AD-A099 508 CALIFORNIA UNIV BERKELEY EARTHQUAKE ENGINEERING RES--ETC F/G 8/11
ANALYSIS OF LOCAL VARIATIONS IN FREE FIELD SEISMIC GROUND MOTIO--ETC(U)
JAN 81 J CHEN, J LYSMER, H B SEED DAAG29-76-G-0257
UNCLASSIFIED UCB/EERC-81/03 ARO-13838.2-GS NL

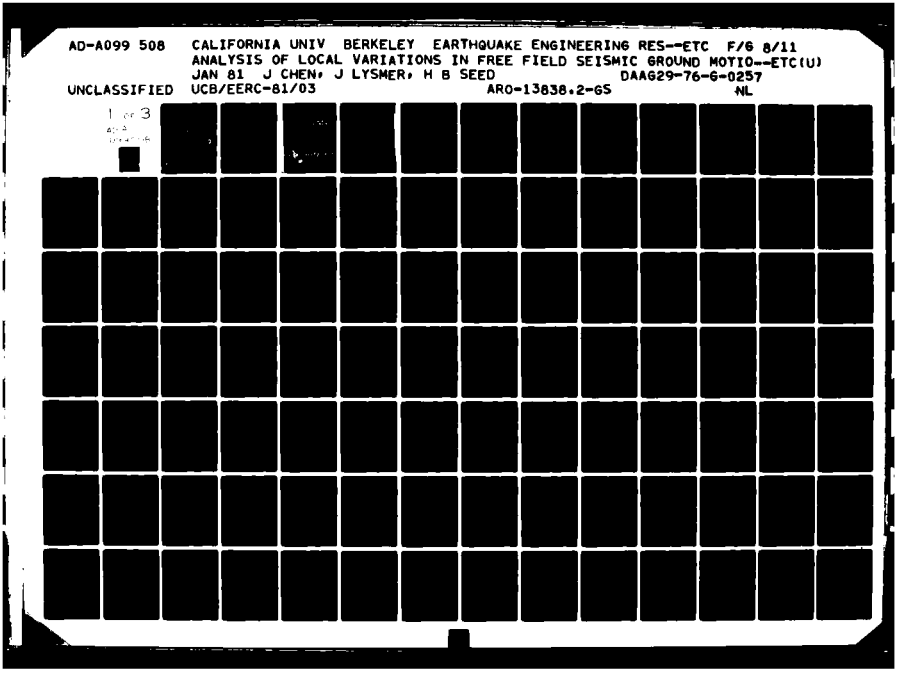

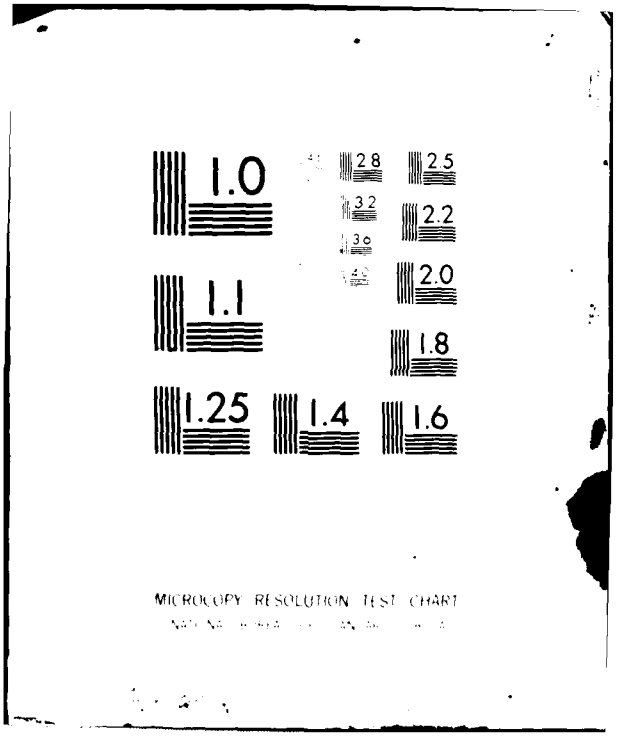
1.0
2.8
2.5
3.2
2.2
3.6
4.0
2.0
1.1
1.8
1.25
1.4
1.6
MICROCOPY RESOLUTION TEST CHART

UNCLASSIFIED

SECURITY CLASSIFICATION OF THIS PAGE (When Data Entered)

AD A099508

REPORT DOCUMENTATION PAGE

READ INSTRUCTIONS BEFORE COMPLETING FORM

1. REPORT NUMBER: 13838.2-GS	2. GOVT ACCESSION NO.: ARO AD-A099508
3. RECIPIENT'S CATALOG NUMBER:	
4. TITLE (and Subtitle): Analysis of Local Variations in Free Field Seismic Ground Motion.	5. TYPE OF REPORT & PERIOD COVERED: Technical
	6. PERFORMING ORG. REPORT NUMBER:
7. AUTHOR(s): Jian-Chu Chen, John Lysmer, H. Bolton Seed	8. CONTRACT OR GRANT NUMBER(s): DAAG29-76-G-0257
9. PERFORMING ORGANIZATION NAME AND ADDRESS: University of California, Berkeley, CA 94720	10. PROGRAM ELEMENT, PROJECT, TASK AREA & WORK UNIT NUMBERS: UCB/EERC-81/03
11. CONTROLLING OFFICE NAME AND ADDRESS: U. S. Army Research Office, Post Office Box 12211, Research Triangle Park, NC 27709	12. REPORT DATE: Jan 81 (12) 282
	13. NUMBER OF PAGES: 261
14. MONITORING AGENCY NAME & ADDRESS (if different from Controlling Office)	15. SECURITY CLASS. (of this report): Unclassified
	15a. DECLASSIFICATION/DOWNGRADING SCHEDULE

LEVEL II

16. DISTRIBUTION STATEMENT (of this Report)

Approved for public release; distribution unlimited.

DTIC ELECTE JUN 1 1981 S D

17. DISTRIBUTION STATEMENT (of the abstract entered in Block 20, if different from Report)

NA

18. SUPPLEMENTARY NOTES

The view, opinions, and/or findings contained in this report are those of the author(s) and should not be construed as an official Department of the Army position, policy, or decision, unless so designated by other documentation.

19. KEY WORDS (Continue on reverse side if necessary and identify by block number)

seismic waves
soil structure
liquefaction
surface waves
wave propagation
interfaces
ground motion

20. ABSTRACT (Continue on reverse side if necessary and identify by block number)

Earthquake engineers are often faced with the problem of determining the temporal and spatial variation of near-surface seismic motions in a site. This type of information is needed for the evaluation of soil-structure interaction effects, liquefaction potential and the effects of local site conditions on surface motions. Actual ground motions are due to a complicated system of body waves and surface waves. However, it is usually assumed that near-surface motions consist only of vertically

DD FORM 1 JAN 73 1473 EDITION OF 1 NOV 65 IS OBSOLETE

UNCLASSIFIED 405 986

SECURITY CLASSIFICATION OF THIS PAGE (When Data Entered)

DTIC FILE COPY

13838.2-GS

20. ABSTRACT CONTINUED

propagating waves. In order to examine the validity of this assumption for engineering design a theoretical investigation has been made into the nature of near-surface motions produced by horizontally propagating waves. These include inclined P-, SV-, and SH-waves, Rayleigh waves and Love waves in horizontally layered sites over a viscoelastic half space. The research involved five phases; (1) review of current knowledge, (2) development of new methods of site response analysis, (3) application to site response analysis, (4) application to soil-structure interaction analysis and (5) evaluation of the relative importance of horizontally propagating waves in engineering design.

REPORT NO.
UCB/EERC-81/03
JANUARY 1981

EARTHQUAKE ENGINEERING RESEARCH CENTER

ANALYSIS OF LOCAL VARIATIONS IN FREE FIELD SEISMIC GROUND MOTION

by

JIAN-CHU CHEN
JOHN LYSMER
H. BOLTON SEED

A report on research sponsored by
the U.S. Army Research Office

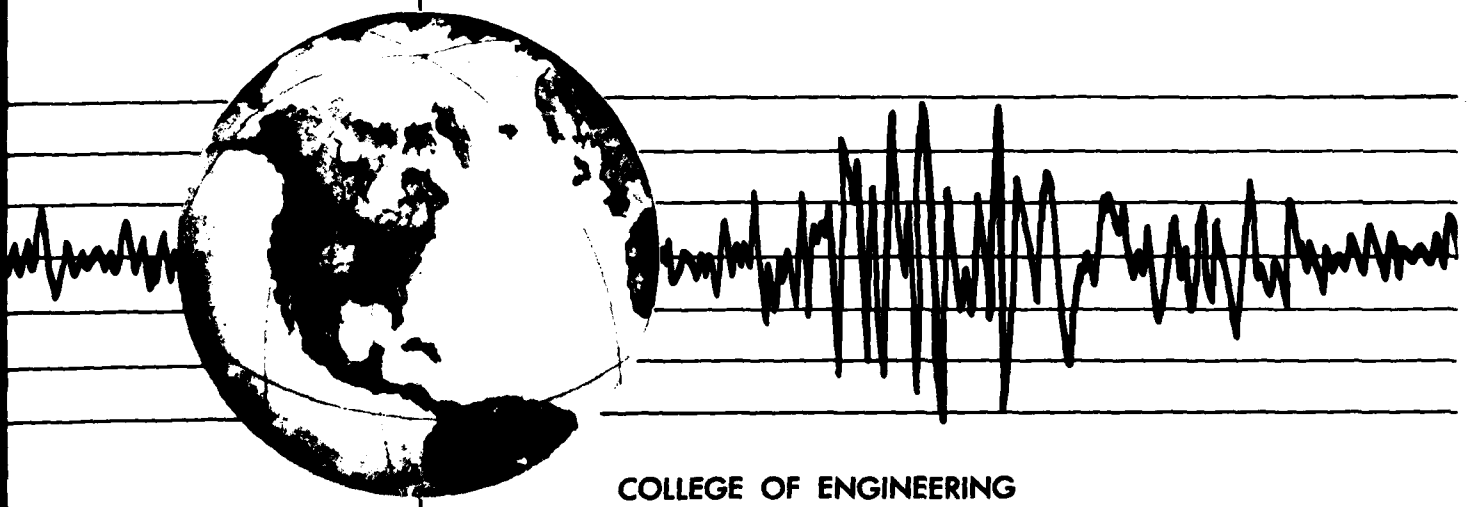

COLLEGE OF ENGINEERING

UNIVERSITY OF CALIFORNIA · Berkeley, California

For sale by the National Technical Information Service, U. S. Department of Commerce, Springfield, Virginia 22161.

See back of report for up to date listing of EERC reports.

EARTHQUAKE ENGINEERING RESEARCH CENTER

ANALYSIS OF LOCAL VARIATIONS IN FREE FIELD SEISMIC GROUND MOTION

by

Jian-Chu Chen

John Lysmer

H. Bolton Seed

Report No. UCB/EERC-81/03

January 1981

A report on research sponsored by
the U.S. Army Research Office

College of Engineering

University of California

Berkeley, California

ABSTRACT

Earthquake engineers are often faced with the problem of determining the temporal and spatial variation of near-surface seismic motions in a site. This type of information is needed for the evaluation of soil-structure interaction effects, liquefaction potential and the effects of local site conditions on surface motions.

Actual ground motions are due to a complicated system of body waves and surface waves. However, it is usually assumed that near-surface motions consist only of vertically propagating waves. In order to examine the validity of this assumption for engineering design a theoretical investigation has been made into the nature of near-surface motions produced by horizontally propagating waves. These include inclined P-, SV-, and SH-waves, Rayleigh waves and Love waves in horizontally layered sites over a viscoelastic half space.

The research involved five phases; (1) review of current knowledge, (2) development of new methods of site response analysis, (3) application to site response analysis, (4) application to soil-structure interaction analysis and (5) evaluation of the relative importance of horizontally propagating waves in engineering design.

The new method of site response analysis involves a finite element type discretization of the site in the vertical direction. According to this method the site is subdivided into thin sublayers and it is assumed that displacements vary linearly between layer interfaces. The method is essentially linear and works in the frequency domain. Nonlinearities are handled by an equivalent linear method according to which the stiffness and damping ratio within each layer are adjusted

iteratively to be compatible with the strains developed in the layer. Transient motions are handled by Fourier techniques.

The method is essentially the same for inclined body waves and surface waves. However, the latter requires the solution of a special eigenvalue problem and identification of the fundamental mode. The procedures have been implemented in the two computer codes, SITE and LOVE. These codes can produce the complete transient field of motion from the knowledge of the motion at one point and the type of wave field producing the motion. Any specified combination of inclined body waves and surface waves can be considered.

The procedure has been applied to a number of sites (rock, sand, and alluvium) assuming different types of wave fields and the motions produced by these fields are compared with those produced by vertically propagating waves. The results show that the realistic analysis of incident body waves produce near-surface motions which vary with depth in essentially the same manner as those produced by vertically propagating body waves. The motions produced by surface waves are somewhat different. However, the study shows that in soil sites surface wave motions decay rapidly in the direction of wave propagation. Within a few hundred feet of the control motion all components of frequencies higher than 1 Hz are reduced to insignificant amplitudes. The same phenomenon occurs in rock sites but at a much slower rate. It is therefore questionable whether high frequency surface waves are important for engineering design.

The study of soil-structure interaction effects show that only the free-field motions within the body of soil replaced by the structure are of importance for design. Thus, with a specified surface control

motion, the spatial variation of free-field ground motions need to be determined only within a shallow zone near the surface.

Examples of soil-structure interaction analyses are provided for a structure on rock, a structure on sand, and a large retaining wall on an alluvial site. The results show that for realistic wave fields the motions of structures on soil site depends only slightly on the type of wave field assumed. On rock sites surface waves may produce somewhat larger motions than vertically propagating body waves.

The study also shows that, while the motions produced in structures by different types of wave fields may not be too different, the dynamic earth pressures on embedded structures depend strongly on the nature of the seismic environment. In particular Rayleigh waves may produce larger dynamic earth pressures than vertically propagating shear waves.

The final conclusions of the study are that the current assumption of vertically propagating waves is probably sufficient for many practical purposes. However, surface waves may be important in rock sites and in the determination of forces acting on structures.

ACKNOWLEDGEMENTS

The work described in this report was performed under Contract No. DAAG 29-76-G-0257 between the U.S. Army Research Office and the University of California at Berkeley. The major part of the research described was performed by Dr. Jian-chu Chen in partial fulfillment of the requirements for the degree of Doctor of Philosophy of the University of California at Berkeley. The soil-structure interaction results presented in Chapter 6 were performed in cooperation with Dr. A. J. Gomez-Masso.

The authors gratefully acknowledge the financial support of the Army Research Office and the interest taken throughout the study by Professor B. A. Bolt of the Seismographic Station of U. C. Berkeley. A special thanks goes to R. C. Murray, J. J. Johnson and O. R. Maslenikov of the Structural Mechanics Group of the NTED of the Lawrence Livermore National Laboratory for their support in the final stages of preparing this report.

CONTENTS

LIST OF FIGURES

LIST OF TABLES

CHAPTER 1

INTRODUCTION

Earthquake engineers are often faced with the problem of determining the spatial and temporal variation of seismic motions in a soil profile from a motion specified at a single point. Solutions to such problems, which are known as site response problems, are necessary for liquefaction and soil-structure interaction analyses.

1.1 Current Methods of Site Response Analysis

Current engineering analyses of site response usually involve three basic assumptions:

- Ground motions developed near the surface of a soil deposit may be attribute only to the vertical propagation of shear waves, Kanai (1950, 1952).
- The ground surface, the interfaces between layers, and the bedrock are essentially horizontal.
- The material in each layer is homogeneous and linearly elastic or viscoelastic.

Using these assumptions, many researchers have developed computational site models and methods of analysis for site response problems, including Idriss and Seed (1967), Tsai (1969), Roesset and Whitman (1969), and Schnabel, Lysmer, and Seed (1972). The first two assumptions above were found to be quite reasonable for many sites involving sedimentary deposits with horizontal layering. The third assumption of linearity might be inappropriate for strong seismic motion. However, the nonlinear behavior of soil can be practically approximated by the equivalent linear method proposed by Seed and Idriss (1969).

In general, the computational methods for site response problems can be separated into continuum or discrete methods. Continuum methods involve either the analytical solution of boundary value problems directly from differential equations, the method of characteristics, or the finite-difference method. These solutions can be obtained either in the frequency or the time domain. Discrete methods use lumped-mass or consistent-mass finite element formulations, which give good results if each layer in the model is thin enough to transmit the shortest wavelength involved. Current discrete methods include the complex response method, modal analysis, direct integration, and the method of characteristics. Each method is briefly reviewed below.

Complex response analysis (linear frequency domain analysis) can conveniently account for material damping through the introduction of complex moduli into the equations of motion. This method can incorporate equivalent linear techniques to approximate nonlinear soil behavior. Furthermore, Fast Fourier Transform and interpolation techniques in the frequency domain make this method effective and economical.

Modal analysis can be performed on a lumped-mass model of a shear beam representing the soil profile. Modal frequencies and mode shapes may be obtained from the geometry and mass distribution of the system. The response in each mode may then be determined, and the total response is obtained by superposition. This technique, however, can not properly account for the spatial variation of damping within the soil mass or for radiation damping.

Direct integration (step-by-step time domain analysis) may also be used. Experience has shown that for a large time step this method

encounters stability and damping problems related to the numerical algorithms. Although smaller time steps will overcome some of these problems, computational costs increase dramatically. Problems may also be encountered in constructing the proper damping matrix from given material properties. Besides, unreliable responses might be obtained in the high-frequency ranges.

The method of characteristics is a mathematical technique for transforming partial differential equations into ordinary differential equations that are then solved by some suitable technique. The method is effective for linear analysis but encounters computational problems for nonlinear analysis.

Recently, efforts have been directed toward the development of better nonlinear analysis methods. Nonlinear total stress analyses of site response problems using vertically propagating shear waves were studied by Streeter et al. (1974), Constantopoulos (1973), Papadakis (1973), Joyner and Chen (1975), Martin (1975), Idriss et al. (1976), and Taylor and Larkin (1978). Several methods of nonlinear effective stress analysis have been proposed by Finn et al. (1977), Liou et al. (1977), and Ghaboussi and Dikmen (1978). These methods are important for the study of liquefaction during earthquakes.

1.2 The Seismic Environment

The above methods assume a simple seismic environment consisting of vertically propagating waves. However, as shown in Fig. 1.1 the motions generated by a source in the Earth's crust are composed of many wave types. The basic wave types are called shear waves (S-waves) and compressional waves (P-waves). When the (perhaps curved) wave fronts of these waves impinge on the ground surface or layer interfaces

surface waves may be generated. These include Rayleigh waves (R-waves) and Love waves (L-waves).

The different wave types can be classified as shown in Fig. 1.2. S-waves involve motions perpendicular to the direction of wave propagation. S-wave motions in the vertical plane are called SV-waves. Horizontal S-wave motions are called SH-waves. P-waves involve motions in the direction of wave propagation. Rayleigh waves involve horizontally propagating elliptical motions in the vertical plane and Love waves consist of horizontal motions perpendicular to the horizontal direction of wave propagating.

All of the above wave types can propagate independently. However, at layer interfaces and other inhomogeneties refraction or reflection may occur which not only may change the direction of wave propagation but which may convert one wave type into another (mode conversion). As a result actual seismic environments are much more complicated than the vertically propagating wave field assumed in current engineering analyses.

The main purpose of the research described herein was to investigate the possibility of developing methods of site response analysis which can consider more realistic, and thus more complicated, seismic environments than that described in Section 1.1. Specifically, the assumption of vertical wave propagation will be dropped.

1.3 Horizontally Propagating Waves

Five types of horizontally propagating wave fields in horizontally layered soil and rock systems will be investigated:

- Inclined P-waves
- Inclined SV-waves

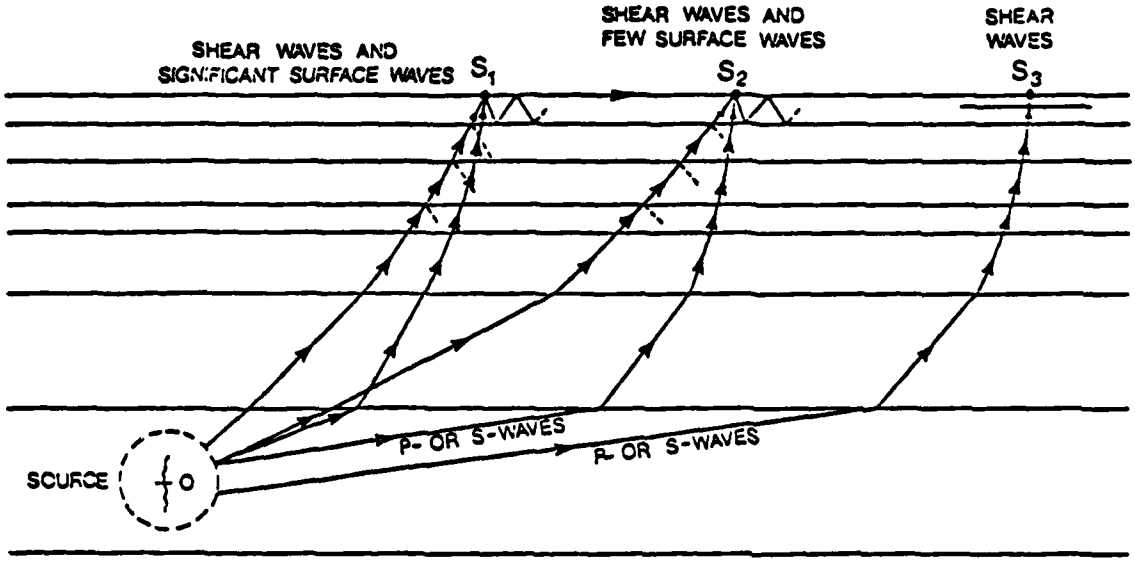

Fig. 1.1 Idealized Relation Among Earthquake Source, Wave Paths and Site (after Tsai, 1969; Nair, 1975)

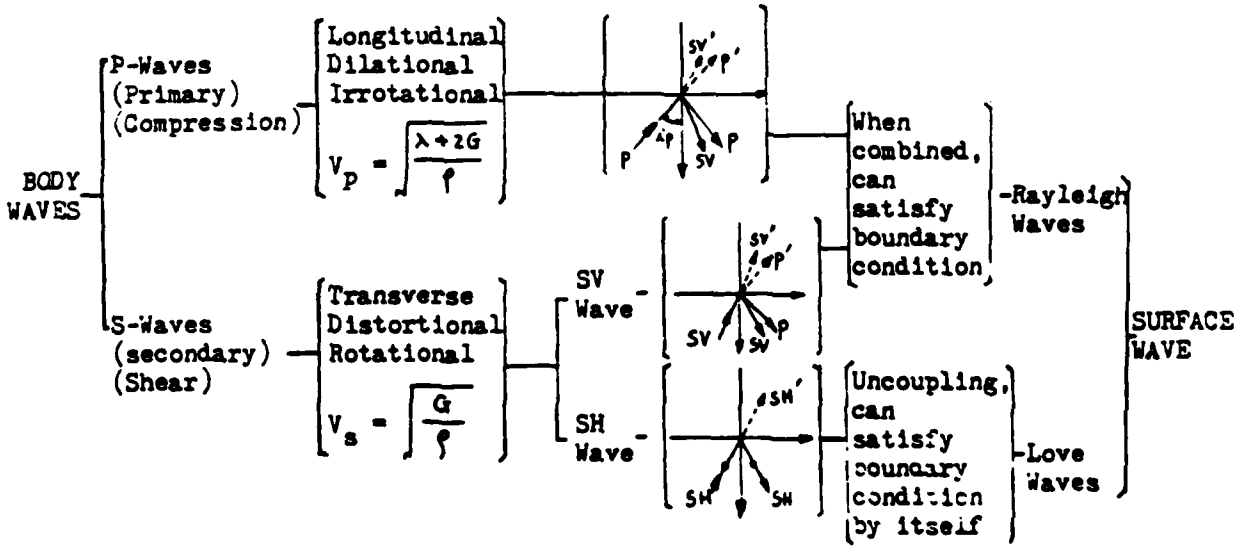

Fig. 1.2 Seismic Waves - Types, Characteristics and Relationships

- Inclined SH-waves
- Rayleigh waves
- Love waves

Also, combinations of such wave systems will be considered.

The relative contributions of the different wave types to the total ground motion and the corresponding arrival times for each type of wave depend on the epicentral distance to the site, the focal depth of the source, and the phenomena of multiple reflection, refraction, and dispersion along the various paths. Realistically, it must be assumed that all observed seismograms contain some components of all of the above motions. However, the exact composition is not and probably never will be known since the exact properties of the source and the physical and geometric details of the geology cannot be determined.

There is today considerable observational evidence that all of the above wave types exist. The existence of inclined body waves has been confirmed by numerous investigators, e.g. Suzuki (1932) who reported a mean angle of incidence of about 4° for the initial motion in about fifty records from Hongo and Mitika, Japan.

The evidence for the existence of surface waves is even stronger. More recent observations include; Shima (1970), Trifunac (1971), Bolt (1972), Anderson (1974), Hanks (1975), Toki (1977), Swanger and Boore (1978). However, the evidence seems to be limited to frequencies below 2 Hz. For example, the surface waves observed by Swanger and Boore (1978) in the records from the 1968 El Centro earthquake occurred in the range 0.1 - 1.0 Hz and the surface waves detected in the 1971 San Fernando earthquake were in the range 0.1 - 2.0 Hz, Toki (1977). The existence of significant surface wave components above 2 Hz, which is

the range of most interest to engineers, has therefore not been confirmed.

In addition to the above evidence there is an overwhelming amount of data which indicate phase differences between motions observed at closely spaced points, e.g. Yamahara (1970) who observed significant phase differences between stations spaced only about 100 feet apart. In most of these cases the wave type was not identified. Nevertheless, the evidence confirms the existence of horizontally propagating waves.

Although a few suggestions have been made, Nair and Emery (1975), Liang and Duke (1978), as to the relative content of different wave types, the literature has a dearth of data on this topic in the frequency range of interest to engineers.

Several researchers have developed theories for the response of a horizontally layered site to plane harmonic body waves arriving at a specified incident angle from an underlying half space. Thomson (1950) and Haskell (1960, 1962) developed a matrix formulation for computing transmission coefficients in a layered continuum. Hannon (1964) extended Haskell's formulation to study transient incident P-waves. Silva (1976) extended the Thomson-Haskell method to include damping in soil layers.

The response of a horizontally layered site to harmonic surface waves has been studied by Sezawa and Kanai (1935), Haskell (1953), and Ewing et al. (1957), Mooney and Bolt (1966). Recently, Bocheva (1977) extended the method to study surface wave amplification factors. Swanger and Boore (1978) simulated strong motion displacement using surface wave modal superposition. Lysmer (1969a), Waas (1972), Lysmer and Waas (1972), and Lysmer and Drake (1972) applied the finite element method to problems involving Rayleigh and Love waves.

Most of the above studies are restricted to linear analysis of harmonic motion of a single type of wave field.

1.4 Purpose and Scope

The main purpose of the research described herein was:

- To develop analytical methods for site response analysis of horizontally layered sites excited by horizontally propagating seismic motions consisting of surface waves and inclined body waves.

The main emphasis is on engineering applications. This means that the geometric dimensions of the model considered are smaller than (and the frequency range higher than) those usually considered by seismologists (100 ft vs. 1 km, 1-20 Hz vs 0.1 - 1 Hz). Also, while the seismologist's problem usually is to determine motions from estimated source parameters or source parameters from observed motions, the engineering site response problem involves determining the spatial and temporal variations of transient motions within a limited distance from a specified motion (control motion) at or near the ground surface. This process is called deconvolution in the engineering profession.

The research involved the following items:

- Review of existing methods and available data on dynamic material properties.
- Development of a finite element method for transient site response analysis of problems involving inclined body waves in a profile consisting of soil layers over a viscoelastic half space.

- Development of a finite element method for transient site response analysis of problems involving Rayleigh waves and Love waves in a profile consisting of soil layers over a viscoelastic half space.
- Development of practical computer codes (SITE and LOVE) to implement the above methods.
- Application of the above methods to realistic site response problems.
- Application of site response solutions to soil-structure interaction problems.

The presentation of the research is organized as follows:

The dynamic properties of soils and rock are described in Chapter 2. The emphasis is on a material description which is suited for the analytical procedures employed in later chapters.

Inclined body waves are discussed in Chapter 3 and surface waves in Chapter 4. The treatment in these chapters involves only harmonic waves. However, these chapters contain most of the theoretical developments for the finite element codes SITE and LOVE.

The transition to transient cases through Fourier techniques is made in Chapter 5 which also contains several case studies of site response analysis.

In Chapter 6 the application of site response solutions to soil-structure interaction problems is discussed and a number of case studies are presented.

The results of the research are summarized in Chapter 7. As will be shown in that chapter the research lead not only to the development of a unified theory for inclined body waves and surface waves in

layered systems and two associated computer programs but to a number of significant conclusions regarding the importance of considering horizontally propagating waves in design and, perhaps surprisingly, the likely contribution of surface waves to near surface seismic motions.

CHAPTER 2

DYNAMIC MATERIAL PROPERTIES

2.1 Introduction

The stress-strain characteristics of soils are strongly nonlinear and may significantly influence the dynamic response of a site subjected to a strong earthquake. A good site response analysis must therefore consider these nonlinear effects.

Details of the dynamic stress-strain behavior of soils have recently been reported in state-of-the-art papers by Hardin (1978) and Yoshimi et al. (1977). It is clear from these reports that the transient stress-strain behavior of soils is extremely complicated and that this behavior can not as yet be fully described by constitutive laws. Most of the data and models available refer to cyclic behavior of soils subjected to constant strain amplitudes. Typical stress-strain relationships of soils subjected to symmetric cyclic loading conditions are curvilinear as shown in Fig. 2.1.

In choosing dynamic soil properties for site response analysis, one should realize that such problems can only be solved by making certain assumptions about the nature of the wave fields involved. Except for the special case of vertically propagating waves, which is not the major topic of this dissertation, appropriate wave fields can only be constructed for linear layered systems. Therefore, it is essential to choose representative linear dynamic properties for the actual analysis. As will be shown, such properties can be determined from the available data, and an approximation to nonlinear analysis can be achieved by the equivalent linear method, which is discussed at the end of this chapter.

2.2 Measurement of Dynamic Properties

Considerable effort has been directed towards the determination of soil properties in recent years. A complete review of the measurement of dynamic properties was given in a state-of-the-art paper by Woods (1978). The most commonly used test procedures are described below.

Determination of Hysteresis Loops

Hysteretic stress-strain relationships of the type shown in Fig. 2.1 can be determined by cyclic triaxial compression tests, cyclic simple shear tests, or cyclic torsional shear tests. These tests are applicable in the amplitude ranges shown in Fig. 2.2a and are usually performed in the frequency range of 1-20 Hz. Test results have indicated that the shape of the hysteresis loops is virtually independent of frequency. From these loops the effective dynamic moduli and fractions of critical damping can be determined. The modulus is the slope of the secant betweeen the ends of the loop, and the damping is proportional to the aspect ratio of the loop, i.e., the ratio between the average width and the length of the loop.

Resonance Column Tests

The dynamic moduli can also be determined from longitudinal or tortional resonance tests, in which a column of soil is excited at different frequencies to determine the natural frequencies from which the moduli can be computed. The damping ratio can be estimated from the height of the resonance peaks or by measurement of the phase difference between the displacement of the specimen and the exciting force. These tests are usually performed at frequencies in the range of 20-260 Hz and are applicable in the strain amplitude ranges shown in Fig. 2.2a.

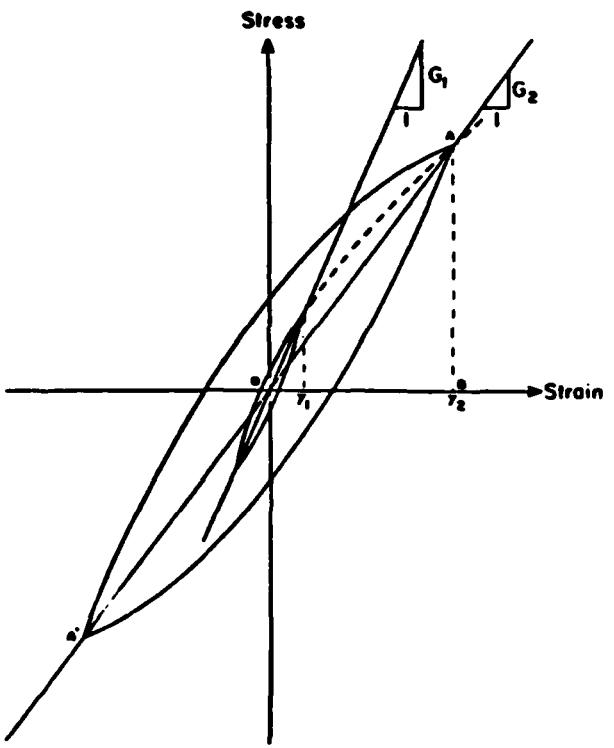

Fig. 2.1 Hysteretic Stress-Strain Relationships at Different Strain Amplitudes

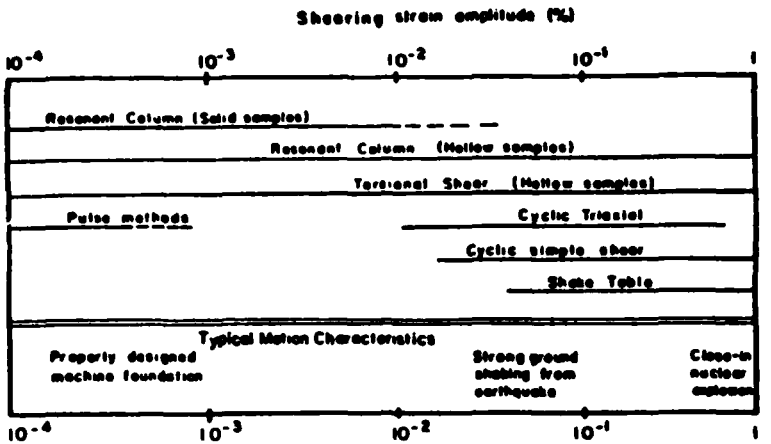

a. Laboratory tests (after Woods, 1978)

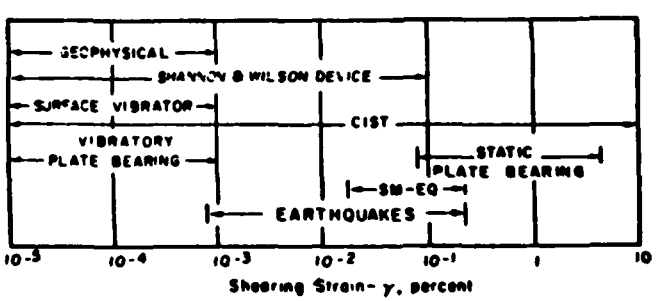

b. Field techniques (after SW-AA, 1974)

Fig. 2.2 Shearing Strain Amplitude Capabilities for Laboratory tests and Field Techniques

Free Vibration Tests

In these tests cylindrical soil samples are set into longitudinal or torsional vibrations, the power is switched off, and the decay of the amplitudes is measured to determine the logarithmic decrement, from which the damping ratio can be computed. These tests can be conducted using a resonant column apparatus with either solid or hollow samples, and good results can be obtained only at relatively low to moderately high strain levels.

Field Measurement of Wave Velocities

In-situ tests are conducted to determine the velocities of propagation of P-, S- and Rayleigh waves. The most usual types of field tests are

a. Geophysical tests: seismic refraction, seismic cross-hole, and seismic down-hole methods.

b. Surface vibration tests: surface wave and resonant footing techniques.

c. Other field techniques: frequency domain measurements; cylindrical in-situ tests, see Woods (1978).

In general, these tests give soil moduli for low strain levels. In-situ tests are inadequate to determine the volumetric characteristics of saturated soil because the measured P-wave velocities are greatly affected by the presence of water. The customary procedure in this case is to conduct laboratory measurements of Poisson's ratio or bulk modulus. Such laboratory tests are usually performed statically because the measurement of lateral deformations and volumetric strains under dynamic conditions is not practical, Shannon and Wilson (1971).

The ranges of shear strain amplitudes over which the field techniques are applicable are shown in Fig. 2.2b.

2.3 Summary of Available Data

As can be seen from Fig. 2.1, the effective dynamic moduli of soils subjected to cyclic excitation will usually decrease with the strain amplitude, and the damping ratio will increase as the strain amplitude is increased. Therefore, it is customary to present the data in the form of curves which show the variation of modulus and damping with strain amplitude, see Figs. 2.3-2.9.

Most available data only consider the variation of shear modulus and damping ratio with shear strain amplitude. In principle, two moduli and two damping ratios should be considered--one set corresponding to S-waves (shear modulus, G, and the corresponding damping ratio, β_s), and a second set corresponding to P-waves (constrained modulus, M, and damping ratio, β_p). Also, the variation of these parameters with the amplitude of normal strain should, in principle, be considered. However, normal strains are usually considered to have only small effects on the dynamic properties and are neglected. Similarly, the two damping ratios β_s and β_p are often assumed to be the same, although data by McDonal (1958) and Eisenburg (1972) indicate that the damping ratio for S-waves is considerably higher than that for P-waves (see below). A detailed study of the factors influencing the shear moduli and damping values of soils has been carried out by Hardin and Drnevich (1972). Seed and Idriss (1970) have proposed simplified practical relations which will be used in this study. Some relationships for rock material were proposed by Schnabel (1973).

Cohesionless Soils

Seed and Idriss (1970) have shown that the dynamic shear modulus of cohesionless soil can be expressed by:

$$G = 1000\ K_2\ (\sigma_m)^a\ F \qquad (2.1)$$

where K_2 is a parameter that depends on the relative density and the shear strain amplitude. Also, σ_m is the mean effective stress, which equals $(\sigma_v + 2K_0 \sigma_h)/3$, where σ_v and σ_h are the vertical and horizontal effective pressures, respectively, and K_0 is the at-rest earth-pressure coefficient. The exponent, a, has been found to vary from 0.3 to 0.8 (Idriss and Seed, 1968; Carriveau, 1970; Drnevich et al., 1966; and Silver and Seed, 1969). Seed and Idriss (1970) proposed the use of a = 0.5 in the above expression. The term F is a coefficient accounting for grain size and shape variation. It ranges from 0.6 for silt to 2 for gravel.

The estimated average value for the combined effects of K_2 and F is about 61 at low shear strain levels (10^{-4} percent) for a wide range of sandy soils at 75% relative density. The attenuations of the shear modulus with increasing strain for sands of different densities are shown in Fig. 2.3. The curves shown in this figure may be normalized to a single attenuation curve as shown in Fig. 2.4.

Measured values of the damping ratio for cohesionless soils and average values proposed by Seed and Idriss (1970) are shown in Fig. 2.5. The average curve shown is adequate for most cohesionless soils up to a confining pressure of 2500 psf. The damping ratio will be affected by overburden pressure, relative density, degree of saturation and the number of loading cycles. The effects of the number of loading cycles and relative density are minor. It has been found that the damping decreases with increasing effective overburden pressure and increases with increasing degree of saturation. Schnabel (1973) suggested that the variation of the damping factor with effective overburden pressure, σ_m,

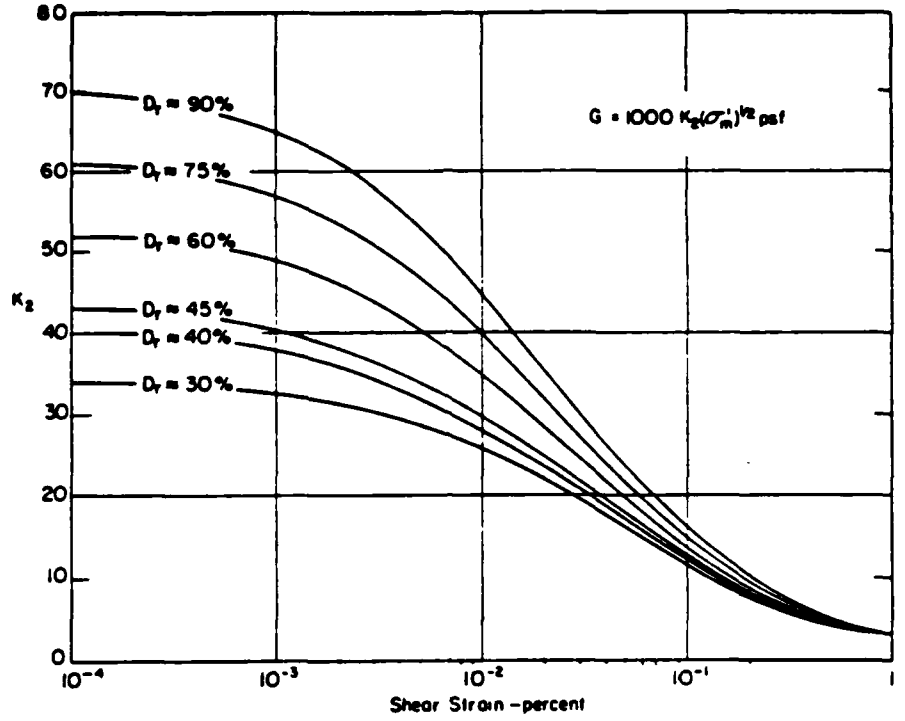

Fig. 2.3 Shear Moduli of Sands at Different Relative Densities (after Seed and Idriss, 1970)

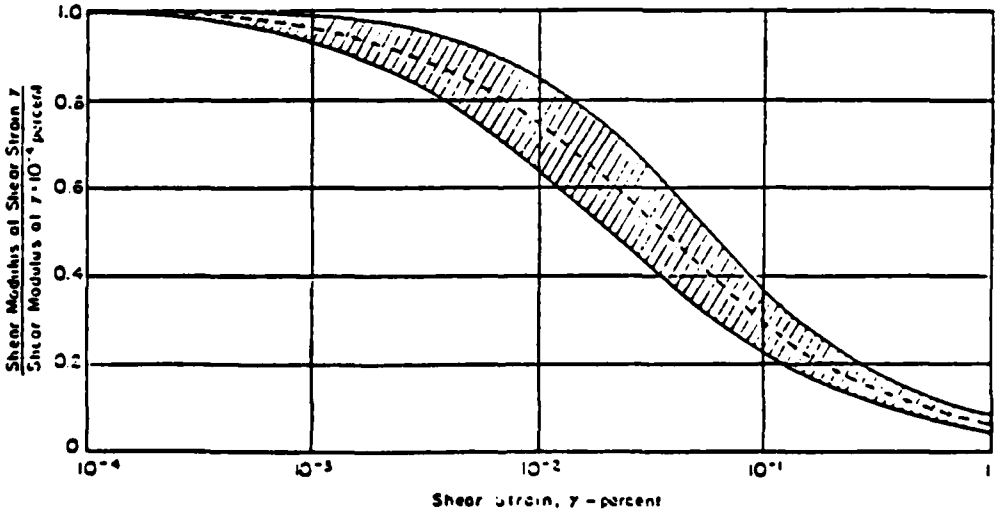

Fig. 2.4 Variation of Shear Modulus with Shear Strain for Sands (after Seed and Idriss, 1970)

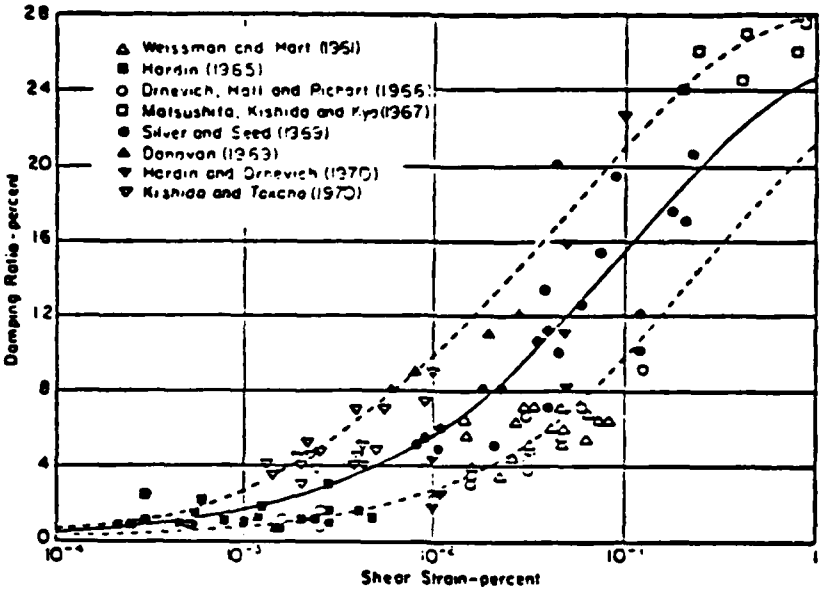

Fig. 2.5 Damping Ratios for Sands (Seed and Idriss, 1970)

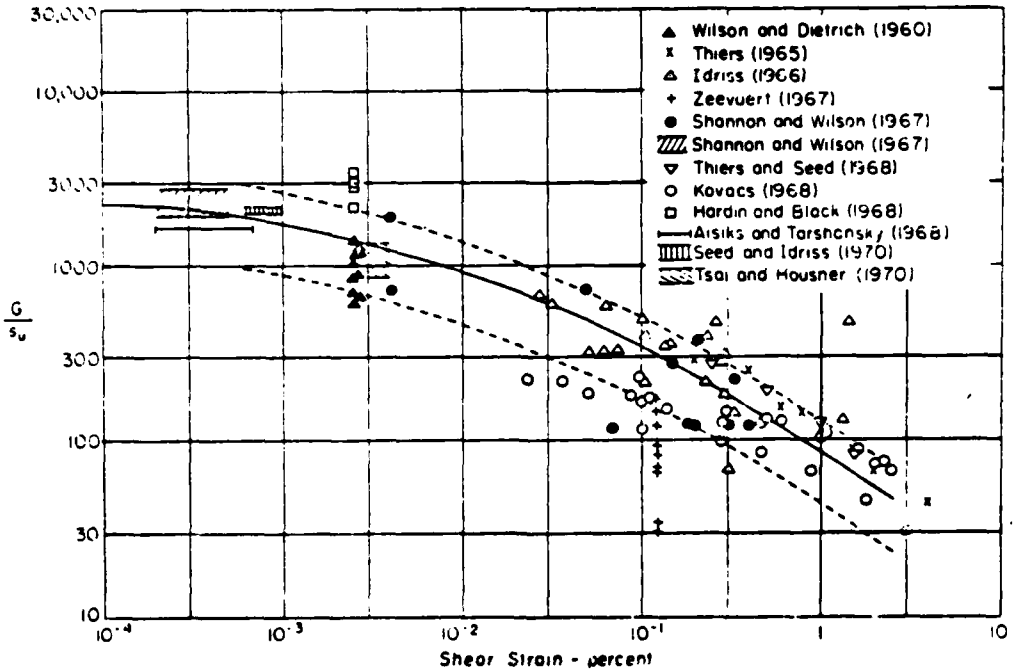

Fig. 2.6 In - Situ Shear Moduli for Saturated Clays (after Seed and Idriss, 1970)

may be expressed by

$$\beta = \left(\frac{2500}{\sigma_m'}\right)^{1/4} F_s \beta_{ave} \qquad (2.2)$$

where F_s is 0.6 for dry sand or 1.0 for saturated sand.

Cohesive Soil

The shear modulus of saturated clays has been found to be essentially proportional to the undrained shear strength S_u, as follows:

$$G = K S_u \qquad (2.3)$$

where K is a coefficient depending mainly on the shear strain amplitude. Average values of the coefficient K obtained from various sources are shown in Fig. 2.6, Seed and Idriss (1970). Some recent results by Stokoe and Lodde (1978) are shown in Fig. 2.7. The shear modulus of clay can be determined in the field for low strain levels and in the laboratory for high strain ranges. Sample disturbance will significantly affect the shear moduli obtained from laboratory tests. Hence, laboratory data must be corrected for sample disturbance. Correction factors can be obtained by comparison of low strain tests in both field and laboratory.

The damping ratio of clays is affected by shear strain amplitude, effective overburden pressure, void ratio, number of loading cycles and water content. Most available data cover only the effect of shear strain amplitude. Measured values of the damping ratio and proposed average values for saturated clay obtained from different sources of data are shown in Fig. 2.8.

Rock

Values of shear modulus for rock are most often obtained from seismic investigations, which yield values only at low strain levels. Very few data are available for strain dependence, but it seems likely that rock will exhibit some decrease of shear modulus with increasing

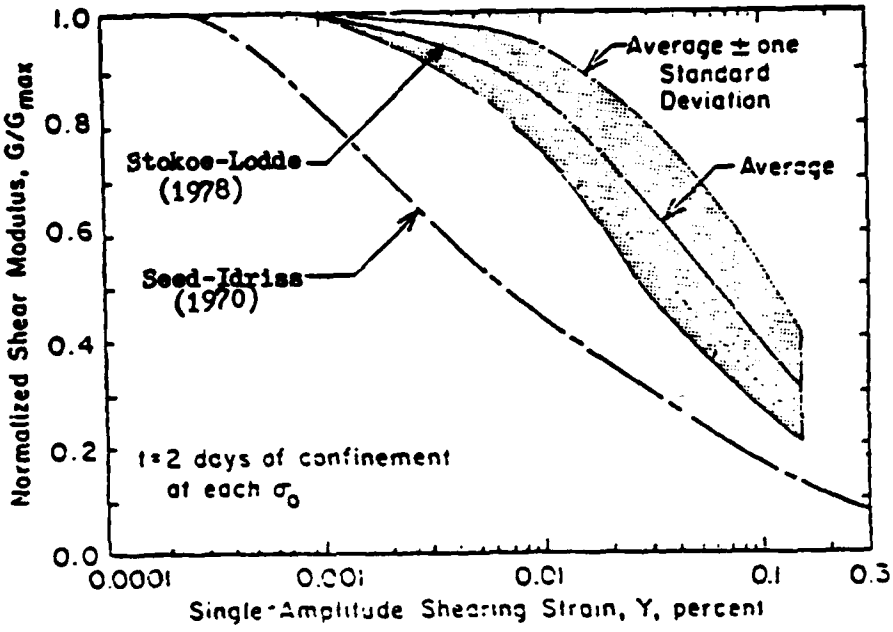

Fig. 2.7 Normalized Shear Modulus with Shear Strain for Saturated Clays (from Stokoe and Lodde, 1978)

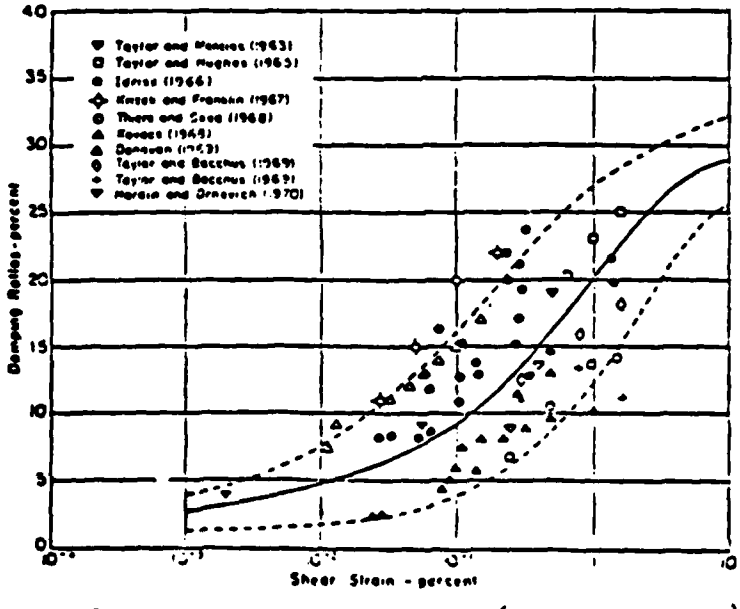

Fig. 2.8 Damping Ratios for Clays (Seed and Idriss)

shear strain. The curves shown in Fig. 2.9 were proposed by Schnabel (1973) for site response analysis of sedimentary rock layers. Schnabel also presented considerable data for low strain properties of different rock types.

A literature survey by Knopoff (1964) provides values of damping ratios for various rock types. These data were obtained from laboratory tests and indicate that the damping ratio for rock varies from 0 to 1.4 percent. A literature survey by Jackson and Anderson (1970) of data obtained from in-situ measurement in the shallow crust of the earth indicates values for the S-wave damping ratio ranging from 2.5×10^{-2}% to 0.5%, and values for the P-wave damping ratio ranging from 0.01% to 1.5%. For surface earth materials, Knopoff's survey (1964) shows values of the P-wave damping ratio ranging from 1% for magnetite hemotite to 7.2% for Pottsville sandstone and values of the S-wave damping ratio of about 5% for *Pierre Shale*.

Damping for shear waves is higher than for P-waves by a factor of 1.8 to 2.6 (McDonal, 1958; Eisenberg, 1972). No data are available regarding the variation of damping with strain in rock, although some increase in damping ratios with increasing strain is to be expected. The strain dependent damping curve shown in Fig. 2.9 was proposed by Schnabel (1973) for sedimentary rock layers with shear wave velocities in the range 2000-4000 fps at 100-3000 ft depth. He also proposed the following method for adjusting the damping values of rock having other shear wave velocities.

a. All materials with $V_s \leq 3000$ fps are treated as soil with the same nonlinear property characteristics as described for soils.
b. All materials with $V_s > 11{,}000$ fps may be treated as linear elastic materials.

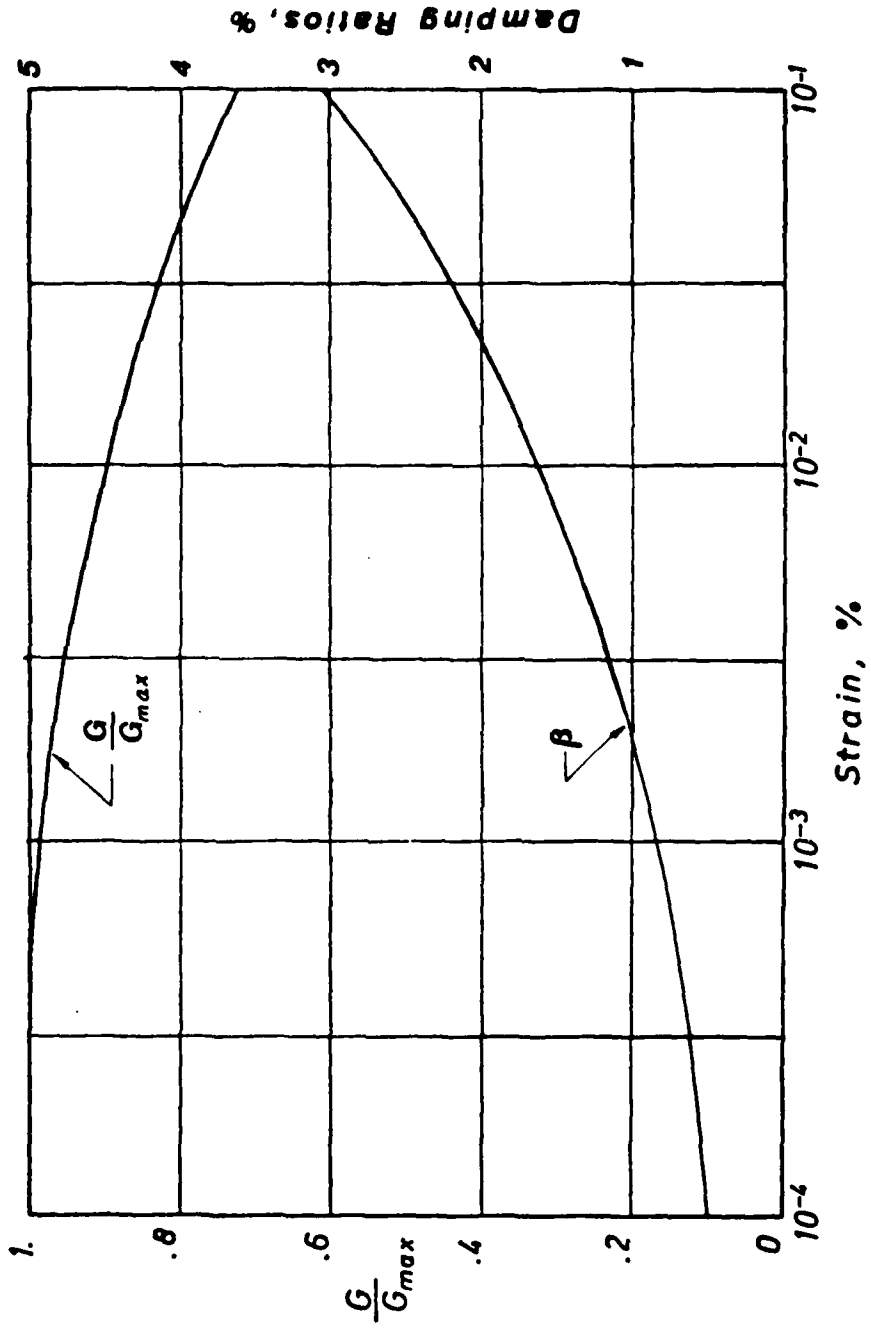

Fig. 2.9 Shear Moduli and Damping Characteristics for Rock

c. A material with 3000 fps<V_s<11,000 fps is treated as a transition material between soil and linear elastic rock. In this case, linear interpolation can be employed between the two extremes described above.

Dynamic Poisson's Ratio

The dynamic Poisson's ratio of soil during cyclic loading has attracted very little attention. Fig. 2.10 shows some laboratory test results for the dynamic Poisson's ratio of clayey soil tested at different shear strain levels, Hara (1973). It can be seen that the dynamic Poisson's ratio for a soft clay and a very stiff clay are essentially independent of the shear strain levels and frequencies of cyclic loading. A statistical analysis of recorded wave velocities of various deposits obtained by seismic exploration was conducted by Ohsaki and Iwasaki (1973). The evaluated dynamic Poisson's ratio versus shear moduli and the total average values are shown in Fig. 2.11. The results demonstrate that the dynamic Poisson's ratio does not change appreciably with shear moduli for sandy soils. Using the experimental results given by Hara (1973), they concluded that the dynamic Poisson's ratio for cohesive soils is almost constant (approximately 0.48) and that for cohesionless soil, the dynamic Poisson's ratio is a function of shear modulus.

In fact, the dynamic Poisson's ratio will significantly affect stress and strain computations as well as the wave propagation characteristics of P-waves in a soil deposit during dynamic excitation.

2.4 Theoretical Models

Several theoretical constitutive models have been proposed which, with cyclic excitation, produce hysteresis loops similar to those shown

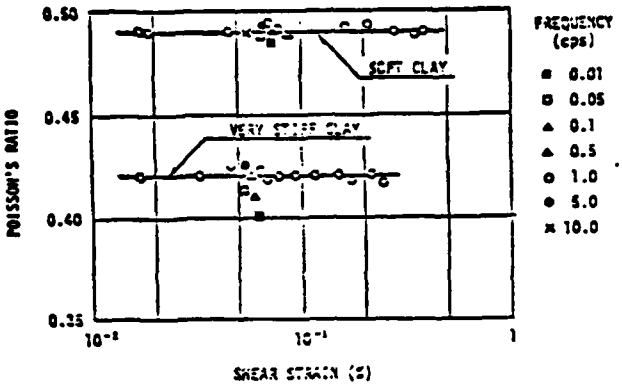

Fig. 2.10 Dynamic Poisson's ratio of clay (after Hara, 1973)

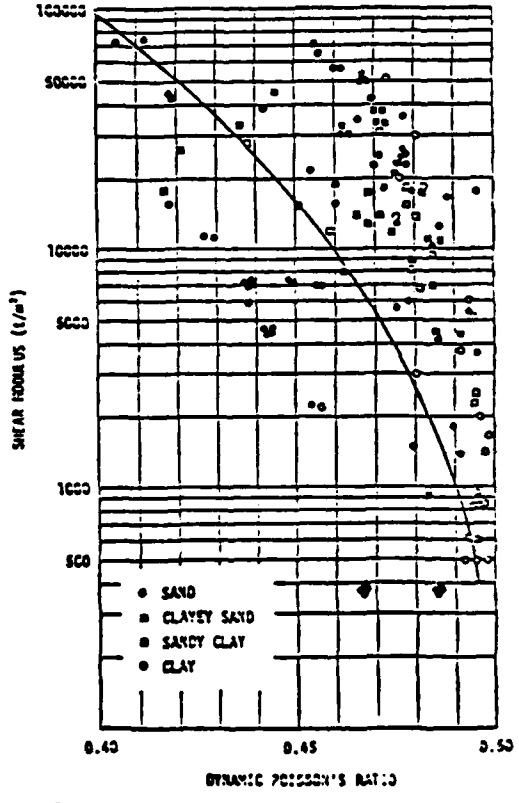

Fig. 2.11 Dynamic Poisson's ratios and shear moduli (after Ohsaki, 1973)

in Fig. 2.1. For the special case of the shear stress-shear strain relationship the most relevant models for soil dynamics analysis are those discussed below.

1. Viscoelastic Models

The general viscoelastic solid produces an elliptical hysteresis loop, the shape and slope of which are rate dependent (i.e., the effective modulus and damping ratio are frequency dependent). However, numerous tests have shown that the shapes of the hysteresis loops for soils are essentially independent of frequency within the frequency range of interest in earthquake engineering. A viscoelastic material which satisfies this condition, as used in this dissertation, can be defined by the complex dynamic modulus:

$$G^* = G(1 - 2\beta_s^2 + 2i\beta_s\sqrt{1 - \beta_s^2}) \tag{2.4}$$

$$\approx G(1 + 2i\beta_s) \; ; \text{ for small } \beta_s$$

where G is the usual shear modulus and β_s is the fraction of critical damping. With this definition the stress-strain law for harmonic excitation becomes

$$\tau = G^*\gamma$$

where τ and λ are the complex amplitudes of stress and strain. A more complex model for two-dimensional stress states will be introduced in Chapter 3.

The hysteresis loops inherent in the above model are independent of the strain amplitude. However, this problem can be overcome by the equivalent linear method discussed later in this chapter.

2. Ramberg-Osgood Generalized Model

A four-parameter model which can be used for nonlinear analysis was proposed by Ramberg and Osgood (1943) and modified by Jennings (1964).

In this model, the shear strain is a function of a given stress as follows:

$$(\gamma/\gamma_y) = (\tau/\tau_{ult}) + \alpha(\tau/\tau_{ult})^r \qquad (2.5)$$

in which r is a positive constant greater than one, α is a real positive parameter, which is a function of r, γ_y is a reference strain, and τ_{ult} is the ultimate shear stress. The shear stress in this equation can not be explicitly represented by the shear strain for a general value of r (r = 1 gives a linear relationship between λ and τ, and r = ∞ gives an elasto-plastic relationship).

The hysteretic damping, β, can be evaluated as described by Jacobsen (1960).

$$\beta = \beta_{max} (1 - \frac{1}{G_{max}})/(1 - \frac{r-1}{2r} \cdot \frac{G}{G_{max}}) \qquad (2.6)$$

where $\beta_{max} = (r - 1)/(\pi r)$, and G/G_{max} can be evaluated from

$$G/G_{max} = 1/\left[1 + \alpha(G\ r/G_{max}\ \gamma_y)^{r-1}\right] \qquad (2.7)$$

The model has been used by Constantopoulos and Christian (1973) and Streeter et al. (1974) for site response analysis and lately by Idriss et al. (1976) for the gradual degrading of clay when subjected to cyclic loading.

3. Hardin-Drnevich Model

Hardin and Drnevich (1972b) proposed the following approximate relationship between stress and strain

$$\tau = G_{max}\ \gamma/(1 + \gamma_h) \qquad (2.8)$$

G_{max} can be measured by resonant column or seismic techniques and γ_h is the hyperbolic strain defined as:

$$\gamma_h = \frac{\gamma}{\gamma_y}\left|1 + ae^{-b\gamma/\gamma_y}\right| \qquad (2.9)$$

in which "a" and "b" are empirical soil constants and "e" is the base of natural logarithms. This model needs four parameters explicitly. The damping ratio is given by

$$\beta = \beta_{max}\, \gamma_h/(1 + \gamma_h) \tag{2.10}$$

For sandy soil β_{max} depends on the number of cycles of loading, and, for clay soil, on the loading frequency and stress state. A similar model--initially used by Kondner (1963) and lately also by Hardin and Drnevich (1972b)--does not include the parameters a and b and defines $\gamma_h = \gamma/\gamma_y$. This model is called the Hyperbolic Model, and only two parameters are needed to determine the stress-strain relationship.

4. Martin-Davidenkov Model

Martin (1975) modified the generalized Davidenkov model by defining a new function for shear strain, and he proposed the following stress-strain law:

$$\tau = G_{max}\,[\,1 - H(\gamma)]\,\gamma \tag{2.11}$$

where $H(\gamma)$ is given by

$$H(\gamma) = \left\{(\gamma/\gamma_y)^{2B}/[1 + (\gamma/\gamma_y)^{2B}]\right\}^{A} \tag{2.12}$$

in which A and B are constant parameters. Four parameters are required for this model. The damping ratio can be evaluated by

$$\beta = \frac{2}{\pi}\left\{\gamma^2 H(\gamma) - 2\int_0^{\gamma} \eta H(\eta)\, d\eta\right\} / \left\{\gamma^2 - 2\int_0^{\gamma} \eta H(\eta)\, d\eta\right\} \tag{2.13}$$

By appropriate choices of the parameters involved all of the above nonlinear models can be made to fit approximately the strain dependency curves for cyclic loading published by Seed and Idriss (1970), see Fig. 2.12 from Kagawa (1978). The Martin-Davidenkov model provides the closest fit.

Parameters Used for Soil Models

Hyperbolic Model	$\gamma_y = 3.16 \times 10^{-4}$, $\beta_{max} = 22\ \%$
Ramberg-Osgood Model	$\gamma_y = 3.16 \times 10^{-4}$, $\alpha = 2.5$, $r = 2$
Hardin-Drnevich Model	$\gamma_y = 3.16 \times 10^{-4}$, $\beta_{max} = 27\ \%$, $a = -0.5$, $b = 0.16$
Martin-Davidenkov Model	$\gamma_y = 3.16 \times 10^{-4}$, $A = 0.9$, $B = 0.413$

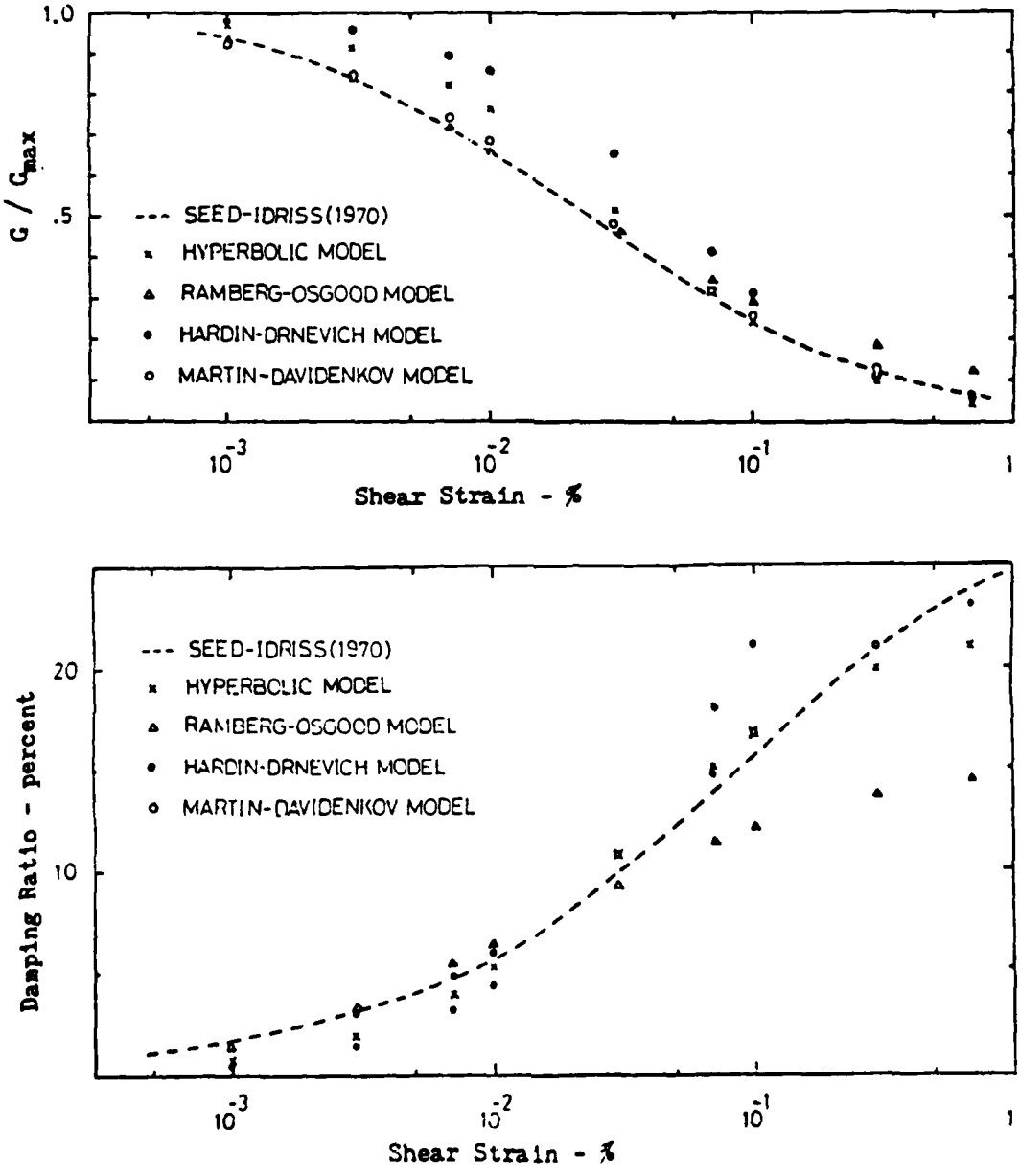

Fig. 2.12 Strain-Dependent Soil Properties from Various Models for Sand

2.5 The Equivalent Linear Method

The nonlinear behavior of soil materials cannot be fully described by constant elastic moduli and damping coefficients. However, a good approximation of the effects of soil nonlinearities on the response can be obtained by the use of constant strain compatible moduli and damping ratios in a sequence of linear analyses. This method, which is known as the equivalent linear method (Seed and Idriss, 1969), can be briefly described in the following manner.

In a site response analysis the equivalent linear method starts with a linear analysis using estimated soil properties in each layer of the soil system. This analysis yields complete time histories of shear strain, from which the effective shear strain amplitudes are calculated in each layer. (The effective shear strain amplitude is usually taken as 65% of the maximum shear strain or as the RMS value of the shear strain time history). Using the computed strain amplitudes, an improved set of soil moduli and damping ratios are obtained from appropriate soil data curves of the type shown in Figs. 2.4-2.9, and a new linear analysis is performed with these properties. The process is repeated until the properties from two consecutive analyses differ by less than a specified tolerance, say 5 percent. This will usually require fewer than 5 iterations. The results of the last iteration are taken as the final solution to approximate a true nonlinear solution. This technique has been widely used in practice because it is an efficient method and is easy to implement in a computer program.

The linear equivalent method can also be used for two-dimensional analysis by the finite element method, Idriss et al. (1973) and Lysmer et al. (1975). In such analyses, strain compatible properties are determined by iteration for each soil element.

The equivalent linear technique has been shown to give surprisingly good approximations to motions computed by truly nonlinear techniques, Martin (1975), although cases have been found where significant differences occured, Martin (1975) and Finn et al. (1978). Good agreement has also been found between observed ground motions and motions computed by equivalent linear methods, Idriss and Seed (1968), Schnabel and Seed (1971), and Valera et al. (1977).

2.6 Combined Loading Effect on Strain-Dependent Properties

The above discussion of shear modulus and S-wave damping is basically for the case of a simplified one-dimensional S-wave analysis. These strain dependent properties can be easily obtained from available laboratory tests such as the resonant column test and the strain control triaxial cyclic test. However, during an earthquake, the soil is excited simultaneously by all kinds of seismic waves travelling in all directions. An element of soil will be subjected to combined shear and compressive strains. How these combined excitations affect the modulus and damping characteristics is still not clear.

A research program to study these combined effects in different soils is currently in progress at the University of California at Berkeley. The research comprises different studies in order that a wide range of loading conditions and strain amplitudes might be explored. For the harmonic simultaneous loading condition, two components of loading can be either out of phase (Rayleigh wave type excitation) or in phase excitation (body waves at small angles of incidence). At low strains, studies involve the cyclic excitation of a triaxial soil specimen in a special resonant column device capable of simultaneous compression and torsion excitation. At high strain ranges, studies involve the cyclic loading of a hollow cylindrical specimen of soil with a special testing

machine capable of reproducing earthquake level strains. While the study is still continuing, the effect on both the shear and constrained moduli and damping appears to be significant in some high strain ranges and some particular loading conditions, Griffin (1979).

Because of a lack of experimental results on strain dependent properties for simultaneous loading conditions, the site response analysis for R-wave excitation is still restricted to linear analysis. However, the developed computer program SITE can handle the approximate nonlinear analysis for R-wave excitation whenever the strain dependent properties are available.

In site response analyses with R-waves or inclined body waves, the strain-dependent property curves for both the shear and the constrained moduli as well as both the S-and P-wave damping ratios will be used simultaneously for the iteration process. The complex constrained modulus, M^*, is defined in a similar way as the complex shear modulus defined in section 2.4:

$$M^* = M(1 - 2\beta_p^2 + 2i\beta_p\sqrt{1 - \beta_p^2}) \tag{2.14}$$

where M is the real constrained modulus and β_p is the damping ratio due to P-waves. However, at this stage, because of a lack of data on strain-dependent P-wave properties, one can assume a constant real Poisson's ratio and follow the conventional iteration procedures by iterating on shear modulus and S-wave damping. This approach implies that the analysis is using the same rate of attenuation on both the shear modulus and constrained modulus and also using the same value of damping for S- and P-waves. On the other hand, as an extreme case one can assume a constant constrained modulus and a constant P-wave damping together with strain-dependent S-wave properties. Analyses iterating on these

sets of property curves will result in a complex Poisson's ratio. The Poisson's ratio will be strain dependent and tend to be larger than that obtained when both G* and M* are assumed to be shear strain dependent.

CHAPTER 3

INCLINED BODY WAVES

3.1 Introduction

In this chapter a method is developed for the evaluation of the seismic response of a horizontally layered site due to a system of plane incident body waves. These waves arrive at an oblique angle at the base of the layered soil system from an underlying uniform half space.

The fundamental equations of motion are presented and partially solved in Section 3.2. The complete solution for the special case of a half space with a free boundary is presented in Sections 3.3 and 3.4. Additionally, an exact solution for a single uniform layer over a viscoelastic half space is developed in Section 3.5. This solution will be later used to verify the discretized method, as developed in Sections 3.6 and 3.7, for a general multi-layered system.

3.2 Governing Equations

The motions created by incident plane body waves will in general involve three components of displacements, however, these components do not vary in the horizontal direction, y, perpendicular to the direction of wave propagation. Hence the problem involves only the space coordinates x and z. The coordinates of x and z are defined as shown in Fig. 3.1.

For the special case of harmonic excitation the equations of motion for an isotropic viscoelastic medium may be written:

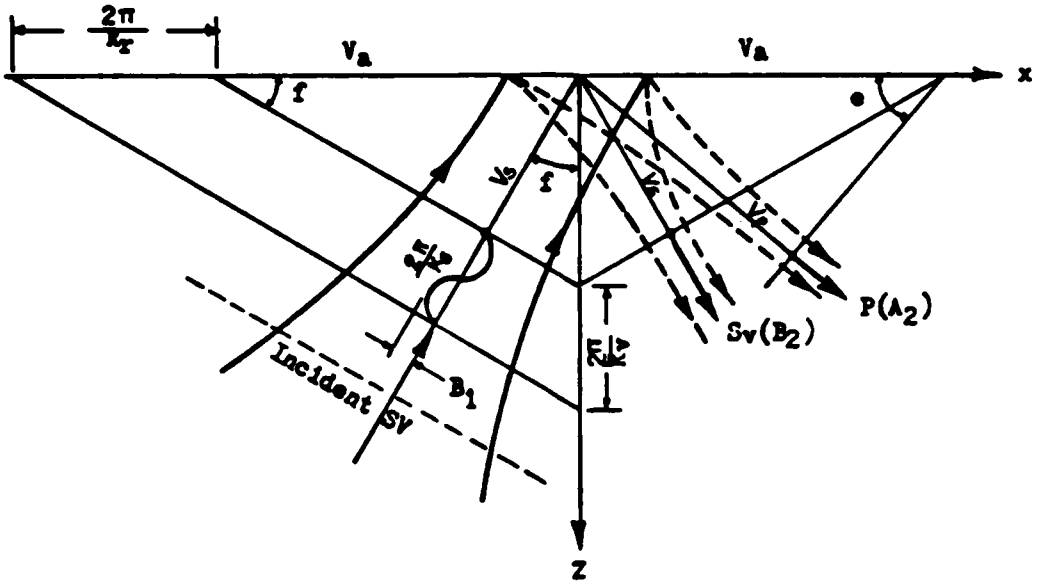

Fig. 3.1 Incidence and Reflection of a SV Wave Arriving at a Free Surface

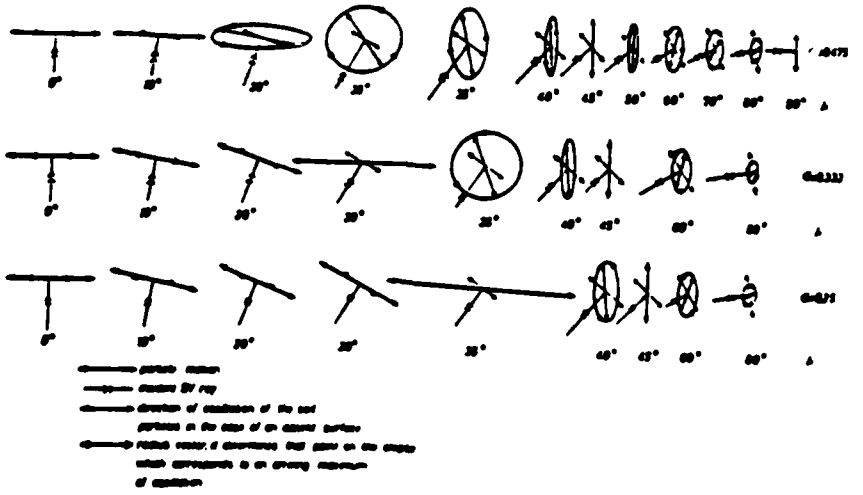

Fig.3.2 Ground Motion at the Free Surface for Incident SV waves (after Meissner, 1965)

$$(M^* - G^*)\frac{\partial \varepsilon}{\partial x} + G^*\nabla^2 u_x = \rho\frac{\partial^2 u_x}{\partial t^2} \qquad (3.1.a)$$

$$(M^* - G^*)\frac{\partial \varepsilon}{\partial z} + G^*\nabla^2 u_z = \rho\frac{\partial^2 u_z}{\partial t^2} \qquad (3.1.b)$$

$$G^*\nabla^2 u_y = \rho\frac{\partial^2 u_y}{\partial t^2} \qquad (3.1.c)$$

where

$$\varepsilon = \frac{\partial u_x}{\partial x} + \frac{\partial u_z}{\partial z} \qquad \text{(Dilation)}$$

$$\nabla^2 = \frac{\partial^2}{\partial x^2} + \frac{\partial^2}{\partial z^2} \qquad \text{(Laplace Operator)}$$

and u_x, u_y, u_z are the displacements in the x, y, z directions, respectively. ρ is the mass density and M^* and G^* are the complex moduli introduced earlier. Equations (3.1.a) and (3.1.b) are coupled. They govern the motion in the vertical x-z plane while Eq. (3.1.c) governs the motion perpendicular to the x-z plane. The waves described by Eqs. (3.1.a) and (3.1.b) will be discussed first.

General Solutions

Using a method based on the work of Helmholtz, see Ewing et al. (1957), Eqs. (3.1.a) and (3.1.b) can be solved by expressing the displacements in terms of displacement potentials ϕ and ψ as follows:

$$u_x = \frac{\partial \phi}{\partial x} - \frac{\partial \psi}{\partial z} \qquad (3.2.a)$$

$$u_z = \frac{\partial \phi}{\partial z} + \frac{\partial \psi}{\partial x} \qquad (3.2.b)$$

where ϕ, ψ satisfy the wave equations:

$$\nabla^2\phi = \frac{1}{V_p^{*2}}\frac{\partial^2 \phi}{\partial t^2} \qquad (3.3.a)$$

$$\nabla^2\psi = \frac{1}{V_s^{*2}} \frac{\partial^2\psi}{\partial t^2} \qquad (3.3.b)$$

The potential functions ϕ and ψ are associated with P and SV wave motions, respectively. The two types of waves propagate through the medium with velocities V_p and V_s, respectively.

Since the motions are assumed to be harmonic at the frequency ω, the wave potentials must also be harmonic, and can be written:

$$\phi = \Phi\, e^{i\omega t} \qquad (3.5.a)$$

$$\psi = \Psi\, e^{i\omega t} \qquad (3.5.b)$$

where Φ and Ψ are complex potential amplitudes. Substitute of Eqs. (3.5) into Eqs. (3.3) yields the time independent equations:

$$\nabla^2\Phi + k_p^2 = 0 \qquad (3.6.a)$$

$$\nabla^2\Psi + k_s^2 = 0 \qquad (3.6.a)$$

where $k_p = \omega/V_p^*$ and $k_s = \omega/V_s^*$ are complex P-wave and S-wave numbers, respectively.

Particular solutions to Eqs. (3.6) corresponding to plane waves propagating in the positive x-direction with the complex wave number $k = k_r + ik_i$ ($k_r > 0$, $k_i < 0$) may be found by separation of variables:

$$\text{Let } \Phi = f(z)\, e^{-ikx} \qquad (3.7.a)$$

$$\Psi = g(z)\, e^{-ikx} \qquad (3.7.b)$$

Substitution of these expressions into Eqs. (3.6) leads to the following ordinary differential equations:

$$\frac{d^2f}{dz^2} + (k_p^2 - k^2)\, f = 0 \qquad (3.8.a)$$

$$\frac{d^2g}{dz^2} + (k_s^2 - k^2)\, g = 0 \qquad (3.8.b)$$

The solutions to Eqs. (3.8) are:

$$f(z) = A_1\, e^{ik_\phi z} + A_2\, e^{-ik_\phi z} \qquad (3.9.a)$$

and

$$g(z) = B_1\, e^{ik_\psi z} + B_2\, e^{-ik_\psi z} \qquad (3.9.b)$$

where k_ϕ and k_ψ are the solutions with positive real parts to the equations.

$$k_\phi^2 = k_p^2 - k^2 \qquad (3.10.a)$$

$$k_\psi^2 = k_s^2 - k^2 \qquad (3.10.b)$$

Introducing the notation

$$k = k_p \sin e = k_s \sin f \qquad (3.11)$$

where e and f are (not necessarily real) angles which, as will be shown in connection with Eq. (3.23), are related to the direction of wave propagation, the wave numbers in Eqs. (3.10) may be written

$$k_\phi = k_p \cos e = k \cot e \qquad (3.12.a)$$

$$k_\psi = k_s \cos f = k \cot f \qquad (3.12.b)$$

Substitution of Eqs. (3.9) and (3.10) into Eqs. (3.7) yields the following solution to the original Helmholtz equations, Eqs. (3.6):

$$\Phi = \left(A_1(\omega)\, e^{ik_\phi z} + A_2(\omega)\, e^{-ik_\phi z}\right) e^{-ikx} \qquad (3.13.a)$$

$$\Psi = \left(B_1(\omega)\, e^{ik_\psi z} + B_2(\omega)\, e^{-ik_\psi z}\right) e^{-ikx} \qquad (3.13.b)$$

A further, complete expression for the displacement amplitudes may be found below, Eq. (3.31). The surface amplitudes follow from Eq. (3.33).

Equations (3.13.a) and (3.13.b) are obviously of the same form. Hence, only solutions corresponding to the first equation will be discussed in full detail. These solutions correspond to P-waves.

P-Waves

The potential function in Eq. (3.13.a) can be written on the form

$$\Phi = \Phi_1 + \Phi_2 \tag{3.14}$$

where

$$\Phi_n = A_n e^{-i(\bar{K}_n \cdot \bar{r})} = A_n e^{-\bar{A}_n \cdot \bar{r}} \cdot e^{-i\bar{P}_n \cdot \bar{r}} \quad ; n = 1,2 \tag{3.15}$$

In this notation r is the location vector, $r = x\hat{x} + z\hat{z}$, where $\hat{x}$ and $\hat{z}$ are unit vectors on the x- and z-axes, respectively, and $\bar{K}_n$ is the vector

$$\bar{K}_n = k\hat{x} + (-1)^n k_\phi z = \bar{P}_n - i\bar{A}_n, \; n = 1,2 \tag{3.16}$$

The real vectors $\bar{P}_n = Re(\bar{K}_n)$ and $\bar{A}_n = -Im(\bar{K}_n)$ are called the propagation vector and the attenuation vector, respectively.

The last form of Eq. (3.15) shows that Φ_n represents a plane wave with the potential amplitude A_n (at the origin) which propagates in the direction $\bar{P}_n$ with the attenuation factor $\exp(-|A_n|)$ per unit length in the direction of the attenuation vector $\bar{A}_n$. Both of these vectors lie in the xz-plane. A wave for which the propagation vector and the attenuation vector do not coincide is called an inhomogeneous wave. For such plane waves the amplitude will vary exponentially along the wavefront, see Borcherdt (1973).

The angle e_n from the z-axis to the propagation vector, $\bar{P}_n$ may be determined by considering the vector product

$$\hat{z} \times \bar{P}_n = \begin{vmatrix} x & y & z \\ 0 & 0 & 1 \\ Re(k) & 0 & (-1)^n Re(k_\phi) \end{vmatrix} = Re(k)\hat{y} \tag{3.17}$$

where $\hat{y}$ is a unit vector on the y-axis. This vector product also satisfies

$$\hat{z} \times \bar{P}_n = |\hat{z}| \cdot |\bar{P}_n| \sin e_n \hat{y} = |P_n| \sin e_n \hat{y} \tag{3.18}$$

thus,

$$\sin e_n = \frac{Re(k)}{\sqrt{Re^2(k) + Re^2(k_\phi)}} > 0 \tag{3.19}$$

Similarly, by considering the "dot" product $\hat{z} \cdot P_n$

$$\cos e_n = \frac{(-1)^n Re(k_\phi)}{\sqrt{Re^2(k) + Re^2(k_\phi)}} \tag{3.20}$$

which, since $Re(k_\phi) > 0$ and $Re(k) > 0$, shows that $n = 1$ corresponds to a wave propagating generally upwards while $n = 2$ corresponds to a wave propagating generally downwards, see Fig. 3.1.

The same procedure applied to the vector product $\bar{P}_n \times \bar{A}_n$ yields the following expression for the angle, α_n, from the propagation vector to the attenuation vector

$$\sin \alpha_n = (-1)^n \frac{Re(k_\phi)Im(k) - Im(k_\phi)Re(k)}{\sqrt{\left[Re^2(k) + Re^2(k_\phi)\right]\left[Im^2(k) + Im^2(k_\phi)\right]}} \tag{3.21}$$

This expression shows that a homogeneous wave ($\alpha_n = 0$) occurs if and only if

$$\frac{Im(k)}{Re(k)} = \frac{Im(k_\phi)}{Re(k_\phi)} \tag{3.22}$$

But this implies, by Eqs. (3.10) that $arg(k) = arg(k_p) = arg(k_\phi)$, and also that the angle e in Eq. (3.11) is real for homogeneous waves. Furthermore, for this case Eqs. (3.19) and (3.20) reduce to

$$\sin e_n = \sin e \tag{3.23.a}$$

$$\cos e_n = (-1)^n \cos e \tag{3.23.b}$$

Thus, e is simply the angle, e_2, which the downgoing wave forms with the z-axis, and the corresponding angle for the upgoing wave is $e_1 = \pi - e$.

SV-Waves

A similar vectorial study of the SV-wave solutions expressed by Eq. (3.13.b) will show that all of the formulas, Eq. (3.14) to Eq. (3.23) are also valid for this case provided k_ϕ, k_p, ϕ_n, A_n and e_n are replaced by k_ψ, k_s, Ψ_n, B_n and f_n, respectively.

SH-Waves

The motions described by Eq. (3.1.c) are called SH-waves. They involve displacements only in the y-direction. The solution for harmonic motions propagating with the wave number k in the positive x-direction is

$$u_y = U_y e^{i\omega t} \tag{3.26.a}$$

where

$$U_y = \left(C_1 e^{ik_\psi z} + C_2 e^{-k_\psi z}\right) e^{ikx} \tag{3.26.b}$$

The wave number k_ψ is as defined by Eq. (3.10.b), and C_1 and C_2 are to be considered arbitrary complex constants. As for the case of the P- and SV-waves discussed above, the terms of this solution may be written in a vector notation similar to Eq. (3.13) and (3.14). However, homogeneous incident SH-waves do not give rise to inhomogeneous reflected waves, and the simple notation of Eq. (3.26) will suffice for wave fields considered in this dissertation. The wave numbers for homogeneous SH-waves satisfy the condition stated by Eq. (3.11), i.e., $k = k_s \sin f$, where f is the angle which the propagation vector forms with the z-axis.

3.3 The Viscoelastic Half Space

The following study of the solution for the case of a homogeneous harmonic body wave obliquely incident on the free surface of a uniform, viscoelastic half space will provide an insight into the nature of the more complicated solutions for multi-layered systems to be discussed in later sections. As shown in Fig. 3.1, an obliquely incident homogeneous SV-wave will in general result in two reflected waves of different types (mode conversion). Furthermore, in certain cases, depending on the incident angle and the material properties, one of the reflected waves may be inhomogeneous, Borcherdt (1971) and Cooper (1967).

Incident SV-Waves

Only the specific case of an incident SV-wave will be discussed in detail. However, the method presented is also applicable to the case of an incident P-wave. Since no incident P-wave exists for the case studied, the form of the solution is given by Eq. (3.13) with $A_1 = 0$. The incident SV wave is represented by the term $B_1 \exp(ikz)$.

The incident angle, $f = -f_s$, shown in Fig. 3.1, is real since the wave is assumed to be homogeneous. The relations in Eqs. (3.23) immediately implies that the reflected SV-wave, represented by the term $B_2 \exp(ik_\psi z)$ is homogeneous and forms the angle $f_2 = f$ with the z-axis. Inversion of Eq. (3.11) and multiplication by ω yields the complex form of Snell's Law

$$V_a^* = V_p^*/\sin e = V_s^*/\sin f \tag{3.27}$$

where $V_a^* = \omega/k$ is the apparent complex phase velocity along the free surface. Hence,

$$\sin e = \frac{V_p^*}{V_s^*} \sin f \tag{3.28}$$

which shows that the reflected P-wave, corresponding to the last term in Eq. (3.13a), will always be inhomogeneous if $\beta_s \neq \beta_p$; and that even if $\beta_s = \beta_p$ a homogeneous reflected P-wave will only occur when f is smaller than a certain critical angle, f_{cr}, defined by

$$\sin f_{cr} = V_s^*/V_p^* \tag{3.29}$$

since sin e > 1, for $f > f_{cr}$.

The amplitudes A_2 and B_2 of the reflected P- and S-waves, respectively, can be computed from the condition that no stresses occur at the free boundary. Introducing the notation

$$a = \cot e;\ b = \cot f \tag{3.30}$$

where b is real while a could be complex, and remembering Eqs. (3.12), the displacement amplitudes are by Eqs. (3.2), (3.5), (3.7), and (3.9)

$$\begin{Bmatrix} U_x \\ U_z \end{Bmatrix} = i\,k\,e^{-ikx}[Z]\begin{Bmatrix} A_1 \\ B_1 \\ A_2 \\ B_2 \end{Bmatrix} \tag{3.31}$$

where

$$[Z] = \begin{bmatrix} -e^{iakz} & -b\,e^{ibkz} & -e^{-iakz} & b\,e^{-ibkz} \\ a\,e^{iakz} & -e^{ibkz} & -a\,e^{-iakz} & -e^{-ibkz} \end{bmatrix} \tag{3.32}$$

Thus at the surface (x = z = 0)

$$\begin{Bmatrix} U_x \\ U_z \end{Bmatrix}_0 = ik\begin{bmatrix} -1 & -b & -1 & b \\ a & -1 & -a & -1 \end{bmatrix}\begin{Bmatrix} A_1 \\ B_1 \\ A_2 \\ B_2 \end{Bmatrix} \tag{3.33}$$

The strain field can be obtained by differentiation of Eq. (3.31) and the stresses then follows on the basis of Hooke's Law. This leads to the following expression for the normal stress, σ, and shear stress, τ, at z = 0.

$$\begin{Bmatrix}\tau\\ \sigma\end{Bmatrix}_0 = G^* k^2 \begin{bmatrix} 2a & -(1-b^2) & -2a & -(1-b^2) \\ (1-b^2) & 2b & (1-b^2) & -2b \end{bmatrix} \begin{Bmatrix} A_1 \\ B_1 \\ A_2 \\ B_2 \end{Bmatrix} \tag{3.34}$$

Since these stresses must vanish, $A_1 = 0$, and B_1 is known, this immediately leads to a system of linear equations from which A_2 and B_2 may be determined.

$$\begin{bmatrix} -2a & -(1-b^2) \\ (1-b^2) & -2a \end{bmatrix} \begin{Bmatrix} A_2 \\ B_2 \end{Bmatrix} = \begin{Bmatrix} 1-b^2 \\ -2b \end{Bmatrix} B_1 \tag{3.35}$$

The solution is:

$$A_2 = \frac{-4b(1-b)^2}{4ab + (1-b^2)^2} B_1 \tag{3.36}$$

$$B_2 = \frac{4ab - (1-b^2)^2}{4ab + (1-b^2)^2} B_1 \tag{3.37}$$

This solution has the properties:

$A_2 \to 0$ and $B_2 \to -1$; for $f \to 0$

and

$A_2 \to 0$ and $B_2 \to 1$; for $f \to 45^\circ$

Thus, no reflected P-waves occur at these angles of incidence. Furthermore, by Eq. (3.33), no vertical displacement occurs at the surface for $f = 0$; and no horizontal displacement occurs for $f = 45^\circ$. Surface displacement amplitudes for other angles of incidence can be computed from Eq. (3.33).

Solutions for the elastic case have been published by Knopoff et al. (1957) and Meissner (1965) for both incidence SV- and P-waves. Figs. 3.3 and 3.4 shows ratios between surface amplitudes and the horizontal component of amplitude of a vertical incident SV-waves. The corresponding particle motions are shown in Fig. 3.2. These figures, which are actually valid for a damped half space as long as $\beta_s = \beta_p$, indicate several interesting features:

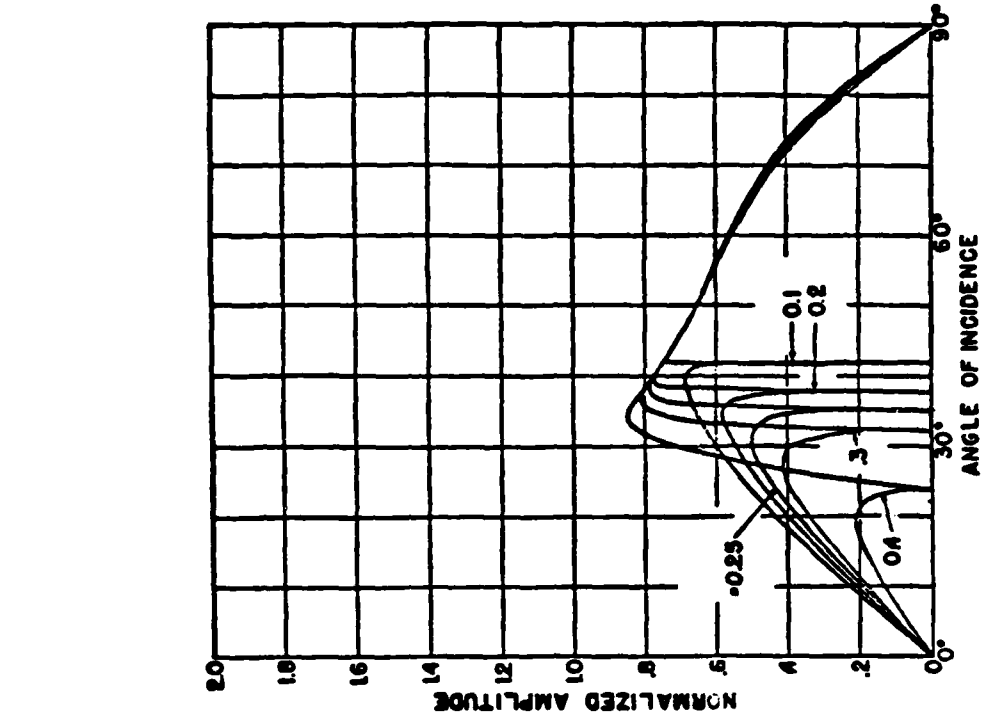

Fig. 3.4 Vertical Component of Surface Motion for Incident SV waves - Elastic Halfspace System (after Knopoff et al., 1957)

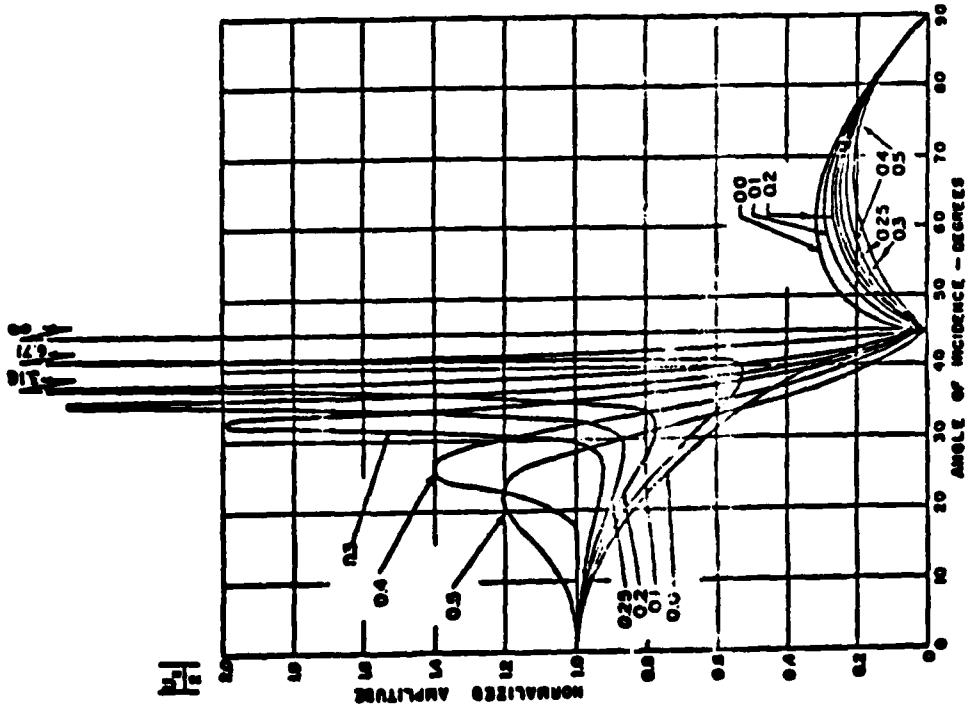

Fig. 3.3 Horizontal Component of Surface Motion for Incident SV waves - Elastic Halfspace System (after Knopoff et al., 1957)

1. For angles of incidence less than the critical angle, see Eq. (3.29), a is real and the horizontal and vertical components are in phase. The particle motion is linear and the horizontal component of motion is larger than the vertical component for usual values of Poisson's ratio.
2. For incident angles larger than the critical angle, a is complex.

The reflected P-wave is inhomogeneous and the reflected (homogeneous) SV-wave is out of phase with the incident wave. The horizontal and vertical motions are 90^{o} out of phase. Thus, the particle motion is elliptical (retrograde for $f < 45^{o}$ and prograde for $f > 45^{o}$). The vertical component is generally larger than the horizontal component.

The comparison between the induced vertical and horizontal amplitudes of surface motion for an incident SV-wave at different angles of incidence is shown in Fig. 3.7. The dotted lines show the cases for all incident angles exceeding the critical angle. A singularity is found at 45 degrees because the horizontal displacement is 0 for all values of Poisson's ratio.

Incident P-Wave

The case of an incident P-wave can be treated by the technique used above. Snell's law, Eq. (3.27) is also valid for this case, but since V_p^* is always larger than V_s^* no critical angle of incidence exists. Surface amplitudes can also be computed from Eq. (3.33) by setting $B_1 = 0$ and assuming that A_1 is given. Figures 3.5 and 3.6 show the normalized vertical and horizontal amplitudes of P-wave at different angles of incidence for a range of Poisson's ratio. Both displacement amplitudes are normalized by the amplitude of the

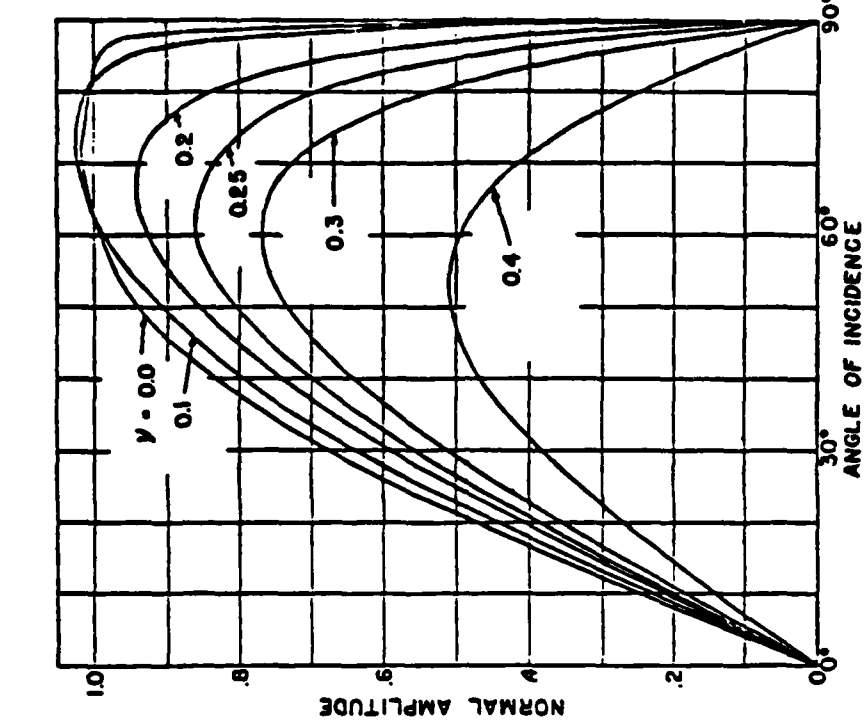

Fig. 3.6 Horizontal Component of Motion for Incident P waves (after Knopoff et al., 1957)

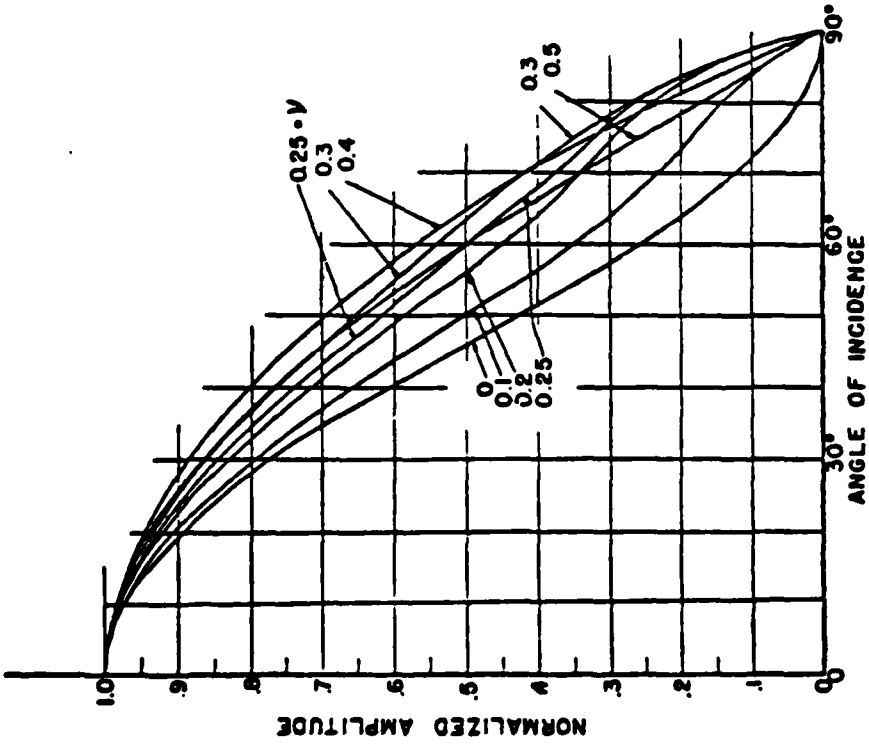

Fig. 3.5 Vertical Component of Motion for Incident P waves (after Knopoff et al., 1957)

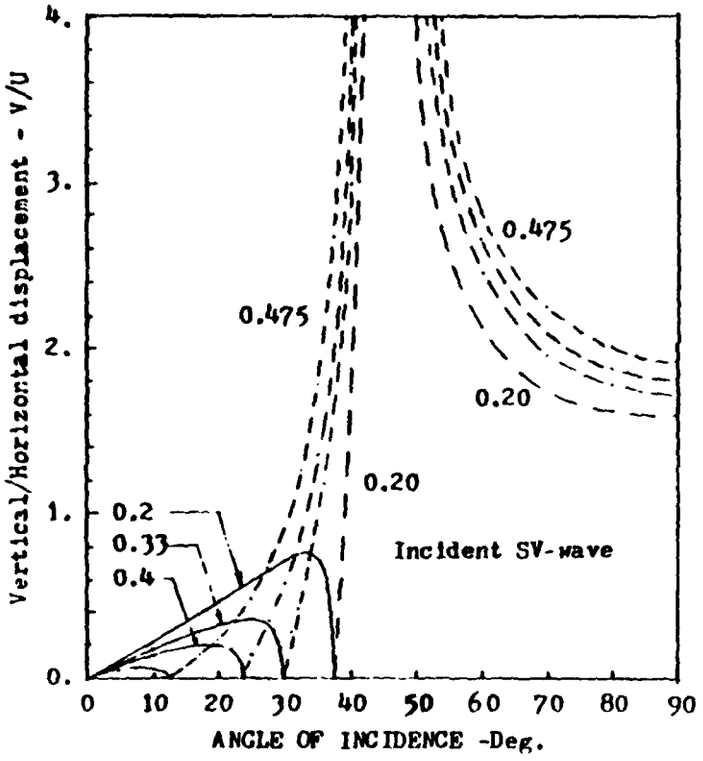

Fig. 3.7 Displacement Ratio of Surface Motion for Incident SV-wave

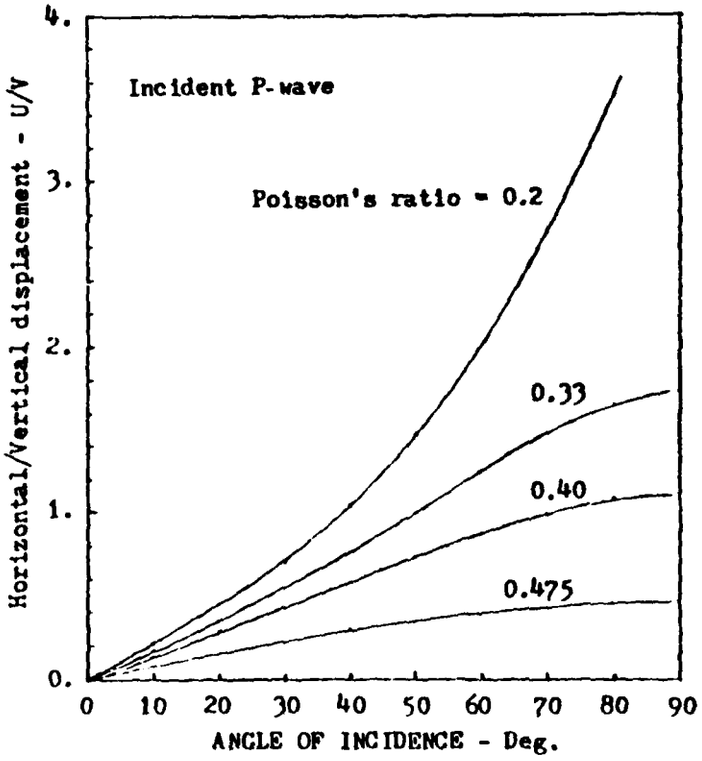

Fig. 3.8 Displacement Ratio of Surface Motion for Incident P-wave

vertically incident P-wave. The features of the motion are summarized as follows:

1. For a medium with Poisson's ratio greater than 0.2, no significant difference is seen in the different amplitude curves and an approximation through a function U_z/V_o = cos e is sufficient for most practical purposes, Meissner (1965). V_o denotes the vertical amplitude of vertically incident P-waves.
2. The induced horizontal components start from 0 at vertical incidence, and increase practically linearly to 35 degrees incidence. The maximum horizontal amplitude is about 52 percent of V_o at 52 degrees incidence for a medium with a Poisson's ratio of 0.4; and is about 93 percent of V_o at 65 degrees incidence for a medium with Poisson's ratio of 0.2.

The ratio of the horizontal to the vertical amplitude of surface motion due to incident P-wave is shown in Fig. 3.8. The angle of incidence has a strong effect on the displacement ratio for materials with a low Poisson's ratio, while for materials with a high Poisson's ratio the effect is relatively small.

3.4 Single Layer over Half Space

In order to verify the algorithm of the computer programs SITE and LOVE which will be described in Section 3.7, the boundary value problem for a viscoelastic uniform layer overlying a viscoelastic half space is solved analytically. The amplification of oblique SV- or P-waves incident to the base with various incident angles were examined. The effects of S-wave velocity ratios between the layer and the half space on response were also studied.

3.4.1. Solutions to Boundary Value Problem

The structural model shown in Fig. 3.9 consists of two uniform isotropic viscoelastic media. A layer with the thickness H, and the properties ρ', $G^{*'}$, $M^{*'}$, $V_s^{*'}$, $V_p^{*'}$, β_s', and β_p' overlies a half space with the properties ρ, G^*, M^*, V_s^*, V_p^*, β_s, and β_p.

Let Φ, Ψ, and Φ', Ψ' be the displacement potentials of the P-and SV-waves in the bottom half space and stratified layer. The general expressions of Φ, Ψ, Φ' and Ψ' are denoted by

$$\Phi = (A_1 e^{iakz} + A_2 e^{-iakz}) e^{-ikx} \tag{3.38.a}$$

$$\Psi = (B_1 e^{ibkz} + B_2 e^{-ibkz}) e^{-ikx} \tag{3.38.b}$$

where

$$a = \left\{(V_a^*/V_p^*)^2 - 1\right\}^{1/2} , \quad b = \left\{(V_a^*/V_s^*)^2 - 1\right\}^{1/2} \tag{3.39}$$

and

$$\Phi' = (C e^{irkz} + D e^{-irkz}) e^{-ikx} \tag{3.40.a}$$

$$\Psi' = (E e^{iskz} + F e^{-iskz}) e^{-ikx} \tag{3.40.b}$$

where

$$r = \left\{(V_a^*/V_p^{*'})^2 - 1\right\}^{1/2} , \quad s = \left\{(V_a^*/V_s^{*'})^2 - 1\right\}^{1/2} \tag{3.40.c}$$

in which A_1, A_2, B_1, B_2, C, D, E, F are arbitrary constants to be determined by the boundary condition. On the basis of assumptions similar to those made in the previous section:

1. Only one incoming wave is incident to the base boundary
2. The incident angle is real
3. $V_a^* = V_s^*/\sin f$

it can be concluded that if only an SV-wave is incident to the base boundary, the coefficient "b" will be the only real quantity and a, r,

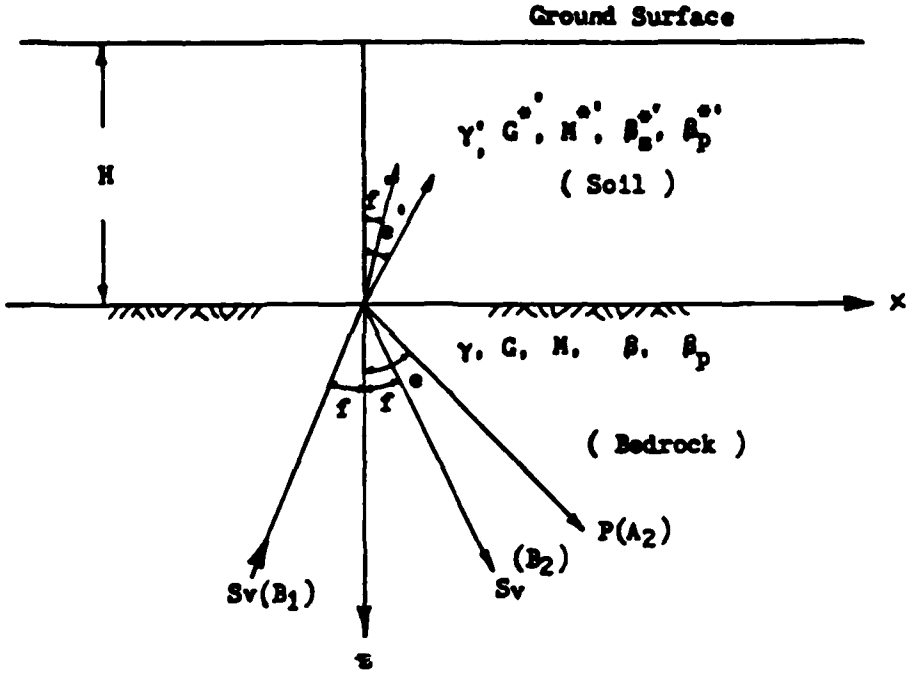

Fig. 3.9 Structural Model - Inclined Body Wave

and s will be complex. If a P-wave is incident, then b, r, and s will be complex in general and the coefficient "a" will be real.

The displacement components can be determined from Eq. (3.2) and stresses can also be obtained from Hooke's Law by the substitution of appropriate quantities for the half space and the surfacial layer. The boundary conditions are:

$$\text{at } z = 0: \quad U_x = U_x', \quad U_z = U_z'$$
$$\tau_{xz} = \tau_{xz}', \quad \sigma_{zz} = \sigma_{zz}'$$
$$\text{at } z = -H: \quad \tau_{xz}' = 0, \quad \sigma_{zz}' = 0$$

Incident SV-Wave From the Base

By setting $A_1 = 0$ and normalizing all coefficients by B_1, a set of linear equations may be formed in terms of the system geometry, system properties, and normalized coefficients. The linear equation is:

$$[\bar{P}]\{Q_s\} = R_s \tag{3.41}$$

where

$$\{Q_s\} = \langle A_2', B_2', C', D', E', F' \rangle^T$$

$$\{R_s\} = \langle -b, 1, -(b^2-1)G^*, -2bG^*, 0, 0 \rangle^T$$

and $[\bar{P}] =$

$$\begin{bmatrix} 1 & -b & -1 & -1 & -s & s \\ -a & -1 & -r & r & 1 & 1 \\ -2aG^* & (b^2-1)G^* & -2rG^{*'} & 2rG^{*'} & -(s^2-1)G^{*'} & -(s^2-1)G^{*'} \\ -(b^2-1)G^* & -2bG^* & (s^2-1)G^{*'} & (s^2-1)G^{*'} & -2sG^{*'} & 2sG^{*'} \\ 0 & 0 & 2re^{-ikhr} & -2re^{ihkr} & (s^2-1)e^{-iksh} & (s^2-1)^{iksh} \\ 0 & 0 & -(s^2-1)e^{-ikhr} & -(s^2-1)e^{ikhr} & 2se^{-iksh} & -2se^{iksh} \end{bmatrix} \tag{3.42}$$

From this equation the normalized coefficients A_2', B_2', C', D', E', F' can be found in terms of given parameters in $[\bar{P}]$ and $\{R_s\}$.

Incident P-Wave From the Base

Again, a real value of an angle of incidence may be specified, then, by setting $B_1 = 0$, and normalizing all coefficients by A_1:

$$[\bar{P}]\{Q_p\} = \{R_p\} \tag{3.43}$$

in which

$$\{Q_p\} = \langle A_2', B', C', D', E', F' \rangle^T$$

and

$$\{R_p\} = \langle -1, -a, -2aG^*, (b^2-1)G^*, 0, 0 \rangle^T$$

Displacements and Stresses

For any wave field expansion of Eq. (3.2) gives the normalized displacements for the surface layer:

$$u' = U' e^{i(\omega t - kx)}$$

$$w' = W' e^{i(\omega t - kx)} \tag{3.44}$$

where

$$\begin{aligned} U' &= -ik\left\{(C' e^{ikrz} + D' e^{-ikrz}) + s(E' e^{iksz} - F' e^{-iksz})\right\} \\ W' &= ik\left\{r(C' e^{ikrz} - D' e^{-ikrz}) - (E' e^{iksz} + F' e^{iksz})\right\} \end{aligned} \tag{3.45}$$

and the stress components

$$\tau_{xz}' = \underline{\tau}\, e^{i(\omega t - kx)}$$

$$\sigma_{xz}' = \underline{\sigma}\, e^{i(\omega t - kx)} \tag{3.46}$$

where

$$\begin{aligned} \underline{\tau} &= G^{*'} k^2\{2r(C' e^{irkz} - D' e^{-irkz}) + (s^2-1)(E' e^{iskz} + F' e^{-iskz})\} \\ \underline{\sigma} &= G^{*'} k^2\{-(s^2-1)(C' e^{irkz} + K' e^{-irkz}) - 2s(E' e^{iskz} - F' e^{-iskz})\} \end{aligned} \tag{3.47}$$

The displacements and stresses at the base boundary due to a specified incident wave take the same forms as shown in Eqs. (3.33) and (3.34)

3.4.2 Numerical Examples

A model consisting of a simple uniform layer overlying a half space was used to investigate the characteristics of displacements at the free surface and the base boundary for the case of SV- or P-waves incident at different angles. The study also included a study of the effects of the incident angle on amplification of both steady state and transient motions. The influence of the variation of shear wave velocity, Poisson's ratio, and damping ratio between surface layer and half space were also studied.

The basic system is shown in Fig. 3.10. The parameters had the values

	Surface Layer	Half Space
Thickness (ft)	128	infinite
Unit weight (pcf)	125	162.5
Shear wave velocity (fps)	1000	1200 - 8000
Poisson's ratio	0.1 - 0.45	0.1 - 0.45
Damping ratio	0.05 - 0.12	0.02 - 0.05

The fundamental fixed base undamped frequencies of the layer were 1.95 Hz and 3.38 Hz for S- and P-waves, respectively. Computations were performed at a frequency of 1 Hz. Thus, the shear wave length in the surface layer was 1,000 ft. The ratio of wave length to the thickness of the layer was about 7.8 and the ratio of densities between half space and the surface layer was 1.3.

Displacements at Layer Surface and Layer Base

The horizontal displacements and vertical displacements at the free surface due to a harmonic inclined SV-wave was computed for an elastic system with Poisson's ratio 0.25. The results are shown in Fig. 3.10. In order to see the influence of the incident angle, both components are normalized by the displacement at ground surface due to a vertically propagating shear wave. The results are very similar to those shown in Section 3.3 for a viscoelastic half space. The horizontal component has a sharp peak at the critical angle whereas the vertical component at this point forms a downward sharp cusp. For most realistic choices of system parameters, the horizontal amplitudes of inclined SV-waves are smaller than those of vertically propagating shear waves except at a very narrow range of angles of incidence around the critical angle. The vertical amplitudes of SV-waves are zero at normal incidence and linearly increase to 40 percent of the amplitudes of vertically propagating shear waves at 30 degrees of incidence. The effects of the shear wave velocity of the half space on the displacements are insignificant, as can be seen from Fig. 3.10 which contains results for four different values of the velocity ratio.

Figure 3.11 shows similar results for the case of incident P-waves. Both components are normalized to the ground surface amplitude of a

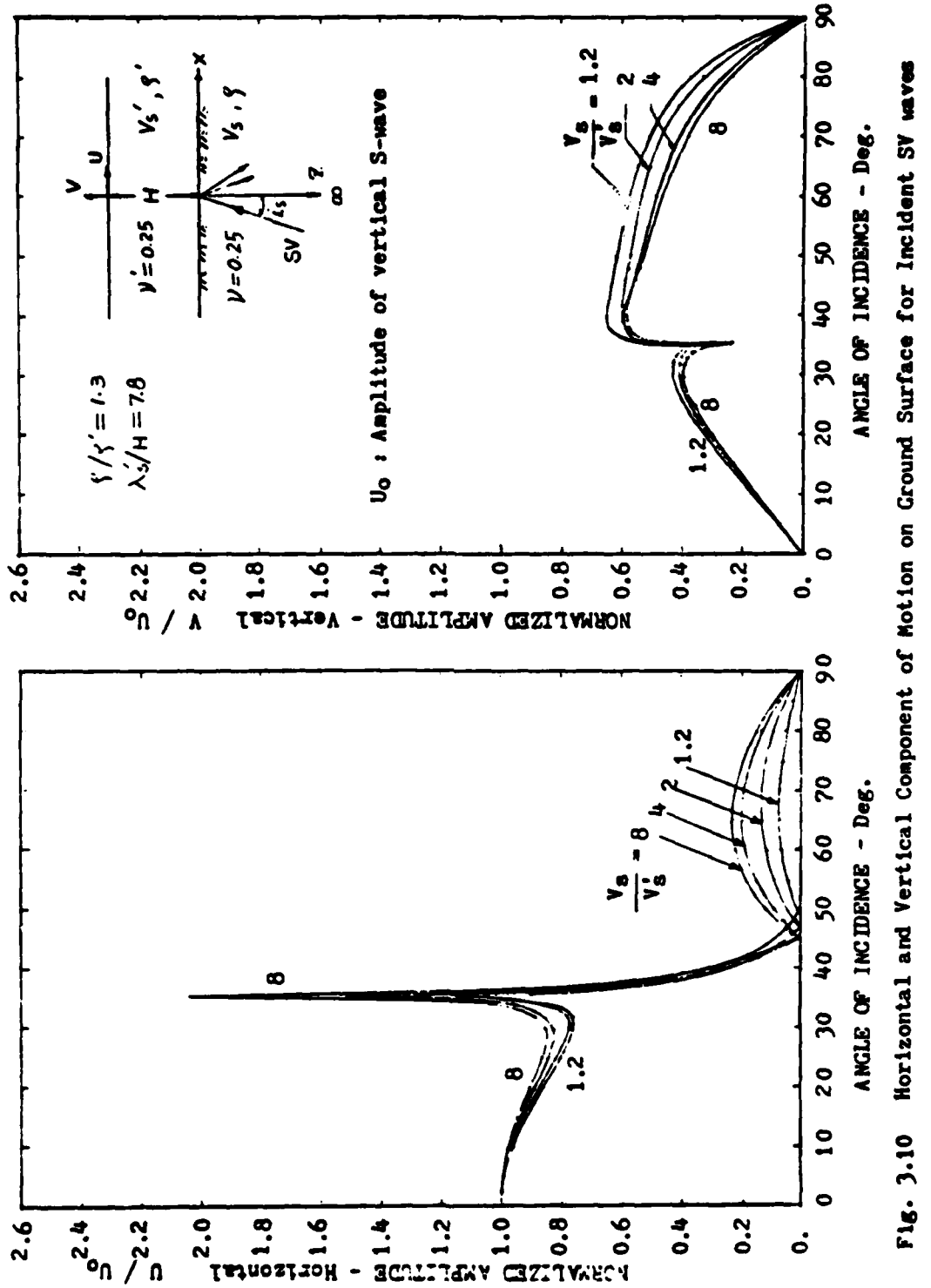

Fig. 3.10 Horizontal and Vertical Component of Motion on Ground Surface for Incident SV waves

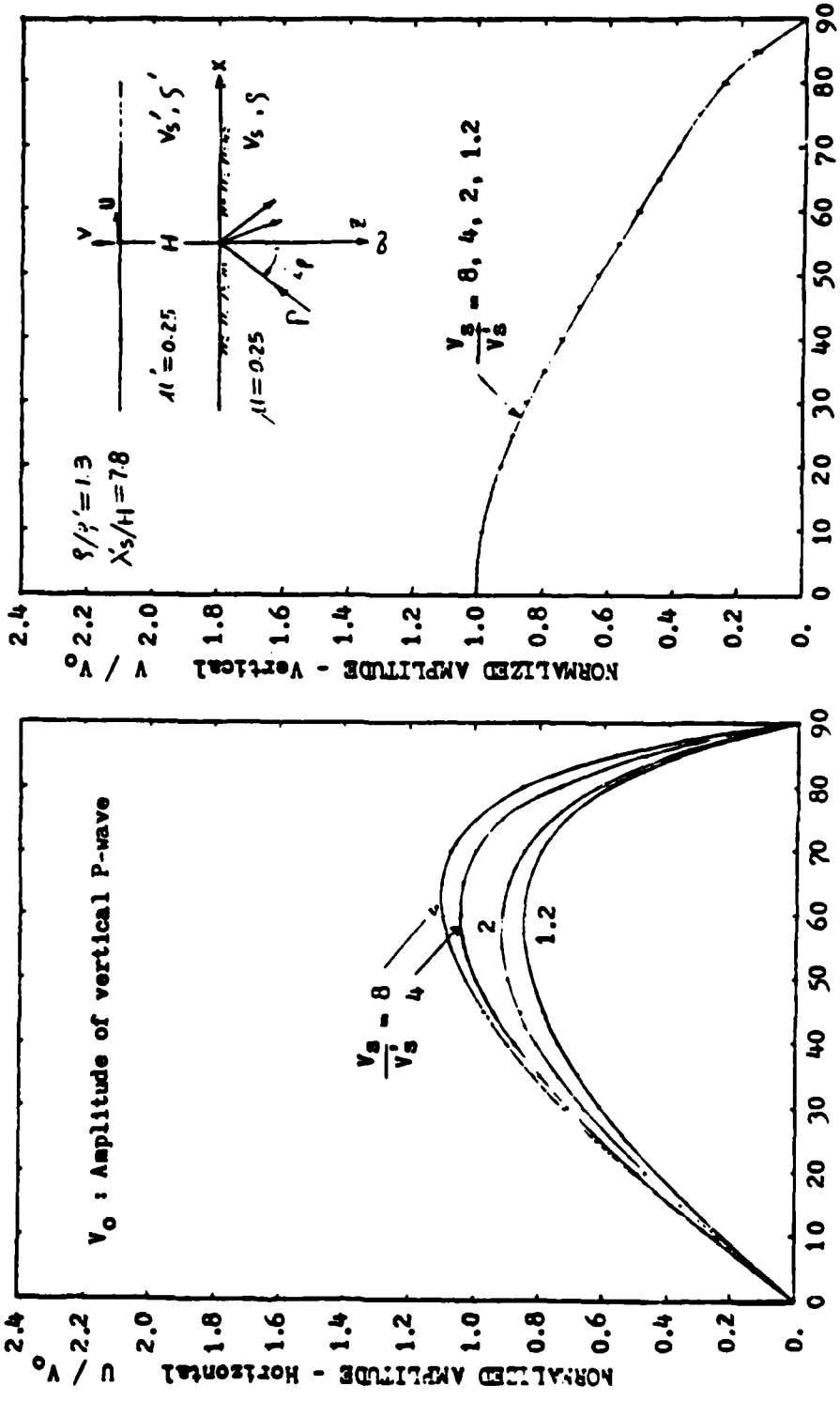

Fig. 3.11 Horizontal and Vertical Component of Motion on Ground Surface for Incident P waves

vertically incident P-wave. All the vertical components of the inclined P-wave are smaller than those corresponding to vertical incidence. No difference can be seen in the amplitude curves for the four values of shear wave velocity ratios. This effect is probably due to the relatively long wave length as compared to the thickness of the surfacial layer. The horizontal components of the inclined P-wave are more sensitive to the shear wave velocity of the half space. The greater the stiffness of the elastic half space, the larger the horizonal displacements due to inclined P-waves. The greatest differences in horizontal amplitudes occur for angles of incidence between 50 and 70 degrees.

Figure 3.12 illustrates similar studies of normalized displacements at the top of the half space for the case of a shear wave velocity ratio equal to 4. Both results indicate that if the angle of incidence is less than 30 degrees, which should be the practical case; the vertically propagating body waves produce larger motions than the inclined body waves.

Amplification at Ground Surface

A study was made of the variation of amplification of a harmonic SV-wave arriving at a wide range of incident angles. The frequency for this harmonic SV-wave was arbitrarily chosen as 1 Hz. Site amplification at ground surface versus angles of incidence have been plotted for four different values of the S-wave velocity ratio as shown in Fig. 3.13. For angles of incidence less than the critical angle, the horizontal components at the ground surface are about 1.4 times the horizontal amplitudes of SV-wave at the base for the cases of an S-wave velocity ratio greater than 2. The vertical components at the normal

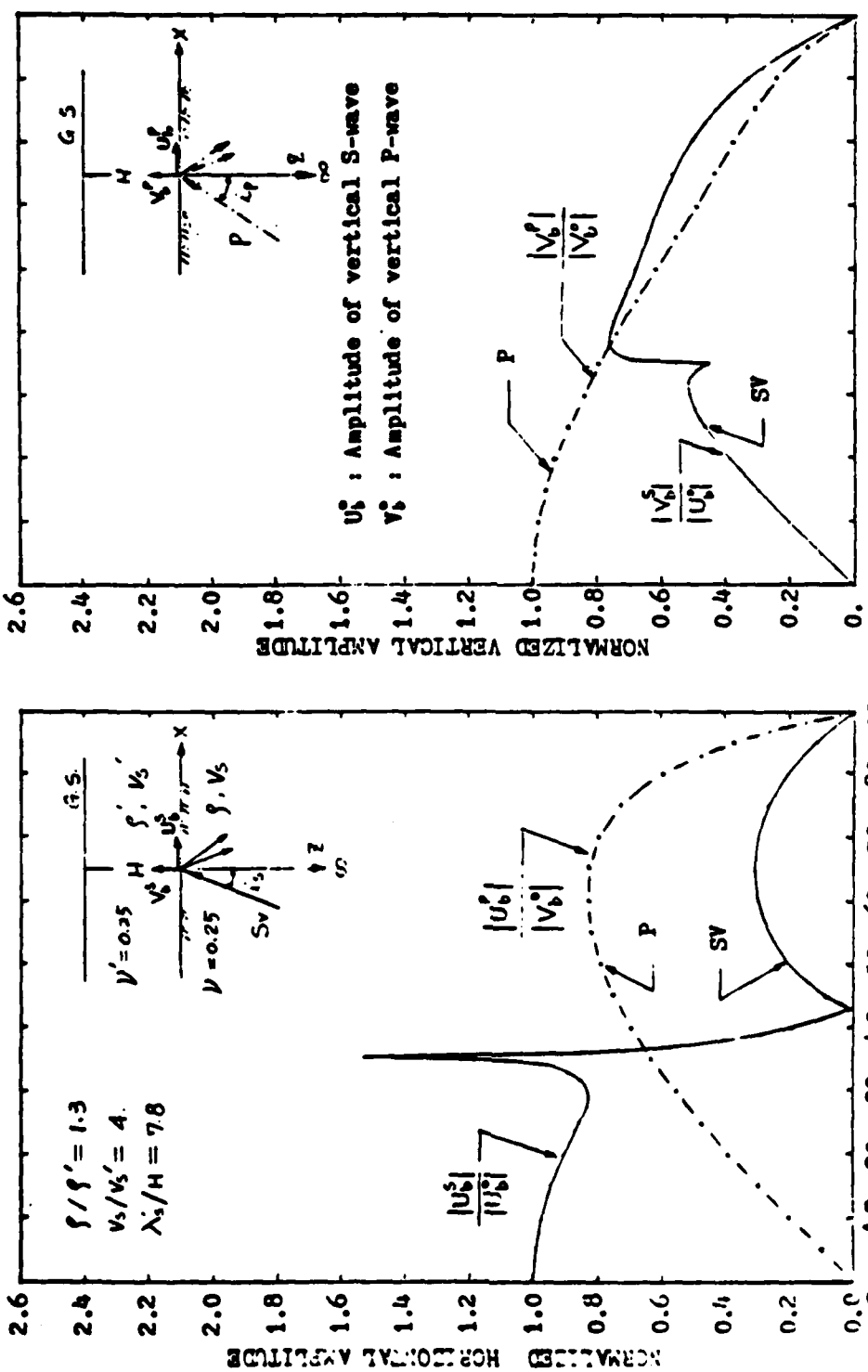

Fig. 3.12 Horizontal and Vertical Component of Motion at Top of Bedrock for Incident Body waves

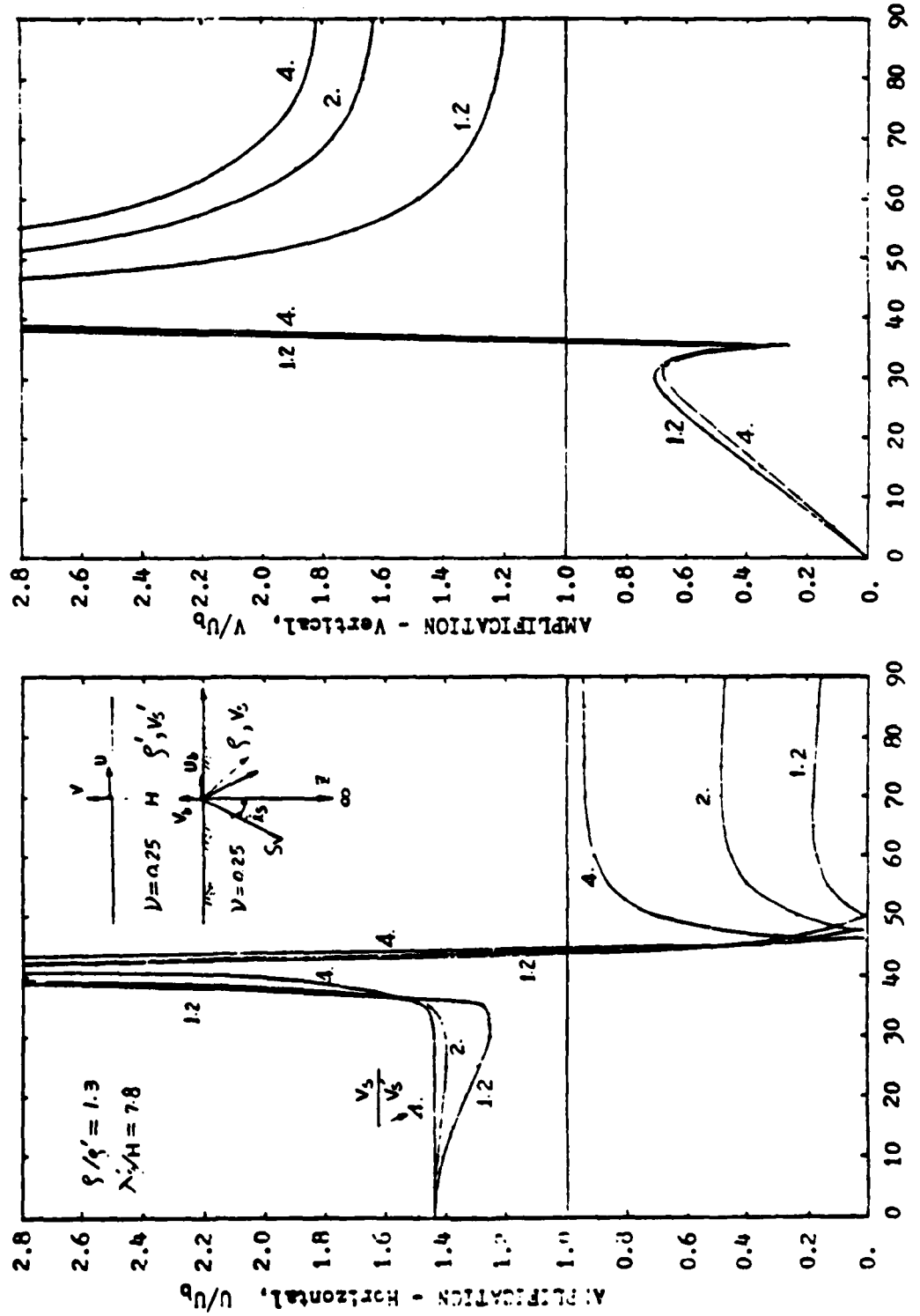

Fig. 3.13 Amplification at Ground Surface for Incident SV waves

incidence are zero and increase linearly to about 70 percent of the horizontal amplitude of the vertical shear wave at 30 degrees of incidence. At the critical angle, vertical components show a very sharp trough because an unusual amplitude spike appears at this angle as seen in Fig. 3.12. The amplification at some particular angle of incidence, say 43 degrees in this case, can not be defined since the horizontal amplitude at the base approaches zero. Fortunately, this case will not appear in practice because the angles of incidence are normally less than the critical angle, and also this phenomenon does not occur in damped systems. The amplifications for inclined P-waves incident to the base are shown in Fig. 3.14. Both components are normalized by the vertical amplitudes of the base at the corresponding angles of incidence. For this case the shear wave velocity ratio is not a significant factor if the angle of incidence is less than the critical angle.

The variation of amplification with frequency for an undamped system is shown in Fig. 3.15 and for angles of incidence of 0, 10, 20, and 30 degrees. The case of normal incidence, shown as a solid curve, is the well known case of a vertically propagating shear wave. Only horizontal amplitudes occur in this case. The peak amplifications occur at 1.95 Hz, 5.86 Hz, 9.77 Hz, 13.67 Hz etc., which are the natural frequencies of the system. For inclined waves, coupling effects occur, and vertical components are induced. Three other cases were shown in the same plot. Some effects of coupled P wave motion may be seen at frequencies near 3.4 Hz and 10.2 Hz, which are the first and second natural frequency of P-waves of the site.

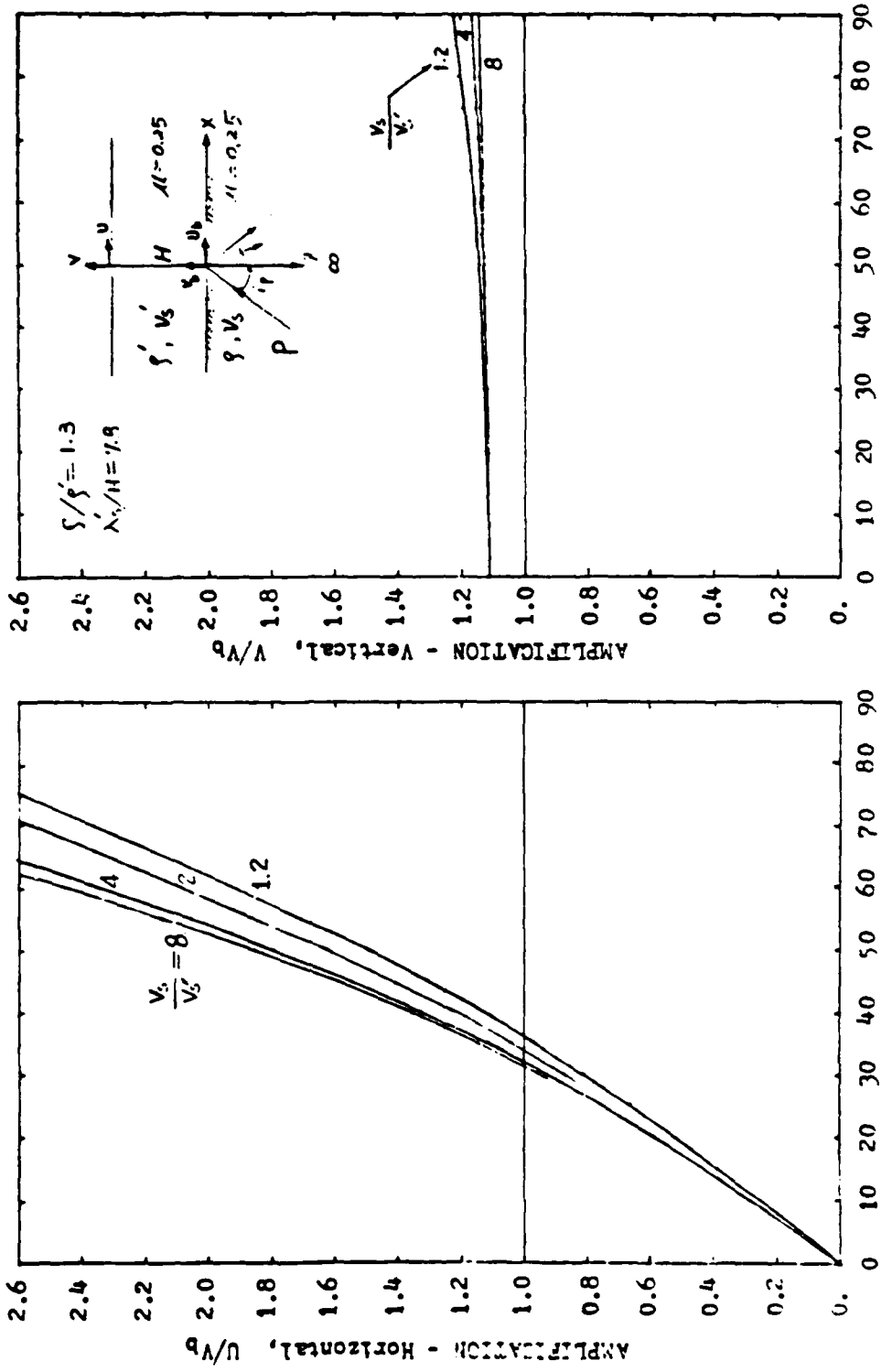

Fig. 3.14 Amplification at Ground Surface for Incident P waves

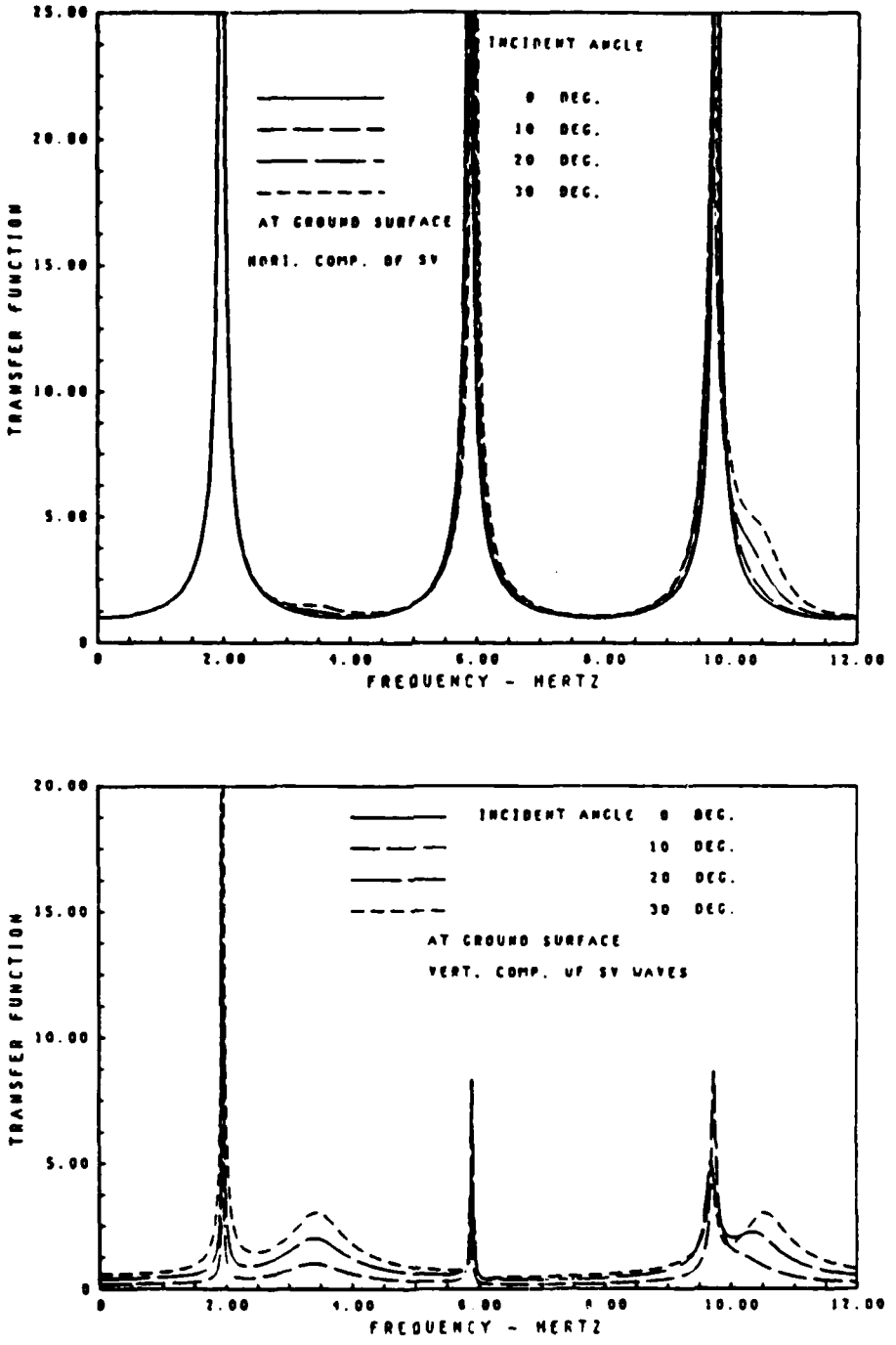

Fig. 3.15 Effect of Incident Angle on Site Amplification at Ground Surface - Closed Form Solution

Computations were performed for the same system assuming a 2 percent damping in the half space, and 5 percent damping in the layer. The results are shown in Fig. 3.16. The resonant peaks for all modes are damped out significantly compared to the undamped cases. However, while the effect of incident angles on the response is not important on the horizontal component, it is quite significant on vertical component of SV-waves as was found in the undamped case.

Effect of Damping Contrast

As shown above the effect of uniform damping is to reduce the surface response significantly. In order to study the effect of a contrast in damping ratio between the surface layer and the underlying half-space surface amplification factors were computed for the special case of an SV-wave with an incident angle of 10 degrees for the following three choices of damping ratios.

	Surface Layer		Half Space	
System	β_s (%)	β_p (%)	β_s (%)	β_p (%)
1	5	5	2	2
2	12	12	5	5
3	12	6	5	2

The result of these computations are shown in Fig. 3.17. As expected the horizontal amplification functions were found to be similar to those computed for vertically propagating shear waves, compare Fig. 3.16. However, some effects were observed in the

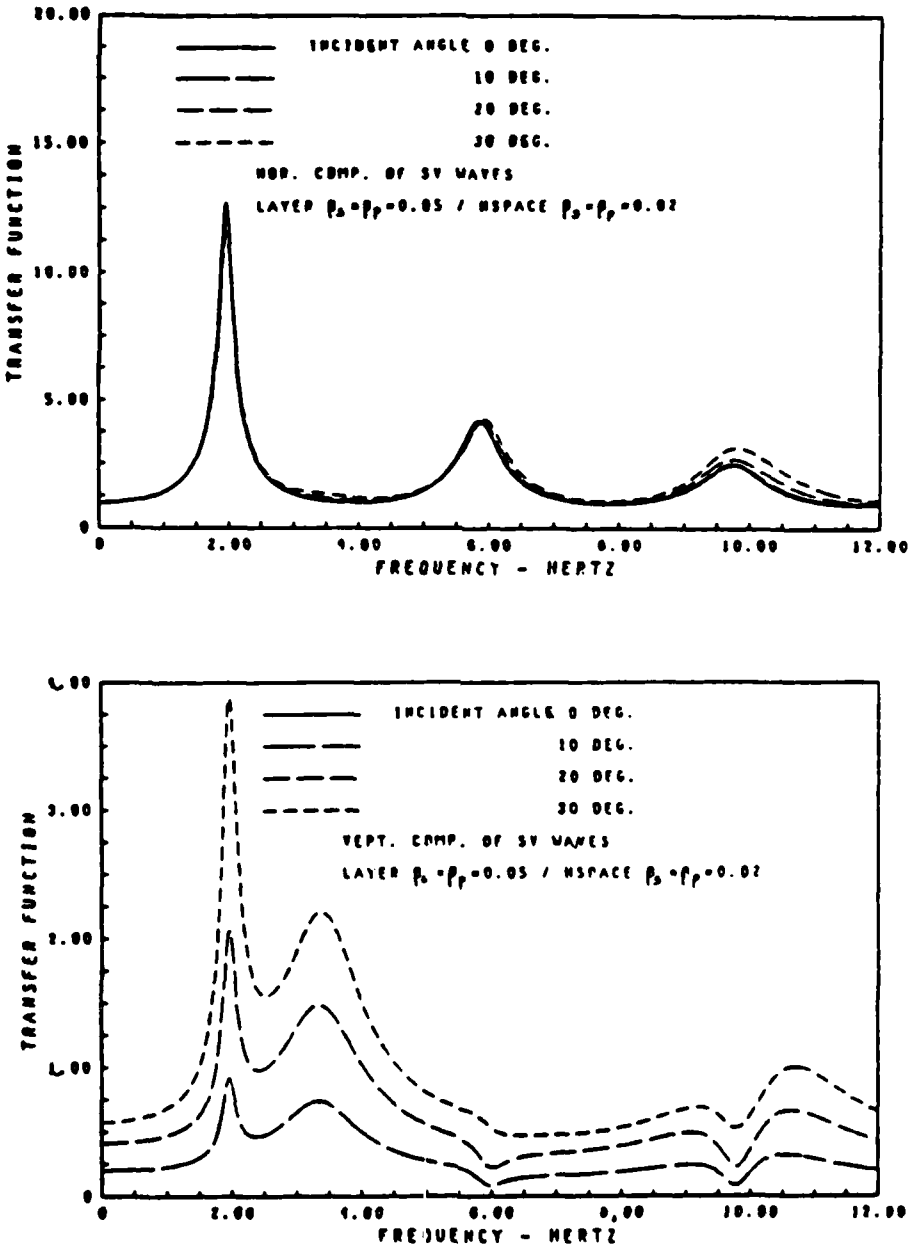

Fig. 3.16 Effect of Incident Angle on Site Amplification Ground Surface

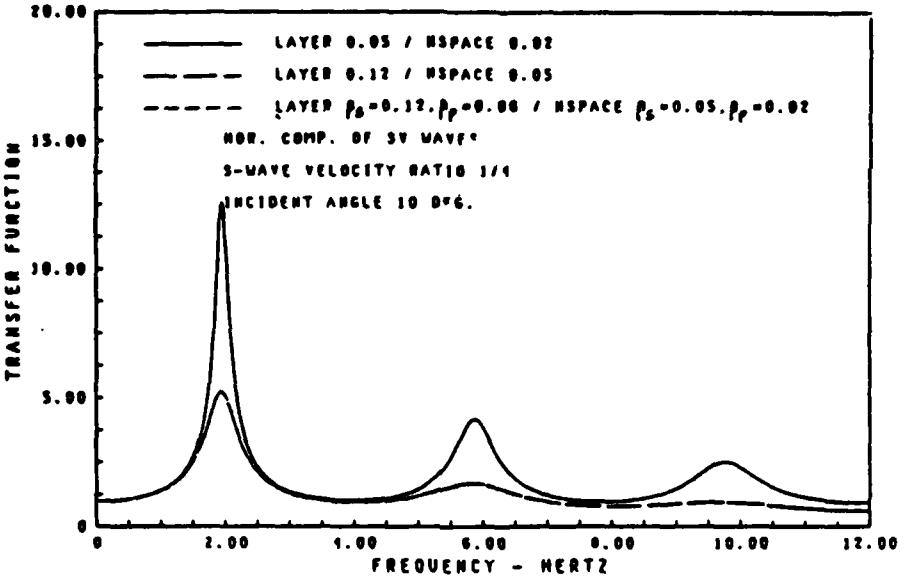

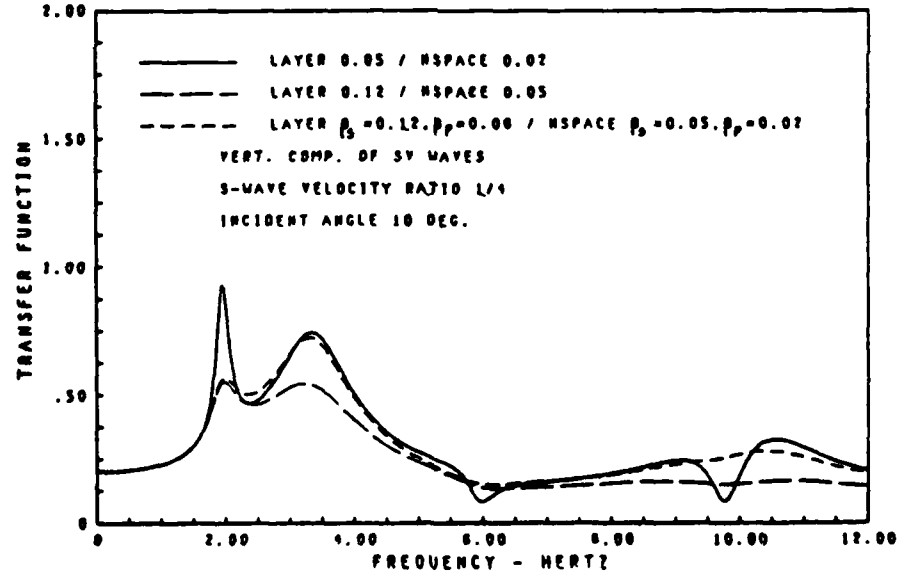

Fig. 3.17 Effect of Damping Ratio on Site Amplification at Ground Surface

amplifications of vertical motions. In particular, it is interesting to observe that Systems 3 (which β_s = 12%, β_p = 6% in the layer) produced nearly as big vertical motions as System 1 (with $\beta_s = \beta_p$ = 5% in the layer). Thus, it appears that horizontal amplification is governed by β_s while vertical amplification is governed by β_p. This observation is perhaps not too surprising if one observed that for System 3 the peaks occur at the natural frequencies for vertically propagating P-waves in the site.

Effect of Poisson's Ratio

Studies were also performed on the above undamped two-layer systems to determine the influence of Poisson's ratio. Again, a SV wave with an incident angle of 10 degrees was assumed.

Figure 3.18 shows the effect of varying Poisson's ratio in the half-space (it was set to 0.25 in the layer) and Fig. 3.19 shows the effect of varying Poisson's ratio on the surface layer (it was set to 0.25 in the half-space). As expected variations in Poisson's ratio has only small effects on the horizontal response while it significantly influenced the vertical response. This of course is due to the strong effect of Poisson's ratio on the P-wave velocity.

3.5 Multi-layered Half-space for SV and P Waves

The propagation of body waves in multi-layered systems is of fundamental interest in seismology and has been studied by Thomson (1950), Matsumoto (1953), Haskell (1960, 1962), Phinney (1964), Hannon (1964), Teng (1967), and Bakun (1970). Their methods of analysis were essentially based on the Thomson-Haskell's matrix formulation. The formulation uses the idea of displacement potential theory and only considers harmonic wave propagation in an undamped elastic media.

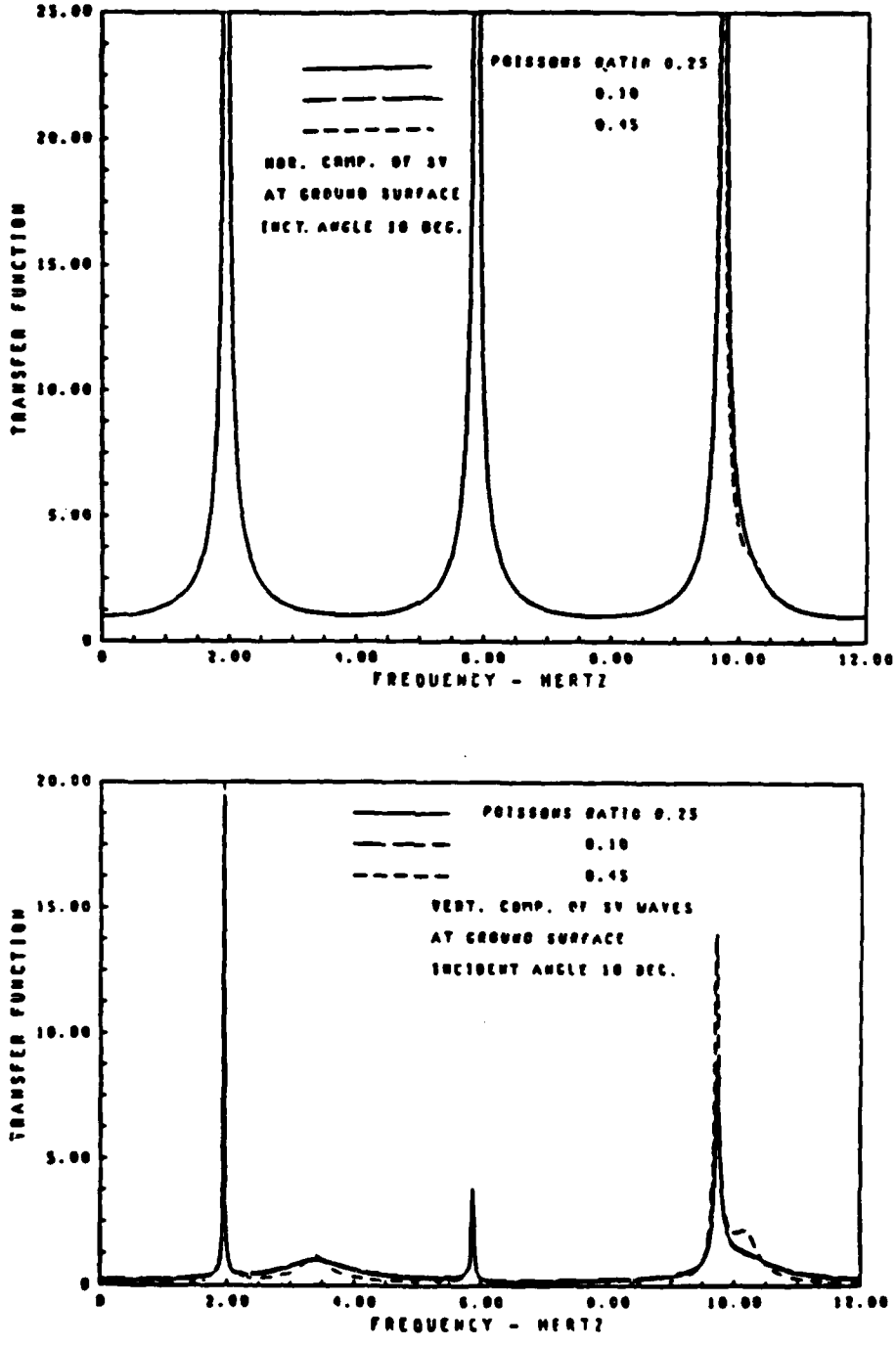

Fig. 3.18 Effect of Halfspace Poisson's Ratio on Amplification - From Closed Form Solution

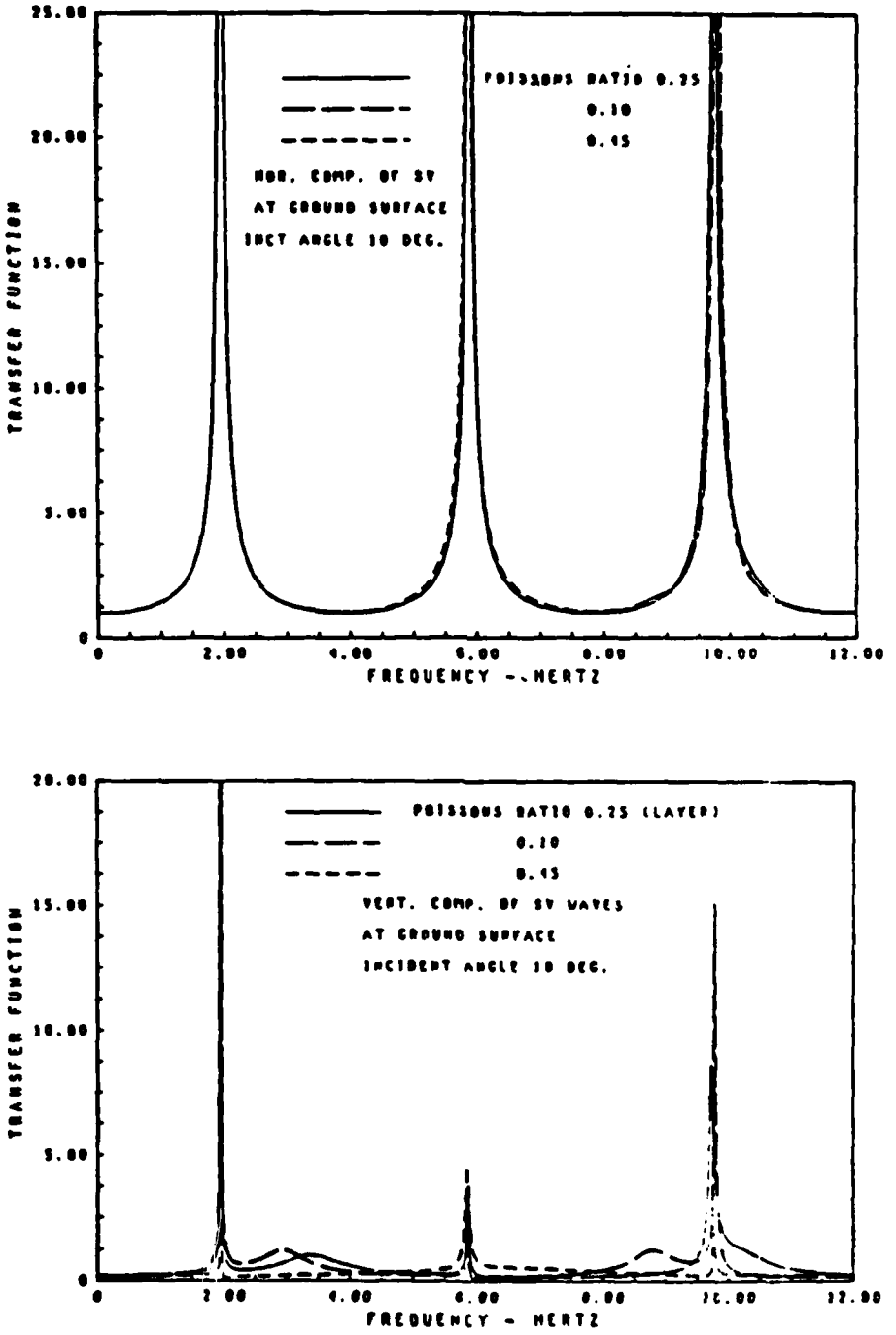

Fig. 3.19 Effect of Layer Poisson's Ratio on Amplification - From Closed Form Solution

Silva (1976) extended Thomson-Haskell's formulation to include damping in a layered system overlying an undamped elastic half space.

The above theories lead to a very complicated equation of motion in which the wave number k, enters through transcendental functions in a form similar to Eq. 3.41. As shown by Lysmer (1969) and Waas (1972) a much simpler equation of motion, see Eq. (3.50), can be obtained by a discretized representation of the layered half space. In this method it is assumed that displacements vary linearly between layer interfaces. As will be discussed this assumption imposes certain restrictions on how thick individual sublayers can be chosen. A major advantage of the method is that it leads to a uniform treatment of inclined body waves and surface waves and it will be used extensively below. In the original applications of the method, Lysmer (1969) and Waas (1972), the underlying half space was considered to be rigid. This lead to a method for analyzing surface waves in layered systems as will be discussed in Chapter 5.

Udaka (1975) used the same method with specified motions at the half-space surface to simulate the effect of traveling waves. In this method a control motion at the half-space surface was assumed to propagate horizontally with a given constant phase velocity. Only one component of motion was allowed at the control point. The method does not consider interaction between the layered soil systems and the underlying half space.

This interaction is properly considered in the present work on the effects of inclined body waves arriving through a viscoelastic half space. The study will show that except for the case of normal incidence, there must be two components of motion at each layer interface. The following cases will be considered:

1. SV-waves at oblique incidence
2. P-waves at oblique incidence
3. Pairs of SV-and P-waves at oblique incidence

3.5.1 Discretized Formulation for Layered System

The layered system considered is shown in Fig. 3.20. It consists of n homogenous, isotropic layers over a half space. All material properties may be undamped elastic or damped viscoelastic.

Assuming linear variation of displacements within each layer the displacement of any point in the system for a plane harmonic wave travelling in the horizontal x-direction at a given frequency, ω, can be written:

$$\delta_x = \alpha U_x(z)\ e^{i(\omega t - kx)} \tag{3.48.a}$$

$$\delta_z = i\alpha U_z(z)\ e^{i(\omega t - kx)} \tag{3.48.b}$$

in which, for $z_j \leq z \leq z_{J+1}$

$$U_x(z) = (Z_{j+1} - z)/h_j\ U_{2j-1} + (z - z_j)/h_j\ U_{2j+1} \tag{3.49.a}$$

$$U_z(z) = (Z_{j+1} - z)/h_j\ U_{2j} + (z - z_j)/h_j\ U_{2j+2} \tag{3.49.b}$$

and α is a mode participation factor that can be found from the given control motion. The displacement functions $U_x(z)$ and $U_z(z)$ are interconnected and can be normalized in any manner. The wave number K may be complex expressing both the phase velocity, $V_a = \omega/Re(k)$, and the attenuation factor, $\exp(-Im(k)x)$.

As shown by Udaka (1975) the equations of motion for the discretized layered system is

$$([K] - \omega^2[M])\ \{U\} = \begin{Bmatrix} 0 \\ P_b \end{Bmatrix} \tag{3.50.a}$$

where

$$[K] = A\ k^2 + [\bar{B}]\ k + [G] \tag{3.50.b}$$

In these equations all matrices are of the order $(2n + 2) \times (2n + 2)$ and the last two terms, P_b, of the load vector are forces at the

interface between the layered system and the half space. The vector U contains (2n + 2) complex displacement amplitudes, U_j, j = 1, 2, ..., (2n + 2) for the (n+1) layer interfaces each having two degrees of freedom U_x and U_z.

The banded, symmetric matrices [A], [$\bar{B}$], [G], and [M], are assembled from sublayer matrices as shown in Fig. 3.21. The submatrices, shown in Eqs. (3.51) to (3.55), are formed using complex shear moduli G_j^*, complex constrained moduli M_j^*, and layer thicknesses h_j as follows:

$$[A]_j = \frac{h_j}{6}\begin{bmatrix} 2M_j^* & 0 & M_j^* & 0 \\ 0 & 2G_j^* & 0 & G_j^* \\ M_j^* & 0 & 2M_j^* & 0 \\ 0 & G_j & 0 & 2Gj \end{bmatrix} \tag{3.51}$$

$$[\bar{B}]_j = \frac{1}{2}\begin{bmatrix} 0 & 3G_j^*-M_j^* & 0 & -(G_j^*-M_j^*) \\ (3G_j^*-M_j^*) & 0 & (G_j^*-M_j^*) & 0 \\ 0 & (G_j^*-M_j^*) & 0 & (G_j^*-M_j^*) \\ -(G_j^*-M_j^*) & 0 & (3G_j^*-M_j^*) & 0 \end{bmatrix} \tag{3.52}$$

$$[G]_j = \frac{1}{h_j}\begin{bmatrix} G_j^* & 0 & -G_j^* & 0 \\ 0 & M_j^* & 0 & -M_j^* \\ -G^* & 0 & G_j^* & 0 \\ 0 & -M_j^* & 0 & M_j^* \end{bmatrix} \tag{3.53}$$

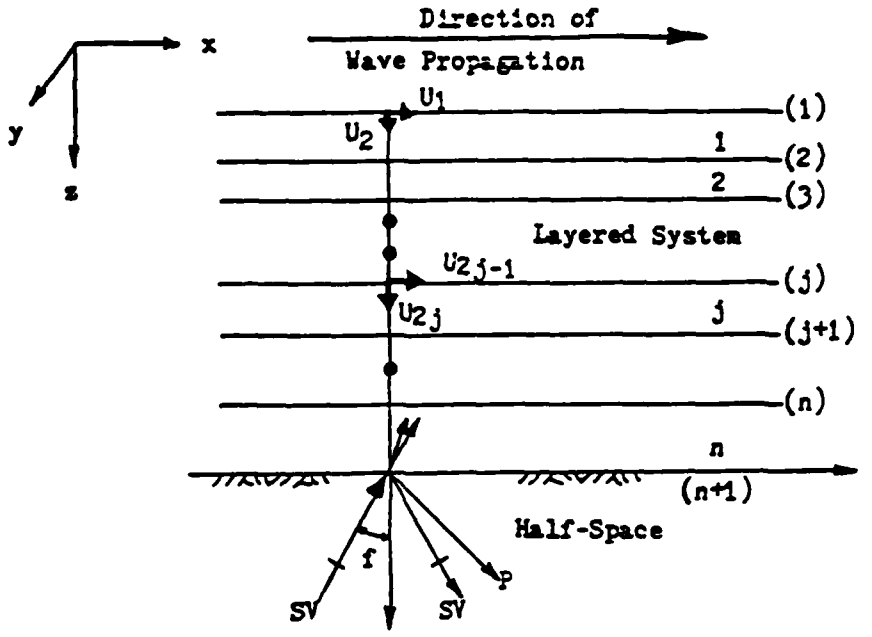

Figure 3.20 Model of Plane SV wave Incidence

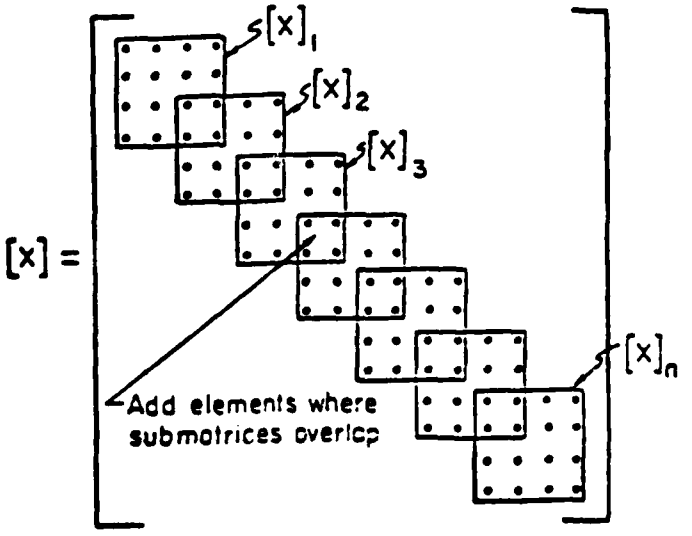

Fig. 3.21 Structure of Matrices [A], [B], [C], and [M]
(For the case of SV and P wave of oblique incidence)

The layer mass matrix M_j can be chosen as consistent mass, or lumped mass, or a combination of both. For consistent mass formulation:

$$[M_c]_j = \rho_j h_j \begin{bmatrix} 1/3 & 0 & 1/6 & 0 \\ 0 & 1/3 & 0 & 1/6 \\ 1/6 & 0 & 1/3 & 0 \\ 0 & 1/6 & 0 & 0 \end{bmatrix} \tag{3.54}$$

For lumped mass:

$$[M_\ell]_j = \rho_j h_j \begin{bmatrix} 1/2 & 0 & 0 & 0 \\ 0 & 1/2 & 0 & 0 \\ 0 & 0 & 1/2 & 0 \\ 0 & 0 & 0 & 1/2 \end{bmatrix} \tag{3.55}$$

For combination of consistent and lumped mass:

$$[M]_j = \alpha_c [M_c]_j + (1 - \alpha_c)[M_\ell]_j \tag{3.56}$$

where α_c is a fraction between 0 and 1. It has been found that with the finite element method, $\alpha_c = 0.5$ gives good results compared with analytical closed form solutions.

The same investigation also showed that when the average mass matrix is used the layer thicknesses, h_j, can be chosen as large as $h_j = \lambda_s/5 = 2\pi V_s/(5\omega)$, where λ_s is the wavelength of shear waves, without impairing the accuracy at the discretized method. This compares with a maximum layer thickness of $\lambda_s/8$ when either the lumped or consistent mass formulations is used.

When the wave number k becomes zero, i.e., the apparent wave velocity approaches infinity, the equation of motion becomes

$$\left\{[G] - \omega^2[M]\right\} \left\{U\right\} = \begin{Bmatrix} 0 \\ P_b \end{Bmatrix} \tag{3.57}$$

which is the case of vertical incidence of body waves. In this case

the shear wave and P-wave are completely uncoupled and Eq. (3.57) can be separated into two simpler matrix equations; one for each wave type.

For the purpose of developing the base boundary equation, it is convenient to express Eq. (3.50a) in partitioned form:

$$\left(\begin{bmatrix} K_\ell & K_c \\ K_c^T & K_b \end{bmatrix} - \omega^2 \begin{bmatrix} M_\ell & M_c \\ M_c^T & M_b \end{bmatrix} \right) \begin{Bmatrix} U_\ell \\ U_b \end{Bmatrix} = \begin{Bmatrix} 0 \\ P_b \end{Bmatrix} \tag{3.58}$$

in which the suffix "ℓ" denotes quantities for the layered system, the suffix "b" refers to the base boundary, and the suffix "c" to interaction between the layered system and the half space. For a given wave number k and frequency ω, this set of linear equations can be further simplified by the notation $[\bar{K}] = [K] - \omega^2[M]$ to:

$$\begin{bmatrix} \bar{K}_\ell & \bar{K}_c \\ \bar{K}_c^T & \bar{K}_b \end{bmatrix} \begin{Bmatrix} U_\ell \\ U_b \end{Bmatrix} = \begin{Bmatrix} 0 \\ P_b \end{Bmatrix} \tag{3.59}$$

or $$\left[\bar{K}_\ell\right] \{U_\ell\} + \left[\bar{K}_c\right] \{U_b\} = \{0\} \tag{3.60}$$

$$\left[\bar{K}_c\right]^T \{U_\ell\} + \left[\bar{K}_b\right] \{U_b\} = \{P_b\} \tag{3.61}$$

Equation (3.60) yields

$$\{U_\ell\} = -\left[\bar{K}_\ell\right]^{-1} \left[\bar{K}_c\right] \{U_b\} \qquad \ell = 1, 2, \ldots\ldots, 2n \tag{3.62}$$

and substitution of this equation into Eq. (3.61) gives the relationship between the displacements, $\{U_b\}$, and the forces, $\{P_b\}$, at the interface between the layered system and the half space (the base boundary)

$$[L] \{U_b\} = \{P_b\} \tag{3.63}$$

where

$$[L] = -\left[\bar{K}_c\right]^T \left[\bar{K}_\ell\right]^{-1} \left[\bar{K}_c\right] + \left[K_b\right] = \begin{bmatrix} L_{11} & L_{12} \\ L_{21} & L_{22} \end{bmatrix}$$

It should be noted that for a system with n layers, K_ℓ is a 2n by 2n matrix, K_b is a 2 by 2 matrix, and K_c is a 2n by 2 matrix.

3.5.2 Half Space

If the displacements and forces at a specified location on the base boundary induced by the incident wave from a homogeneous viscoelastic half space can be determined, then the complex displacement functions $\{U_\ell\}$ at the interfaces between each layer in the system can also be easily determined. It is thus necessary now to find the displacements and forces at the base boundary due to a specified incident plane wave striking at the base. It may be shown that the boundary displacements and forces take the same forms as Eqs. (3.33) and (3.34); after rearrangement, they are:

$$\{U_b\} = ik\left[\bar{\alpha}\right]\begin{Bmatrix} A_1 \\ B_1 \end{Bmatrix} + ik\left[\bar{\beta}\right]\begin{Bmatrix} A_2 \\ B_2 \end{Bmatrix} \tag{3.64}$$

and

$$\{P_b\} = G^* k^2\left[\alpha'\right]\begin{Bmatrix} A_1 \\ B_1 \end{Bmatrix} + G^* k^2\left[\beta'\right]\begin{Bmatrix} A_2 \\ B_2 \end{Bmatrix} \tag{3.65}$$

where

$$\left[\bar{\alpha}\right] = \begin{bmatrix} -1 & -b \\ a & -1 \end{bmatrix}, \quad \left[\bar{\beta}\right] = \begin{bmatrix} -1 & b \\ -a & -1 \end{bmatrix},$$

$$\left[\alpha'\right] = \begin{bmatrix} 2a & (b^2-1) \\ -(b^2-1) & 2b \end{bmatrix}, \quad \left[\beta'\right] = \begin{bmatrix} -2a & (b^2-1) \\ -(b^2-1) & -2b \end{bmatrix}$$

and A_1, B_1, A_2, and B_2 are complex coefficients representing wave amplitudes of displacement potentials.

Elimination of boundary forces and displacements by substitution of Eqs. (3.64) and (3.65) into Eq. (3.63), produces two linear equations containing four unknown coefficients. As discussed earlier, some

AD-A099 508 CALIFORNIA UNIV BERKELEY EARTHQUAKE ENGINEERING RES--ETC F/G 8/11
ANALYSIS OF LOCAL VARIATIONS IN FREE FIELD SEISMIC GROUND MOTIO--ETC(U)
JAN 81 J CHEN, J LYSMER, H B SEED DAAG29-76-G-0257
UNCLASSIFIED UCB/EERC-81/03 ARO-13838.2-GS NL

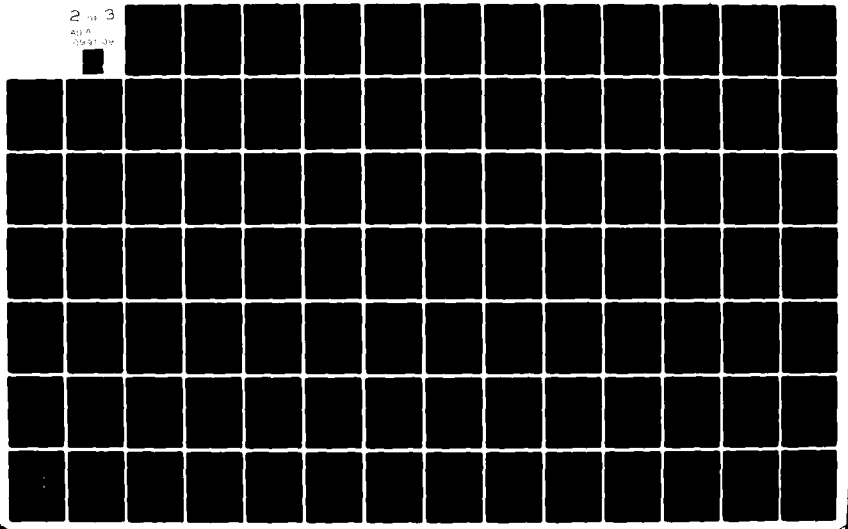

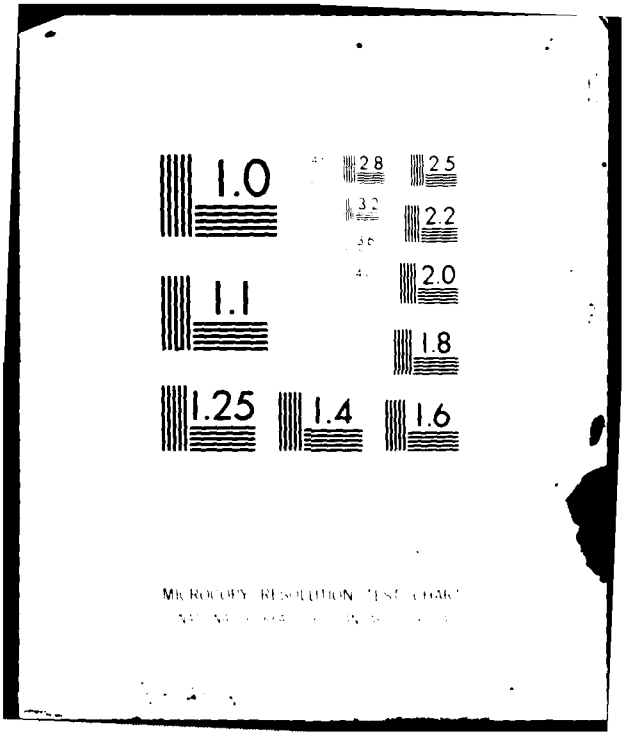
1.0
2.8
2.5
3.2
2.2
2.0
1.1
1.8
1.25
1.4
1.6
MICROCOPY RESOLUTION TEST CHART

restrictions and assumptions must be made in order to determine the coefficients and to obtain normalized boundary displacements and boundary forces at the base boundary. By specifying only one type of body wave incident to the base by a given real incident angle and normalizing two reflection coefficients by this incident coefficient, the two unknown normalized reflection coefficients can be determined from the following equations:

$$\begin{Bmatrix} A_2 \\ B_2 \end{Bmatrix} = [D]^{-1} \begin{Bmatrix} Q_1 \\ Q_2 \end{Bmatrix} \tag{3.66}$$

where

$$D = \begin{bmatrix} (D_{11} - D_{12}) & (D_{13} - D_{14}) \\ (D_{21} - D_{22}) & (D_{23} - D_{24}) \end{bmatrix} \tag{3.67}$$

in which D_{11}, D_{12}, D_{13}, D_{14}, D_{21}, D_{22}, D_{23}, and D_{24} are defined as:

$$D_{11} = i\,k\,L_{11}$$

$$D_{12} = k\,a\,L_{12} + 2\,a\,G^*\,k^2$$

$$D_{13} = -k\,L_{12} + (b^2 - 1)\,G^*\,k^2$$

$$D_{14} = i\,k\,b\,L_{11}$$

$$D_{21} = -i\,k\,L_{21} - (b^2 - 1)\,G^*\,k^2$$

$$D_{22} = k\,a\,L_{22}$$

$$D_{23} = k\,L_{23}$$

$$D_{24} = -i\,(k\,b\,L_{21} + 2b\,G^*\,k^2)$$

where parameters a and b are complex parameters as defined earlier and L_{11}, L_{12}, L_{21}, L_{22}, are elements of the layer stiffness matrix defined in Eq. (3.63).

It should also be noted that the coefficients A_2 and B_2 are "Normalized reflection coefficients" which are different from the

coefficients A_2 and B_2 in Eqs. (3.64) and (3.65). They are related to the reflection coefficients for the case of unit incident coefficeint. It should also be noted that the quantities Q_1 and Q_2 will be redefined from case to case for different incident waves.

Only SV Wave Incidence

Assuming that the angle of incidence, f, is real and that the angle, α_1, between the propagation vector and the attenuation vector is equal to zero, one may obtain $k = k_s \sin f$ as shown in Eq. (3.11). Thus, for a system having a common phase velocity and attenuation factor along the boundary, the complex wave velocity, V_a^* is

$$V_a^* = \omega/(k_s \sin f) = V_s^*/\sin f = V_a^* e^{-i\delta_s/2} \tag{3.68}$$

in which

$$\tan \delta_s = 2\beta_s \sqrt{1 - \beta_s^2}/(1 - 2\beta_s^2) \quad 2\beta_s \text{ for small } \beta_s$$

This assumption will force the complex parameter "b" to become real as long as $V_a > V_s$. If $\beta_p = \beta_s$ the parameter "a" is complex and

$$a = \{(V_a^*/V_p^*)^2 \cdot e^{i(\delta_p - \delta_s)} - 1\}^{1/2}$$

where

$$\tan \delta_p = 2\beta_p \sqrt{1 - \beta_1^2}/(1 - 2\beta_p^2) \quad 2\beta_p \text{ for small } \beta_p \ .$$

If $\delta_s = \delta_p = \delta$, the solution is similar to the elastic case, i.e., both "a" and "b" are real but the wave attenuates in the direction of propagation. For SV wave incidence, A_1 is set to 0 and A_2, B_2 can be determined by defining Q_1 and Q_2 in Eq. (3.66) by

$$Q_1 = -(D_{11} + D_{14})$$
$$Q_2 = -(D_{23} + D_{24}) \tag{3.69a}$$

Once two normalized coefficients A_2, B_2 are found the normalized displacements and boundary forces can be determined.

Only P-Wave Incidence

In this case B_1 is set to zero and the reflection coefficients are normalized by A_1. If a real incident angle, e, is specified we have $V_a^* = V_s^*/\sin e$ and $k = \omega/V_a^*$. From the complex Snell's law, $V_a^* = V_s^*/\sin f = /V_p^*/\sin e$, the reflected angle f can be determined. Generally, if damping due to the shear and P waves are not equal, the reflection angle of the SV wave will be complex which is different from the elastic case. For a viscoelastic half-space, a phase shift at the boundary base will generally be expected regardless of the type of wave incidence. The reflection coefficients can be found by using Eq. (3.66) by replacing Q_1 and Q_2 as follows:

$$Q_1 = -(D_{11} + D_{12})$$
$$Q_2 = -(D_{21} + D_{22}) \qquad (3.69.b)$$

SV-and P-Waves Obliquely Incident

It is assumed that the amplitude of the incident P wave A_1 is given and that the ratio, $\eta = B_1/A_1$, of the displacement coefficients for the incident SV wave and the incident P wave is also known. With these assumptions Q_1 and Q_2 in Eq. (3.66) will be defined as:

$$Q_1 = -(D_{11} + D_{12}) - \eta(D_{13} + D_{14})$$
$$Q_2 = -(D_{21} + D_{22}) - \eta(D_{23} + D_{24}) \qquad (3.69.c)$$

Thus, the normalized reflection coefficients can be determined. In this case, the reflection angles can be either real or complex and will depend on the damping ratio assumed for the half-space and the specified angle of incidence.

3.6 SH-Waves in Multi-layered Half Space

Harmonic motion under plane strain conditions in a semi-infinite layered system due to an inclined SH-wave incident to the base is here considered. The model for plane SV-and P-wave is used, and is replotted for the case of incident SH-waves as shown in Fig. 3.22. All displacements are perpendicular to the x-z plane and are described by

$$\delta_y = \alpha\, U_y(z)\; e^{i(\omega t - kx)} \tag{3.70}$$

in which ω is the circular frequency, and α is the mode participation factor.

The equation of motion take the same form as Eq. (3.50a) but the stiffness matrix [K] is now defined as

$$[K] = [A]\, k^2 + [G] \tag{3.71}$$

where [A], and [G] are n by n tridiagonal, symmetric matrices, which consist of the contributions from individual layers and which can be conveniently assembled from the layer submatrices as shown in Fig. 3.23. The submatrices for the layer j are:

$$[A]_j = h_j\, G^* \begin{bmatrix} 1/3 & 1/6 \\ 1/6 & 1/3 \end{bmatrix} \tag{3.72}$$

$$[G]_j = \frac{G^*}{h_j} \begin{bmatrix} 1 & -1 \\ -1 & 1 \end{bmatrix} \tag{3.73}$$

The mass matrix (see Eq. 3.56) may be a combination of

(consistent) $$\left[M_c\right]_j = \rho_j\, h_j \begin{bmatrix} 1/3 & 1/6 \\ 1/6 & 1/3 \end{bmatrix} \tag{3.74}$$

and

(lumped) $$\left[M_\ell\right]_j = \rho_j\, h_j \begin{bmatrix} 1/2 & 1/6 \\ 0 & 1/2 \end{bmatrix} \tag{3.75}$$

Following the procedures described in Section 3.5, through Eqs. (3.58) to (3.63), the relationships between the boundary force and

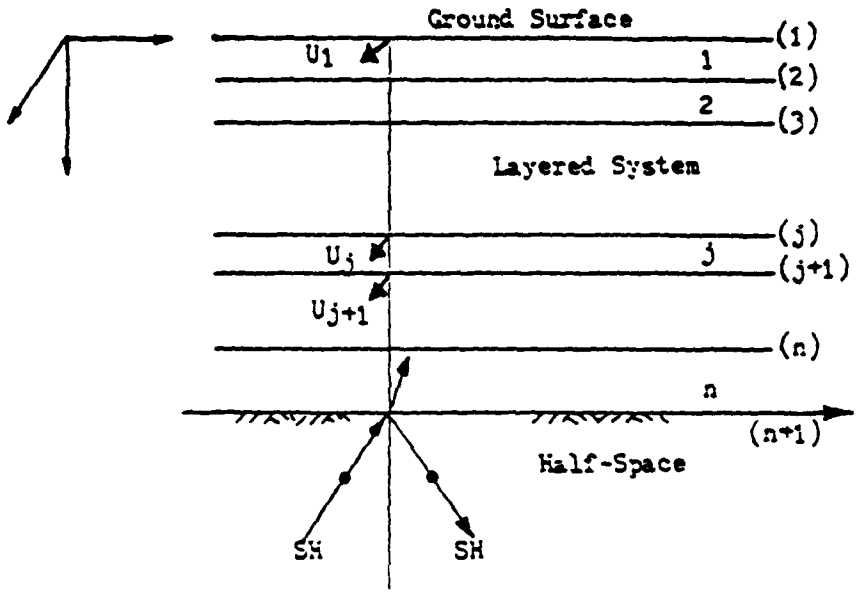

Fig. 3.22 Model of Plane SH Wave Incidence

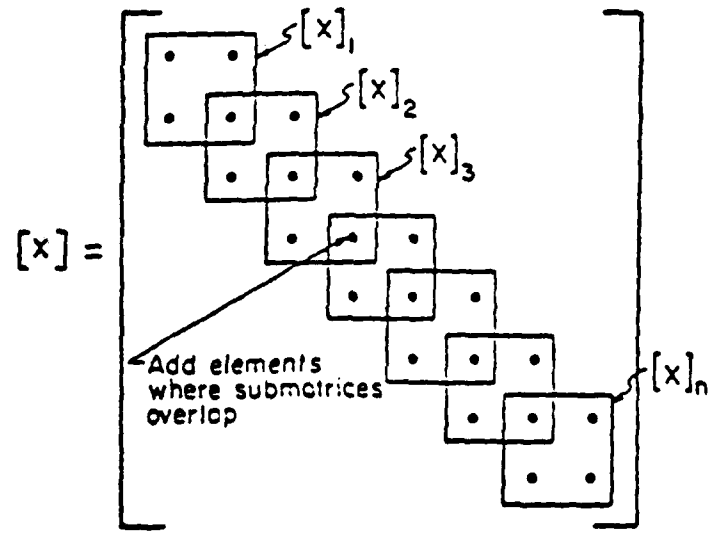

Fig. 3.23 Structure of Matrices [A], [G], and [M]
(For the case of SH wave of oblique incidence)

displacement may be established. On the other hand, the boundary force and displacement induced by the incident SH-wave from the underlying half space can be derived from Eq. (3.26) in the way similar to the case of SV-waves. The boundary force and the displacement are normalized by the amplitude of the incident wave and can be expressed in terms of wave number, shear modulus and and unknown reflection coefficient. By elimination of the displacement and the boundary force between the layered system and the half space, the normalized reflection coefficient can be found and the boundary force and displacement can be determined. Accordingly, the amplitudes of each layer can be easily found from a set of simple linear equations for any given wave number and frequency.

3.7 The Computer Programs SITE and LOVE

The above discretized procedures were implemented in two computer codes, SITE and LOVE. The first program handles the cases of inclined P- and SV-waves. It also handles the case of Rayleigh waves which will be discussed in Chapter 4. The second program handles the cases of inclined SH-waves and Love waves (also to be discussed in Chapter 4).

Both computer codes were verified against the exact solutions provided in Fig. 3.5, 3.6, 3.10 to 3.12 and 3.15 to 3.17 using a model consisting of 18 sublayers to represent the surface layer. The computed data points agreed with the exact solutions to within 3 significant digits and have not been plotted in the above figures.

The two codes can handle not only harmonic motion but also transient motions by the Fourier techniques described in Chapter 5.

3.8 Summary

The fundamental theories of harmonic inclined body waves propagating in a viscoelastic half space and a layered half space are

presented in this chapter. Based on analytical solutions developed for a model of a single layer over a half space, several numerical examples were given to show the characteristic of amplitudes at the free surface and the interface boundary for the case of SV- and P-wave incident at different angle. The study of the effect of incident angle on the amplication of both steady state and transient motion was also included. The effect of damping and Poisson's ratio contrast (between the layer and the half space) on site amplifications was also investigated. Numerical examples for site response to inclined body waves for a more complicated layered half-space system will be given in Chapter 5.

CHAPTER 4

PLANE SURFACE WAVES

4.1 Introduction

The theory of plane Rayleigh and Love waves propagating in an undamped elastic or damped viscoelastic half space, a layered rigid base system, or a layered half space has been well developed. Basically, the available theories can be classified into continuum methods or discretized numerical methods. In principle, continuum theories provide analytical solutions which are valid for any choice of layer thicknesses. However, numerical difficulties are encountered in the numerical evaluation of complete solutions especially for damped systems. The discretized methods are based on finite element techniques and offer easier and more convenient numerical solutions for viscoelastic layered systems. However the accuracy of the solution is affected by the choice of discretization scheme, especially in the high frequency range.

In this chapter, the general theory and characteristics of Rayleigh waves in homogeneous elastic and viscoelastic half spaces are briefly discussed in Section 4.2. In Section 4.3, the discretized method of treating Rayleigh waves in a layered system with a rigid base is briefly reviewed, and several methods are proposed to extend this method for the approximate solution of layered systems resting on a viscoelastic half space. The selection of the fundamental Rayleigh mode is also explained in this section. The discretized method for Love waves in a layered system with a rigid base is briefly presented in Section 4.4.

Several published solutions were used for verification of results from the computer programs SITE and LOVE which were developed as part

of the research described herein for site response analysis by the discretized method. The comparative study, presented in Section 4.5, confirms that the discretized method can be used for analyses of surface wave propagation in a viscoelastic layered half space. Additional analyses of the seismic response of multi-layered sites excited by Rayleigh waves will be presented in Chapter 5.

4.2 Rayleigh Wave in a Viscoelastic Half Space

It is assumed that a simple harmonic wave train with motions in the xz-plane only travels in the x-direction such that the motion is independent of the y-coordinate and that the amplitude of this motion decreases asymptotically with the distance z form the free surface. Waves satisfying these conditions are called Rayleigh waves and were first studied by Rayleigh (1885). A solution corresponding to this definition may be derived from the general equations of motion for two-dimensional waves presented in Chapter 3. Since the boundary condition at $z=\infty$ requires that the wave potentials approach zero as z approaches infinity, the solutions for Rayleigh waves can be written:

$$\Phi = A\, e^{-qz}\, e^{-ikx} \tag{4.1a}$$

$$\Psi = B\, e^{-sz}\, e^{-ikx} \tag{4.1b}$$

where

$q = (k^2 - k_p^2)^{1/2}$; taking the principal value,

$s = (k^2 - k_s^2)^{1/2}$; taking the principal value.

and A and B are unknown complex constants.

Equation (4.1), in connection with Eq. (3.2) defines the form of the displacement and stress field in the half space. By introducing the boundary condition that all stresses must vanish on the plane, z=0, the following relationship between the wave numbers involved can be obtained:

$$4\,(1 - k_s^2/k^2)^{1/2}\,(1 - k_p^2/k^2)^{1/2} = (2 - k_s^2/k^2)^2 \qquad (4.2)$$

By squaring each side of Eq. (4.2) and using the relationships

$$X = (k_s/k)^2 = (V_r^*/V_s^*)^2$$

$$Y = (k_s/k_p)^2 = (V_p^*/V_s^*)^2$$

the following equation is obtained:

$$X^3 - 8X^2 + (24 - 16Y)X + 16(Y - 1) = 0 \qquad (4.3)$$

This is of exactly the same form as the equation developed by Rayleigh for an undamped elastic medium except that real velocities are replaced by complex velocities for a damped system. This equation is a cubic polynomial with coefficients in the complex plane. It has three complex roots, X, which may not be distinct. The root which satisfies the original unsquared equation, Eq. (4.2), provides the fundamental solution for the surface wave, Borcherdt (1971).

The solution may be found by Cardan techniques, as shown by Hall (1964). The solution was also carried out by Borcherdt (1971), who showed that if V_r^{*2}/V_s^{*2} is a root of the complex Rayleigh equation such that $0 < |V_r^*|^2 / |V_s^*|^2 < 1$, then V_r^{*2}/V_s^{*2} also satisfies Eq. (4.2). This restriction on the roots of Eq. (4.3) is the same for the damped and the undamped case and is used for the selection of the root corresponding to the Rayleigh wave. In the undamped case, the solution will consist of three real roots for Poisson's ratio less than 0.26, and there will be one real root plus a conjugate pair of complex roots for Poisson's ratio larger than 0.26.

Once the ratio, X, between the Rayleigh and shear wave velocities has been determined, the normalized displacements, mode shape, of the Rayleigh wave may be obtained by substituting Eqs. (4.1) into Eqs. (3.2).

The mode shape or normalized amplitude distributions as a function of dimensionless depth for four different values of Poisson's ratio are shown in Fig. 4.1 for the case of undamped elastic media. The dimensionless depth is defined as the actual depth divided by the wave length which is inversely proportional to frequencies. The particle motion at different depths is shown in the same plot. Since the horizontal and vertical components of Rayleigh waves are out of phase by the angle $\pi/2$, the trajectories of the particle motions are ellipses. The magnitude and direction of the elliptical motion is dependent on depth. The following characteritic may be summarized from the plot shown.

1. The horizontal amplitude decays rapidly with depth near the surface and becomes zero at a depth of approximately one fifth of the wave length. The maximum negative amplitude occurs at a depth of approximately two fifths to one half of the wave length and then gradually decays to zero.

2. The vertical amplitude first increases slightly with depth and reaches its maximum value at a depth of 0.05 to 0.15 times the wave length below which it decays rapidly to zero, except for materials with zero Poisson's ratio for which the maximum vertical displacement occurs at the surface.

3. The major horizontal and vertical disturbances associated with Rayleigh waves are concentrated within one wave length from the surface.

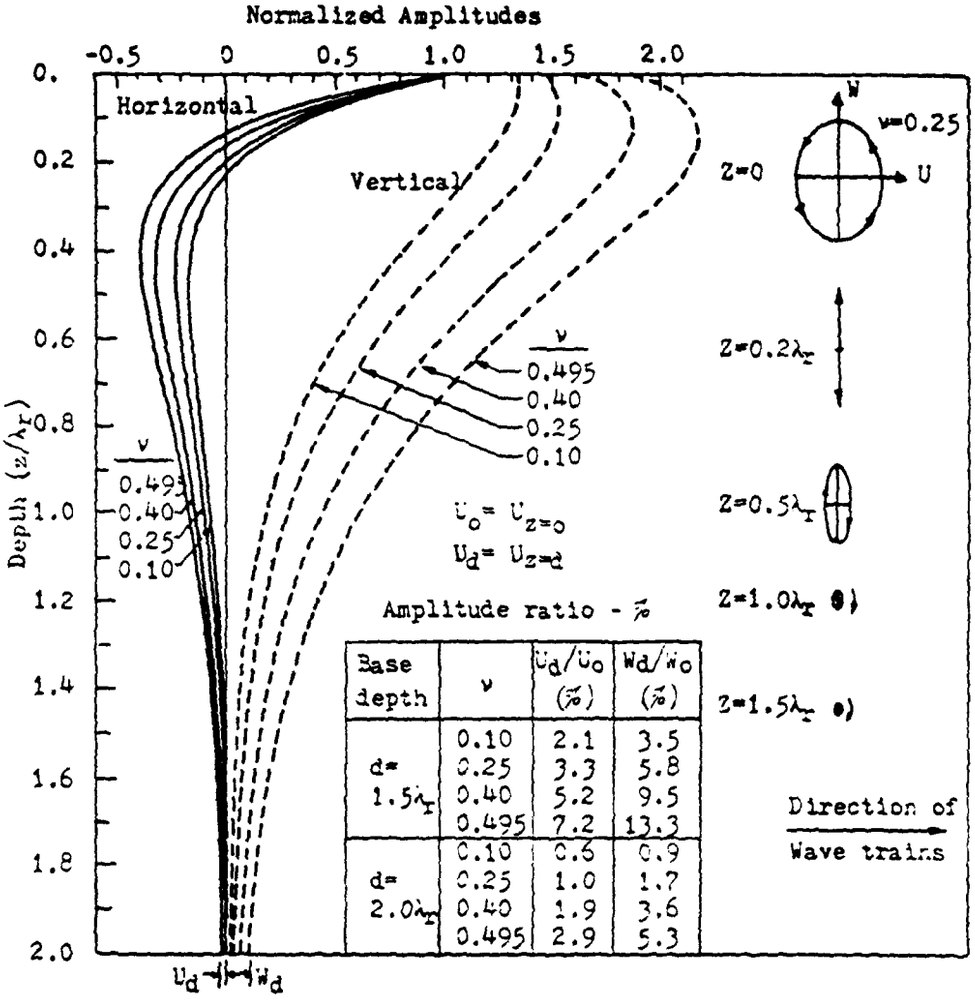

Base depth	ν	Ud/Uo (⁄)	Wd/Wo (⁄)
d= 1.5λr	0.10	2.1	3.5
	0.25	3.3	5.8
	0.40	5.2	9.5
	0.495	7.2	13.3
d= 2.0λr	0.10	0.6	0.9
	0.25	1.0	1.7
	0.40	1.9	3.6
	0.495	2.9	5.3

Fig. 4.1 Normalized Amplitudes Versus Dimensionless Depth for R-Waves

4. The amplitudes at depth decrease as Poisson's ratio decreases.

5. For wave propagation in the positive x-direction, the elliptical particle motion at the surface proceeds counterclockwise. At the depth $z \approx 0.2\ \lambda_r$ where the horizontal amplitude changes sign, the direction of rotation reverses. The minor axes of the ellipses are perpendicular to the free surface of the half space; i.e. the vertical motion is stronger than the horizontal motion at all depths.

The distribution of the stress components with depth is shown in Fig. 4.2. The curves were calculated for Poisson's ratio equal to 0.25 (dashed line) and for Poisson's ratio equal to 0.34 (solid line). It is apparent from the plot that σ_{xx} changes sign at $z=0.25\lambda_r$, whereas δ_{zz} and τ_{zz} reach their maxima at approximately $z/\lambda_r = 0.3$ and then falls off exponentially with depth.

Rayleigh waves in a viscoelastic half space have been studied by Borcherdt(1971). Computed mode-shapes for the special case of Poisson's ratio equal to 0.35 are shown in Fig. 4.3. It may be seen from this figure that the effect of damping on the distribution of motions with depth is insignificant for the magnitudes of damping usually encountered in practice. Another small effect of damping is a slight tilt of the elliptical orbits of particle motion. The major effect of damping is that the waves will decay exponentially as they propagate in the x-directions. The decay factor is approximately $\exp(-2\pi\beta)$ per wavelength in the x-direction.

4.3 Rayleigh Waves in a Layered System

Rayleigh wave propagation in layered media is of great interest to seismologists and has been treated in standard textbooks. A complete theoretical summary may be found in Ewing et al. (1957) and a brief

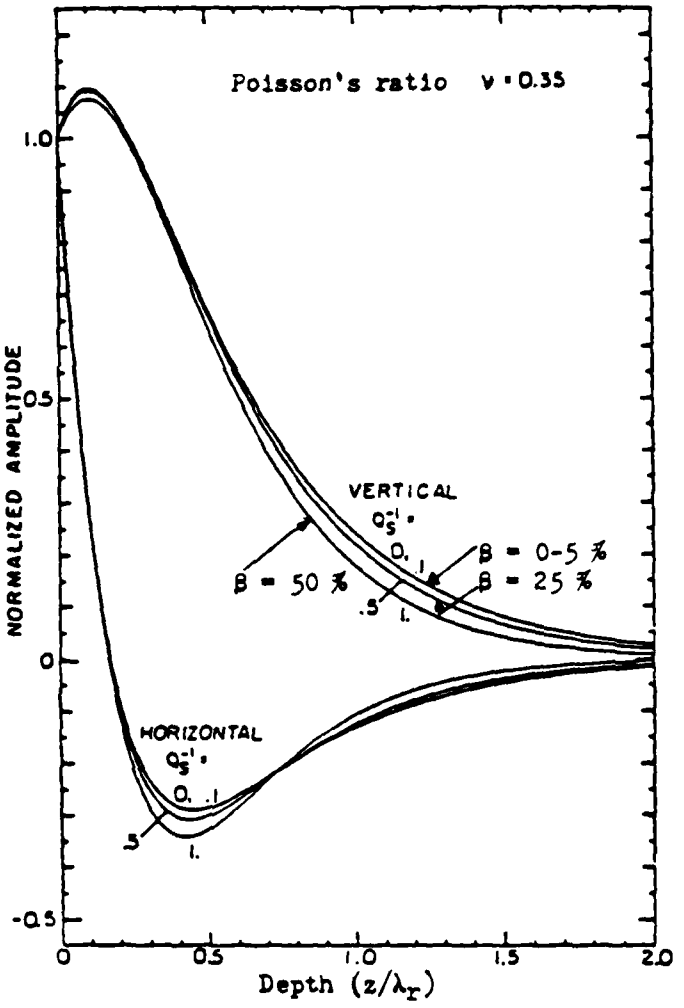

Fig. 4.3 Normalized Amplitude Versus Depth for Materials with Different Values of Shear Wave Damping Ratios, $Q_k^{-1} = 0$ (after Borcherdt, 1971)

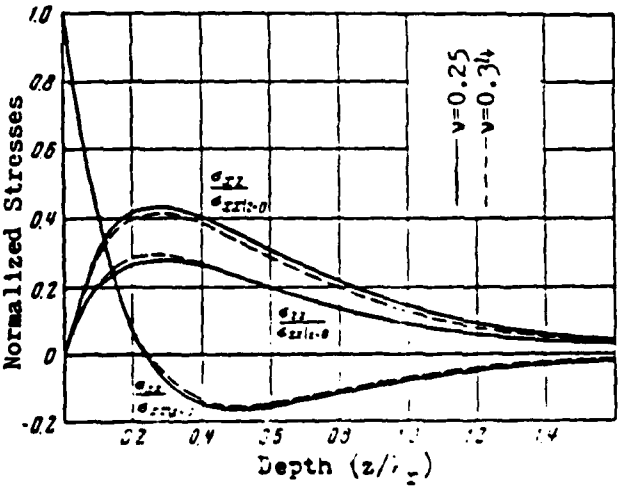

Fig. 4.2 Rayleigh Wave Stress Distribution for ν=0.25 and ν=0.34 (after Viktorov, 1967)

description of geophysics applications has been given by Grant and West (1964). The equation of motion for a system of elastic layers overlying an elastic half space was formulated in matrix algebra by Thomson (1950) and improved by Haskell (1953). An equivalent formulation which makes calculations possible for higher frequencies was presented by Knopoff (1964), Dunkin (1965) and Thrower (1965). A modification of the matrix formulation to give faster machine computations for modal solutions to a layered half space was provided by Watson (1970). Formulations which include damping were later presented by Boncheva (1977) and Silva (1978). The fundamental approach for all of these methods is based on continuum theory which eventually leads to a complicated nonlinear eigenvalue problem. Solution of this problem involves serious numerical difficulties in many cases and is complicated by the fact that in layered systems infinitely many Rayleigh waves (modes) can exist simultaneously.

A lumped mass finite element formulation for a multi-layered system with rigid base was developed by Lysmer (1969). This method leads to a simple quadratic eigenvalue problem which can be transformed to a linear eigenvalue problem of the double dimension. This problem can be solved completely by standard techniques. Lysmer's method was extended by Waas (1972) to include a consistent mass formulation and Love waves. This method, which will be briefly reviewed below, is the basic numerical method employed in the research described herein. As part of this research several methods will be introduced which facilitate the use of the method for cases involving a layered system supported on a viscoelastic half space. These methods will be discussed in Section 4.3.2. Methods for identifying the fundamental

mode among the many Rayleigh waves which can exist in a layered system will be presented in Section 4.3.3.

4.3.1 Layered System With Rigid Base

Consider the semi-infinite layered system shown in Fig. 4.4a. All motions occur in the xz-plane and any point in the system has two degrees of freedom. The layered system is treated as a continuum in the horizontal direction but is discretized in the vertical direction by assuming that the displacement is continuous at each interface and varies linearly within each layer. As shown by Wass (1972), the equation of motion for an n-layer system may be written as:

$$([A]\ k^2 + i[B]k + [G] - \omega^2[M])\ \{v\} = \{0\} \tag{4.6}$$

In this equation, $\{v\}$ is a vector containing the 2n layer interface displacements and [A], [B], [G], and [M] are the 2n by 2n matrices, assembled by addition of layer submatrices as shown in Fig. 3.21 for the case of body waves except that the last two rows and columns of each total matrix are not used because of the assumption of a rigid base for which the displacements are zero. The submatrices [A] and [G] for each layer may be expressed in terms of complex shear moduli, constrained moduli, and the layer thicknesses as shown in Eqs. (3.51) and (3.53) and the submatrix [B] is redefined as follows:

$$[B]_j = \frac{1}{2}\begin{bmatrix} 0 & (3G_j^* - M_j^*) & 0 & -(G_j^* - M_j^*) \\ -(3G_j^* - M_j^*) & 0 & -(G_j^* - M_j^*) & 0 \\ 0 & (G_j^* - M_j^*) & 0 & (G_j^* - M_j^*) \\ (G_j^* - M_j^*) & 0 & -(3G_j^* - M_j^*) & 0 \end{bmatrix} \tag{4.7}$$

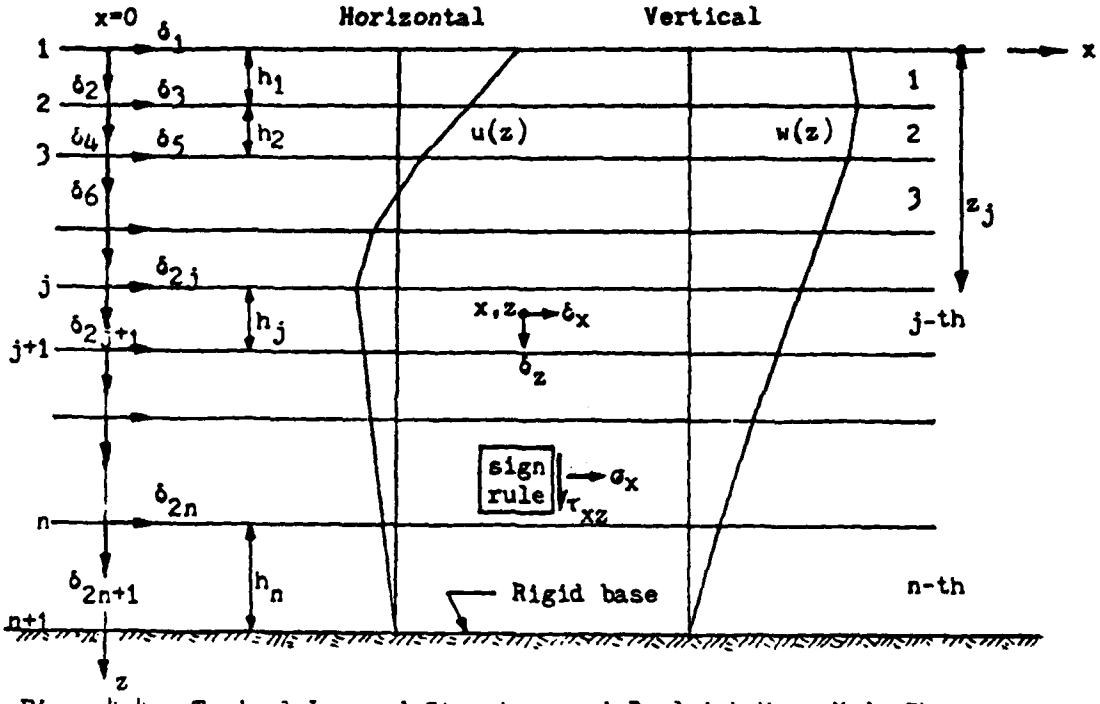

Fig. 4.4a Typical Layered Structure and Rayleigh Wave Mode Shapes

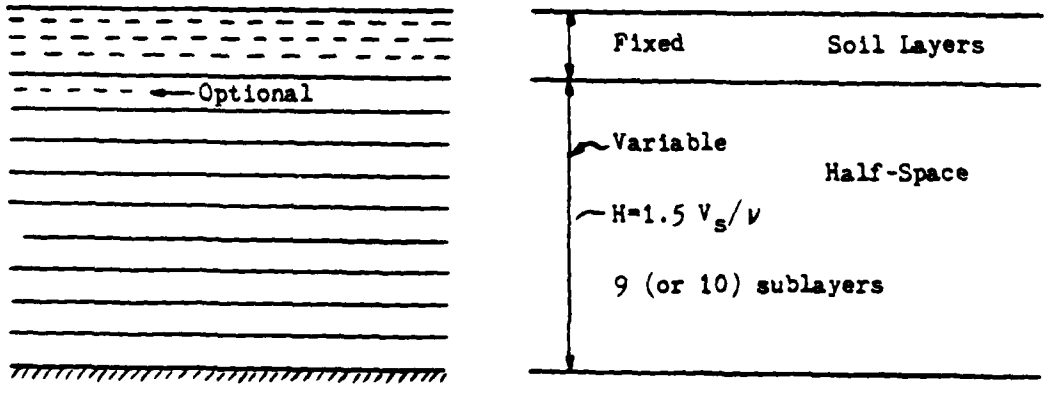

Fig. 4.4b Computation Model for Layered Soil System over Half-Space

Each submatrix of $[M]$ may be expressed in terms of consistent mass, lumped mass or a combination of both as shown in Eq. (3.56). For a given frequency ω, it is convenient to introduce a matrix $[C]$ such that $[C] = [G] - \omega^2 [M]$. This reduces Eq. (4.6) to:

$$([A] k^2 + i[B]k + [C]) \{v\} = \{0\} \tag{4.8}$$

This is a quadratic eigenvalue problem which has a solution $\{v\}$ if, and only if, the determinant of the coefficient matrix vanishes. Hence, for any given frequency the secular equation:

$$|[A]k^2 + i [B] k + [C]| = 0 \tag{4.9}$$

defines the possible wave numbers for Rayleigh waves in the layered system. A numerical technique for finding the eigenvalues and the corresponding eigenvectors in Eq. (4.8) has been presented by Waas (1972). It can be shown that this equation gives 4n eigenvalues, k_s, $s = 1,2,...4n$ and their corresponding eigenvectors, $\{v\}_s$, $s = 1,2,....4n$.

The case, $k = 0$, can occur only in an undamped system and when the frequency is equal to one of the natural frequencies of the layered systems. In this case the motion consists of vertically propagating P- or S-waves. The particle motion is vertical or horizontal.

The case, k real, can occur only in an undamped system. The motion is similar to Rayleigh's original surface wave in that it propagates with constant amplitude in the x-direction with the phase velocity $c = \omega/k$. The particle motion is generally elliptical but may be linear at certain depths.

The case, k purely imaginary, may occur in both damped and undamped systems. It corresponds to a motion which does not propagate but simply decays in the x-direction. The particle motion is linear

for undamped systems and generally elliptical for damped systems. Motions are in phase at all points.

The case, $k = k_r + ik_i$, $k_i = 0$, may occur in both damped and undamped systems and is the case of most interest for applications. The particle motions are generally elliptical and the motions propagate in the x-direction with the apparent phase velocity $V_a = \omega/k_r$ and it decays as exp $(k_i x)$. Generally, k_r and k_i will be of opposite sign, i.e. the motion decays in the direction in which it propagates. However, the unusual case may occur that k_r and k_i have the same sign, i.e. the motion decays in the opposite direction of the phase velocity. This is not a contradiction since it can be shown that for these cases the group velocity, see below, is negative, i.e. energy transmission occurs in the opposite direction of the phase velocity.

It can be shown, Waas (1972), that if k is a solution to the eigenvalue problem in Eq. (4.8) and $\{v\}$ is the corresponding eigenvector (mode shape) then -k is also a solution and the corresponding eigenvector $\{v\}$ is the adjoint of $\{v\}$; i.e. the vector obtained by simply changing the sign of all horizontal components of $\{v\}$. The physical significance of this is that the same motion can propagate in both the positive and negative x-direction. In the applications only the modes which decay (propagate energy) in the positive x-direction are of interest. Thus, in a damped system, only the 2n modes with $k_i < 0$ are of interest and the general solution to the equation of motion may be expressed in the form:

$$\{\delta\} = \sum_{s=1}^{2n} \alpha_s \{v\}_s \, e^{\,i(\omega t - k_s x)} \qquad (4.10)$$

in which α_s is the mode participation factor for mode s. Undamped systems are most conveniently handled by introducing a very small damping ratio and selecting the appropriate modes by the condition, $k_i<0$.

Stresses and Strains

Once the displacements at the interface of each layer are determined the strains at the midpoint of the j-th layer may be easily obtained. The following expressions are for the case of a single mode; if several modes are considered, then the total strain and stress can be found by superposition. The strains are:

$$\begin{aligned} \varepsilon_x &= -ik\left\{(v_{2j-1} + v_{2j+1})/2\right\} e^{-ikx} \\ \varepsilon_z &= \left\{(v_{2j+2} - v_{2j})/h_j\right\} e^{-ikx} \\ \gamma_{xz} &= \left\{(v_{2j+1} - v_{2j-1})/h_j - ik(v_{2j} + v_{2j+2})/2\right\} e^{-ikx} \end{aligned} \tag{4.11a}$$

Stresses may be obtained by the substitution of these strains into Hooke's law:

$$\begin{Bmatrix} \sigma_x \\ \sigma_z \\ \tau_{xz} \end{Bmatrix} = \begin{bmatrix} M_j^* & M_j^* - 2G_j^* & 0 \\ M_j^* - 2G_j^* & M_j^* & 0 \\ 0 & 0 & G^* \end{bmatrix} \begin{Bmatrix} \varepsilon_x \\ \varepsilon_z \\ \gamma_{xz} \end{Bmatrix} \tag{4.11b}$$

Group Velocity

For each mode Eq. (4.6) determines k as a complex-valued function of ω. A plot of this function is called a spectral (or dispersion) curve, see Figs. 4.5 and 4.6. The slope of this curve, U, is called the group velocity.

$$U = \frac{d\omega}{dk} = c + k\frac{dc}{dk} \tag{4.12}$$

where c is the complex phase velocity. The group velocity controls the amount and direction of energy propagation, see Eq. (4.16), and can be computed from Eq. (4.6) by first differentiating by parts and then premultiplying by $\{\tilde{v}\}^T$

$$\{\tilde{v}\}^T([A]\,k^2 + i[B]\,k + [G] - \omega^2\,[M])\,d\{v\} +$$
$$\{\tilde{v}\}^T((2k\,[A] + i[B])\,dk - 2\,\omega d\omega\,[M])\,\{v\} = 0 \qquad (4.13)$$

The first term must vanish since upon transposition and remembering that $[B]^T = -[B]$ and that the other matrices are symmetric, we obtain

$$\{dv\}^T([A]k^2 - i[B]k + [G] - \omega^2\,[M])\{\tilde{v}\}$$

which is zero since $(-k, \{\tilde{v}\})$ satisfies Eq. (4.6). The remaining term gives

$$U = \frac{d\omega}{dk} = \frac{\{\tilde{v}\}^T(2k^2\,[A] + ik\,[B])\,\{v\}}{2k\omega\,\{\tilde{v}\}^T[M]\,\{v\}} \qquad (4.14)$$

This expression can be further reduced if the mode shapes are normalized according to Waas (1972), i.e.

$$\{\tilde{v}\}^T(k^2[A] - [C])\,\{v\} = 2k^2$$

which by Eq. (4.8), multiplied by $\{\tilde{v}\}^T$ implies that

$$\{\tilde{v}\}^T(2k^2[A] + ik[B])\,\{v\} = 2k^2 \qquad (4.15)$$

Thus the group velocity may be computed by

$$U = \frac{k/\omega}{\{\tilde{v}\}^T[M]\,\{v\}} \qquad (4.16)$$

which was developed by Lysmer and Drake (1972) for real modes but is actually valid for the general case.

Energy Transmission

Each of the Rayleigh modes in the general motion defined by Eq. (4.10) can propagate independently: this would simply correspond to the case when only one of the mode participation factors, α_s, is non-zero. However, if more than one, mode propagating energy is

transmitted between the modes. Thus, the amount of energy transmitted through a vertical plane, say of x=0, depends on the composition of the mode participation factors, α_s, s=1,..., 2n.

This problem has been solved by Waas (1972) who showed that the rate of energy transmission per unit width in the y-direction of x=0 is:

$$E = \frac{\omega}{2} \text{Im} \left[\{U\}^* [R] \{U\} \right] \tag{4.17}$$

where ω is the frequency, Im indicates the imaginary part and $\{U\}$ is the complex amplitudes at x=0. Hence, by Eq. (4.10)

$$\{U\} = \sum_{s=1}^{2n} \alpha_s \{v\}_s = [V] \{\alpha\} \tag{4.18}$$

where $[v]$ is a matrix which contains the mode shapes in its columns and $\{\alpha\}$ is a vector containing the mode participation factors α_s, s=1,...,2n.

The matrix $[R]$ is the transmitting boundary matrix developed by Waas (1972), i.e.

$$[R] = i [A] [V] [K] [V]^{-1} + [D] \tag{4.19}$$

where $[K]$ is a diagonal matrix which contains the waves numbers, k_s, s=1,..., 2n, on the diagonal and $[D]$ is a banded matrix assembled from the layer submatrices

$$[D]_j = \frac{1}{2} \begin{bmatrix} 0 & (M_j^* - 2 G_j^*) & 0 & -(M_j^* - 2 G_j^*) \\ G_j^* & 0 & -G_j^* & 0 \\ 0 & (M_j^* - 2 G_j^*) & 0 & -(M_j^* - 2 G_j^*) \\ G_j^* & 0 & -G_j^* & 0 \end{bmatrix} \tag{4.20}$$

j = 1,..., n. this matrix is related to $[B]$ through $[B] = [D]^T - [D]$.

For the special case of an undamped layered system, it can be shown that real modes transmit the following energy per time unit per

unit width in the y-direction

$$E_s = \pm \frac{1}{2} \omega k_s |\alpha_s|^2 \qquad (4.21)$$

where the sign follows the sign of the group velocity, see Eq. (4.16). In the undamped case complex and purely imaginary modes transmit no energy.

Dispersion curves for the first few real modes of Rayleigh waves in an undamped homogeneous layer over a rigid base are shown in dimensionless form in Fig. 4.5. Since the group velocity is proportional to the slope of these curves only points with positive slope corresponds to waves which propagate energy in the positive x-direction. A more complete picture of the variation of the wave numbers with frequency can be obtained by plotting both the real and imaginary parts of these. This has been done in Fig. 4.6 which corresponds to the same case. In this graph only the spectral lines show as full lines correspond to waves which propagate energy in the positive x-direction. The broken lines correspond to motions which decay in the positve x-direction but transmit no energy.

4.3.2 Layered System over Half Space

The theory summarized above is applicable only to a layered system over a fixed rigid base. Actual sites are more similar to a layered system over a viscoelastic half space. This problem can in principle be overcome by using a very deep model with many sublayers. However, such an approach will lead to very large matrices and thus expensive calculations. Hence, some effective method for better approximating the half-space condition is currently needed. Three methods have been investigated in this research:

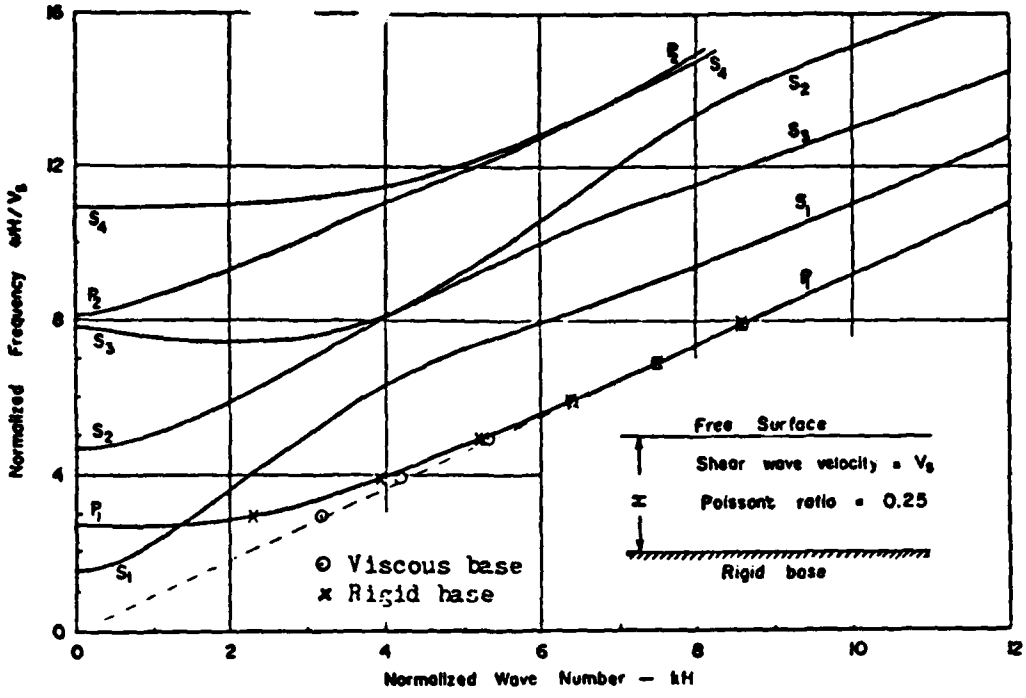

Fig. 4.5 Frequencies of Real Rayleigh Waves in Elastic Layer on Rigid Base

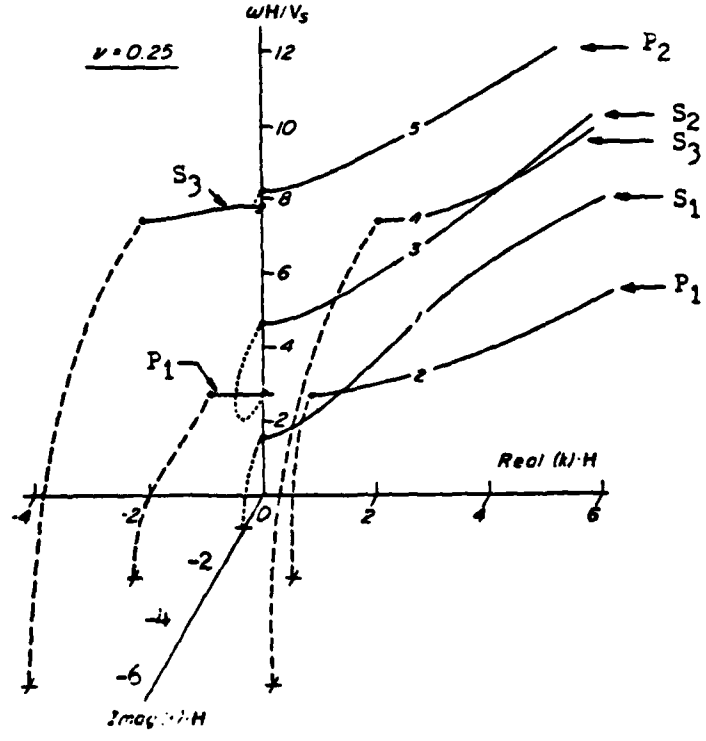

Fig. 4.6 Spectral Lines for Waves with Positive Group Velocity in Homogeneous Elastic Layer over Rough Rigid Base

Viscous Boundary

The first method investigated involved the use of Lysmer-Kuhlemeyer (1969) viscous boundary condition (dashpots) at the bottom of the layered system. According to this method the existence of the lower half space can be simulated by adopting the following relationship between the amplitudes of forces (stresses) and the horizontal, U, and vertical, V, displacements at the interface with the half space

$$\begin{bmatrix} H_c \end{bmatrix} \begin{Bmatrix} U \\ V \end{Bmatrix} = \begin{Bmatrix} \tau_{xz} \\ \sigma_z \end{Bmatrix} \tag{4.22}$$

where

$$\begin{bmatrix} H_c \end{bmatrix} = i\omega\rho \begin{bmatrix} V_s^* & 0 \\ 0 & V_p^* \end{bmatrix} \tag{4.23}$$

and ρ, V_s^* and V_p^* corresponds to the mass density, S-wave and P-wave velocities of the half space, respectively. The above forces can be added to the equation of motion for the n-layer systems. This results in the equation

$$\{[A]\ k^2 - i[B]\ k + ([C] + [H])\}\ \{v\} = \{0\} \tag{4.24}$$

which is similar to Eq. (4.8) except that all matrices now have the dimension $(2n + 2) \times (2n + 2)$. [H] is the expanded matrix

$$[H] = \left[\begin{array}{c|c} 0 & 0 \\ \hline 0 & H_c \end{array}\right] \tag{4.29}$$

For any given frequency, ω, Eq. (4.24) has the same form as Eq. (4.8) and the eigenvalue problem can be solved as for that equation.

The method is hard to justify theoretically since the Lysmer-Kuhlemeyer boundary condition was originally developed for plane

vertically propagating waves and thus implies energy propagation in the vertical direction which does not occur within Rayleigh waves in undamped systems. However, experience with the method has shown a pronounced improvement in the ability of the discretized method to simulate a uniform half space. Some results are shown in Fig. 4.5 which shows (in full lines) dispersion curves computed by Lysmer (1969) for a uniform layer over a rigid base. The dotted line through the origin is the exact solution for a complete half space and the circles indicate points computed using the above viscous boundary condition. The improvement is limited to the lower modes however. Eq. (4.24) predicts higher modes which do not exist in a perfect half space.

Travelling Wave Boundary

When a plane wave travels in the x-direction through a viscoelastic half space the boundary condition at the surface can be shown to be

$$\begin{Bmatrix} \tau_{xz} \\ \sigma_z \end{Bmatrix} = \left[H_e\right] \begin{Bmatrix} U \\ V \end{Bmatrix} e^{-ikx} \tag{4.30}$$

where

$$\left[H_e\right] = \begin{bmatrix} (M^*\bar{A} - ik\lambda^*) & M^*\bar{B} \\ G^*\bar{C} & G^*(\bar{D} - ik) \end{bmatrix} \tag{4.31}$$

and τ_{xz}, σ_z, U and V are the stress and displacement amplitudes at x=0. The constants

$$\begin{aligned} \bar{A} &= kq\,(q - s)/(sq - k^2) \\ \bar{B} &= s\,(k^2 - q^2)/(sq - k^2) \\ \bar{C} &= q\,(k^2 - s^2)/(sq - k^2) \\ \bar{D} &= sk\,(s - q)/(sq - k^2) \end{aligned} \tag{4.32}$$

where $q^2 = k^2 - \omega^2/V_p^{*2}$, $s^2 = k^2 - \omega^2/V_p^{*2}$ are rather complicated functions of k and the above boundary condition cannot be used directly in connection with the discretized method discussed above. However, by expanding the constants in Eq. (4.32) into Maclaurin series about k = 0, the following approximation can be obtained

$$[H_e] \approx [H_a]\, k^2 + i\,[H_b]\, k + [H_c] \tag{4.33}$$

where

$$[H_a] = \frac{i}{2\omega} \begin{bmatrix} (V_s^* + 2v_p^*)\, G^* & 0 \\ 0 & (V_p^* + 2V_s^*)\, M^* \end{bmatrix} \tag{4.34}$$

$$[H_b] = \rho \begin{bmatrix} 0 & (i-1)\, V_s^* + iV_s^*V_p^* \\ (i-1)\, V_p^* + iV_s^*V_p^* - 2V_s^* & 0 \end{bmatrix} \tag{4.35}$$

and $[H_c]$ is the matrix given by Eq. (4.23). As for the case of the viscous boundary discussed above the expanded forms of the matrices in Eq. (4.33) can now be added to the expanded forms of the matrices [A], [B] and [C] for the n-layer system. This results in the following equation of motion

$$\{([A] + [H_a])\, k^2 - i([B] - [H_b])k + ([C] + [H_c])\}\, \{v\} = \{0\} \tag{4.36}$$

This eigenvalue problem can, in principle, be solved and should lead to better solutions for low values of k. However, the matrix $([A] + [H_a])$ is not symmetric and the matrix $([B] - [H_b])$ is not skew-symmetric. Hence, the solution of Eq. (4.36) is considerably more difficult than the eigenvalue problems stated by Eqs. (4.8) or (4.24). Further research needs to be performed to investigate the performance of this approach.

Variable Depth Method

As shown in Fig. 4.1 Rayleigh waves in a uniform half space attenuate rapidly with depth. The table shown in the same figure indicates that for most solids only small amplitudes occur at a depth of 1.5 × the wavelength, λ_r, and at a depth of 2 × the wavelength the amplitudes are insignificant compared to the surface amplitudes. Thus it is to be expected, that the fundamental Rayleigh mode computed from a discretized model with a rigid base at a depth of $H = 1.5\lambda_r$ will be similar to the corresponding wave travelling in a complete half space. This suspicion is confirmed by Fig. 4.5 which shows that for $KH > 2\pi$; i.e. $H > \lambda_r$ the correct wave number is computed from a rigid base model. Further confirming evidence will be presented in Section 4.6.

In a typical layered soil system over a half space it can be assumed that the shear wave velocity of the half space will be larger than the velocity of the fundamental Rayleigh wave. Thus λ_r in the above expression can be safely replaced by λ_s for the half space, and the half space can be simulated by a uniform layer of the thickness $H = 1.5\lambda_s = 1.5\ V_s/\nu$ where ν is the frequency in Hz. Subdividing this layer into 9 sublayers the element height becomes 1/6 Vs/ν which as described in Chapter 3 is sufficiently small to ensure numerical accuracy. Thus, no matter what the frequency the underlying half space can be represented by 9 layers as shown in Fig. 4.4b. As will be discussed in Section 4.6, when the half space extends all the way to the surface or if the surface layers are very soft compared to the half space even better accuracy in the mode shape can be obtained by subdividing the top layer into two equal sublayers as indicated by the dotted line marked "optional" in Fig. 4.4b.

The variable depth method is simple to implement and will be used in the remaining part of this dissertation and in the associated computer programs, SITE and LOVE, which at each frequency automatically adjust the depth of the computational model as indicated in Fig. 4.4b. The method ensures the computation of good lower modes which, as will be discussed below, are the modes of primary interest for the research presented herein.

4.3.3 Mode Selection

Having adopted the variable depth method the motions of a layered system over a uniform half space are given by Eq. (4.10) which unfortunately contains 2n unknown mode participation factors. These can, in principle, be determined by 2n boundary conditions; say by a set of forces acting on the plane x = 0. This was the method used by Waas (1972) to compute the transmitting boundary matrix [R] in Eq. (4.19). Alternatively, the mode participation factors could be computed from 2n given displacement amplitudes at x = 0. This would correspond to solving Eq. (4.18) for $\{\alpha\}$. However, in the usual site response problem, only one control motion and thus only one displacement amplitude is known at each frequency; say the horizontal surface amplitude at x = 0. It is therefore not possible to determine the general motion from a single control motion. A particular solution can be obtained, however, if it is assumed that only the fundamental mode produces the motion at the control point in which case Eq. (4.10) reduces to

$$\{\delta\} = \alpha_f \{v\}_f \, e^{i(\omega t - k_f x)} \tag{4.37}$$

where α_f, $\{v\}_f$ and k_f correspond to the fundamental mode. This is a reasonable approach since it can be expected that, if Rayleigh

waves exist at the site, the fundamental mode is the major contributor to the motion.

Fundamental Mode

Adopting this idea, the remaining problem is to select the fundamental mode from among the 2n solutions to the eigenvalue problem, Eq. (4.8). For an undamped system the fundamental mode will be among the real modes which are the only modes which transmit energy in the x-direction. Among these modes the fundamental mode will be the one with the largest wavenumber k (shortest wavelength, lowest phase velocity). This definition coincides with that used by seismologists. For a homogeneous half space it corresponds to Rayleigh's original wave and the straight part of the dispersion curve P_1 in Fig. 4.5.

The total number of real modes which can exist in a given system depends on the frequency of excitations and the natural frequencies of the system. The latter, which correspond to vertical wave propagation between the free surface and the rigid base, can be determined by solving the eigenvalue problem in ω which results from setting $k = 0$ in Eq. (4.9). For a homogeneous layer over a rigid base these frequencies can be read off at $k = 0$ in Fig. 4.5. In general, at any given frequency, ω, the number of real modes which propagate energy in the positive x-direction will be equal to the number of natural frequencies below this frequency. Thus, for the special case of a homogeneous layer over a rigid base with $H = 1.5\lambda_s$ ($\omega H/V_s = 9.425$) five real modes will exist. This can be seen by counting the number of dispersion curves which intersect the horizontal line $\omega/HV_s = 9.475$ in Fig. 4.5. This observation implies that real modes will always exist when the variable depth method is used. Since the same line

intersects the straight part of curve P_1 in Fig. 4.5, a good fundamental mode will always be computed by this method.

Actual sites cannot be properly modeled by undamped materials. Thus the cases of major interest involve damped layered systems. For such systems the definition and selection of the fundamental mode is a much more complicated matter. As discussed in Section 4.4 all modes are complex, i.e. they have complex wave numbers with negative imaginary parts corresponding to decay in the direction of wave propagation. One can therefore not make a simple statement to the effect that the fundamental mode is the real mode with the largest wave number. On the other hand the introduction of damping does have some simplifying effect on the computations. For example, as discussed in Section 4.4, it does simplify the selection of the 2n appropriate wave numbers (the ones with negative imaginary parts). Also, damping tends to eliminate singularities in transfer functions and dispersion curves. For example, all of the nondifferential points on the dispersion curves shown in Fig. 4.6 will become differentiable points.

With the magnitude of damping which has to be introduced in practical problems the changes in numerical values of wave numbers, mode shapes, etc. from the corresponding values obtained by undamped analysis are not large. This was already indicated by the results presented in Fig. 4.3 which show that mode shapes are virtually unchanged by the presence of damping. As a further illustration of this point a 450 ft homogenous layer over a rigid base was subdivided into 15 sublayers and analyzed by program SITE at different frequencies using four different damping values (β = 0%, 0.001%, 3% and 10%). Computed wave numbers are shown in Table 4.1 which also show the values

for the corresponding undamped half space. At each frequency the number of modes included corresponds to the number of real modes for the undamped systems, as can be seen from the natural undamped frequencies of the system shown below the table. The number of real modes is equal to the number of natural frequencies below the frequency of excitation as discussed above.

The wave numbers shown for the damped cases are those corresponding to low attenuation. These were selected by first ordering all of the modes in order of the least magnitude of the imaginary part of the wave number and then selecting as many as indicated by the undamped case. The argument for this procedure is that if it is true that damping has a small effect on the wave modes then the damped mode corresponding to the fundamental mode in the undamped case (which does not decay) should be among the low attenuation modes for the damped case. That this is indeed so can be seen by comparison of the wave numbers marked by an asterisk in Table 4.1.

It can also be seen from Table 4.1 that among the modes selected the fundamental mode is the one with the largest real part of the wave number. This of course is not surprising in view of the above definition of the fundamental mode for the undamped case.

In view of the above considerations the following procedure, which also serves herein, as the definition of the fundamental mode, has been adopted for selection of the fundamental mode in a damped (or undamped) system:

a) Compute the undamped natural frequencies of the system (by setting k=0 in Eq. 4.6).

Table 4.1 Effect of Damping Ratio on Wave Numbers of R-waves in a Fixed-base System

Freq. (Hz)	H-space $\beta = 0.$	Fixed-base $\beta = 0.$		Fixed-base $\beta = 0.00001$		Fixed-base $\beta = 0.03$		Fixed-base $\beta = 0.1$	
	k_r ($\times 10^{-2}$)	k_r ($\times 10^{-2}$)	k_i	k_r ($\times 10^{-2}$)	k_i ($\times 10^{-7}$)	k_r ($\times 10^{-2}$)	k_i ($\times 10^{-3}$)	k_r ($\times 10^{-2}$)	k_i ($\times 10^{-3}$)
7.5 (3 modes)	1.4509	* 1.4341	0.	0.8140	-1.1548	0.8125	-0.3456	0.7987	-1.1209
		0.8140	0.	0.4483	-1.2726	0.4483	-0.3816	0.4483	-1.2618
		0.4483	0.	* 1.4341	-1.5054	* 1.4335	-0.4518	* 1.4280	-1.5047
12.5 (5 modes)	2.4182	* 2.4062	0.	1.1577	-1.5779	1.1573	-0.4731	1.1534	-1.5638
		1.9672	0.	* 2.4062	-2.3929	* 2.4051	-0.7181	* 2.3947	-2.3931
		1.3138	0.	1.3138	-2.6235	1.3103	-0.7856	1.2727	-2.5512
		1.1577	0.	0.5196	-2.6981	0.5206	-0.8075	0.5284	-2.6299
		0.5196	0.	1.9672	-2.7846	1.9667	-0.8355	1.9621	-2.7806
20.0 (8 modes)	3.8290	* 3.8293	0.	1.8410	-2.4094	1.8408	-0.7218	1.8386	-2.3681
		3.4728	0.	1.9217	-3.4451	1.9188	-1.0292	1.8920	-3.2712
		3.1188	0.	* 3.8293	-3.7668	* 3.8277	-1.1304	* 3.8111	-3.7677
		2.4780	0.	3.4728	-3.7932	3.4714	-1.1383	3.4567	-3.7925
		1.9217	0.	1.3440	-4.3501	1.3512	-1.2927	1.4086	-3.9525
		1.8410	0.	3.1188	-4.3954	3.1178	-1.3189	3.1080	-4.3917
		1.3440	0.	2.4780	-5.1973	2.4754	-1.5634	2.4539	-5.3300
		0.9209	0.	0.9209	-6.3408	0.9220	-1.8853	0.9091	-5.7067

*** Fundamental Rayleigh Mode**

Natural frequencies of the fixed-base system (undamped) - Hz

S-waves : 1.95, 5.84, 9.73, 13.62, 17.51, 21.40,

P-waves : 3.64, 10.92, 18.20,

Model - Fixed base at 450 ft below ground surface

15 sublayers at 30 ft each = 450 ft

V_s= 3502 fps, V_p= 6552 fps, ν = 0.3, γ = 140 pcf

b) Determine m = the number of natural modes below the frequency of excitation.

c) Solve the eigenvalue problem, Eq. 4.8.

d) Sort the modes in order of magnitude of the imaginary part of the wave number.

e) Select from among the first m modes the one with the largest real part. This mode is the fundamental mode.

Experience with the above method for a large range of site conditions has shown that the above procedure and definition of the fundamental mode leads to motions which have all the usual characteristics of fundamental Rayleigh waves; decay with depth, simple mode shape and low phase and group velocity. For the undamped case the definition coincides with that used by seismologists.

Least-Decay Mode

Several other schemes were investigated for selecting the fundamental mode of Rayleigh waves. Among these one method, herein named the least-decay method, deserves some discussion. Consider a typical Rayleigh wave with the wave number $k = k_r + ik_i$, $k_i < 0$. According to the theory presented in Section 4.3 the wave has the wave length $2\pi/k_r$ and it attenuates as $\exp(k_i x)$ in the direction of wave propagation. Hence the decay factor per wavelength is $\exp(2\pi k_i/k_r)$. The ratio $(-k_i/k_r)$ is thus a measure for how fast a wave decays.

It is to be expected that the fundamental mode, which does not decay in the undamped case, will have a very small attenuation for damped cases. The idea thus arose to define, for damped cases, the fundamental mode as the mode with the smallest value of the ratio $(-k_i/k_r)$. This is the least-decay method.

In order to test this method on the case discussed above the modes were sorted according to increasing values of the above ratio. The result of this scheme is shown in Table 4.2 which also shows values of the ratio $(-k_i/(k_r\beta))$. As can be seen from this table the least-decay method works perfectly for this case.

Table 4.2 also illustrates the interesting fact that for all modes the ratio $(-k_i/(k_r\beta))$ is independent of the damping ratio and for the fundamental mode this ratio is near unity. The reason for this follows from the continuum theory for Rayleigh waves in a homogeneous half space presented in Section 4.4. Suppose $\beta_s = \beta_p = \beta$, then simple substitution of complex wave velocities $V_s^* = V_s(1-i\beta)$ and $V_p^* = V_p(1-i\beta)$ into Eq. 4.2 will show that $k_r + ik_i = k(1-i\beta)$, where k is the wave number for the undamped case. Thus, by separation of the real and imaginary part and division, it follows that $-k_i/(k_r\beta) = 1$. The deviation of this ratio from unity in Table 4.2 is therefore a measure of the inaccuracy with which the discretized models represent the half space.

In spite of the good results which the least-decay method achieved in this case it was not adopted as the method for selecting the fundamental mode. This is so because in cases involving a soft highly damped layer over a stiff half space with low damping it does not select a mode which agrees with the definition of the fundamental mode used by seismologists. Rather, it tends to select a mode which corresponds to the classic Rayleigh mode in the half space without the surface layer. This mode may attenuate slower than the fundamental mode but will have a longer wavelength. In fact, as will be explained in Chapter 5, this least-decay mode may be of more interest to engineers than the fundamental mode.

Table 4.2 The Least Decay Method

Damping Ratio	β = 0			β = 0.0001			β = 0.03			β = 0.1		
Frequency	k_r ($\times 10^{-2}$)	k_i	$\frac{-k_i}{k_r\beta}$	k_r ($\times 10^{-2}$)	k_i ($\times 10^{-7}$)	$\frac{-k_i}{k_r\beta}$	k_r ($\times 10^{-2}$)	k_i ($\times 10^{-3}$)	$\frac{-k_i}{k_r\beta}$	k_r ($\times 10^{-2}$)	k_i ($\times 10^{-3}$)	$\frac{-k_i}{k_r\beta}$
7.5 Hz	1.4341	0.	0.	1.4341	-1.5054	1.051	1.4335	-0.4518	1.051	1.4280	-1.5047	1.054
	0.8140	0.	0.	0.8140	-1.1548	1.419	0.8125	-0.3456	1.418	0.7987	-1.1209	1.403
	0.4483	0.	0.	0.4483	-1.2726	2.839	0.4483	-0.3816	2.837	0.4483	-1.2618	2.815
12.5 Hz	2.4062	0.	0.	2.4062	-2.3929	0.994	2.4051	-0.7181	0.995	2.3947	-2.3931	0.999
	1.9672	0.	0.	1.1577	-1.5779	1.363	1.1573	-0.4731	1.363	1.1534	-1.5638	1.356
	1.3138	0.	0.	1.9672	-2.7846	1.416	1.9667	-0.8355	1.416	1.9621	-2.7806	1.417
	1.1577	0.	0.	1.3138	-2.6235	1.997	1.3103	-0.7856	1.998	1.2727	-2.5512	2.005
	0.5196	0.	0.	0.5196	-2.6981	5.193	0.5206	-0.8075	5.170	0.5284	-2.6299	4.977
20.0 Hz	3.8293	0.	0.	3.8293	-3.7668	0.984	3.8277	-1.1304	0.984	3.8111	-3.7677	0.989
	3.4728	0.	0.	3.4728	-3.7932	1.092	3.4717	-1.1383	1.093	3.4567	-3.7925	1.097
	3.1188	0.	0.	1.8410	-2.4094	1.309	1.8408	-0.7218	1.307	1.8386	-2.3681	1.288
	2.4780	0.	0.	3.1188	-4.3954	1.409	3.1178	-1.3189	1.410	3.1080	-4.3917	1.413
	1.9217	0.	0.	1.9217	-3.4451	1.793	1.9188	-1.0292	1.788	1.8920	-3.2712	1.729
	1.8410	0.	0.	2.4780	-5.1973	2.097	2.4754	-1.5634	2.105	2.4539	-5.3300	2.172
	1.3440	0.	0.	1.3440	-4.3501	3.237	1.3512	-1.2927	3.189	1.4086	-3.9525	2.806
	0.9209	0.	0.	0.9209	-6.3408	6.885	0.9220	-1.8853	6.816	0.9091	-5.7067	6.277

4.4 Love Waves

Love waves which are of the form

$$u_y = U(z) \exp i(\omega t - kx) \tag{4.25}$$

with $u_x = u_z = 0$ can exist only in layered systems. The simplest case involving a layer of thickness H over an elastic half space has been studied by Love (1927) and Bullen (1963). Continuum methods for the evaluation of Love wave mode shapes and wave numbers in undamped multi-layered systems over a half space have been presented by Haskell (1953) and Ewing et al (1957).

As was the case for Rayleigh waves infinitely many generalized (complex) Love modes can exist in a layered system. However, at any given frequency real modes, which are the only ones usually considered by seismologists, can exist only when the material properties satisfy certain relations.

For multi-layered viscoelastic systems the mode shapes and wave numbers are most conveniently evaluated by discretized methods similar to that used for Rayleigh waves above. Such a method has been described by Lysmer and Waas (1970) and Waas (1972). As was the case for Rayleigh waves this method assumes linear variation of displacements within layers and the existance of a rigid base at some finite depth which can be varied with frequency to ensure proper simulation of a half space.

For an n-layer system of the type shown in Fig. 4.7 the method leads to the equation of motion

$$([A]k^2 + [G] - \omega^2[M])\{v\} = \{0\} \tag{4.26}$$

where [A], [G] and [M] are symmetric n × n matrices which may be assembled from sublayer matrices as shown in Fig. 3.23 for the case of SH-waves, except that the last row and column of each total matrix are

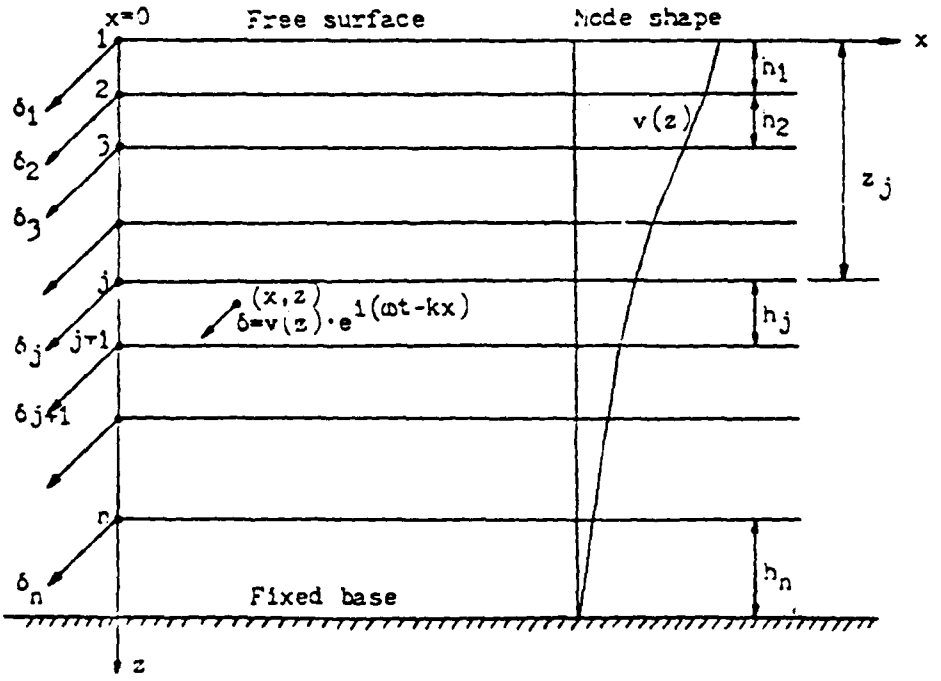

Fig. 4.7 Layered Model for Love Wave Case

not used because of the rigid base assumption. The submatrices are defined by Eqs. (3.72) to (3.75).

Equation (4.26) states an eigenvalue problem similar to, but simpler than, Eq. (4.8) for Rayleigh waves. For any given frequency, ω, this problem can be solved by standard methods for the n eigenvalues k_s^2, s = 1,..., n and corresponding mode shapes, $\{v\}_s$. Assuming a small amount of damping each eigenvalue will lead to a pair of complex wave numbers $\pm k_s$. Since only waves which decay in the x-direction are of interest, the wave numbers with negative imaginary parts are retained and the complete solution can be written as a linear combination of the remaining modes

$$\{\delta\} = \sum_{s=1}^{n} \alpha_s \{v\}_s \, e^{i(\omega t - k_s x)} \tag{4.27}$$

where $\{\delta\}$ is a vector containing the displacements at the layer interfaces and α_s, s = 1,..., n, are unknown mode participation factors.

As was the case for Rayleigh waves these factors cannot be determined from a single control motion. However, by assuming that only the fundamental mode (selected as described above for Rayleigh waves) exists Eq. (4.27) reduces to

$$\{\delta\} = \alpha\{v\} \, e^{i(\omega t - kx)} \tag{4.28}$$

and the mode participation factor can be determined.

The non-vanishing strain amplitudes in the jth layer are

$$\begin{aligned} \gamma_{xy} &= -\frac{1}{2} k\alpha \, (v_{j+1} + v_j) \, e^{ikx} \\ \gamma_{zy} &= \alpha \, \frac{v_{j+1} - v_j}{h_j} \, e^{ikx} \end{aligned} \tag{4.29}$$

These values, at x=0, may be used to evaluate the maximum shear strain in each layer when iterating on the soil properties according to the equivalent linear method.

The group velocity of Love waves may be computed from Eq. (4.16); except that $\{\tilde{v}\}^T$ in this formula should be replaced by $\{v\}^T$.

A computer program, LOVE, has been developed to perform the required computations not just for a single frequency but for transient motions as explained in Chapter 5.

4.5 Numerical Examples

In order to verify the Rayleigh wave and Love wave solutions produced by programs SITE and LOVE, respectively, these programs have been applied to several problems for which exact solutions have been published. Numerical examples are also presented which illustrates the sensitivity of the results to variations in material properties and geometrical conditions.

4.5.1 Uniform Half Space

The exact solution for Rayleigh waves in an undamped uniform half space is readily available and was presented in Section 4.2. The exact mode shapes for Poisson's ratio equal to 0.25 and 0.45 are shown as solid lines in Fig. 4.8 which also shows several fundamental mode solutions obtained by program SITE.

The first solution, dashed line, for Poisson's ratio equal to 0.25 was obtained from a model which consisted of nine sublayers of equal thickness. The depth to the rigid base was 1.5 times the wavelength of shear waves. The solution is generally good except near the free surface where the piecewise linear approximation is too coarse to model the curvature of the exact mode shape. This problem can be overcome by

subdividing the top layer(s) as shown by the other two solutions for the case of Poisson's ratio equal to 0.25.

As Poisson's ratio approaches 1/2 the discretized method tends to overestimate the vertical displacements. As can be seen from Fig. 4.8 the error is about 15% for Poisson's ratio equal to 0.45. This error can probably be reduced by further subdivision and the choice of a deeper rigid base. However, the error appears to be related to the well-known problems associated with the use of the finite element method for plane strain problems with high Poisson's ratio. In any case the error has been judged acceptable for engineering applications. The phase velocity predicted by program SITE is in excellent agreement with the exact value for all the models used.

It is clear from the above results that as far as the fundamental mode is concerned a ten-layer model with the fixed base at a depth of 1.5 × the wavelength of shear waves provides an excellent approximation to an elastic half space.

4.5.2 Single Layer over Half Space

The characteristics of Rayleigh waves in an undamped system consisting of a single layer over an elastic half space have been studied by Mooney and Bolt (1966). The physical model with the notation used for system properties is shown in Fig. 4.9. The curves shown in Figs. 4.10-4.12 are the solutions produced by Mooney and Bolt for the ratio between horizontal and vertical displacements at the ground surface, phase velocity and group velocity, respectively. In these graphs, T is the period of the motion and B_2/B_1 ($= V_s/V_s'$) the shear wave velocity contrast between the half space and the surface layer. The solutions correspond to the special case: $\gamma = \gamma' = 0.25$, $\gamma = 162.5$ pcf, $\gamma' = 125$ pcf (i.e. $\rho/\rho' = 1.3$).

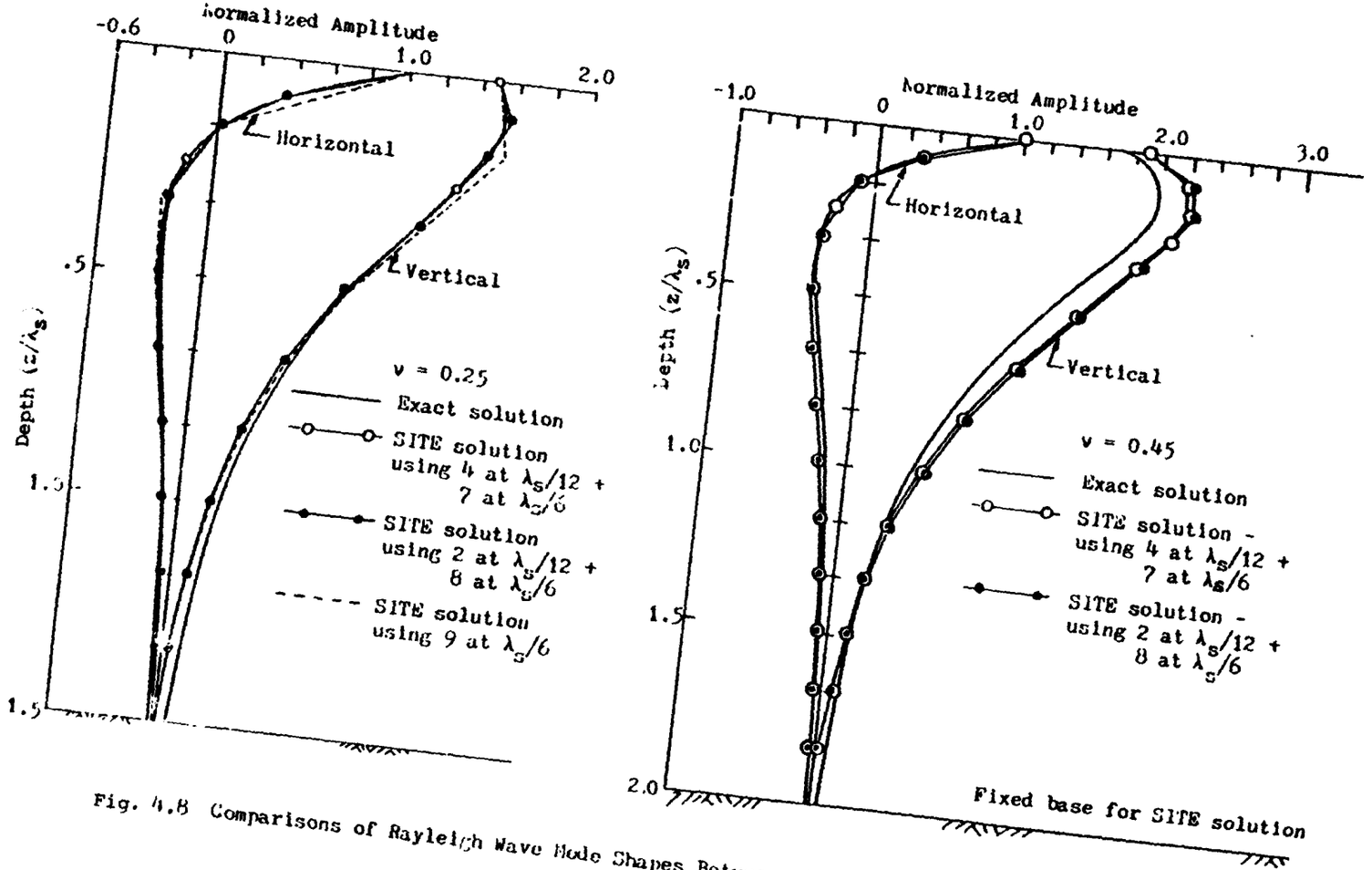

Fig. 4.8 Comparisons of Rayleigh Wave Mode Shapes Between The Exact Solution and The SITE Solution

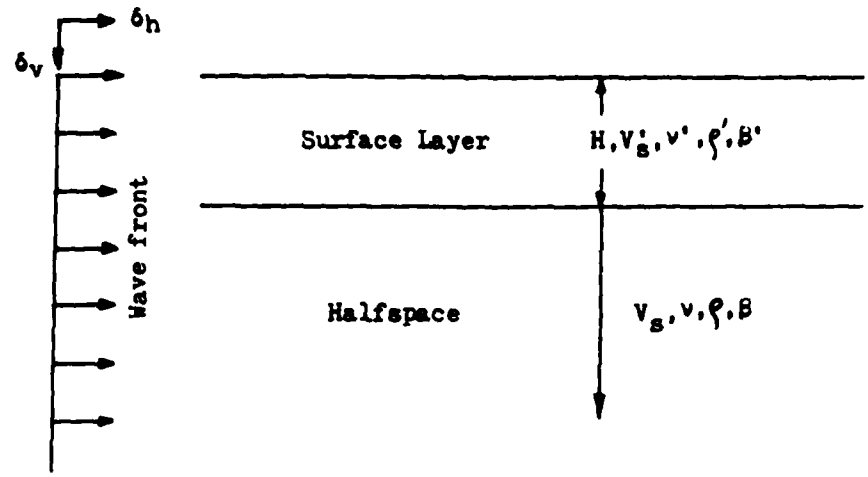

Fig. 4.9 Computational Model

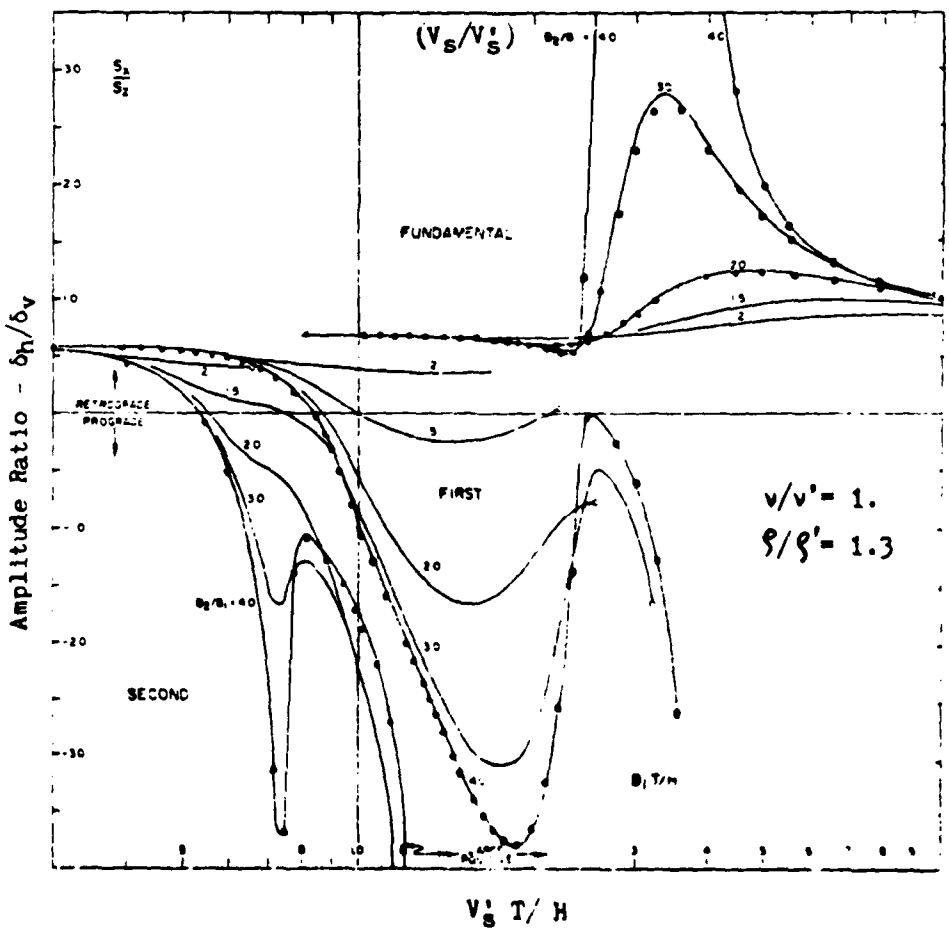

Fig. 4.10 Amplitude Ratio Versus Shear Wave Velocity Rario
($\nu = \nu' = .25$, $\gamma = 162.5$ pcf, $\gamma' = 125$ pcf)

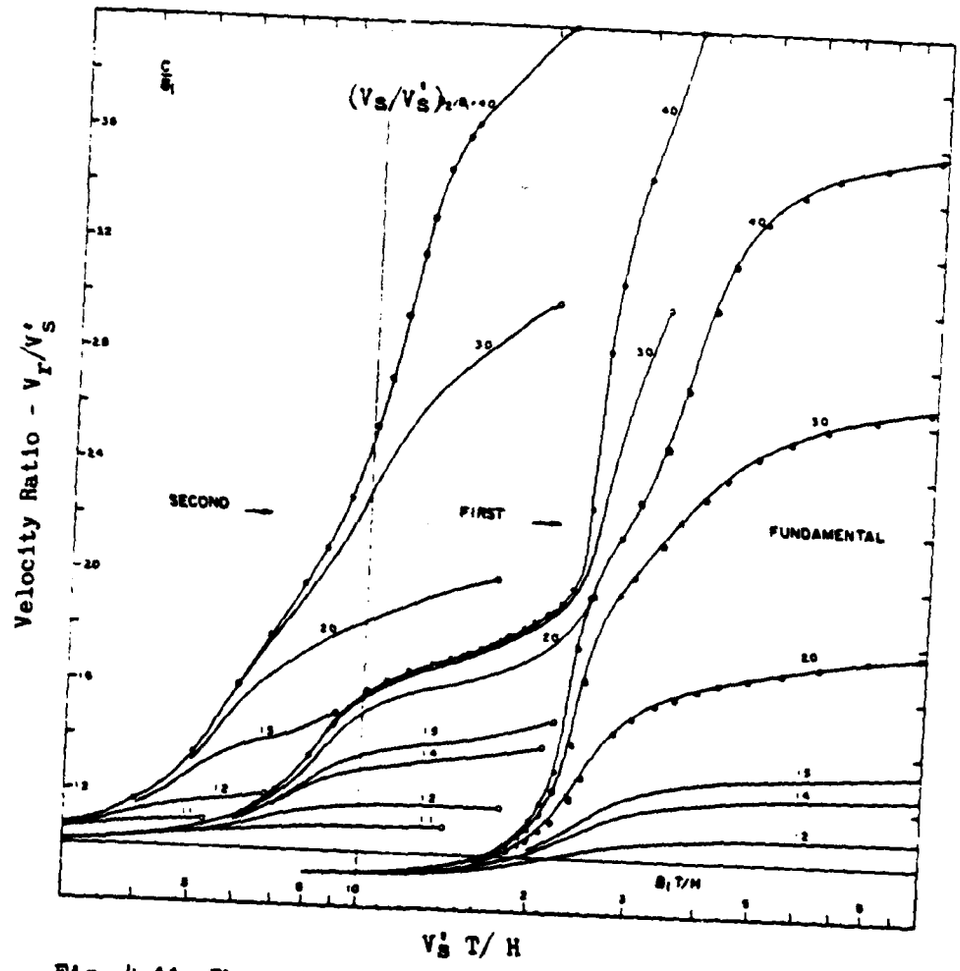

Fig. 4.11 Phase Velocity Versus Shear Wave Velocity Ratio
($\nu = \nu' = 0.25$, $\gamma = 162.5$ pcf, $\gamma' = 125$ pcf)

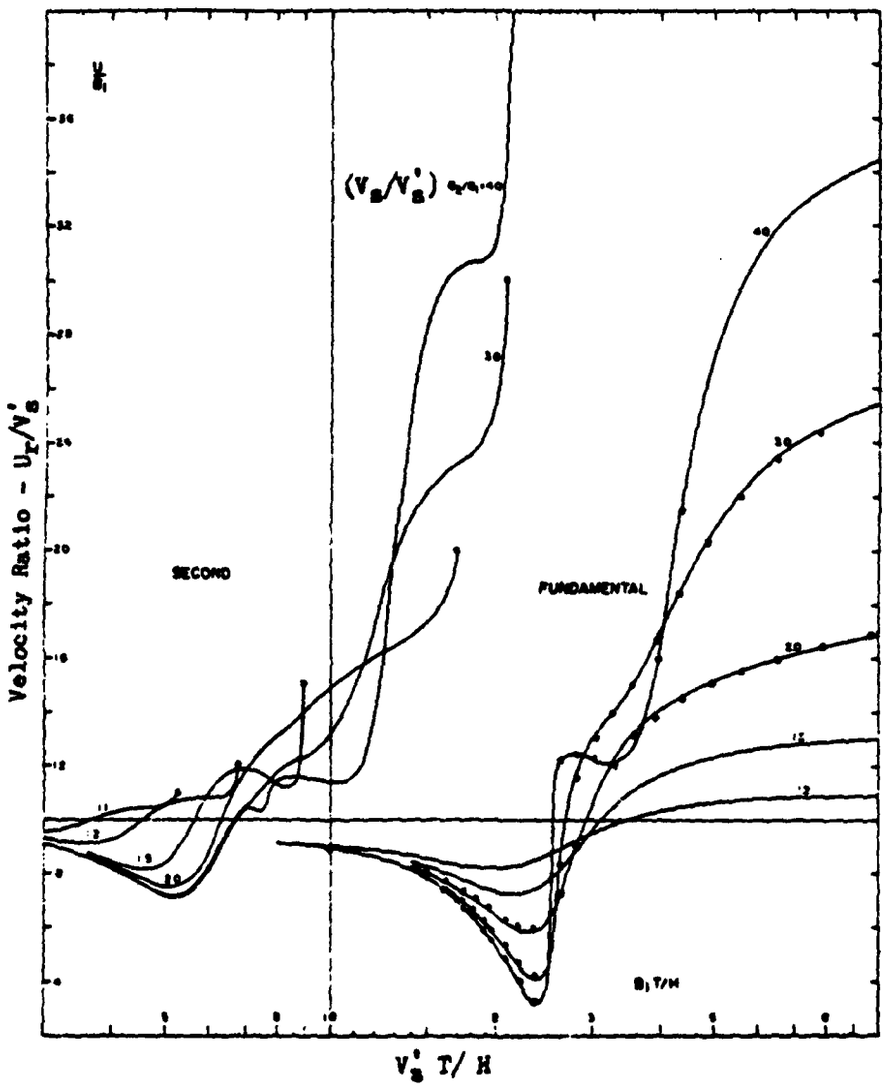

Fig. 4.12 Group Velocity Versus Shear Wave Velocity Ratio
($\nu = \nu' = 0.25$, $\gamma = 162.5$ pcf, $\gamma' = 125$ pcf)

Discretized models were prepared for these values of the S-wave velocity ratio, $V_s/V_s' = 2.0$, 3.0 and 4.0. In each case the surface layer was modeled by 18 sublayers and the half space was handled by the variable depth method. These models were then analyzed using program SITE. The results obtained are indicated by dots in Figs. 4.10-4.12. They are in excellent agreement with the exact solution and clearly demonstrate the adequacy of the discrete method and the associated variable depth method for layered systems over half spaces even for modes beyond the fundamental mode.

The equivalent problem in terms of Love waves has been studied by Stoneley (1955). His model is shown in Fig. 4.13 which also shows the discretization for the surface layer used for the corresponding discretized model. The half space was modeled by the variable depth method with 10 sublayers. In Fig. 4.14 Stoneley's exact dispersion curves for this case are compared with points obtained from the discretized model using program LOVE. Again, excellent agreement was obtained.

4.5.3 Two Layers over Half Space

Stoneley (1957) also studied the propagation of Rayleigh waves in an undamped system consisting of two layers over a half space.

His model for Rayleigh waves is shown in Fig. 4.15 which also shows the discretization used in the corresponding SITE model. The variable depth method was used to simulate the half space. Figure 4.16 shows computed amplitude ratios at the ground surface, phase velocities and group velocities for the fundamental mode. The agreement between the exact solution and the discretized solution produced by program SITE is excellent.

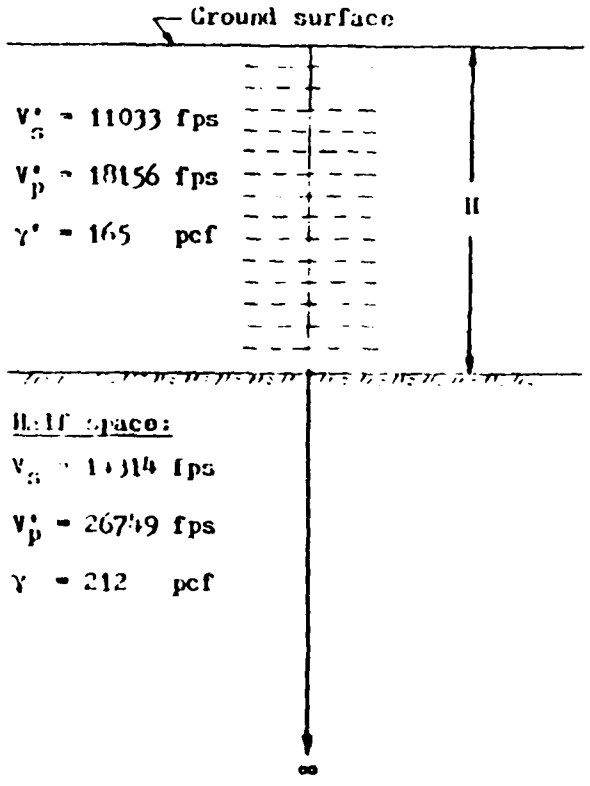

Fig. 4.13 An Uniform Elastic Layer Over an Elastic Half-space

Stoneley's Love Wave Model

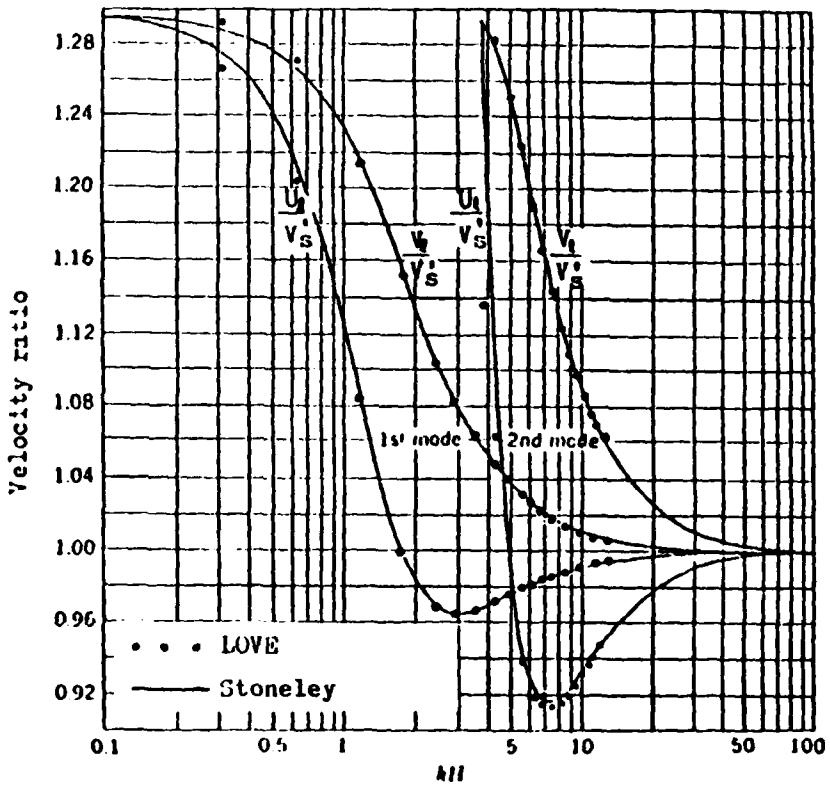

Fig. 4.14 Phase and Group Velocity Curves for First and Second-mode Love Waves for Case V_s/V_s'=1.297

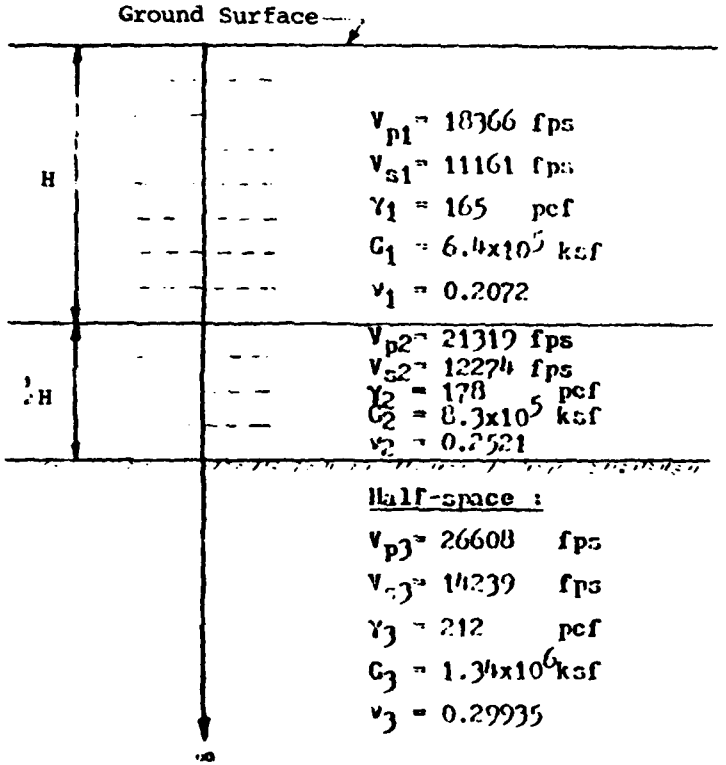

Fig . 4.15 Two Layers on Elastic Half-space
Stanley's Rayleigh Wave Model

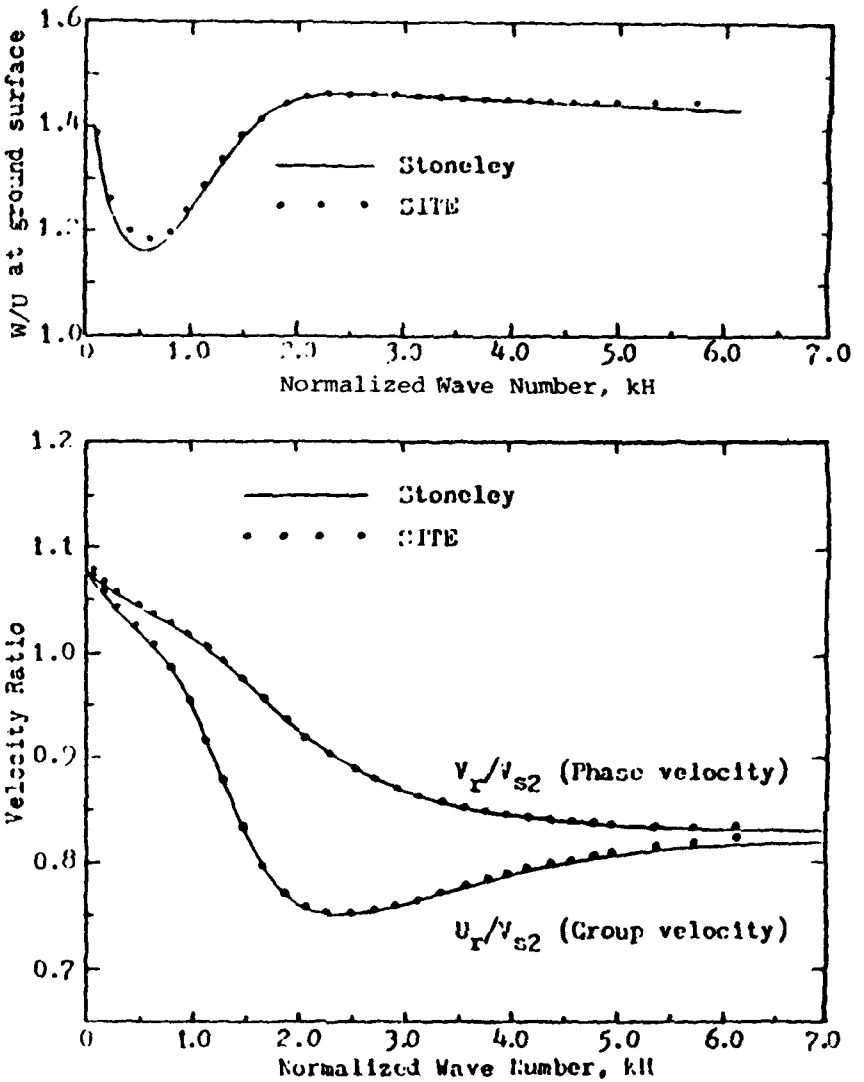

Fig. 4.16 Comparison of SITE Solution and Stanley Solution

CHAPTER 5

EXAMPLES OF SITE RESPONSE ANALYSIS

5.1 Introduction

In this chapter, the steady state methods presented in Chapters 3 and 4 will be applied to solve a number of transient site response problems of the general type shown in Fig. 5.0. The results presented have been selected to illustrate the major effects of horizontal wave propagation in the form of fundamental mode surface waves or inclined body waves.

In all cases the site is assumed to be horizontally layered and to be underlain by a homogeneous half space. For cases involving surface waves this half space is modeled by the variable depth method, see Section 4.4.2.

All materials are assumed to be isotropic and viscoelastic. Nonlinearitics are approximated by the equivalent linear method, see Section 2.5. This implies that the possibility of complete failure and large permanent deformations of the site are not considered.

The sites investigated include a typical rock site, a cohesionless (sand) site and a typical alluvial site with high ground water level and alternating layers of sands, silts and clays. Some of these sites are related to the soil-structure interaction problems discussed in Chapter 6. Although horizontal wave propagation is the main theme of this chapter, all sites have been analyzed, using standard deconvolution procedures (Program FLUSH), for the special case of vertically incident body waves. Since these are well-known procedures, results will be presented without futher comments in the following section whenever a

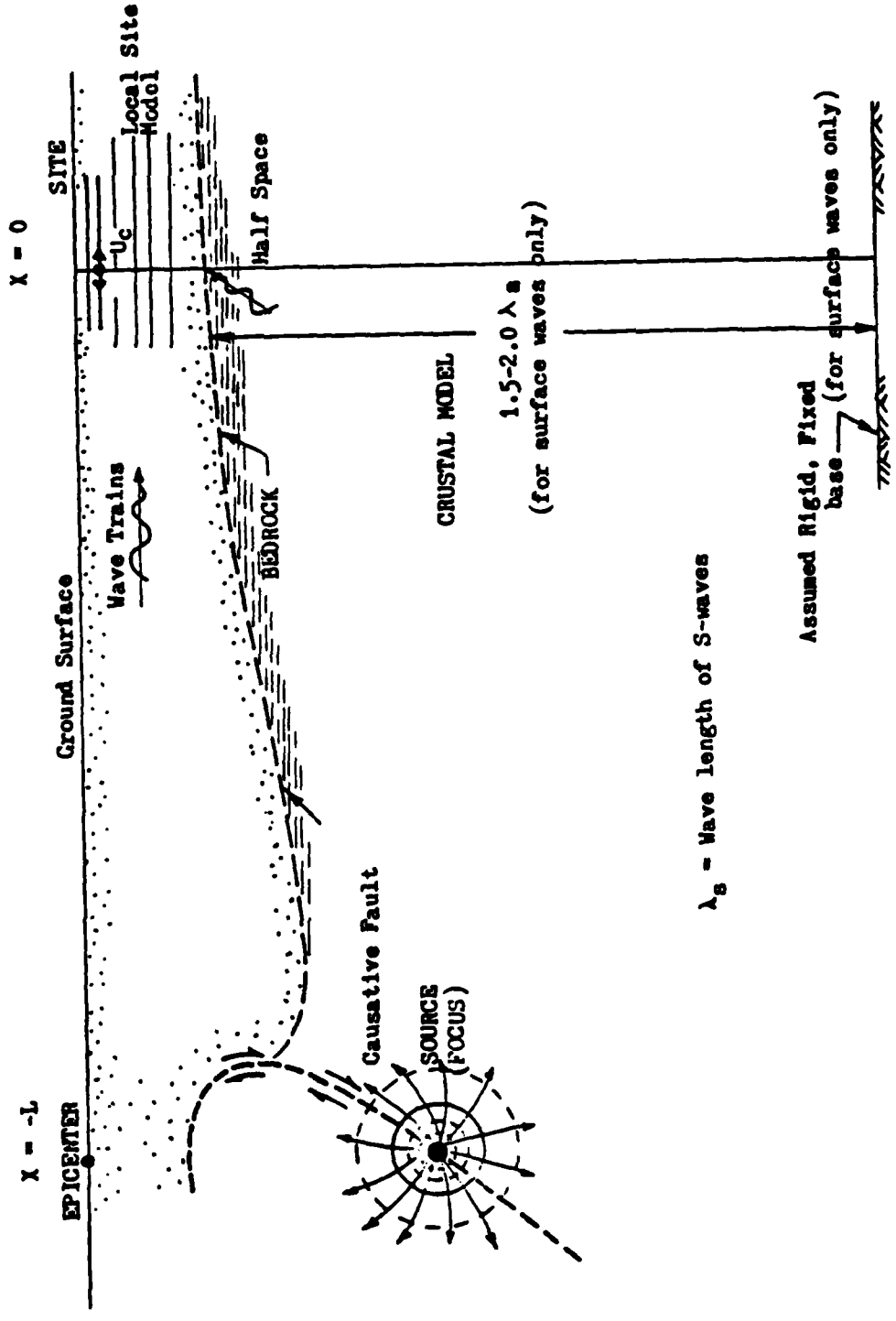

Fig. 5.0 Idealized Local Site Model and Crustal Model for Site Response Analysis

comparison is warranted. Such results will be identified in graphs by the notation; "S-wave" or "P-wave" whatever the case may be.

5.2 Transient Motions

All of the methods described in the previous chapters have been limited to steady state harmonic motions. The remaining part of this dissertation will be dealing with transient motion of finite duration which better model earthquake motion. This transition is achieved through the use of Fourier techniques which involve a discrete Fourier transform, complex transfer function and interpolation on the latter in the frequency domain. This technique, known as the complex response method, has been used extensively in recent years and has previously been described by Schnabel et al (1973), Lysmer et al (1974, 1975) and Idriss et al. (1973).

5.2.1 The Fast Fourier Transform

The basic input to any seismic analysis is a digitized control motion, y(t), which will be assumed to be given at N (even) points at the uniform time interval Δt. Under these conditions the control motion can be written

$$\ddot{y}(t) = \mathrm{Re} \sum_{s=0}^{N/2} \ddot{Y}_s e^{i\omega_s t} \tag{5.1}$$

where

$$\omega_s = \frac{2\pi s}{N \cdot \Delta t} \quad , \quad s=0,1,\ldots, \frac{N}{2} \tag{5.2}$$

The differentiable function defined by Eq. (5.1) may be thought of as a smooth interpolation function between the given points of the control motions.

Equation (5.1) is a truncated Fourier series which implies that the function $\ddot{y}(t)$ is periodic with the period $T = N \cdot \Delta t$. Actual earthquakes are not periodic. However, this problem can be handled by adding a "quiet zone" consisting of a limited number of zeroes to the given control motion, Schnabel (1972); thus increasing N (and T). If the quiet zone is sufficiently long the strong motion occuring at the beginning at each cycle will decay because of material damping before the beginning of the next cycle. Thus the response within each cycle is virtually identical to that of a single earthquake.

The complex coefficients, $\ddot{Y}s$, in Eq. (5.1) can be computed from the given values, $\ddot{y}_k = \ddot{y}\ (k \cdot \Delta t)$, $k = 0,1,\ldots, N-1$, of the control motion. By choosing the length of the quiet zone such that N is a power of 2 this can be done extremely efficiently by the Fast Fourier Transform algorithm developed by Cooley and Tukey (1965). The inverse version of this algorithm can be used to convert from frequency domain to time domain, i.e. to compute the $\ddot{y}_k$ values from the $\ddot{Y}_s$ values.

In seismic applications it is usual to neglect the first term of the sum in Eq. (5.1). This is equivalent to assuming that the control motion has a zero mean value.

5.2.2 The Complex Response Method

According to the complex response method the response of any linear system to the real excitation defined by Eq. (5.1) can be determined as the real part of the response of the system to the complex excitation

$$\ddot{y}(t) = \sum_{s=1}^{N/2} \ddot{Y}_s e^{i\omega_s t} \qquad (5.3)$$

which simply states that the excitation is a finite sum of harmonic excitations.

Using the methods developed in the previous chapters the response of any point to each of these harmonics can be expressed in the form

$$\ddot{U}_s = H(\omega_s)\, \ddot{Y}_s \tag{5.4}$$

where $\ddot{U}_s$ is a complex amplitude and $H(\omega_s)$ are discrete values of a smoother transfer function.

Since superposition is valid for linear systems the real response in the time domain is

$$\ddot{U}(t) = \mathrm{Re} \sum_{s=1}^{N/2} \ddot{U}_s e^{i\omega_s t} \tag{5.5}$$

which is similar to Eq.(5.1) and can be evaluated by the inverse Fast Fourier Transform algorithm.

Since the number, N, of points in the time domain is typically 1024 or 2048, up to 1024 values are needed for the transfer functions $H(\omega_s)$. However, since these functions are smooth only 30-40 points need actually to be determined by the rather complicated methods described in the previous chapters. The intermediate points can be obtained by a special interpolation technique in the complex plane, Lysmer et al (1975).

5.3 Linear Rock Site

The first site considered consists of a 50 feet layer of well-cemented sandstone over harder bedrock. Typical properties for such a site are shown in Table 5.1. These properties were assumed to be independent of shear strain amplitude. Thus the analysis discussed in this chapter is linear.

5.3.1 Computational Model

In the computational model the upper 370 ft of the site were represented by 13 sublayers as indicated in Table 5.1. The half space below this depth was handled by the variable depth method as described in Chapter 4. This resulted in a computational model with a total of 23 sublayers. Details of the discretization are shown in Fig. 5.3. This discretization easily satisfies the requirements discussed in Section 3.4.2 up to a frequency of 20 Hz which was the cut-off frequency for all analyses discussed in this chapter.

Table 5.1 Properties of Linear Rock Site

Main Layer	Thickness (ft)	No Sublayers	V_s (fps)	V_p (fps)	Damping Ratio
1	40	5	3600	2900	0.02
2	10	1	3900	6100	0.02
3	320	7	5600	6600	0.02
half space	varies	10	5600	8700	0.02

All unit weights are 150 pcf.

5.3.2 Control Motion

The control point is at the ground surface at x=0. The horizontal control motion has a maximum acceleration equal to 0.75g. Its time history of acceleration is shown in Fig. 5.1. As can be seen from the upper part of this figure the motion has a broad-band spectrum which fits approximately an NRC-type design spectrum. In the computations discussed below a total of 4096 points (Δt=0.01) were used in the Fast Fourier computations, and frequencies above 20 Hz were not considered. As a result of this low-pass filtering, the computational maximum acceleration was 0.76 g.

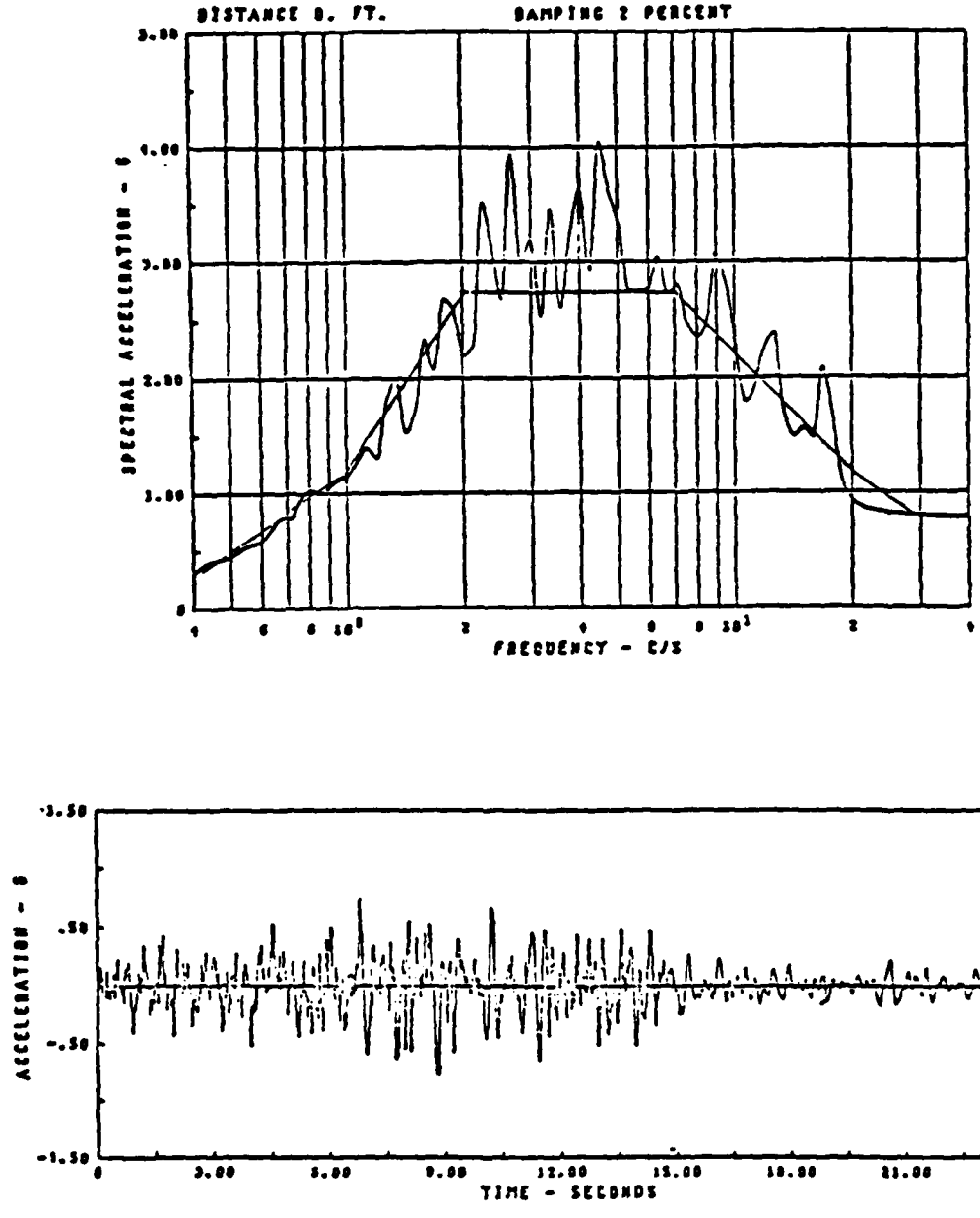

Fig. 5.1 The Control Motion and Its Response Spectrum

5.3.3 Strain Compatibility

The above control motion is extremely strong. Hence, the appropriativeness of a linear analysis for this case might be questioned. Actually, the following comments will confirm that for practical purposes the linear approach is quite appropriate.

While our current knowledge of the behavior of rock at large strain amplitudes is sketchy, approximate relationships between effective dynamic shear modulus, damping ratio and shear strain amplitude have been established. Typical relationships of this type are shown in Fig. 5.2 which also shows the effective shear strain range computed for the linear rock site. It may be seen from this figure and also from the strain compatible properties shown in Fig. 5.3 that the maximum nonlinear effects amount to a 15% reduction in the effective shear modulus and a 50% reduction in the damping ratio assumed for this site. These effects are within the range of accuracy with which engineers can currently determine these properties in the field. Hence, it may be argued that a nonlinear analysis for this case would be a purely academic exercise and that the likely changes in the results from those obtained by a linear analysis would be small. Nevertheless, an attempt to evaluate the maximum nonlinear effects for this site will be made in Section 5.4.

5.3.4 Steady State Results

Before discussing the transient motion results it is interesting to study the behavior of steady state fundamental Rayleigh waves on the site.

The dispersion curves shown in Fig. 5.4 are nearly constant in the frequency range of interest. This indicates that the site behaves

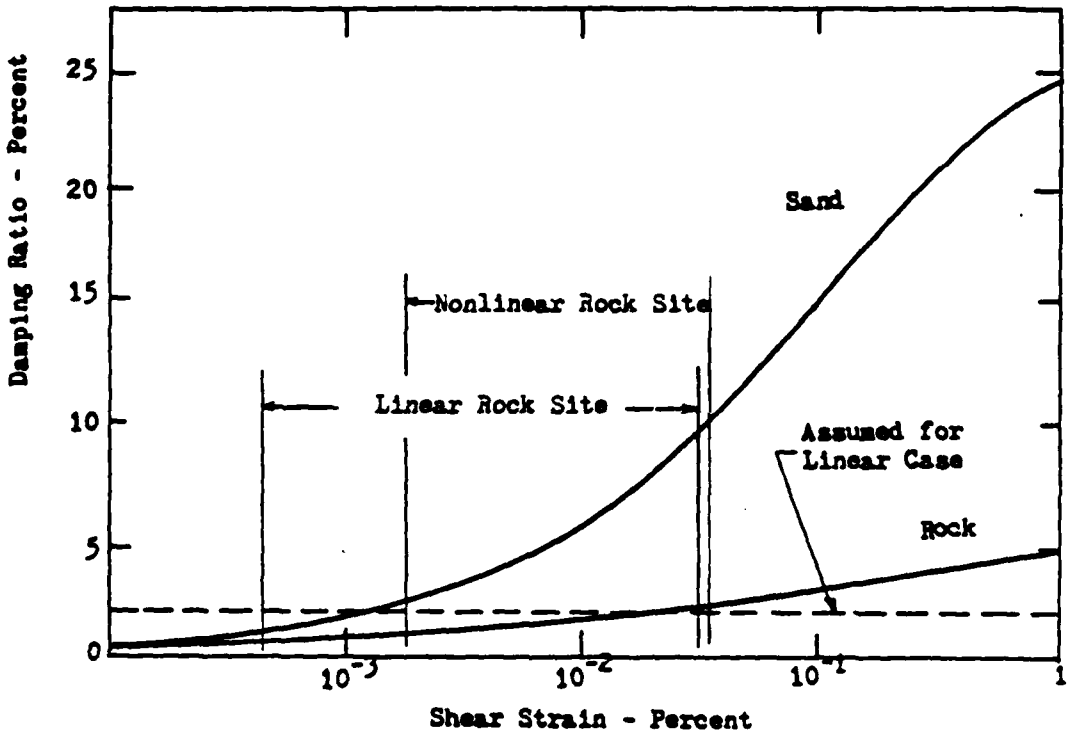

Fig. 5.2a Variation of Damping Ratio with Shear Strain

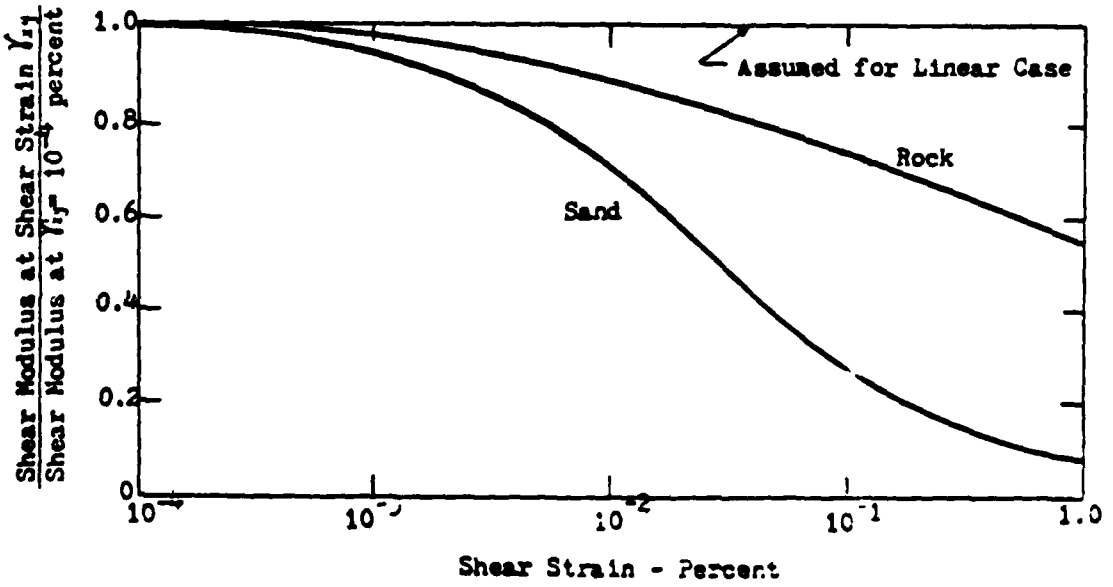

Fig. 5.2b Variation of Shear Modulus with Shear Strain

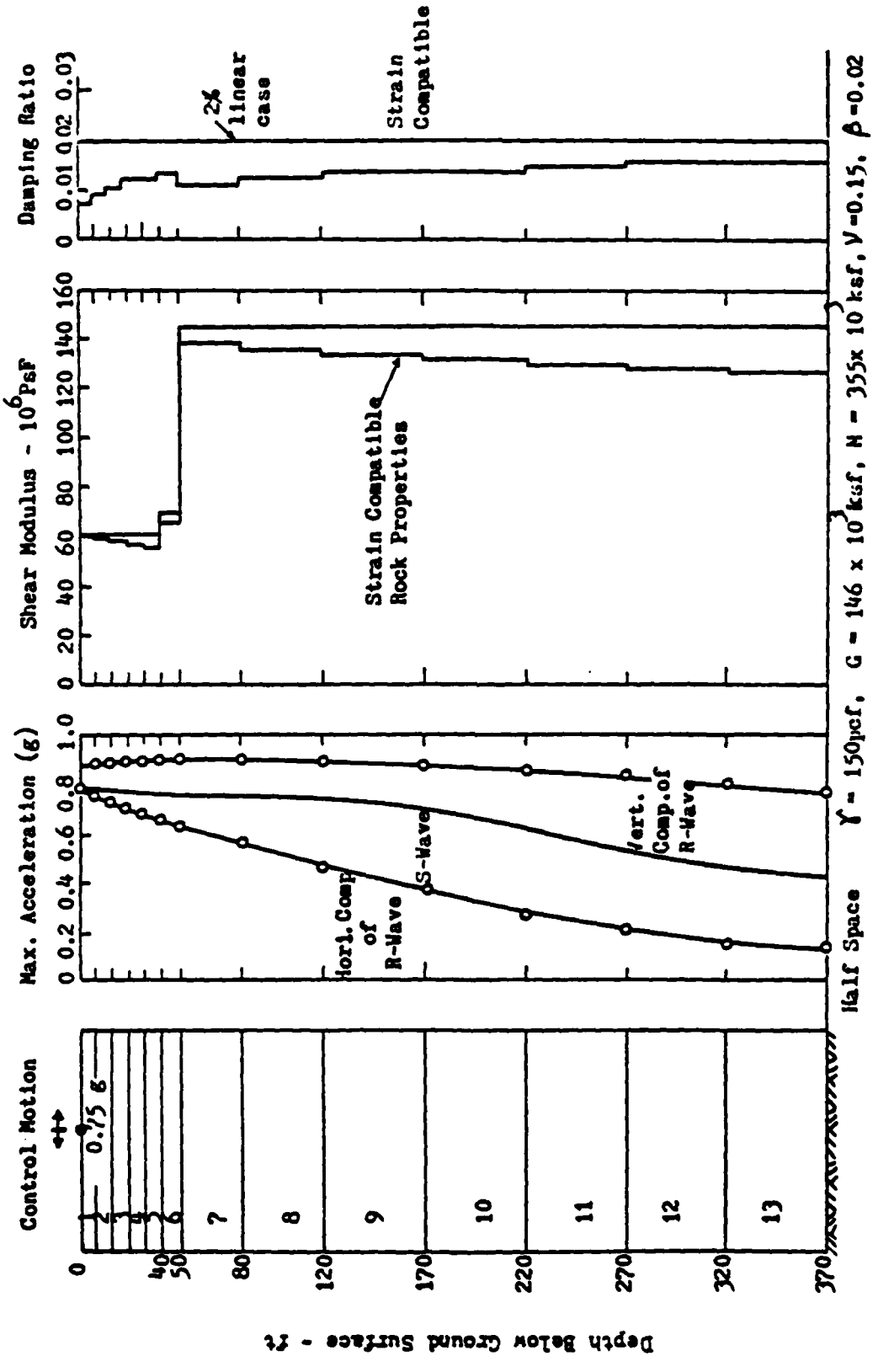

Fig. 5.3 Analysis of Rock Site

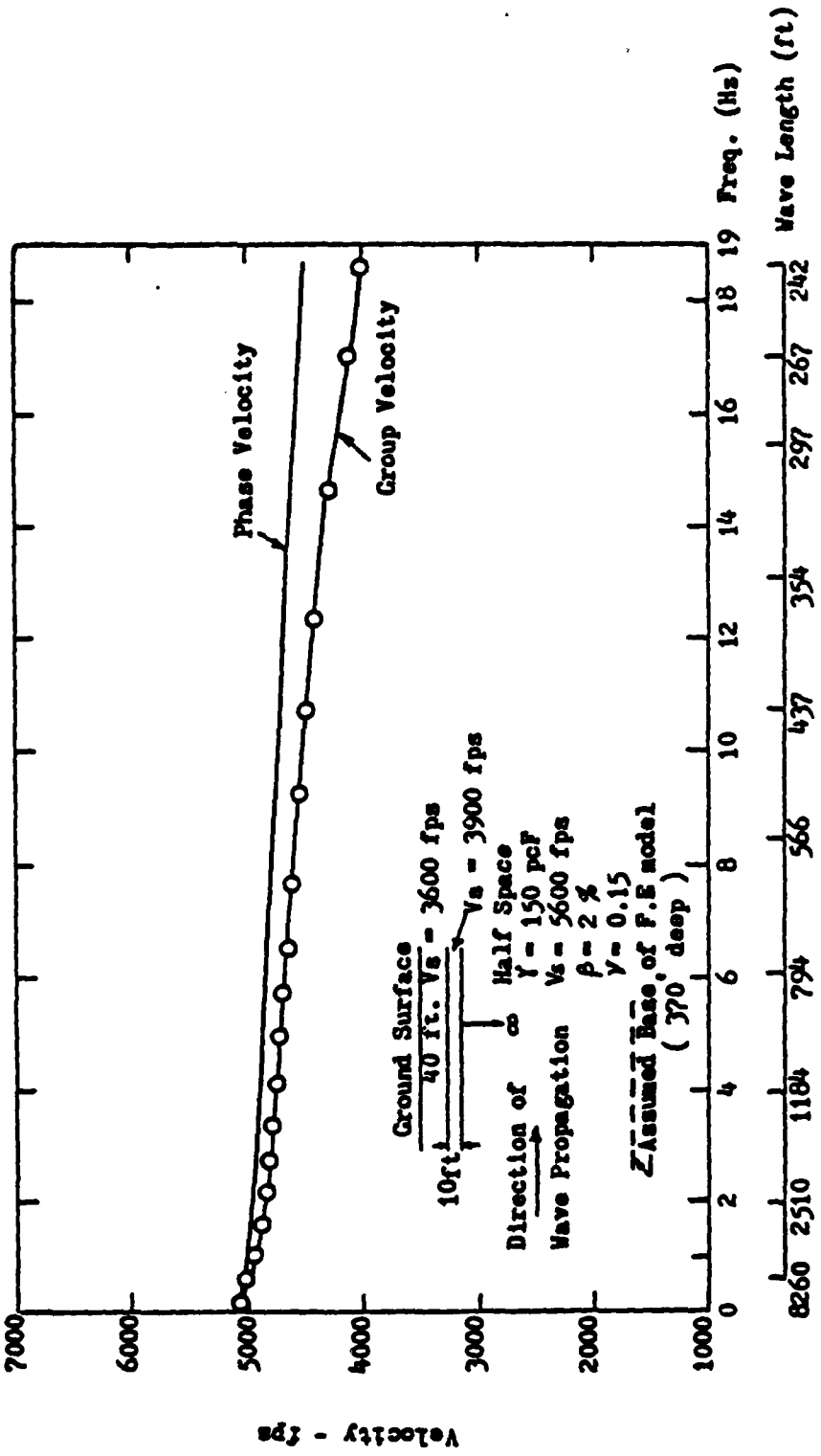

Fig. 5.4 Rayleigh Wave Dispersion Curves for Linear Rock Properties

essentially like a uniform half space with the properties of the bedrock. This is not surprising since the wavelength of the shortest Rayleigh wave is about five times the thickness of the weathered crust.

As expected the mode shapes of the Rayleigh waves, shown in Fig. 5.5, are similar to those observed for a half space. Their depth of penetration is inversely proportional to frequency and motions below a depth of one wavelength are insignificant.

5.3.5 Transient Results

The computed variations of maxumum accelerations with depth below the control point are shown in Fig. 5.3 for both the case of pure Rayleigh wave excitation and the case of vertically incident shear waves. The variation is typical for what would be expected for a half space. The horizontal motions are lower than the vertical motions. Also, they attenuate faster with depth than those determined from the S-wave analysis.

The variation of frequency content with depth is illustrated by the response spectra shown in Fig. 5.6. Within the upper part of the site the frequency distributions of the Rayleigh wave motion do not differ greatly from that determined from S-wave analysis. At greater depth the vertical R-wave components predominate. They are longer than those determined by S-wave analysis especially in the low frequency range.

As discussed in Chapter 4 the Rayleigh wave field will attenuate in the direction of wave propagation. For steady state waves the approximate decay factor for the linear rock site is $\exp(-2\pi\beta) = 0.75$ per wavelength. The effect over a traveling distance of 1000 ft is clearly illustrated by the surface motion response spectra shown in

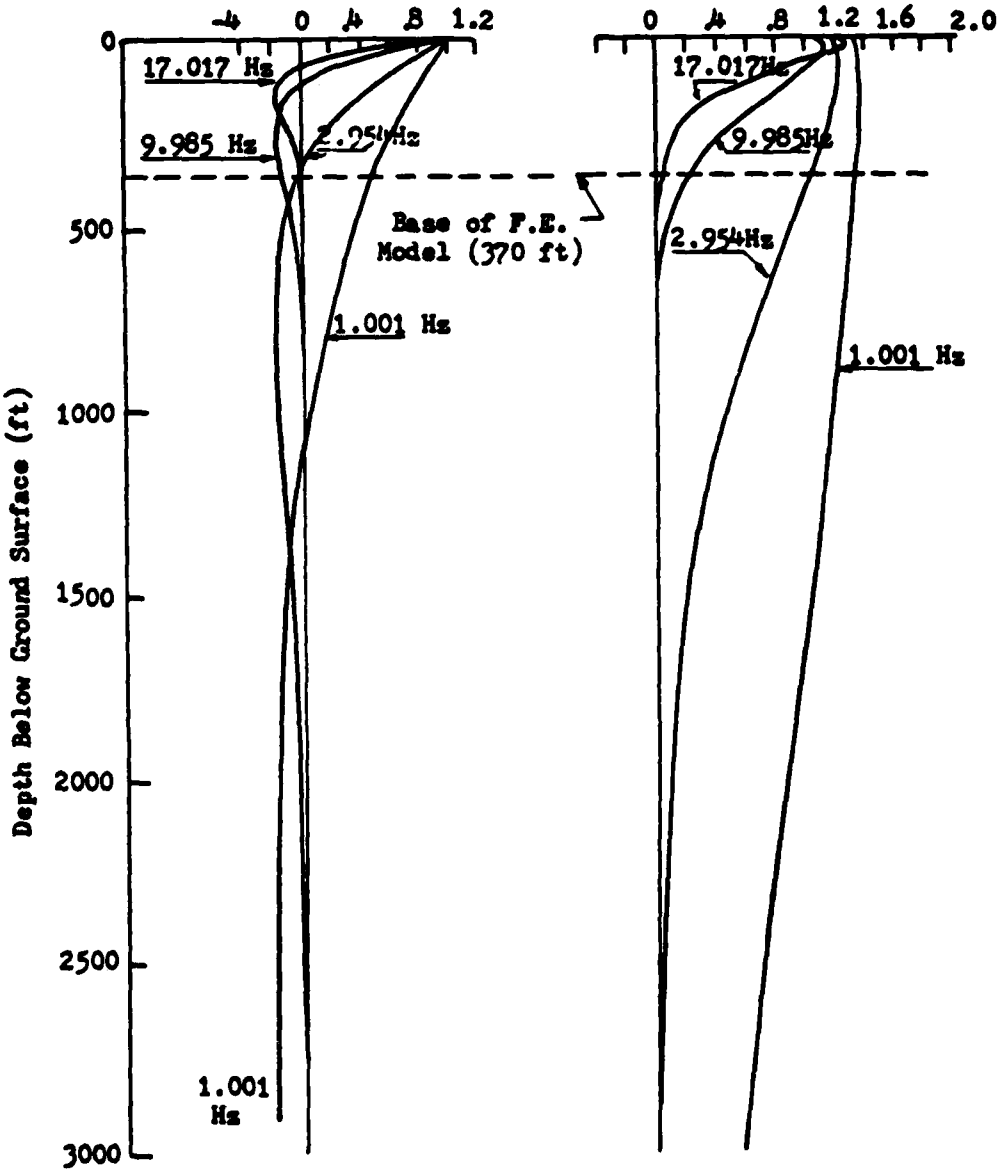

Fig. 5.5 Normalized Mode Shapes for Fundamental Rayleigh Waves - Linear Rock Properties

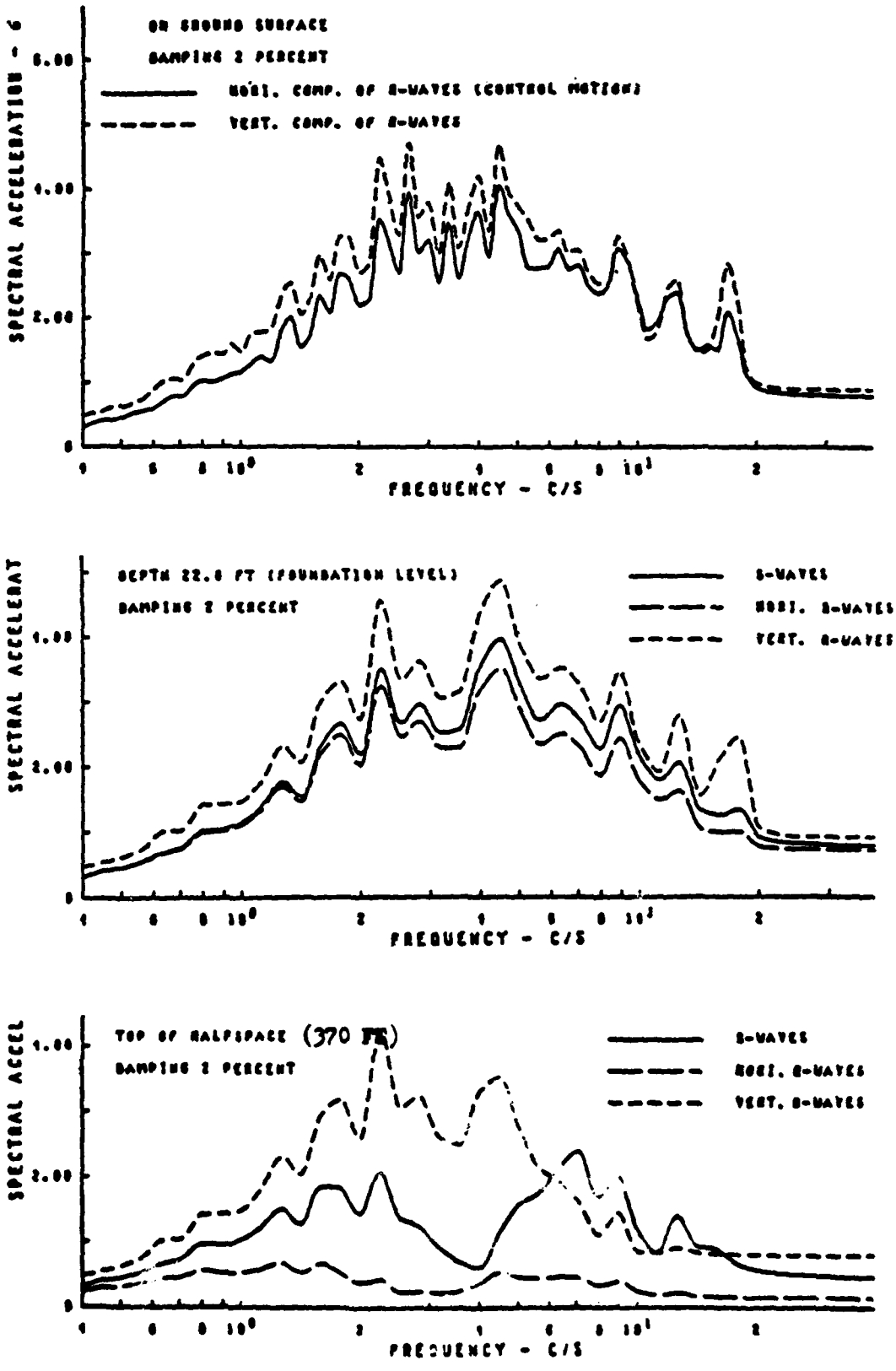

Fig. 5.6 Variation of Frequency Content with Depth - Linear Rock Site

Fig. 5.7. The rate of attenuation indicated for this site is hardly important for engineering design. However, it should be observed that over a distance of several thousands of feet all the high frequency components of the original control motion will vanish. This is a strong indication that even on rock sites high frequency surface waves cannot exist several miles from the epicenter of an earthquake.

5.4 Nonlinear Rock Site

As discussed above linear analysis of competent rock sites is probably appropriate even for very strong motions. However, in order to investigate the maximum credible nonlinear effects on the above site the following modifications were made regarding the properties of the site. First it was assumed that the upper 15 feet of the site is weathered to the point where its low-strain seismic wave velocities are reduced to V_s=1500 fps and V_p=2900 fps and, second, it was assumed that the sandstone, down to a depth of 370 ft, disintegrates during the presumed earthquake to the point where it behaves like sand, i.e. its modulus and damping ratio depends on strain amplitude as shown by the curves marked "Sand" in Fig. 5.2. The above considerations lead to the computational model defined in Table 5.2.

Table 5.2 Low-Strain Properties of Nonlinear Rock Site

Main Layer	Thickness (ft)	Sublayers (No.)	V_s (fps)	V_p (fps)	Damping Ratio
1	15	2	1500*	2900*	*
2	25	3	3600*	6100*	*
3	10	1	3900*	6600*	*
4	320	7	5600*	8700*	*
half space	varies	10	5600	8700	0.02

All unit weights are 150 pcf.

* Computational values vary according to Fig. 5.8.

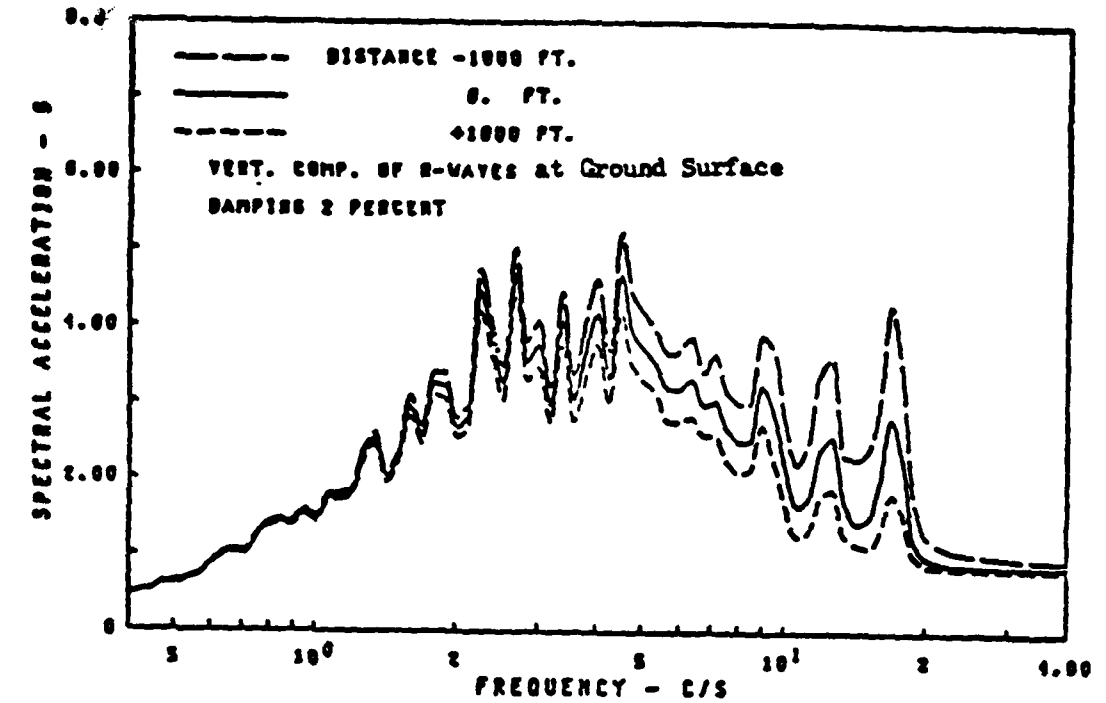

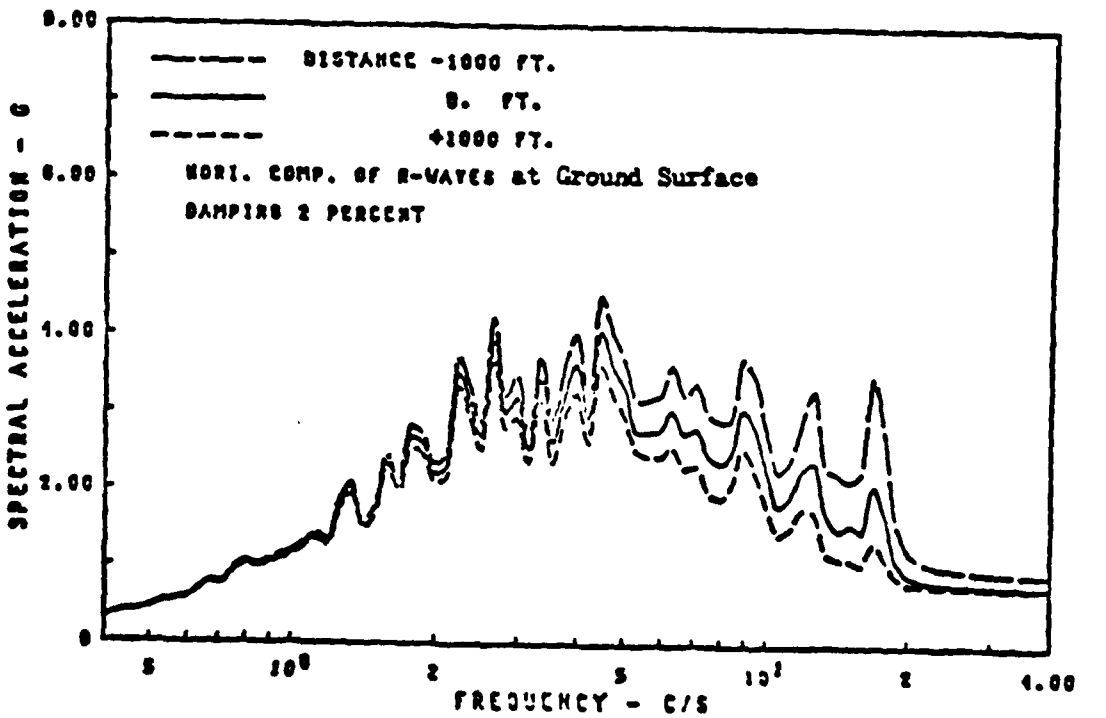

Fig. 5.7 Attenuation of Rayleigh Wave Motion with Travelling Distance - Rock Site

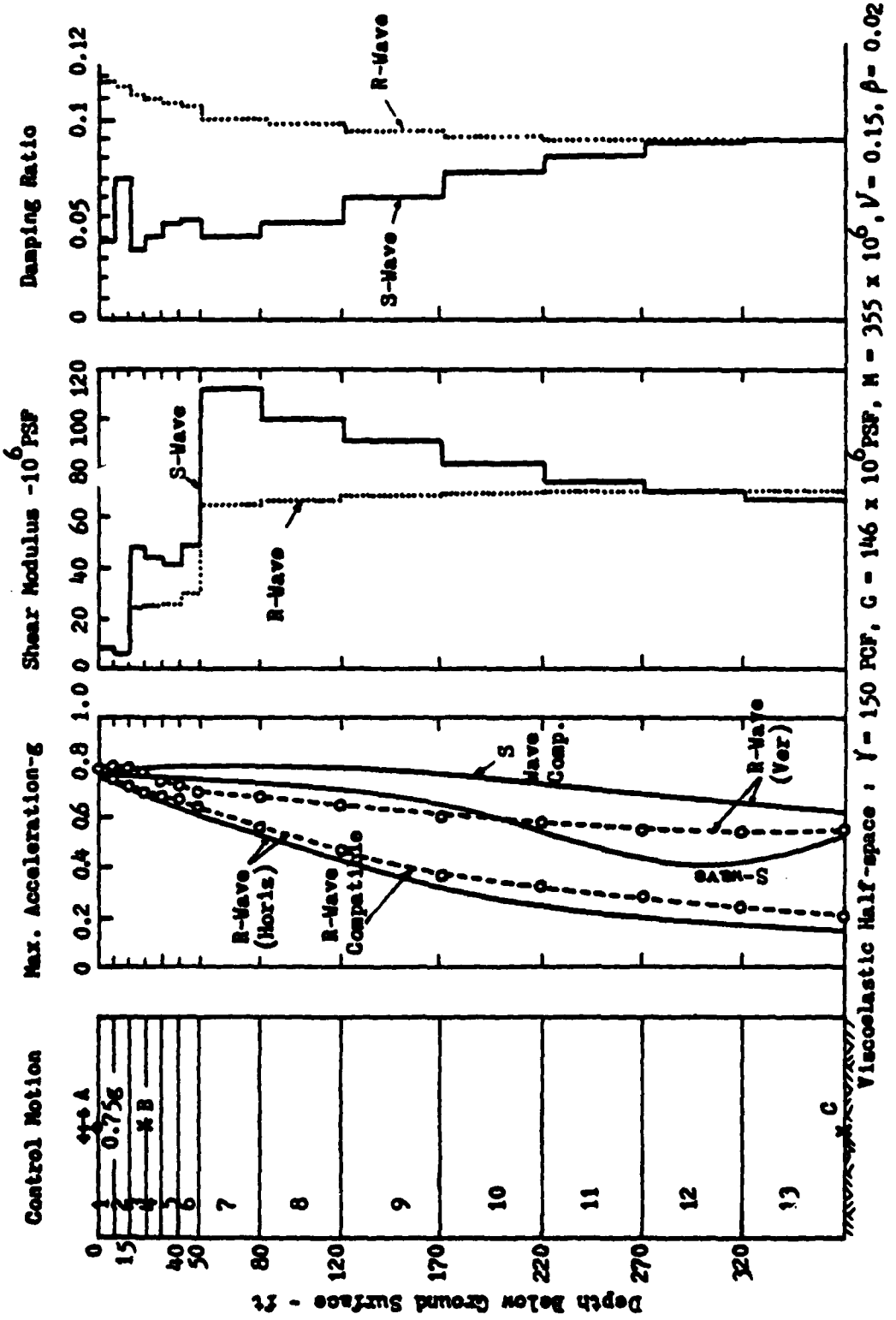

Figure 5.8 Analysis of Nonlinear Rock Site

The model easily satisfies the discretization criteria described in Chapter 3 up to the 20 Hz cut-off frequency of the analysis performed, even when reduced strain-compatible moduli are used.

5.4.1 Strain Compatibility

The above model was analyzed using the equivalent linear method and the same control motion as for the linear rock site. This lead to the strain-compatible properties shown in Fig. 5.8. It is evident from this figure that the nonlinear effects and thus the maximum stresses produced by a Rayleigh wave field in this site are considerably larger than those produced by the corresponding S-wave field. Incidentially, the principal stress directions of the two fields are also completely different. In an S-wave field maximum shear stresses occur on horizontal planes while in an R-wave field they tend to occur on the 45° planes, at least within depths of interest to engineers.

It might at this point be argued that the strain-compatible soil properties determined from the R-wave analysis should be used for all futher R-wave calculations. However, it might also be argued that from a practical standpoint it makes more sense to use the S-wave compatible properties for R-wave calculations. This is so because actual near-surface ground motions consist mainly of vertically or nearly vertically propagating body waves and it is these waves, and especially the shear waves, which produce the major part of the shear strains in the ground. The additional strains produced by a weak superimposed Rayleigh wave field are too small to influence the choice of strain-compatible properties.

The latter approach has been used to produce most of the results presented below. It has the futher advantage that it facilitates the

superposition of different types of wave fields, an operation which would not be valid if the fields were determined from different strain-compatible models. Thus, in the following, unless otherwise mentioned, it may be assumed that S-wave strain-compatible properties were used in all computations involving transient motions.

5.4.2 Steady State Results

Fundamental Rayleigh wave mode shapes at selected frequencies in the range of interest are shown in Fig. 5.9. The dependency of the mode shapes on the choice of rock properties indicate two major effects of increasing nonlinearity:

- A significant decrease in the ratio between the vertical and horizontal motions.
- A decrease in the motions at depth, especially in the high frequency range.

The classic half space theory for Rayleigh waves would predict the second observation. It also predicts that vertical surface motions are always larger than the horizontal motions; a prediction which does not agree with field observations. Thus the first of the above observations about the effect of nonlinearities may be part of the explanation for this discrepancy. In fact, it is only part of the explanation. The smaller vertical motions observed in the field can also be explained as an effect of stiffness contrasts between the surface layers and the bedrock. Nonlinearities tend to increase this contrast when strong motions occurs. Hence, the two explanations are closely interconnected.

Another effect of nonlinearities (or layering if one prefers that explanation) is to increase the dispersiveness of the site. This can

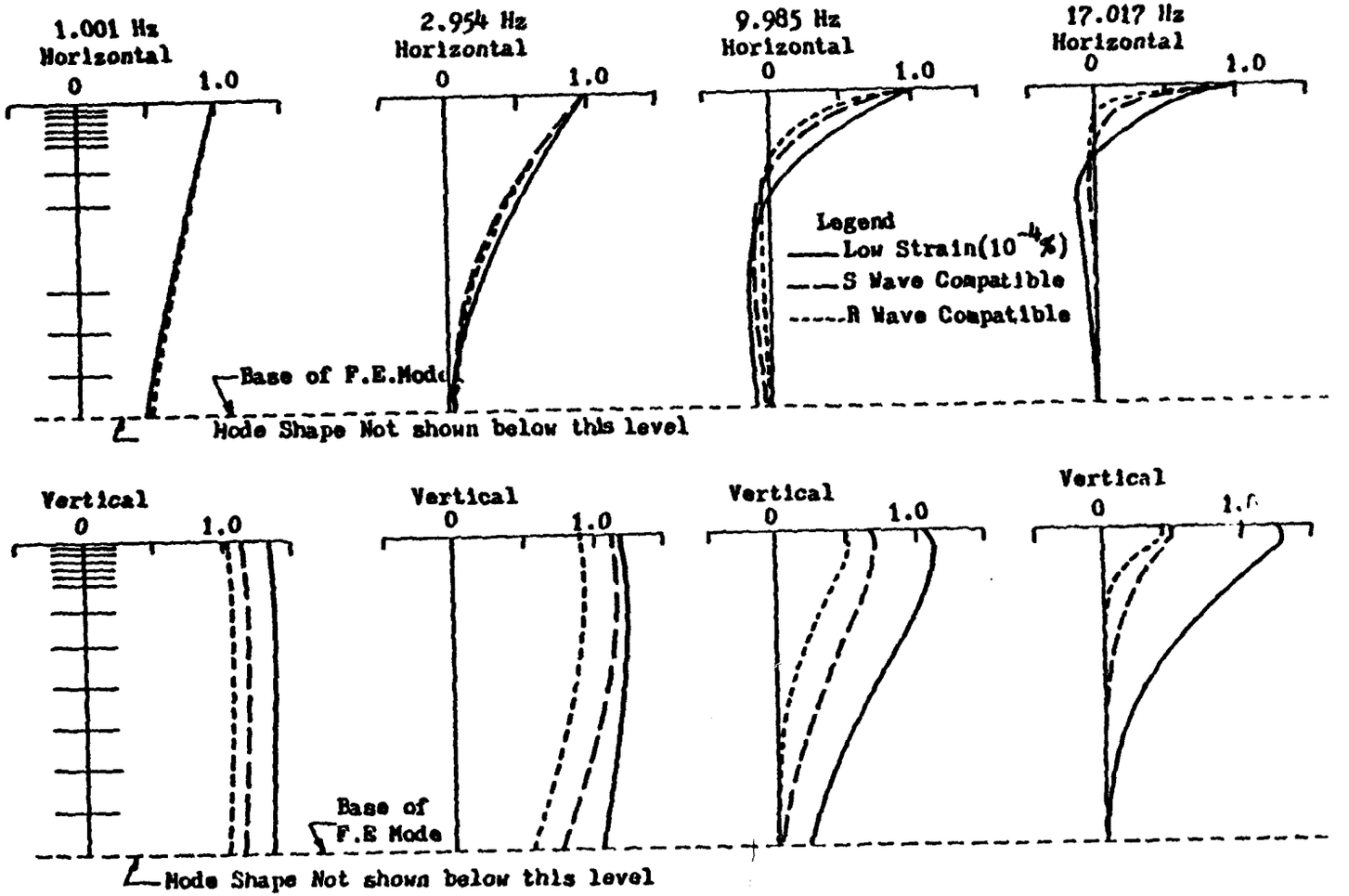

Fig. 5.9 Effect of System Properties on Normalized Mode Shape at Various Frequencies

be seen from the dispersion curves presented in Fig. 5.10. These curves which were computed using S-wave compatible properties show that the modes shown in Fig. 5.9 propagate with completely different velocities. Generally the velocity decreases with frequency from a high velocity corresponding to the velocity of the bedrock to a low velocity corresponding to the velocity of the surface layer.

The rate of attenuation in the direction of wave propagation, $\exp(-k_2 x)$, increases rapidly with frequency and increasing magnitude of nonlinearity. This can be seen from the variation of wave numbers shown in Fig. 5.11. The same graph shows that dispersion, which is proportional to k_1, increases with increasing nonlinearities.

5.4.3 Transient Results

Transient results for the variation of maximum accelerations with depth are shown in Fig. 5.8. The horizontal motions are similar to those computed for the linear rock site, see Fig. 5.3, independent of the choice of strain-compatible rock properties. The vertical motions are smaller that those computed for the linear rock site and they are as expected smallest when R-wave compatible properties are used. Thus, for this site, it may be considered conservative to use S-wave compatible properties for engineering computations. For this reason, and for the reasons given in the previous section, S-wave compatible properties will be used in all further computations.

The variation of frequency content with depth is illustrated by the response spectra shown in Figs. 5.12 to 5.14. The spectra are quite similar to those computed for the linear rock site, Fig. 5.6, except that for the nonlinear rock site the vertical accelerations contain fewer high frequency components.

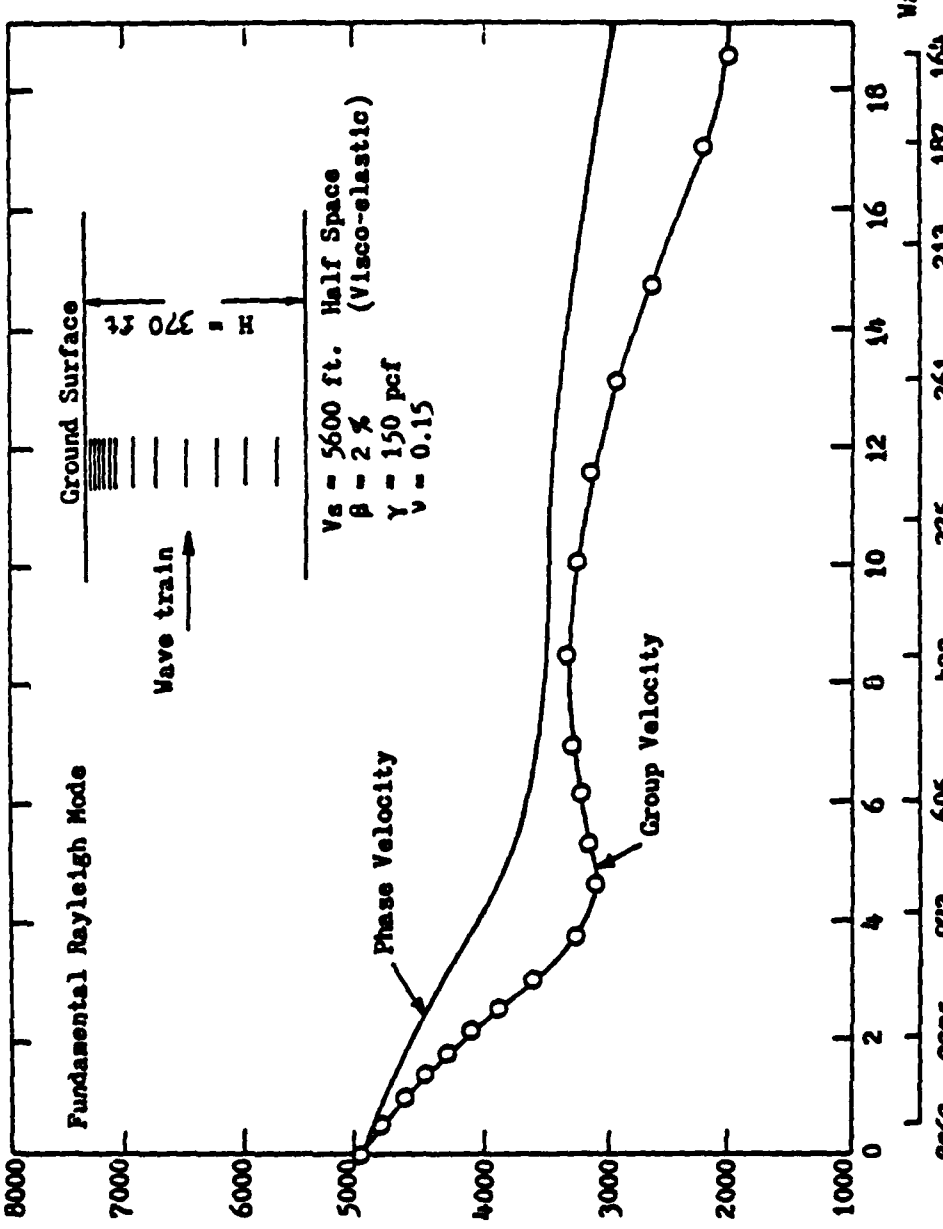

Fig. 5.10 Rayleigh Wave Dispersion Curves for S-Wave Compatible Properties

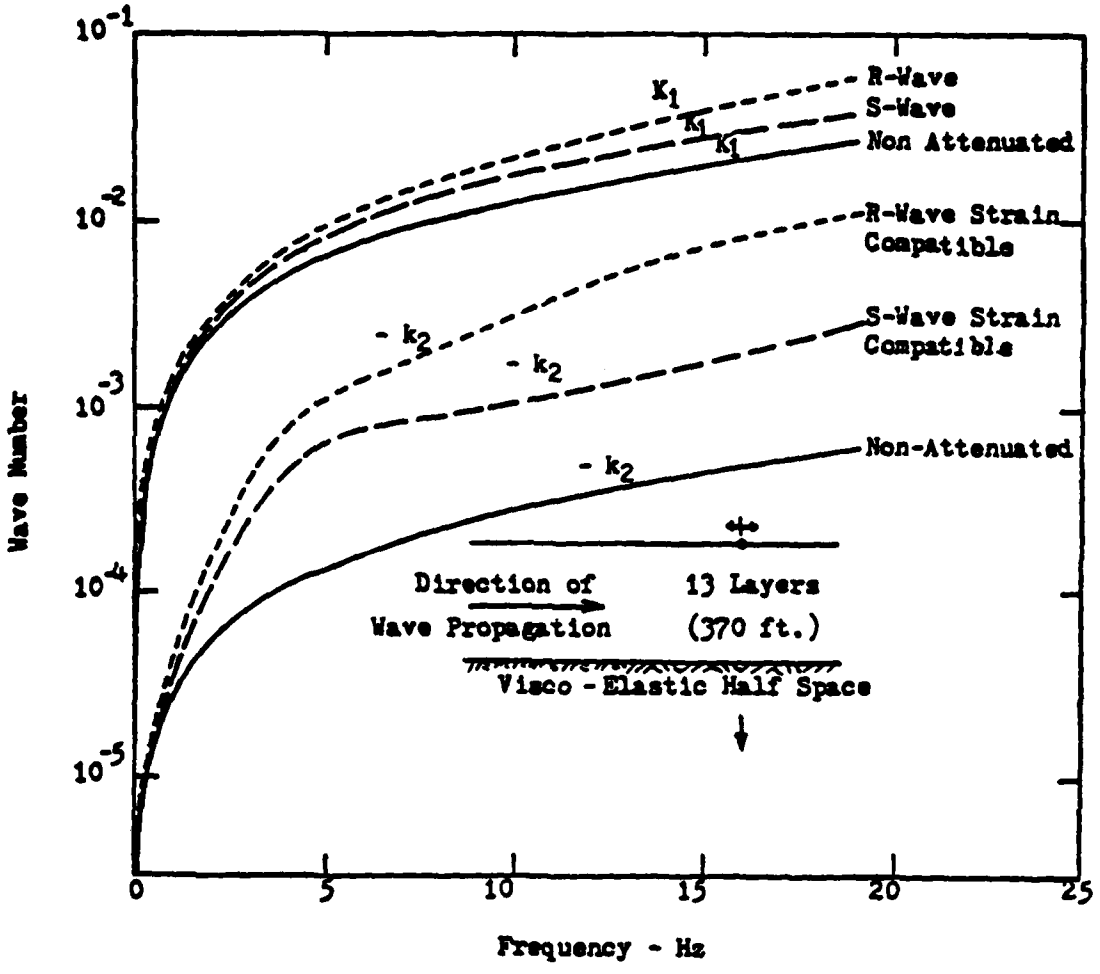

Figure 5.11 Effect of System Properties on Wave Numbers - Nonlinear Rock Site

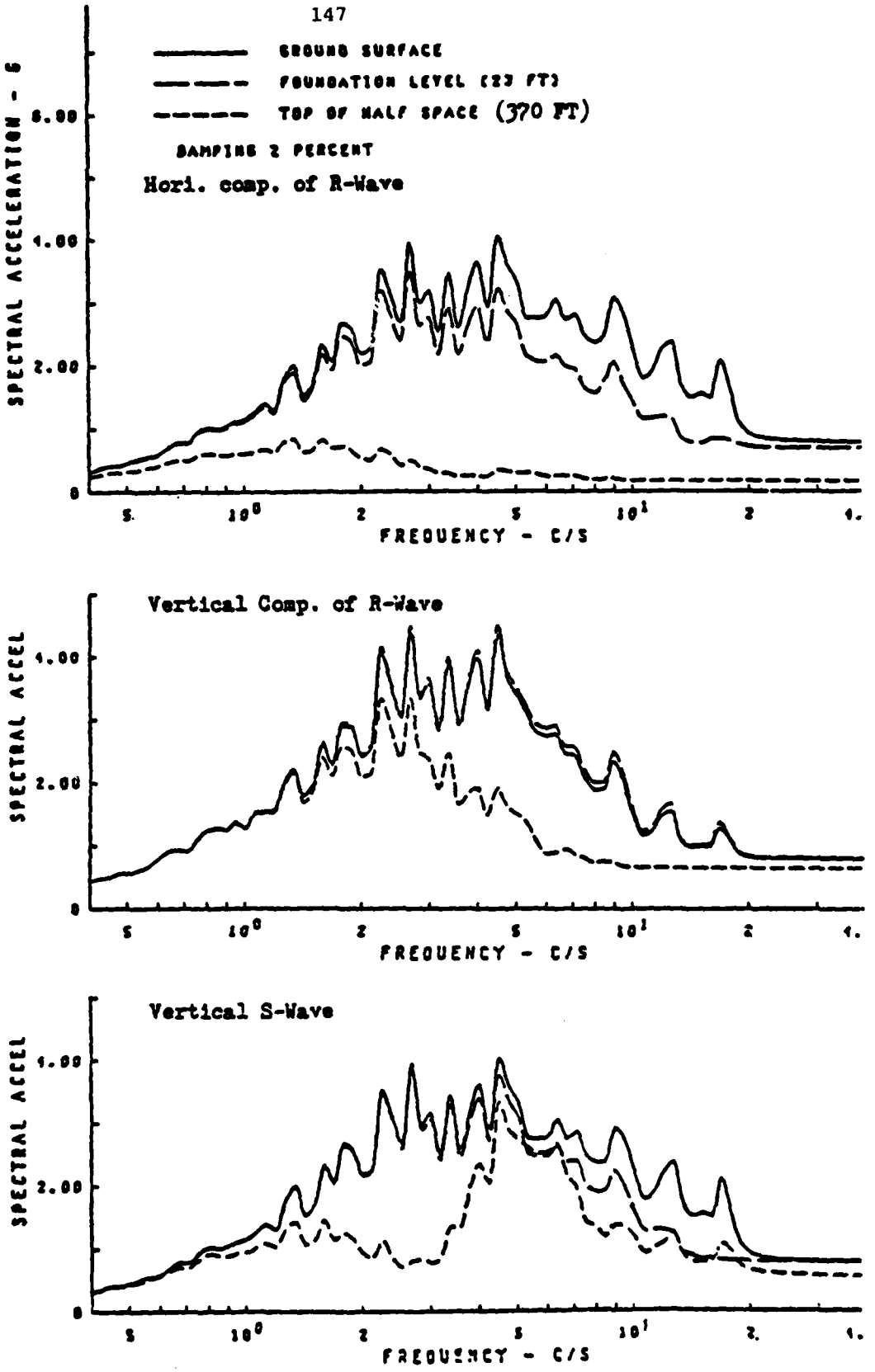

Fig. 5.12 Comparison of Response Spectra at Different Levels in Nonlinear Rock Site

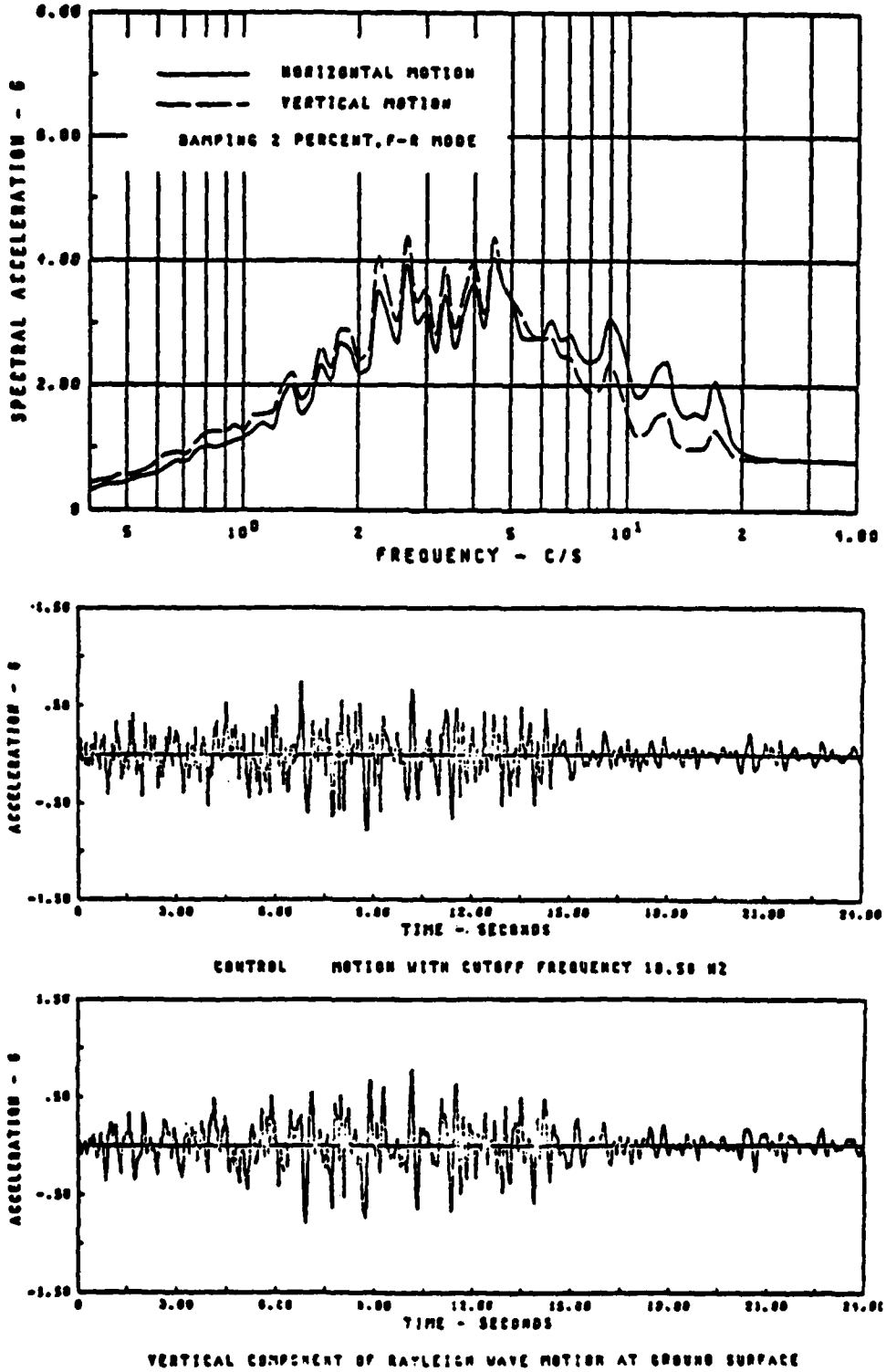

Fig. 5.13 Comparison of Horizontal and Vertical Component of R-Wave Motion at Ground Surface - Nonlinear Rock Site

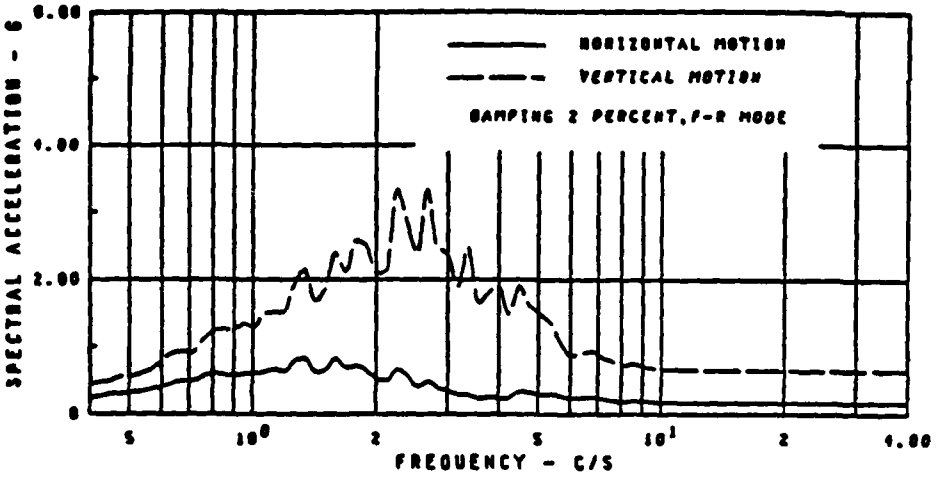

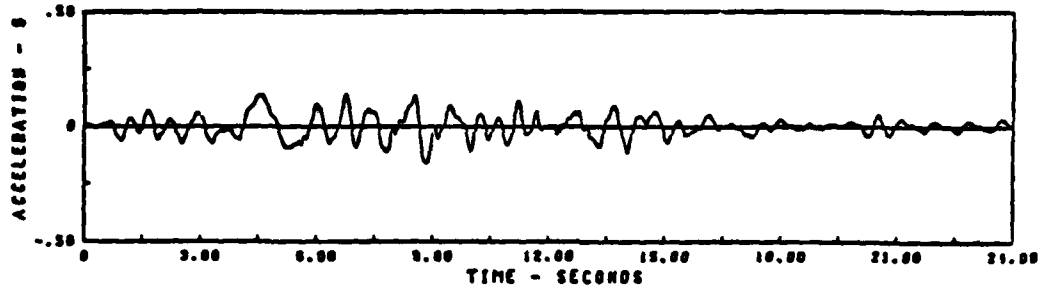

HORIZONTAL COMPONENT OF RAYLEIGH WAVE MOTION AT TOP OF HALF SPACE

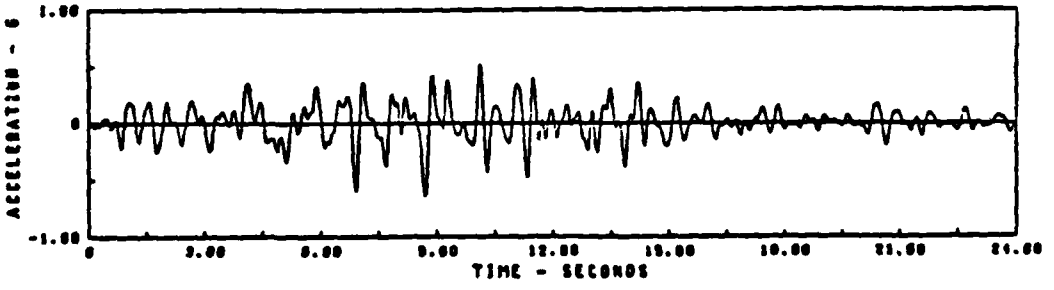

VERTICAL COMPONENT OF RAYLEIGH WAVE MOTION AT TOP OF HALF SPACE

Fig. 5.14 Comparison of Horizontal and Vertical Component of R-Wave Motion at Top of Half-space - Nonlinear Rock Site

The attenuation of the Rayleigh wave field in the direction of wave propagation is illustrated by Figs. 5.15 and 5.16 which shows computed response spectra at different distances from the control point. The results are similar to those obtained for the linear rock site, Fig. 5.7, except that the attenuation is considerably stronger.

5.4.4 Conclusions for Rock Sites

A rock site has been analyzed using two extreme models. The first model assumed linear behavior and the second extreme nonlinear behavior. Except for some minor differences the two models, when analyzed for the same control motion at a surface control point, lead to similar results within depths and distances of interest to foundation engineers. The major conclusion of the above study must therefore be that for engineering purposes nonlinear effects need not to be considered in site response analyses of rock sites.

It was also found that within depths and horizontal distances from the control point of normal interest to foundation engineers the horizontal motions computed on the basis of the assumption of a vertically incident S-wave field are very similar to those computed from a pure R-wave field. This similarity does not extend to the phase difference between distant points on a horizontal plane.

As opposed to vertically incident fields, Rayleigh wave fields attenuate in the direction of wave porpagation. However, for rock sites this attenuation is too small to be of interest to engineers. It might, however, explain why high frequency Rayleigh waves are not observed by seismologists.

5.5 Cohesionless Site

As an example of a site for which nonlinear effects are important it was decided to study a hypothetical site consisting of 128 ft of

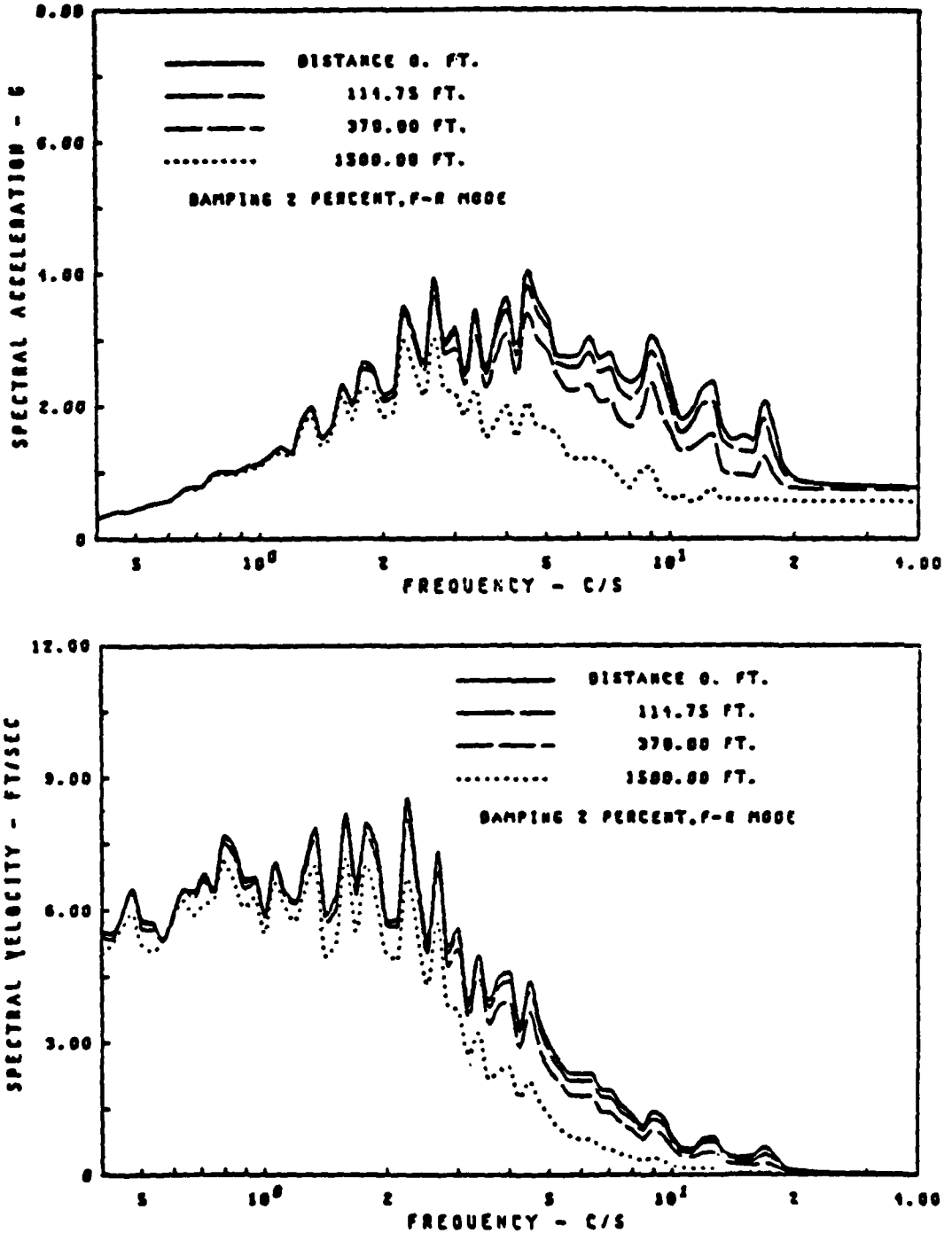

Fig. 5.15 Response Spectra of Horizontal Component of R-Wave Motion at Ground Surface - Nonlinear Rock Site

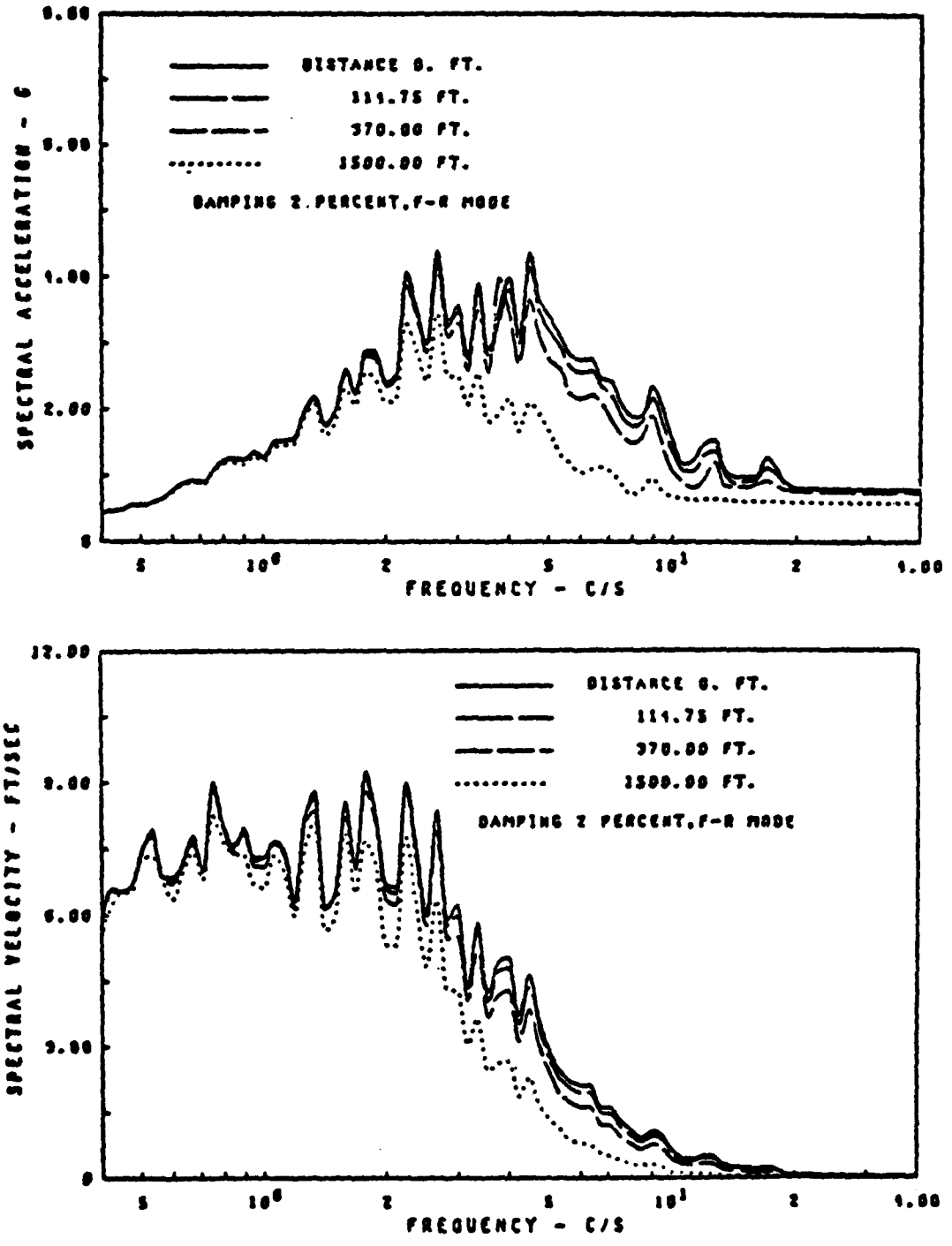

Fig. 5.16 Response Spectra of Vertical Component of R-Wave Motion at Ground Surface - Nonlinear Rock Site

uniformly dense dry sand. This site will be analyzed for the effects of Rayleigh waves, inclined body waves and a combination of such.

The sand was assumed to have the following properties:

Unit weight = 125 pcf

Relative density = 75%

Poisson's ratio = 0.3

Experimental data for the variation of the modulus and damping ratio with effective dynamic shear strain amplitude and confining pressure for such a material were presented in Chapter 2, Fig. 2.3. This data will be used below in connection with the equivalent linear method. The bedrock is considered as a half space with the strain-independent properties: Unit weight 145 pcf; Poisson's ratio, 0.2; V_s = 4000 fps, V_p = 6532 fps and damping ratio, 2%, for both S- and P-waves.

5.5.1 Harmonic Rayleigh Wave

The site, discretized as shown in Fig. 5.21, was first studied for the effect of a harmonic Rayleigh wave at the frequency 2.5 Hz. This frequency corresponds to the predominant frequency of the transient control motion to be discussed in Section 5.5.1. The wave was normalized to produce a horizontal acceleration amplitude of 0.25 g at the ground surface. This corresponds to the acceleration level of the transient control motion to be used in the next section.

Two solutions are presented. The first solution, shown in Fig. 5.17, involves what many may consider common engineering approximations for this type of problem: The sand layer, which actually increases in stiffness with depth was replaced by a uniform layer with the constant shear wave velocity, 1148 fps, and the constant damping ratio, 5%. The

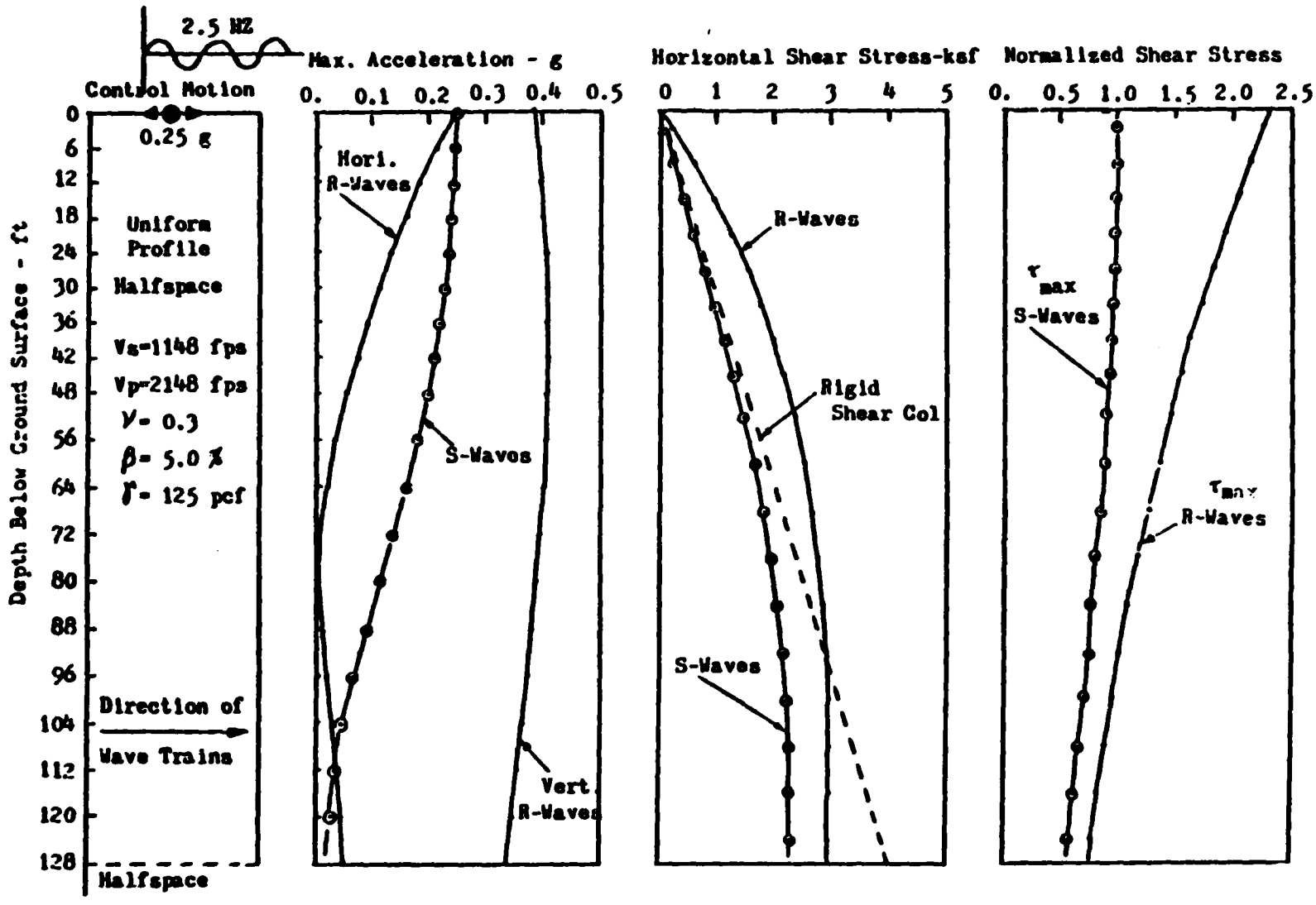

Fig. 5.17 Harmonic Rayleigh Wave and Vertical Shear Wave in Uniform Layer over Half Space - Frequency 2.5 HZ

shear wave velocity corresponds to the average value within the profile at small strains. The damping ratio, which turns out not to be unimportant for the conclusions to be drawn later, is an engineering estimate. Furthermore, in the analysis no attempt was made to adjust the above values for strain compatibility, i.e. a linear analysis was performed.

From the solution one may draw the conclusions that:

- Rayleigh waves produce larger vertical than horizontal motions.
- Horizontal Rayleigh wave motions decrease faster with depth than shear wave motions.

Both of these conclusions are in perfect agreement with classic half space theories for Rayleigh waves. The first is rarely in agreement with field observations.

Now compare the above conclusions with the results of the more complete solution shown in Fig. 5.18. In producing this solution the sand profile was modeled as a layered system, see Fig. 5.21, which increased in stiffness according to Eq. (2.1) and the equivalent linear method was used with S-wave compatible properties to account for nonlinearities. This procedure actually underestimates the nonlinear effects for the R-wave results, since, as will be discussed in Section 5.5.5, R-waves cause larger shear stresses in the upper part of the profile than S-waves.

It is clear from the results shown in Fig. 5.18 that both of the above conclusions made on the basis of the results from the simplified model are wrong for this case. As they will be for some of the transient cases to be presented below, details of layering and non-linearities must be considered in site response analyses of soil profiles.

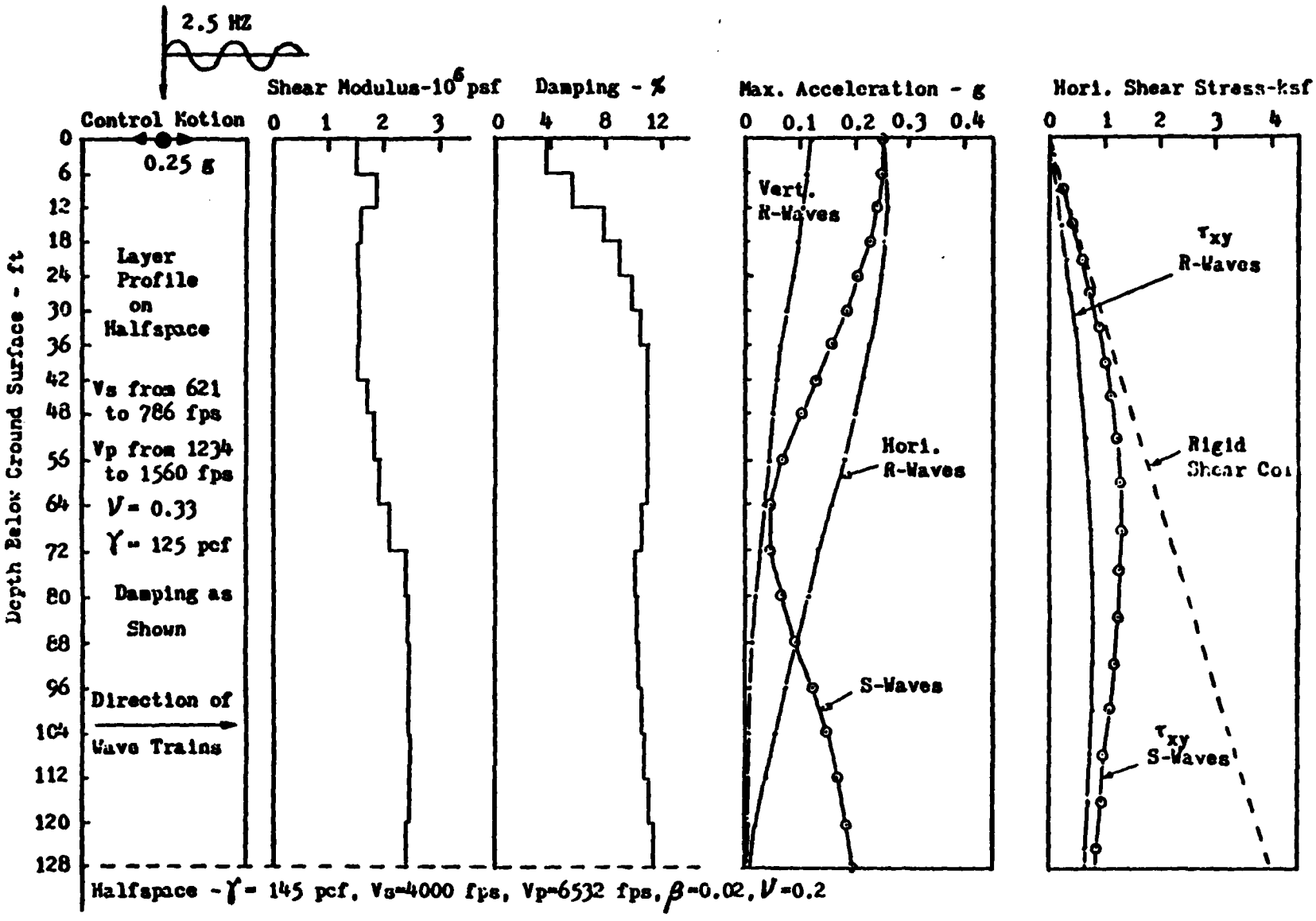

Fig. 5.18 Harmonic Rayleigh Wave and Vertical Shear Wave in Layered Sand Site - Frequency 2.5 HZ

Perhaps the strongest effect is that of nonlinearity which in this case change the average shear wave velocity of the sand layer from about 1148 fps to about 772 fps, a change which will have a pronounced effect on the behavior of both R- and S-waves.

5.5.2 Transient Rayleigh Waves

The above study was repeated using a transient Rayleigh wave field defined by the motion shown in Fig. 5.19. This motion was scaled to 0.25 g and used as the horizontal control motion at the ground surface. 1024 points (Δt=0.02 sec) were used in the Fast Fourier Transform computations and frequencies above 20 Hz were neglected. Results compatible with Figs. 5.17 and 5.18 are shown in Figs. 5.20 and 5.21. They generally confirm the conclusion made in the previous section.

The response spectra for the motions at the control point, Fig. 5.22, shows that, although the maximum acceleration of the horizontal and vertical components are similar, the vertical component contains higher frequencies. Fig. 5.23 shows the variation of frequency with depth. As expected the major effect appears to be a reduction in amplitude approximately proportional to frequency.

The average damping ratio in the sand layer is about 10% and it is therefore to be expected that the attenuation of the Rayleigh wave field on the x-direction is very strong. This is confirmed by the results presented in Fig. 5.24. Within only 250 feet from the control point all motions above 5 Hz have attenuated to insignificant values. This especially influences the vertical component which already at a distance of about 200 ft becomes smaller than the horizontal component at the ground surface. As discussed at the end of section 5.4 the high attenuation computed is strong evidence that fundamental mode Rayleigh

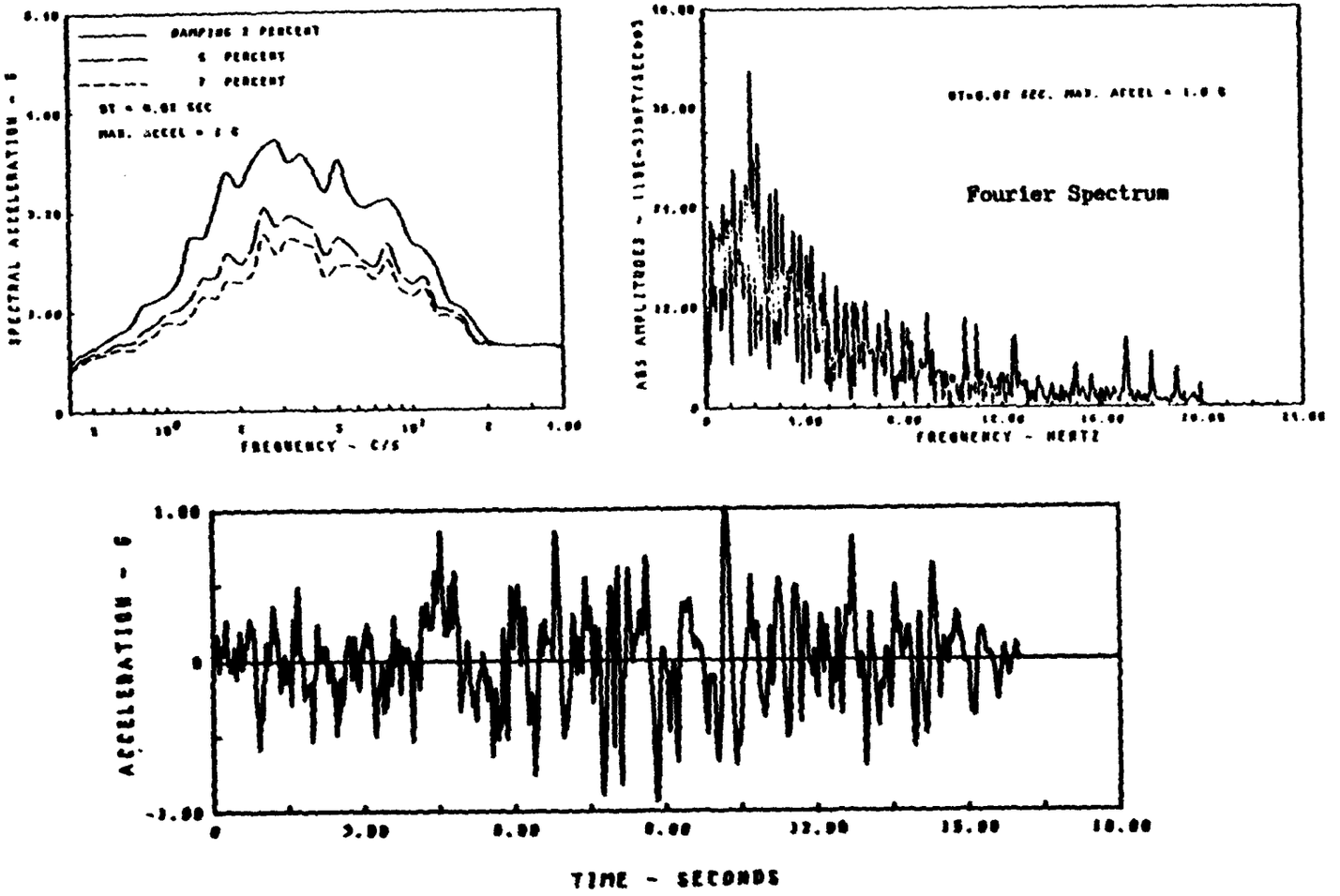

Fig. 5.19 Control Motion for Cohesionless Site

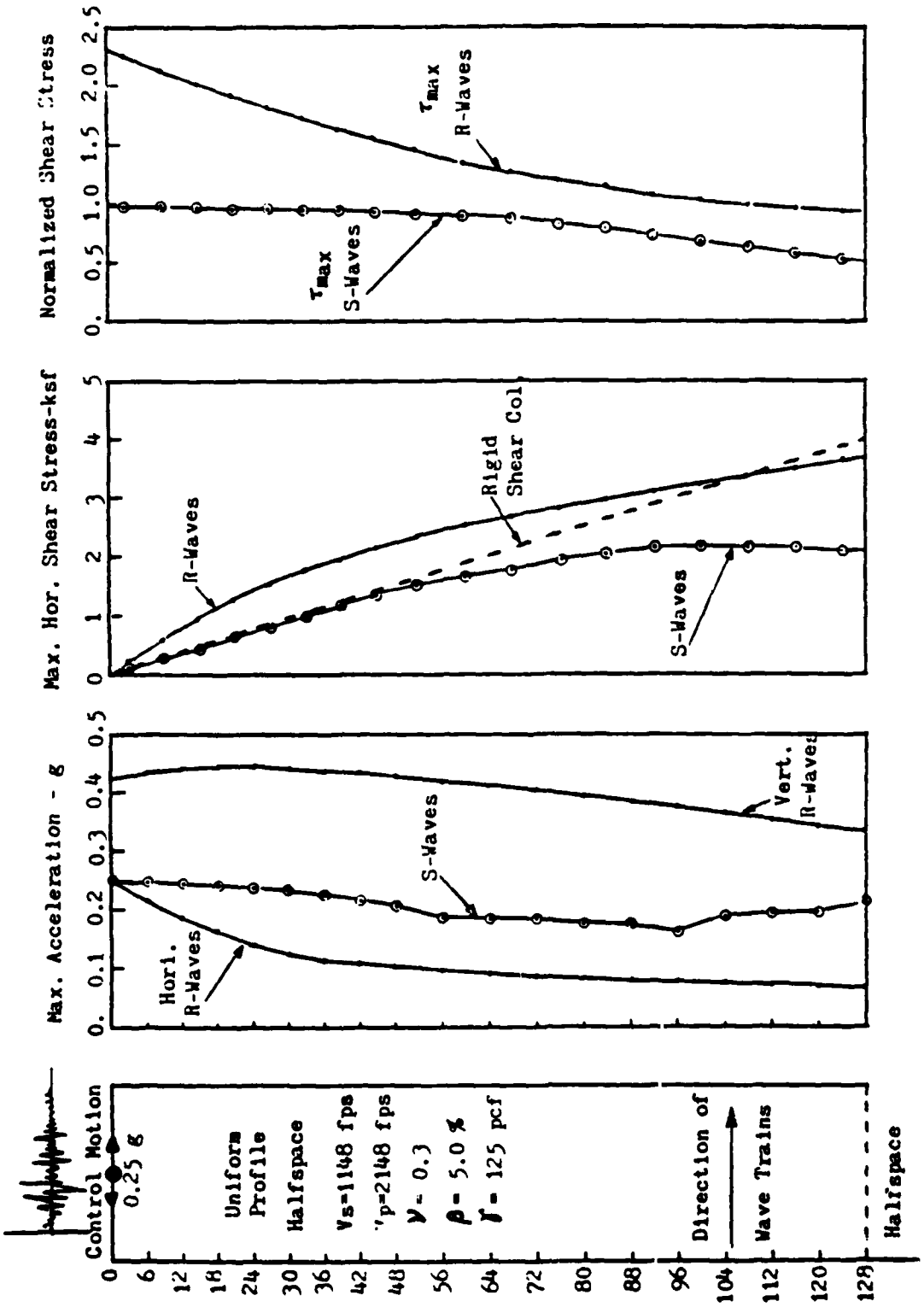

Fig. 5.20 Site Response by Rayleigh Waves and Vertical Shear Waves - Transient Motion

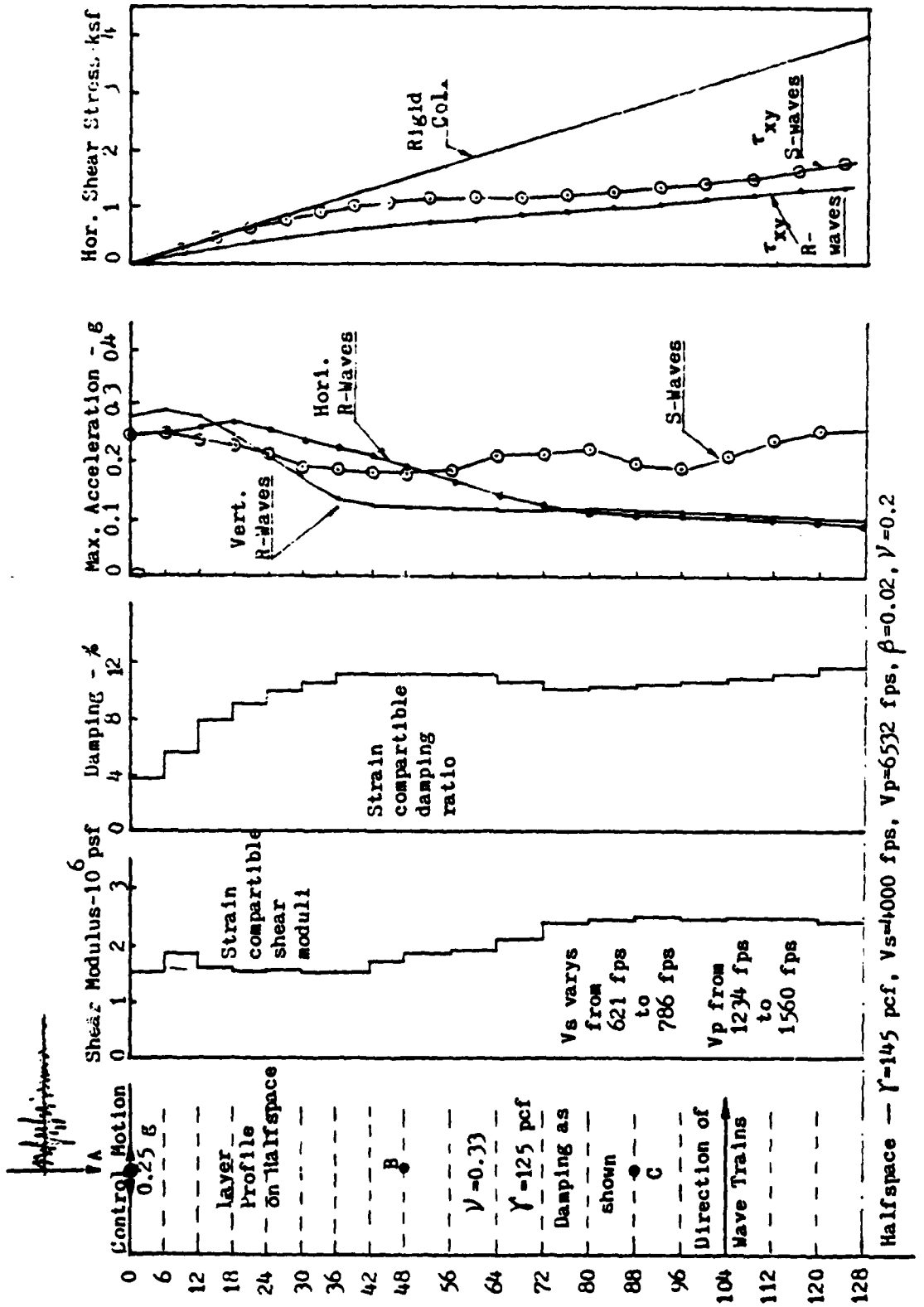

Fig. 5.21 Site Response by Rayleigh Waves and Vertical Shear Waves Transient Motion in Layered Sand Site

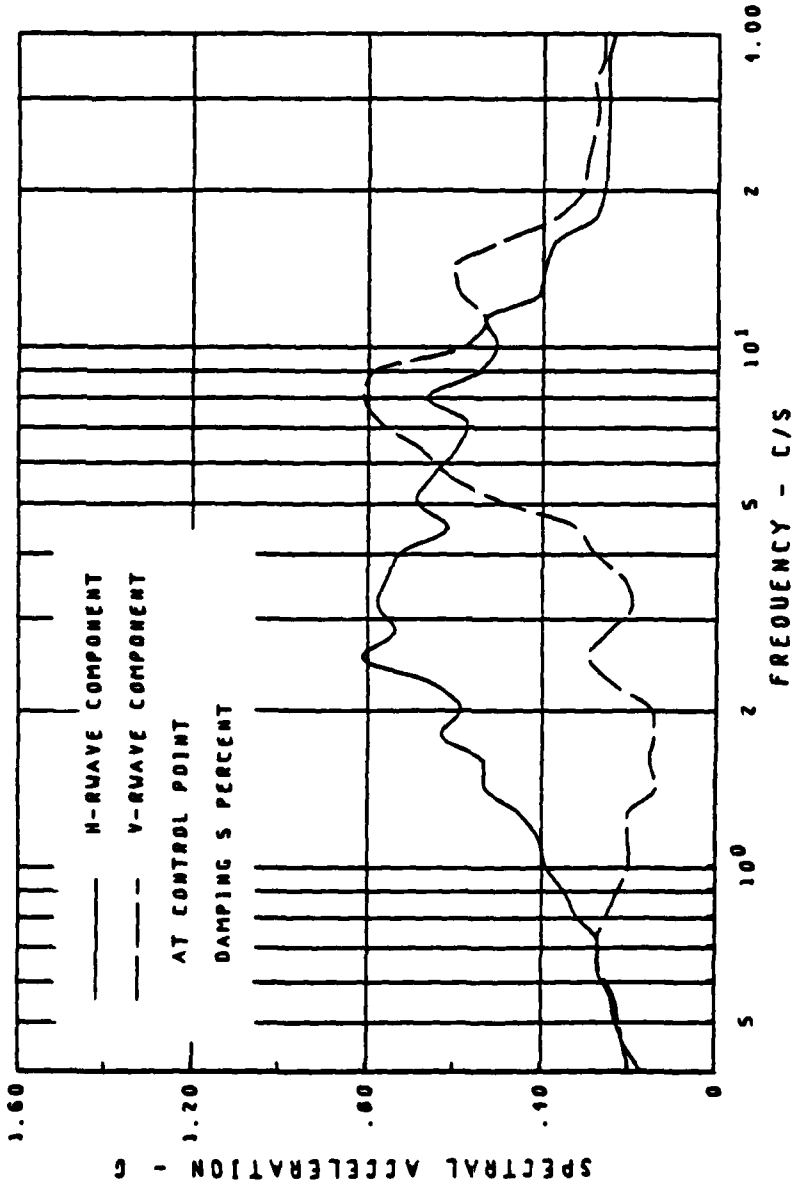

Fig. 5.22 Response Spectra of R-Wave Motions on Ground Surface of the Layered Sand Site

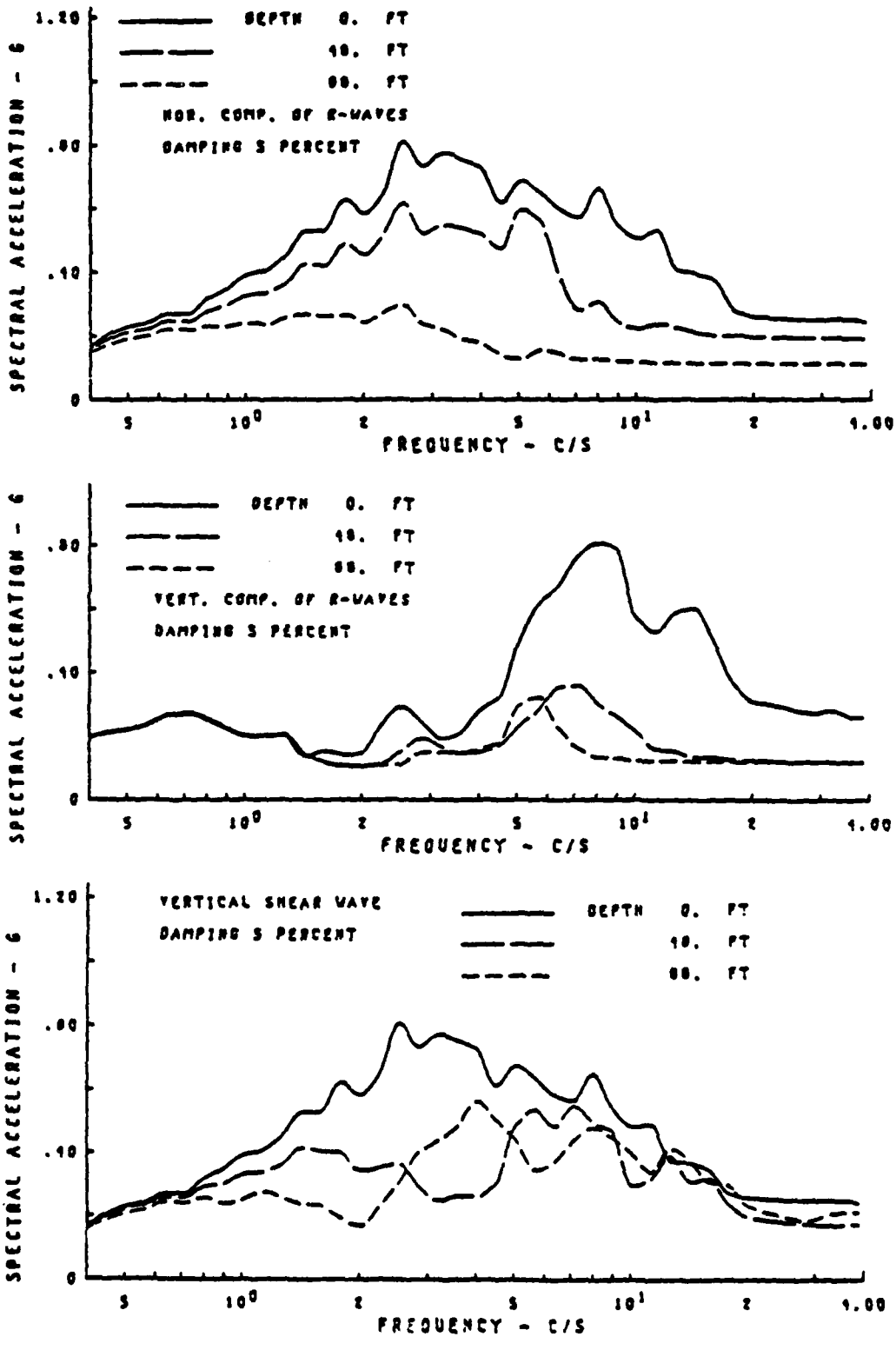

Fig. 5.23 Site Response by Rayleigh Waves and Vertical Shear Waves

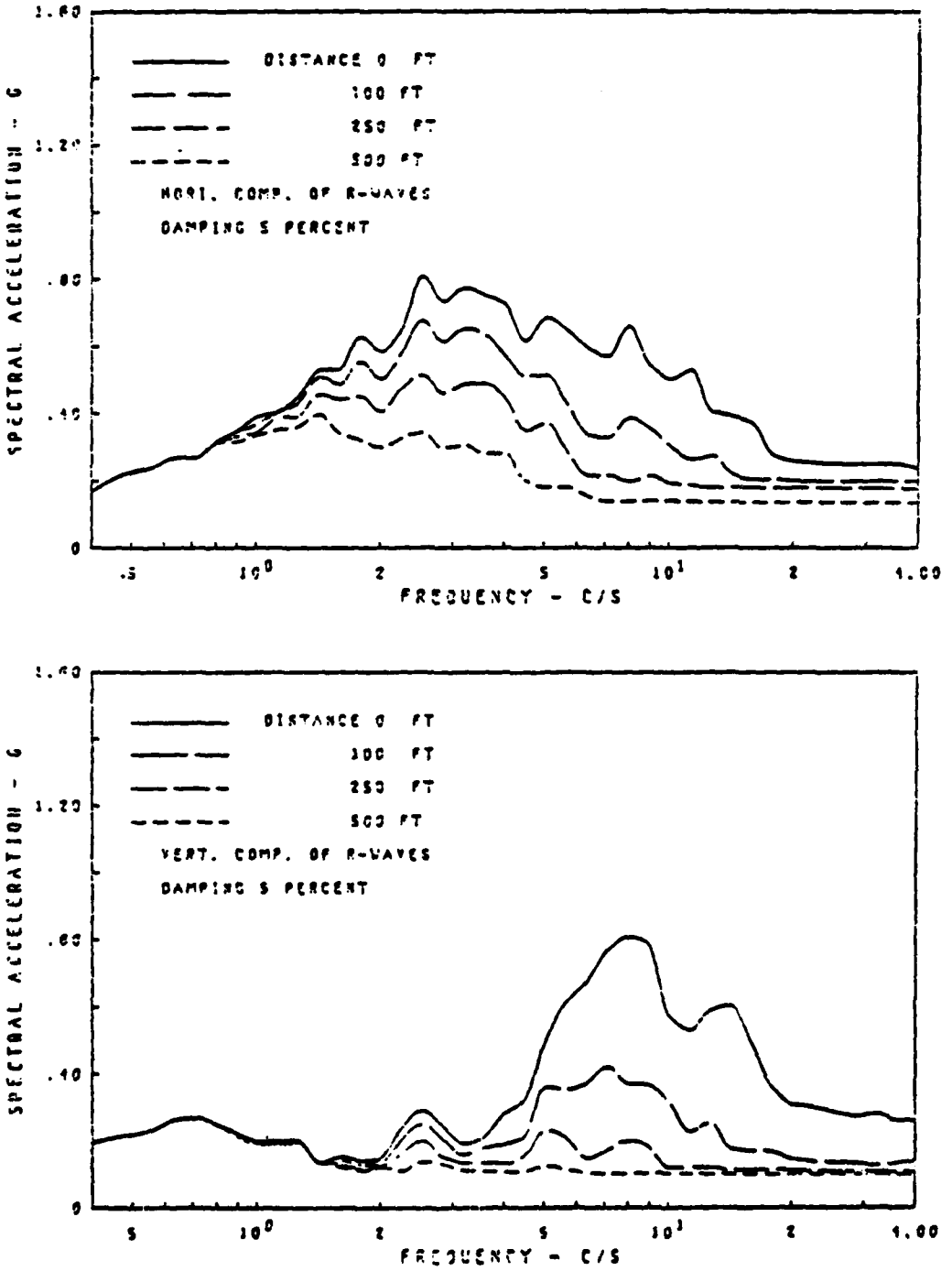

Fig. 5.24 Effect of Travelling Distance of R-Wave Motion on Site Response at Ground Surface of Sand Site

waves are not an important contributor of near-surface motions in cohesionless sites, at least not at frequencies higher than about 1 Hz.

5.5.3 Rayleigh Wave Stress Field

Another factor which may impede the propagation of strong Rayleigh waves in cohesionless sites is the characteristics of the near-surface stress field produced by Rayleigh waves as opposed to that produced by vertically propagating shear wave fields. These characteristics are:

- Shear wave fields produce no normal stresses on vertical and horizontal planes while R-wave fields produce very large stresses; especially on the vertical plane.
- In a shear wave field the maximum shear stresses occur on horizontal and vertical planes while for R-wave fields these stresses occur on the 45° planes near the ground surface and on the horizontal and vertical planes of depth.

Both of these characteristics are confirmed by the data presented in Fig. 5.25 which shows details of the stress field corresponding to the above nonlinear transient solution for cohesionless site. Similar data are shown in the right hand parts of Figs. 5.17, 5.18, 5.20 and 5.21. It should, however, be observed that the stresses shown in Figs. 5.17 and 5.20 are maximum stresses normalized with respect to the S-wave stress at the ground surface, while the stresses in Figs. 5.18 and 5.21 are maximum normal stresses on the horizontal plane. The data is confused by the fact that S-wave strain-compatible properties, see Fig. 5.21, were used in the R-wave analysis. Hence, the stiffness of the upper part of the sand layer is not compatible with the high maximum shear stresses, τ_m (R-wave) in Fig. 5.25, developed by the Rayleigh wave field near the surface. Nevertheless, it is clear that these

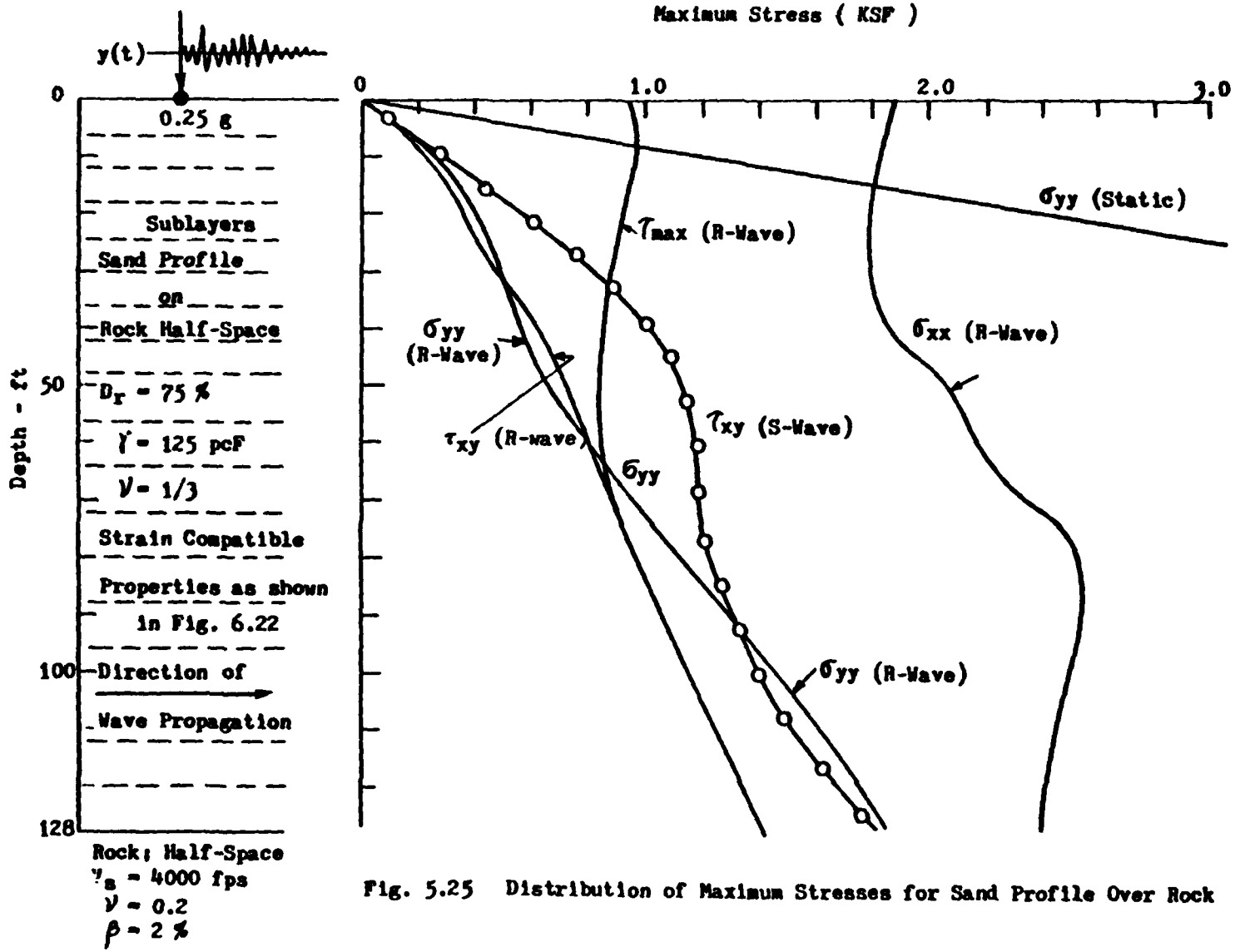

Fig. 5.25 Distribution of Maximum Stresses for Sand Profile Over Rock

stresses cannot be sustained by the near surface sand which, due to the low confining pressure, have very low strength. Thus a near failure condition, which cannot be handled well by the equivalent linear method, will develop in the top layers. This will further impede the propagation of strong Rayleigh waves. Even if the top layer had some strength due to cohesion, tension cracks would develop due to the high normal stress on the vertical plane. Any Rayleigh wave motion in a cohesionless site must therefore be relatively weak.

The high normal stress on vertical planes produced by Rayleigh wave fields may, even for weak fields, induce high pressures on embedded structures. The problem will be considered in Chapter 6.

5.5.4 Inclined Body Waves

Since it is unlikely that Rayleigh waves are of importance for cohesionless sites the above site was analyzed, by the method described in Section 3.5.1, with the same control point and motion, for the effects of inclined SV-waves. As will be shown such waves produce essentially the same motions and stresses on the site as vertically propagating S-waves. For this reason all analysis were performed linearly using the S-wave compatible model shown in Fig. 5.21.

The fixed base complex natural frequencies of the 18-layer model are shown in Table 5.3. In this table the columns marked "S-waves" and "P-waves" corresponds to horizontal and vertical modes, respectively.

The inclined shear waves arrive at the base of the sand profile through the underlying viscoelastic half space at the incident angles, 0, 5, 10 and 20 degrees from the vertical axis. Site transfer functions (defined as the absolute ratio between the amplitude in question and the horizontal amplitude at the top of bedrock) for horizontal and vertical

Table 5.3 Fixed Base Complex Natural Frequencies of Sand Site

Freq. No.	S-waves (Hz)		P-waves (Hz)	
	Real	Imag.	Real	Imag.
1	1.4803	0.1597	2.9387	0.3171
2	4.0958	0.4354	8.1312	0.8644
3	6.9444	0.7051	13.7863	1.3999
4	9.7657	0.9834	19.3872	1.9522
5	12.5171	1.2536	24.8494	2.4886
6	15.3489	1.5282	30.4712	3.0339
7	18.1037	1.7904	35.9402	3.5543
8	20.7286	2.0332	41.1513	4.0365
9	23.4591	2.3297	46.5719	4.6251
10	25.9610	2.4938	51.5388	4.9509
11	28.2083	2.8073	56.0003	5.5732
12	30.8749	3.0326	61.2941	6.0204
13	32.2445	3.1404	64.0131	6.2344
14	34.8634	3.6592	69.2123	7.2644
15	35.9375	3.3149	71.3446	6.5809
16	37.6328	3.9796	74.7102	3.9004
17	39.4701	3.9002	78.3577	7.7427
18	41.4184	2.5956	82.2255	5.1530

motions at different depths are shown in Figs. 5.26 and 5.27, respectively. The horizontal transfer functions are for practical purposes independent of angle of incidence within the range investigated. So are the shapes of the vertical transfer functions. However, the vertical components increase with the angle of incidence. The horizontal transfer functions exhibit peaks at the S-wave natural frequencies of the sand layer and the vertical transter functions exhibit peaks at the P-wave natural frequencies, see Table 5.3. Considering that the approximate velocity ratio between the sand layer and bedrock is equal to 5.5, these results are in excellent agreement with the transfer functions presented in Chapter 3, Fig. 3.16, for a similar profile with the velocity ratio 4.

The fact that the peaks of the vertical transfer functions tend to occur at higher frequencies than the peaks for the horizontal transfer functions means that, in nature, there will be a tendency for vertical surface motions to contain higher frequencies than horizontal surface motions. This, incidentially, is in general agreement with field observations.

A transient analysis, using the same control motion as for the Rayleigh wave case discussed in Section 5.2.2 but with the control point at the top at the bedrock, produced the response spectra shown in Figs. 5.28 and 5.29. As might be expected from the above amplification study the horizontal motions are virtually independent of the angle of incidence, see Fig. 5.28, while the vertical motions increase with increasing angles of incidence, see Fig. 5.29.

A second transient analysis in which the control point was at the ground surface gave similar results. Horizontal response spectra from this analysis are shown in Fig. 5.30.

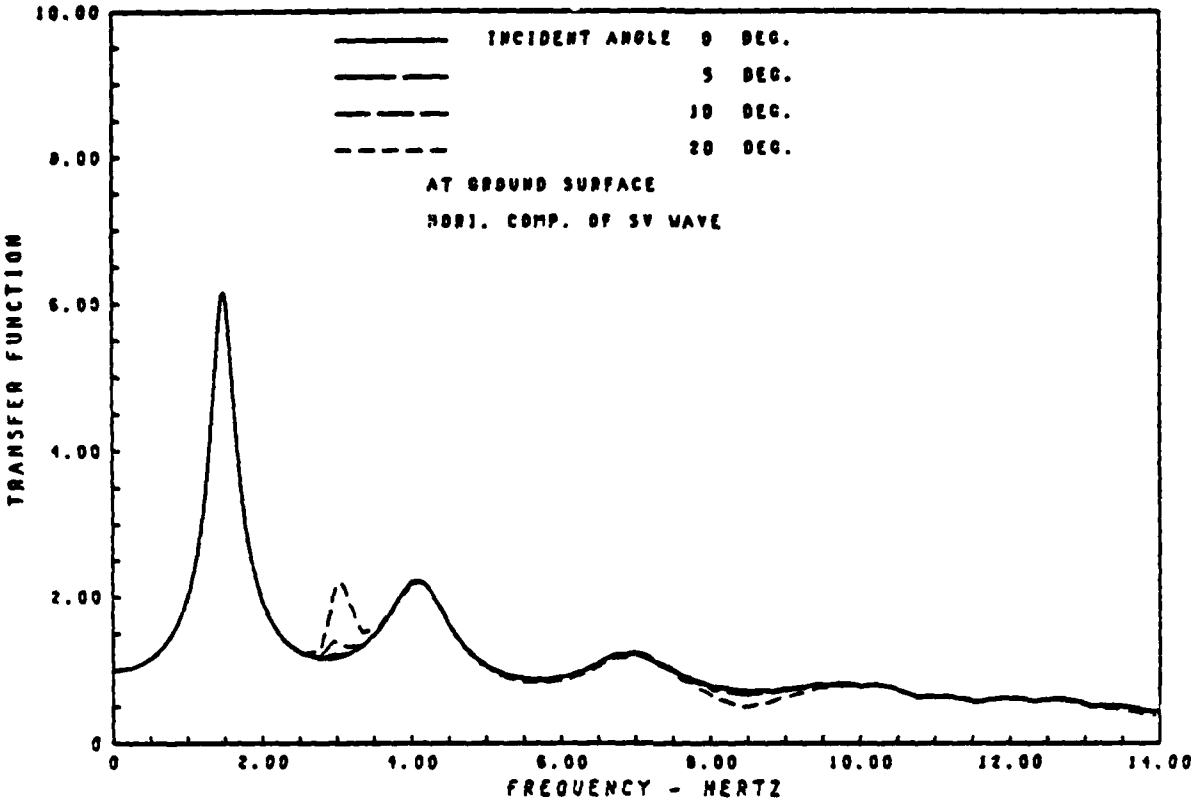

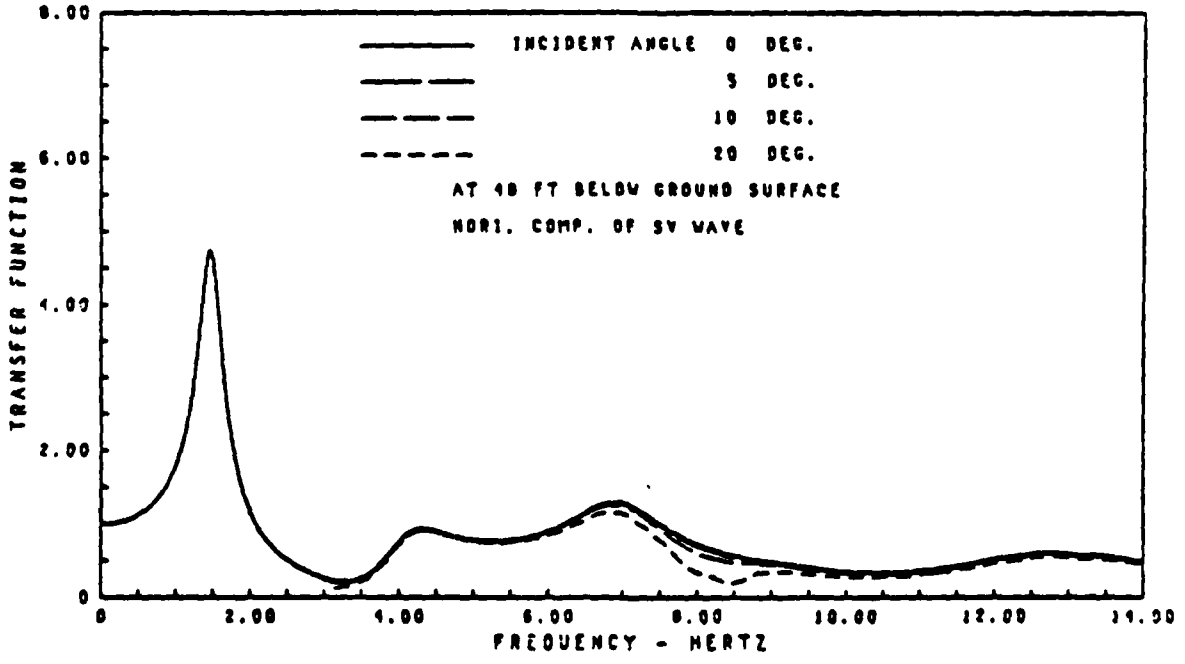

Fig. 5.26 Site Transfer Function on Horizontal Component of SV Wave Motion - Sand Site Response to Inclined SV Waves at Different Angle of Incidence

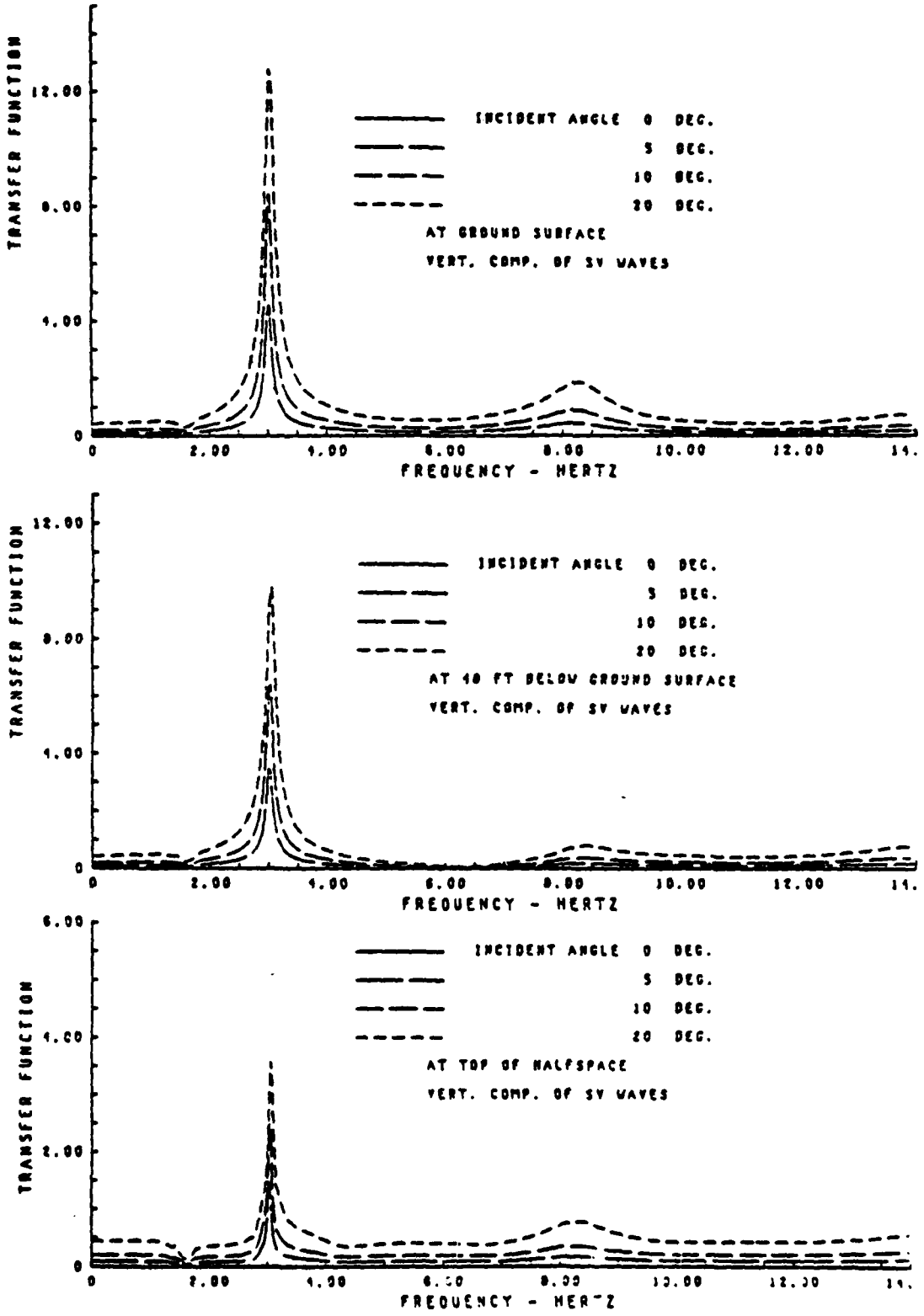

Fig. 5.27 Site Transfer Function on Vertical Component of SV Wave Motion - Sand Site Response to Inclined SV Waves at Different Angle of Incidence

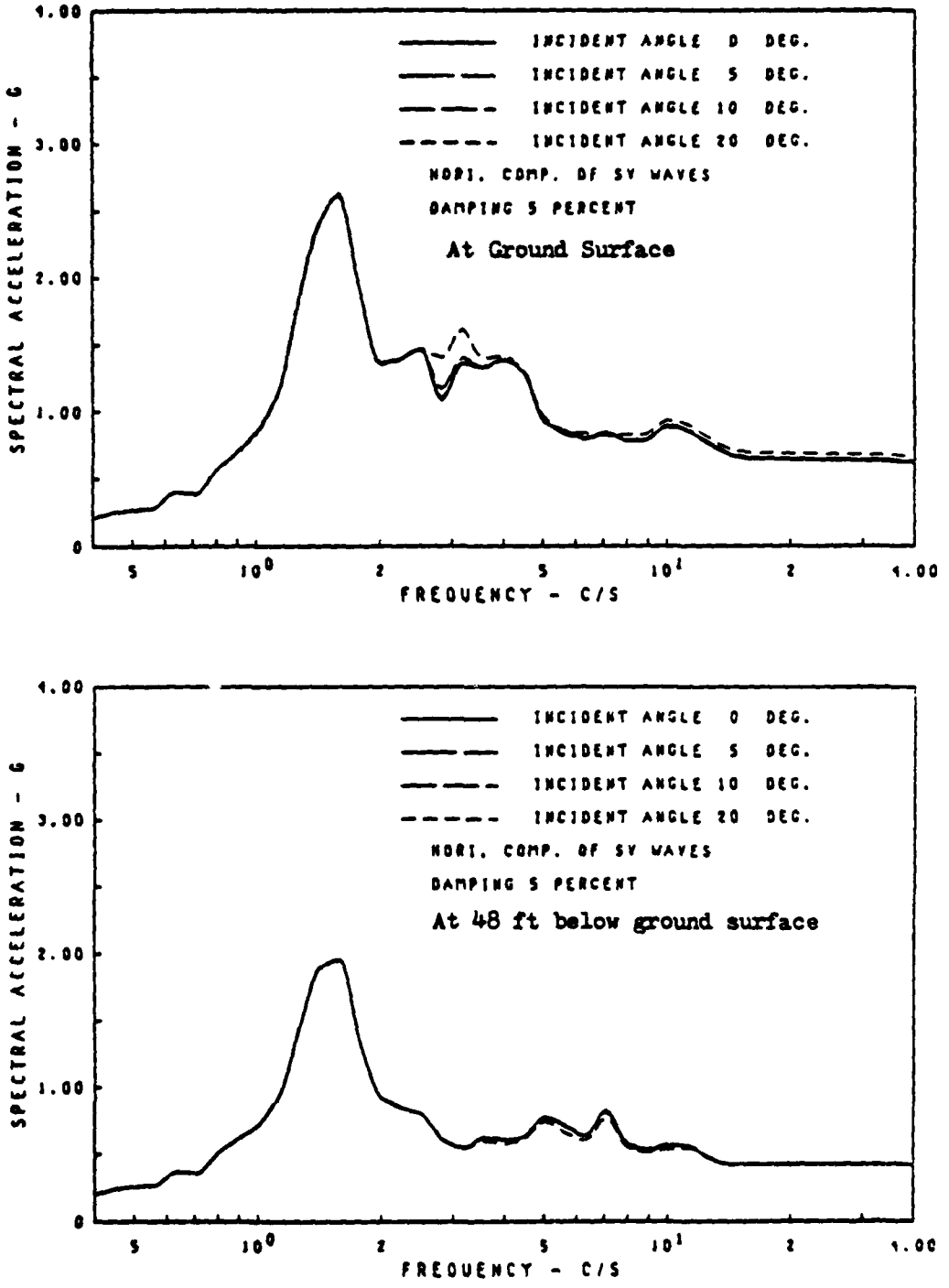

Fig. 5.28 Response Spectra of Horizontal Component of SV Wave Motion Sand Site Response to Inclined SV Waves at Different Angle of Incidence

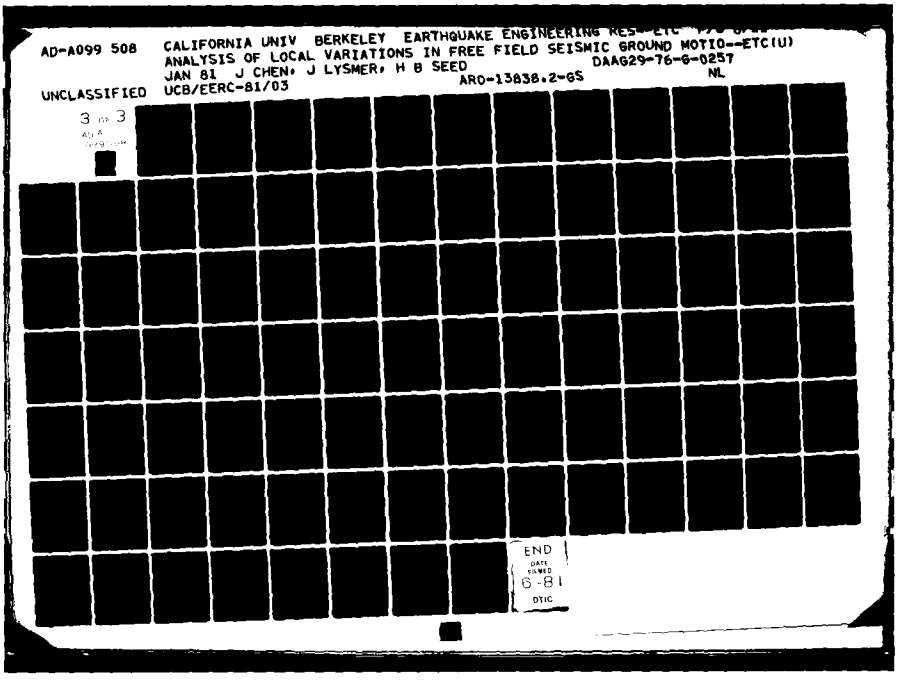
AD-A099 508 CALIFORNIA UNIV BERKELEY EARTHQUAKE ENGINEERING RES...
ANALYSIS OF LOCAL VARIATIONS IN FREE FIELD SEISMIC GROUND MOTIO--ETC(U)
JAN 81 J CHEN, J LYSMER, H B SEED DAAG29-76-G-0257
UNCLASSIFIED UCB/EERC-81/03 ARO-13838.2-GS NL
3 OF 3
END
DATE FILMED
6-81
DTIC

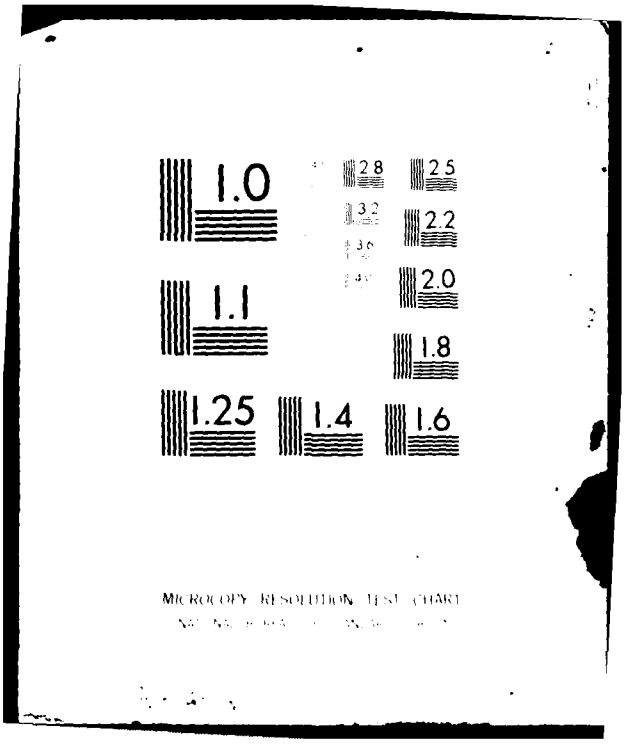
1.0
2.8
2.5
3.2
2.2
3.6
4.0
2.0
1.1
1.8
1.25
1.4
1.6
MICROCOPY RESOLUTION TEST CHART

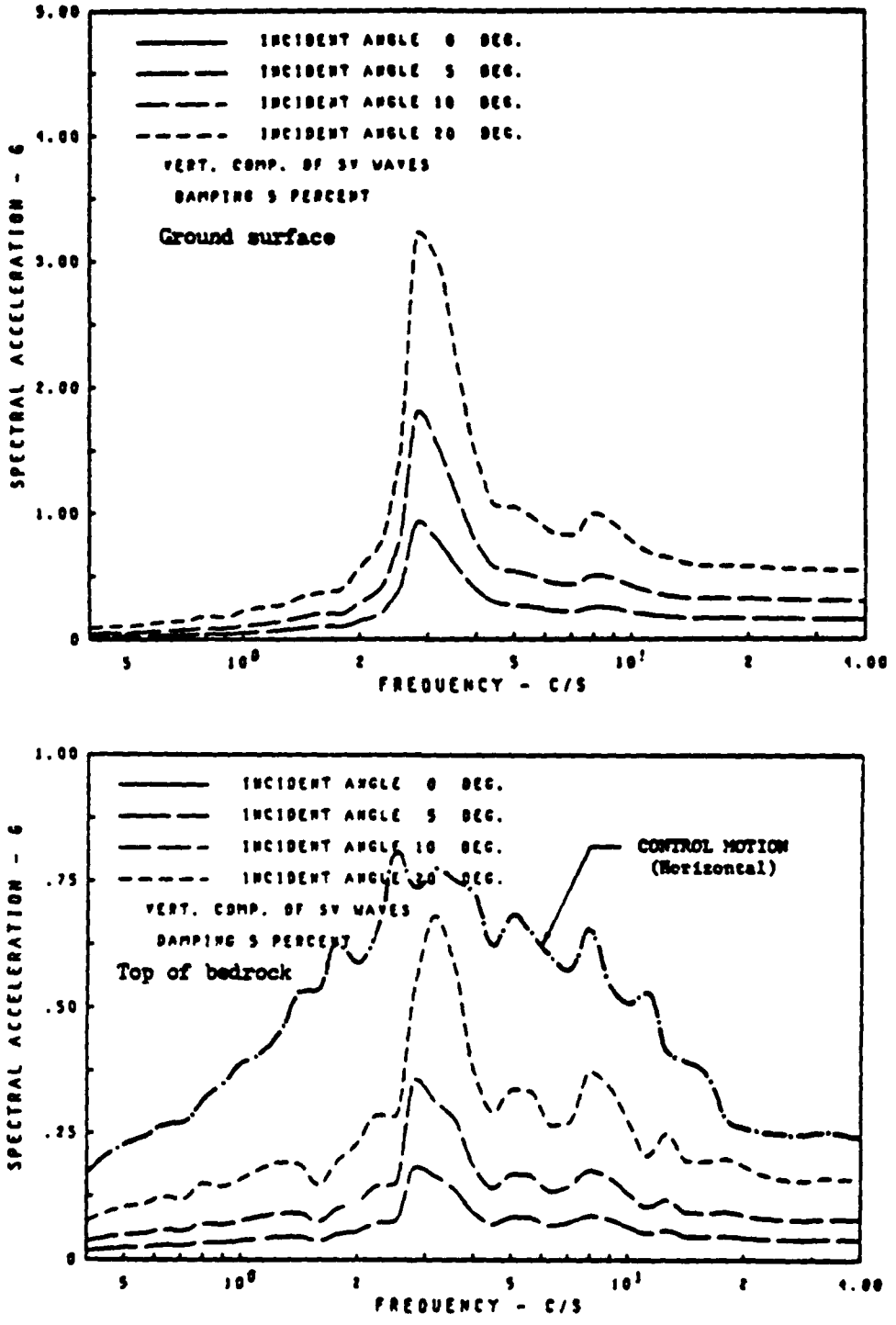

Fig. 5.29 Response Spectra of Vertical Component of SV Wave Motion - Sand Site Response to Inclined SV Waves at Different Angle of Incidence

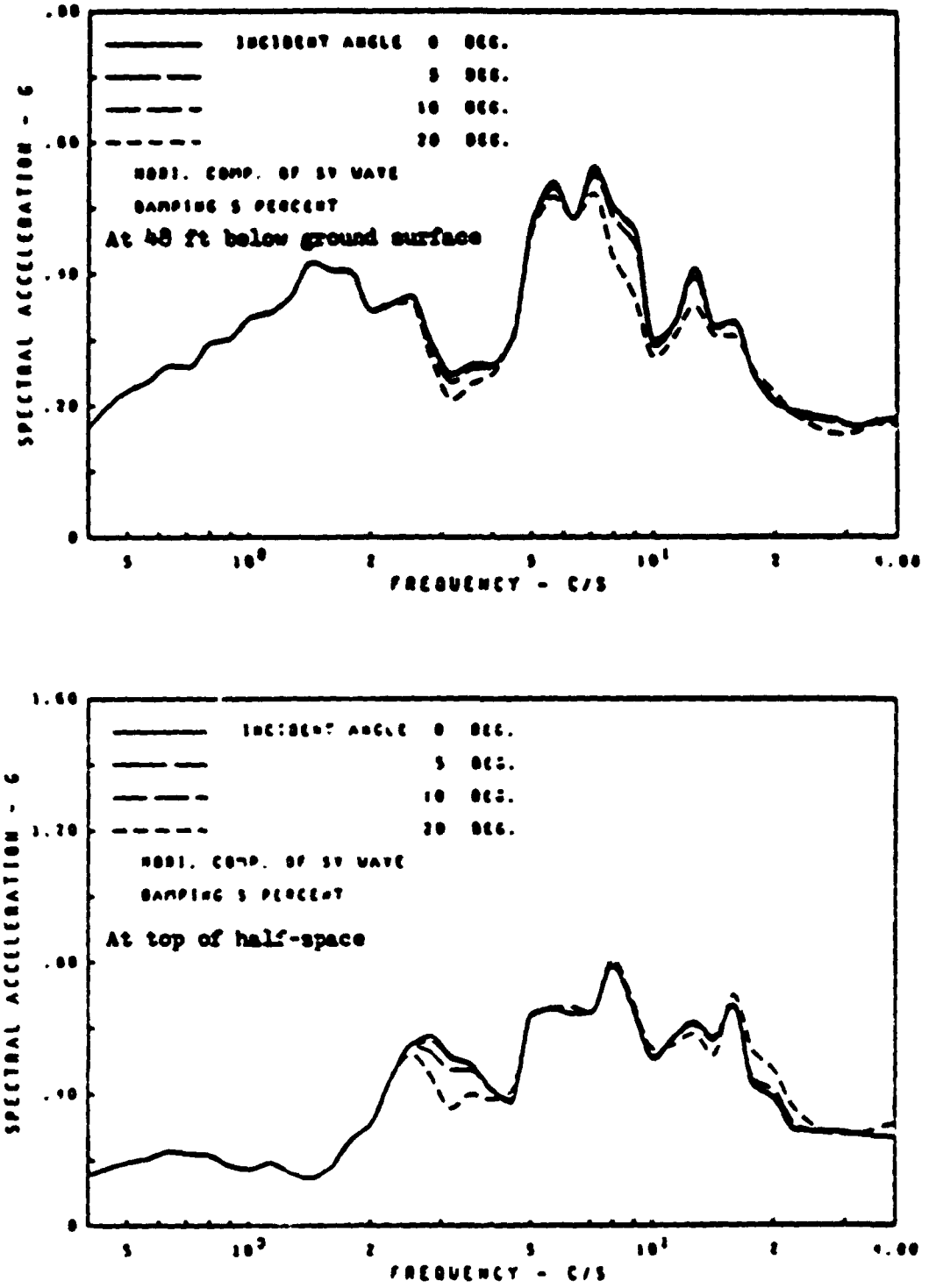

Fig. 5.30 Response Spectra of Horizontal Component for SV Wave Motion in Sand Site - Control Motion on Ground Surface

The basic conclusions from the above study are that for cohesionless sites over bedrock:

- The variation of horizontal motions with depth is independent of the angle of incidence, and
- Vertical motions increase approximately proportionally with the angle of incidence, and tend to contain somewhat higher frequencies than the horizontal motions.

For practical purposes the first conclusion implies that the conventional assumption of vertical propagation can be used to compute the variation of motions with depth. It should, however, be remembered that for cases involving inclined body waves the motions vary in phase from point to point in the horizontal direction and that they decay in that direction in relation to the damping ratio of the bedrock.

5.5.5 Mixed Wave Field

As discussed at several points above, the fact that high frequency fundamental surface waves decay rapidly as they propagate through soil sites is a strong indication that such waves may not exist in nature. When this evidence is combined with the fact that such waves have not been observed in the field, the conclusion must be that the partitioning of the wave types which produce the control motion must be frequency dependent, i.e. the relative content of surface waves must decrease with frequency. The computer programs SITE and LOVE developed in the course of the research described herein have the ability to consider such frequency-dependent partitionings of wave types. This is achieved by the use of partitioning functions which specify the relative content of each wave type. Admittedly, such partitioning functions have not yet been established by seismologists. Nevertheless, it was decided to

analyze the enhancement site for a combination of Rayleigh waves and inclined SV-waves arriving from the same direction. The partitioning was defined as follows: The Rayleigh wave content was set to 100% at zero frequency. It then decreased linearly to 33 1/3% at 7 Hz and remained at this percentage at higher frequencies. The incident angle for the SV-waves was set to 10 degrees with vertical.

Computed response spectra at different depths are shown in Figs. 5.31 and 5.32. The variation of the field in the direction of wave propagation is illustrated by the response spectra shown in Fig. 5.33. These latter spectra were obtained using a slightly different partitioning in which the frequency at which the Rayleigh wave content reached 33 1/3% was changed to 4 Hz. Also, the incident angle of the SV-waves was reduced to 10 degrees.

As can be seen from these results the use of partitioning functions enable the engineer to create complex environments which may have realistically in space that fields consisting of only one wave type for example, as can be seen from Fig. 5.31, at the ground surface the vertical component is 1.7 to 1.9 of the horizontal component, which is about the ratio observed by earthquakes. Also, the attenuation in the direction of wave propagation indicated by the results in Fig. 5.33 are much more realistic than what was found for pure Rayleigh wave fields, e.g. Fig. 5.28.

The high peak indicated at 7 Hz for the vertical surface motions in all of the above figures is a resonance phenomenon associated with the inclined body waves. As can be seen from Table 5.3 this frequency coincides with the first S-wave natural frequency of the sand layer.

A comparison between the transfer functions shown in Figs. 5.28 and 5.27 will show that at this frequency the ratio between vertical and

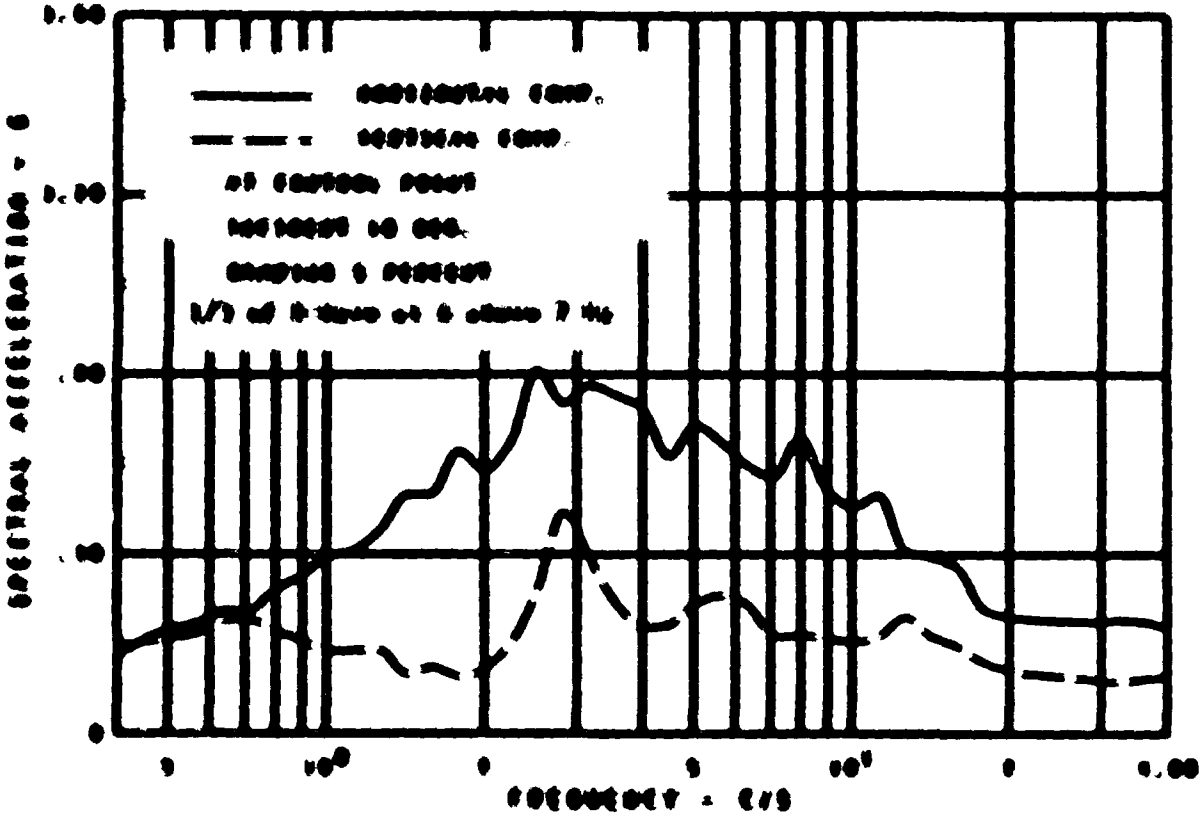

Fig. 5.31 Strike frequency by combination of P-wave and horizontal SV wave frequency spectra of ground surface motion on shell strike

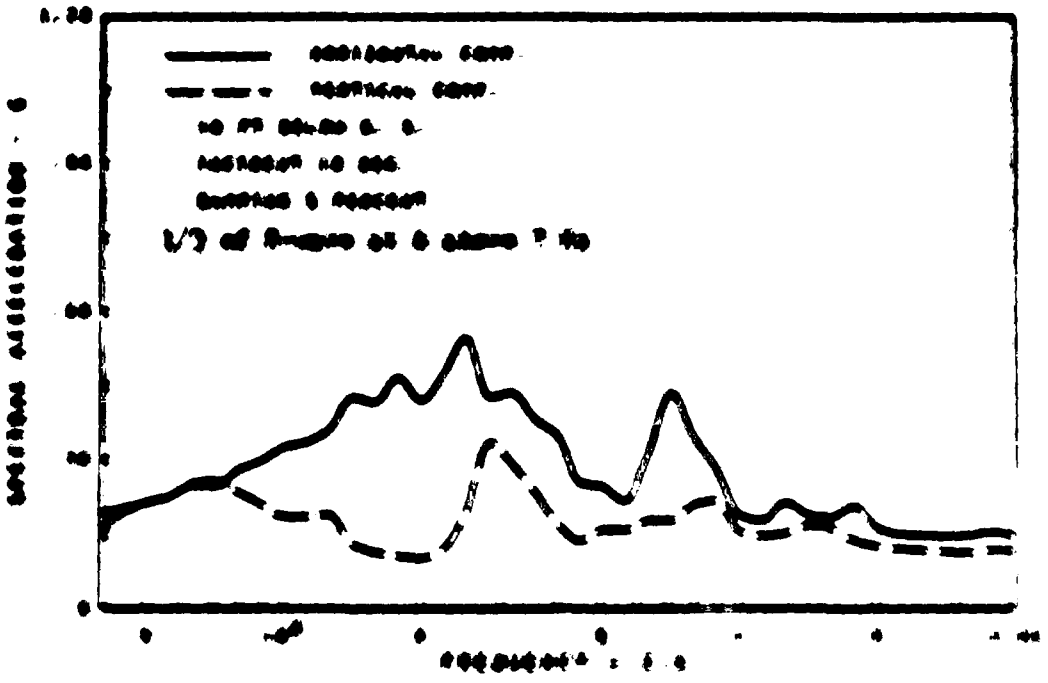

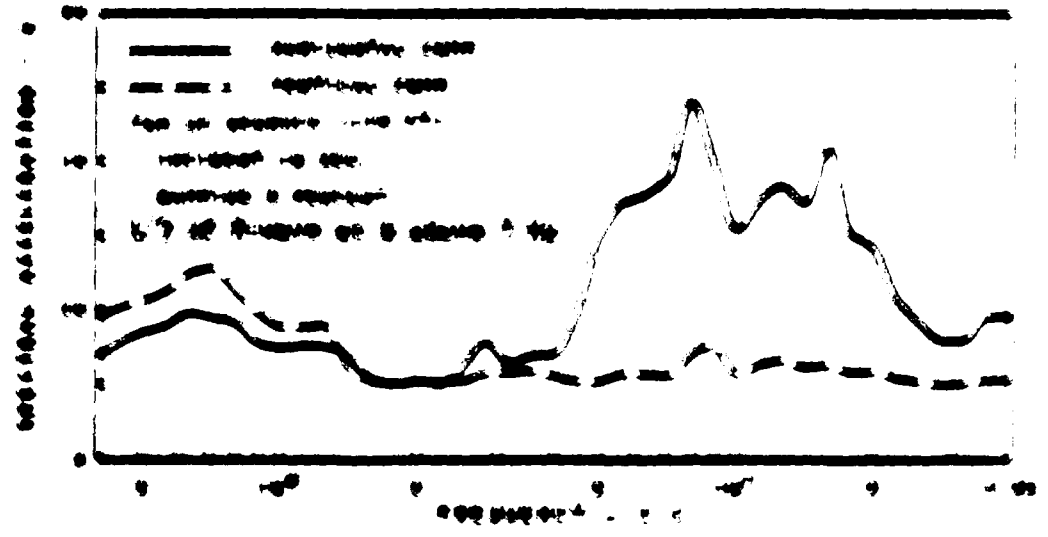

Fig. 7.10 Stress Response to Deformation of Sample with Intermediate Curve - Response Specimen of Different Thickness at Same Strain

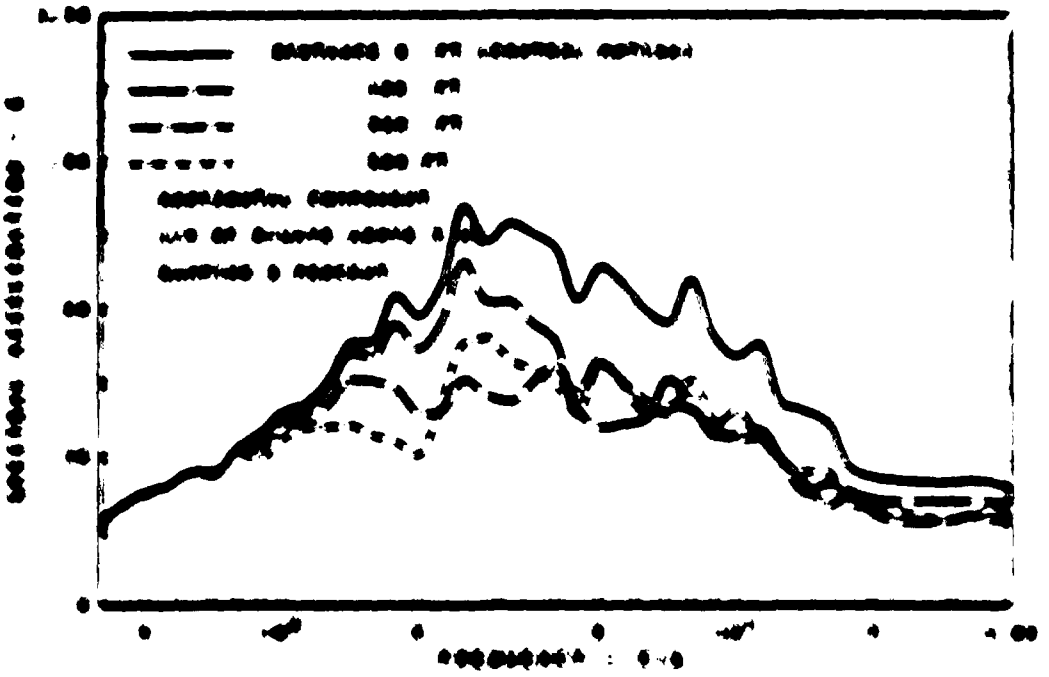

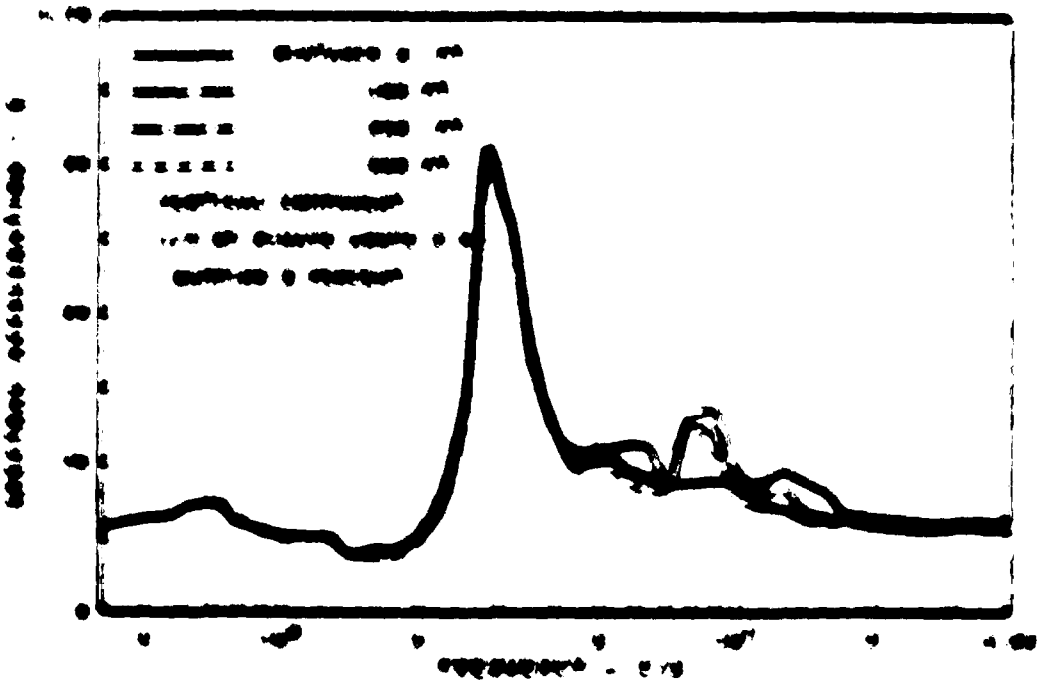

Fig. [illegible] [illegible]

[illegible]

3.6 [illegible]

[illegible]

[illegible]

[illegible]

[illegible]

[illegible]

[illegible]

Layer No.	Depth* (ft.)	Soil Type	SPT (blows/ft.) or Su (psf)	Unit Wt. (pcf)	δ (deg) (Eq.)	δ (deg) (Eq.)
1	[illegible]	Clay	[illegible]	[illegible]	[illegible]	[illegible]
2	[illegible]	Clay	[illegible]	[illegible]	[illegible]	[illegible]
3	[illegible]	Clay	[illegible]	[illegible]	[illegible]	[illegible]
4	[illegible]	[illegible]	[illegible]	[illegible]	[illegible]	[illegible]
5	[illegible]	Clay	[illegible]	[illegible]	[illegible]	[illegible]
6	[illegible]	[illegible]	[illegible]	[illegible]	[illegible]	[illegible]
7	[illegible]	Clay	[illegible]	[illegible]	[illegible]	[illegible]
8	[illegible]	[illegible]	[illegible]	[illegible]	[illegible]	[illegible]
9	[illegible]	Clay	[illegible]	[illegible]	[illegible]	[illegible]
10	[illegible]	[illegible]	[illegible]	[illegible]	[illegible]	[illegible]
11	[illegible]	Clay	[illegible]	[illegible]	[illegible]	[illegible]
12	[illegible]	[illegible]	[illegible]	[illegible]	[illegible]	[illegible]
13	[illegible]	Clay	[illegible]	[illegible]	[illegible]	[illegible]
14	[illegible]	[illegible]	[illegible]	[illegible]	[illegible]	[illegible]
15	[illegible]	Clay	[illegible]	[illegible]	[illegible]	[illegible]
16	[illegible]	[illegible]	[illegible]	[illegible]	[illegible]	[illegible]
17	[illegible]	Clay	[illegible]	[illegible]	[illegible]	[illegible]
18	[illegible]	[illegible]	[illegible]	[illegible]	[illegible]	[illegible]

* [illegible]

** [illegible]

*** [illegible]

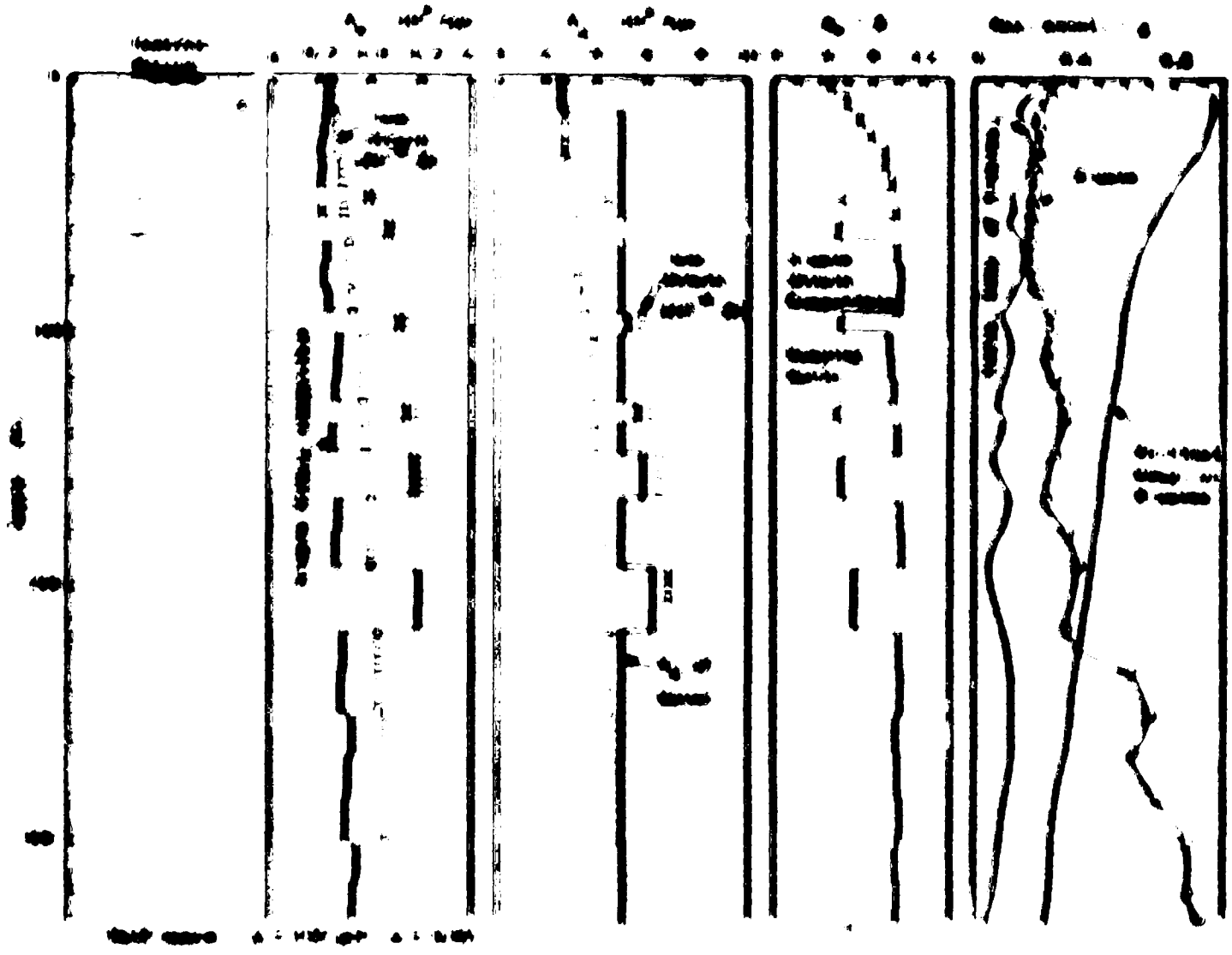

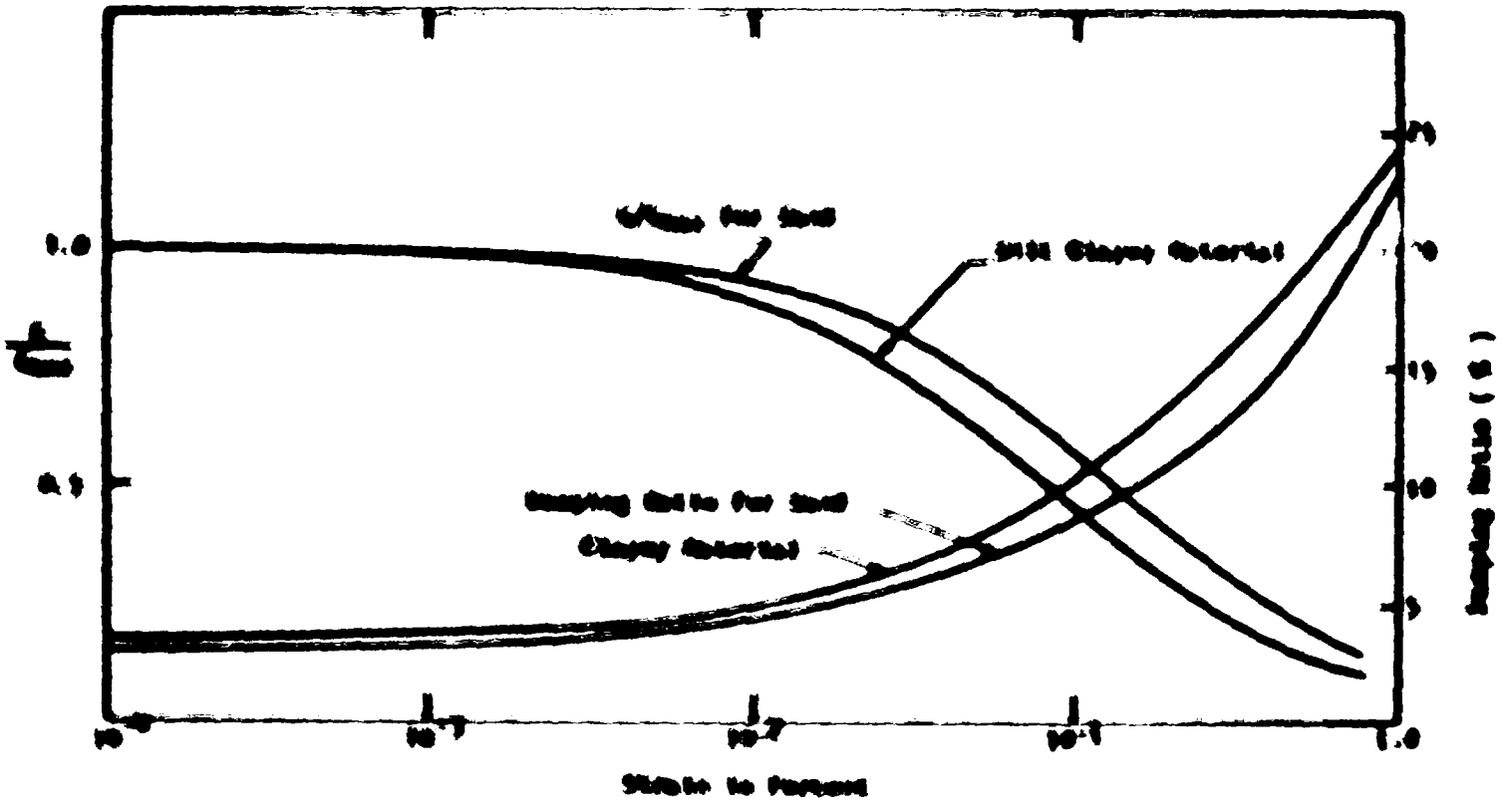

Figure 5.25 Stable Compatible Soil Properties for Saturated Silo

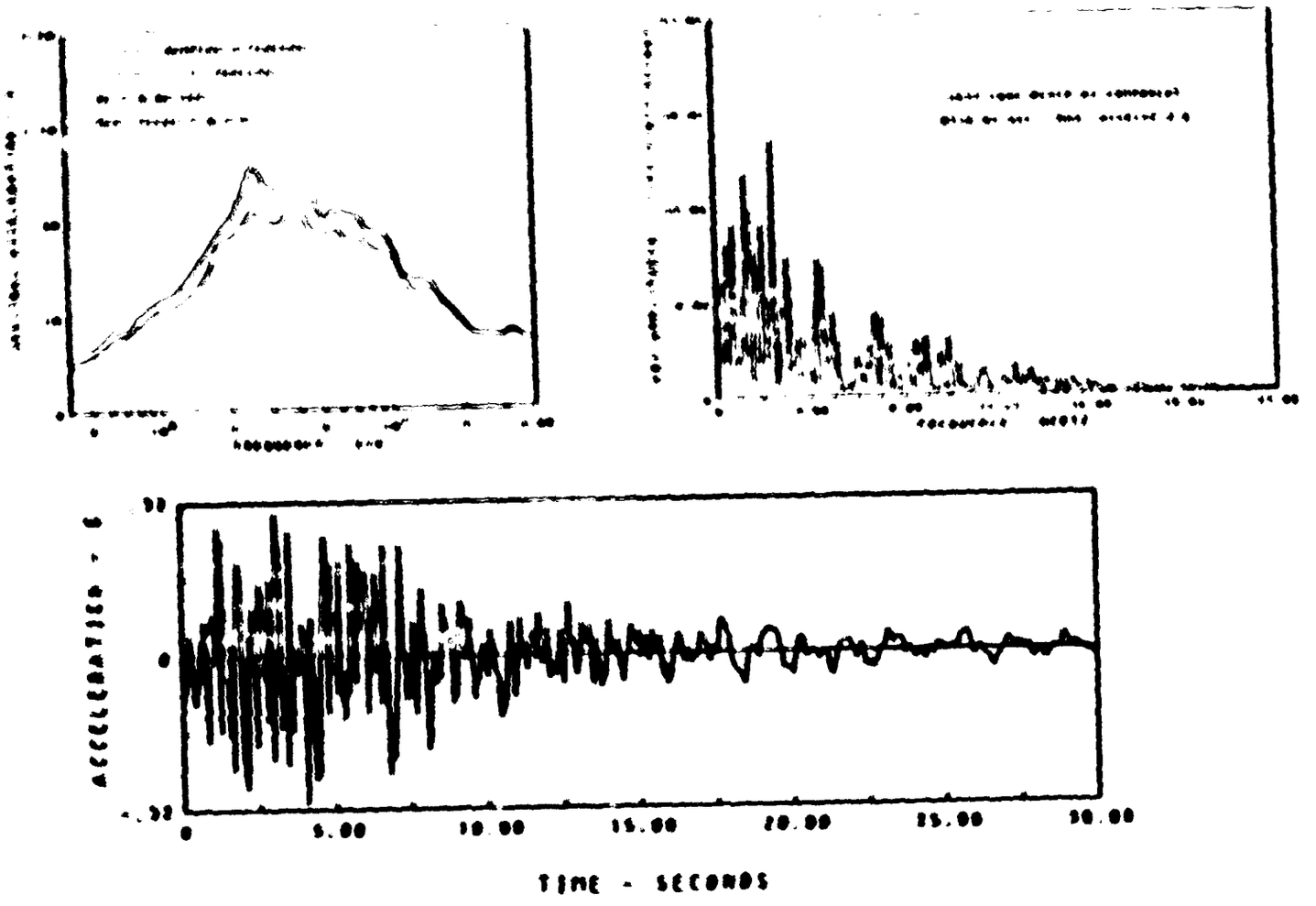

Fig. 5.36 Control Motion for the Saturated Site - Long Beach 1933 NS Matching 5% Reg. Guide

At points below the ground water level, whenever the P-wave velocity computed by the above procedure fell below 5000 fps it was increased to this value. This modification was made to account for the fact that in a saturated soil mass P-waves cannot propagate slower than the velocity of P-waves in water. Physically this means that if the soil frame is not stiff enough to carry the P-wave at this velocity the wave will travel through the pore water rather than through the soil frame. Experimentally, this phenomenon is often observed when seismic refraction tests for P-waves are carried out on a soft site with high ground water level. In fact it is a commonly used method to establish the location of the water table. Since the ground water level was assumed to be located 12 ft below the surface the above procedure lead to the strain-compatible P-wave velocity profile shown as a full line in the third column of Fig. 5.34.

5.6.1 Steady State Results

Steady state Rayleigh wave computations were performed using the discretized model and the strain-compatible soil properties shown in Fig. 5.34. The dispersion curves for fundamental-mode Rayleigh waves, Fig. 5.37, show that the site is highly dispersive.

The mode shapes shown in Fig. 5.38 indicates much higher vertical than horizontal motions. This is probably true for this site in view of the high Poisson's ratio induced by saturation. However, as discussed in connection with Fig. 4.8, the procedure used probably overestimates the vertical motions slightly for high values of Poisson's ratio. Another effect of the high Poisson's ratio, but not an error, is the unusual difference in smoothness between the horizontal and vertical mode shapes at higher frequencies. Transfer functions for the

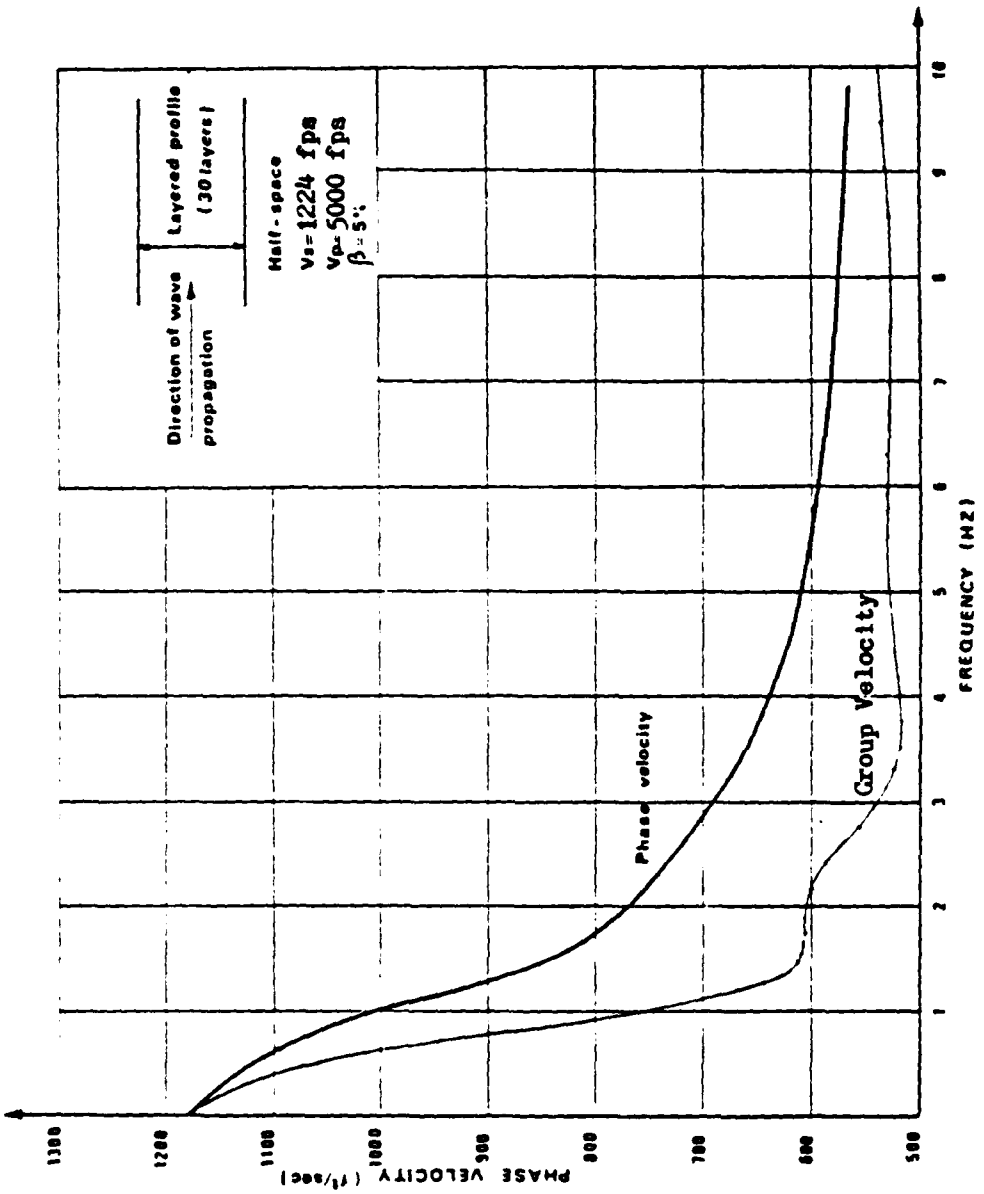

Fig. 5.37 Dispersion Curve for Fundamental Rayleigh Wave - Deep Alluvial Site

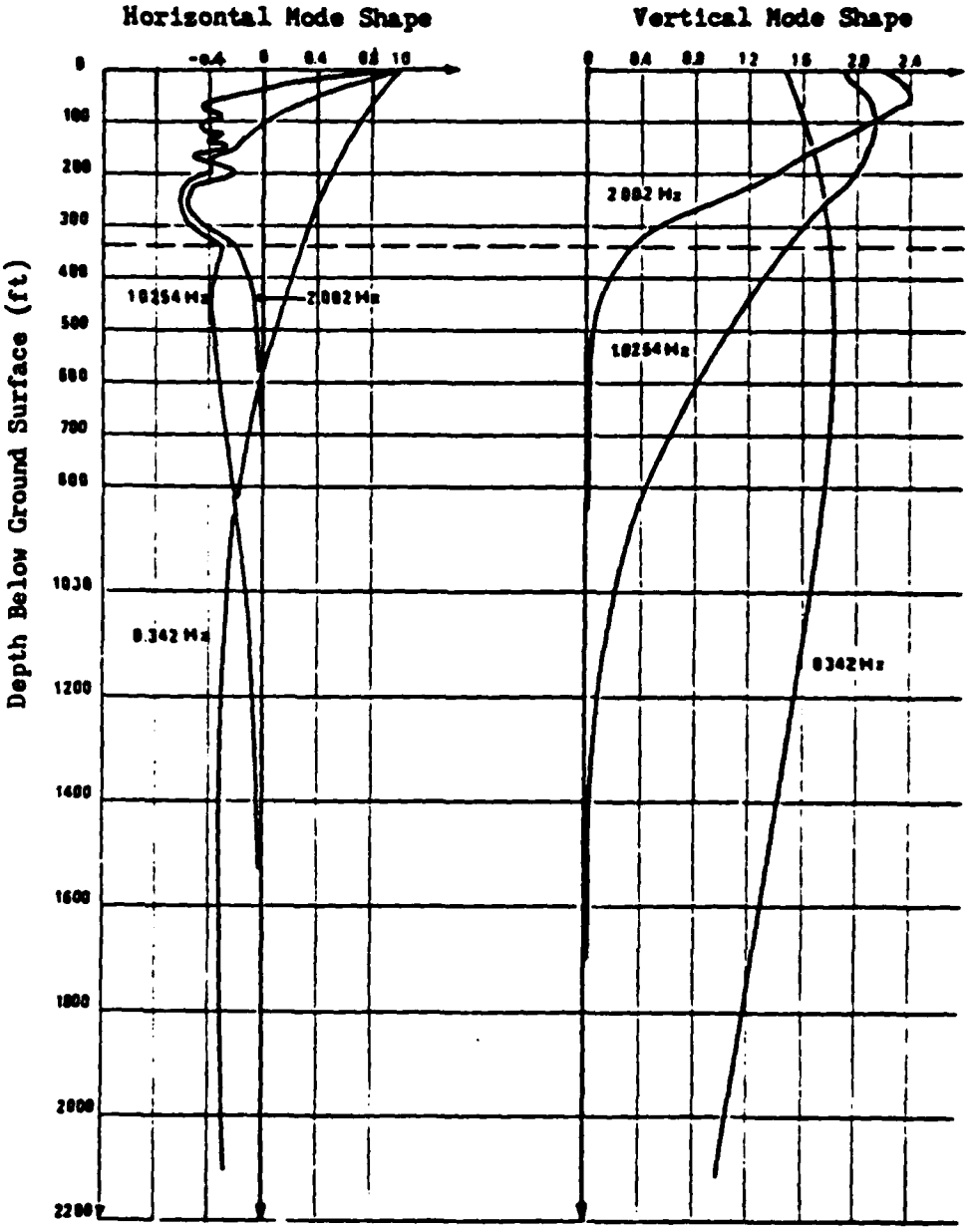

Fig. 5.38 Normalized Mode Shape for Fundamental Rayleigh Mode - Deep Alluvial Site

horizontal and vertical components and different depths and distances from the surface control point are shown in Figs. 5.39 and 5.40. They indicate significant attenuation of all components above 2 Hz within a few hundred feet from the control point.

5.6.2 Transient Results

The transient S-wave analysis produced the acceleration profile shown in Fig. 5.34. The steady increase below a depth of 200 feet is probably due to the fact that an unlikely control motion was used for this analysis. As shown by Hayashi et al. (1971) and Seed et al. (1976) surface motions observed of deep alluvial sites do not contain as many high frequency components as indicated by the control motion spectra in Fig. 5.36. In fact, due to the low velocities (short wavelength) and high attenuation of shear waves in such sites high frequency motions at depth are highly attenuated by the time they reach the ground surface. As a result, if a strong high-frequency component is specified at the ground surface, the deconvolved motion at depth becomes unrealistically strong in the high frequency range. Consequently the accelerations at depth becomes unrealistically high as shown in Fig. 5.34.

The acceleration profile for the corresponding Rayleigh wave analysis is shown in Fig. 5.41. The response spectra of the horizontal and vertical component of R-wave motions at three different ground levels (at ground surface, at 44 ft and 332 ft below ground surface) are shown in Figs. 5.42 and 5.43. Motions were computed directly under the control point and at a horizontal distance of 500 ft from this point.

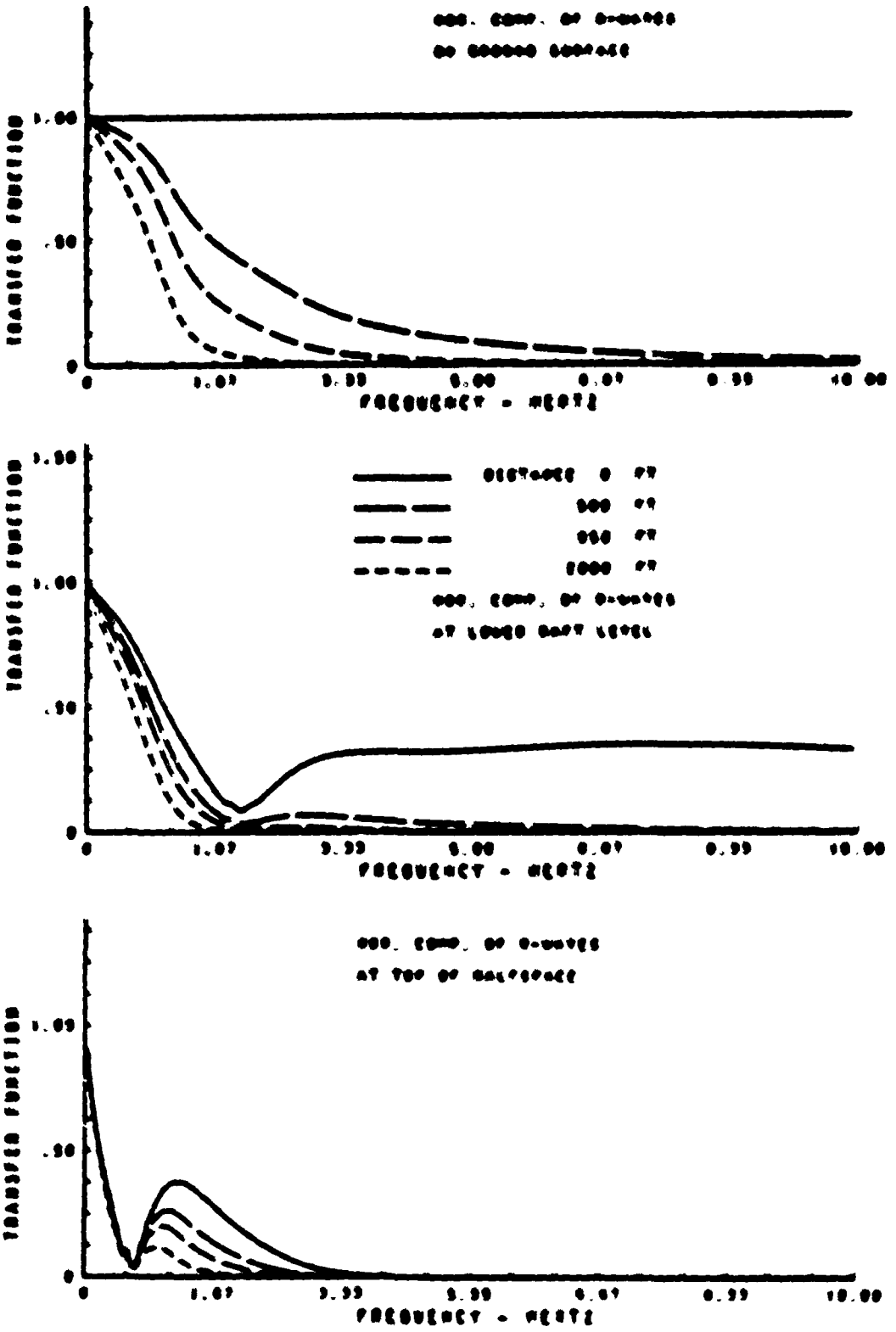

Fig. 5.39 Site Transfer Function on Horizontal Component of R-Wave - Deep Alluvial Site

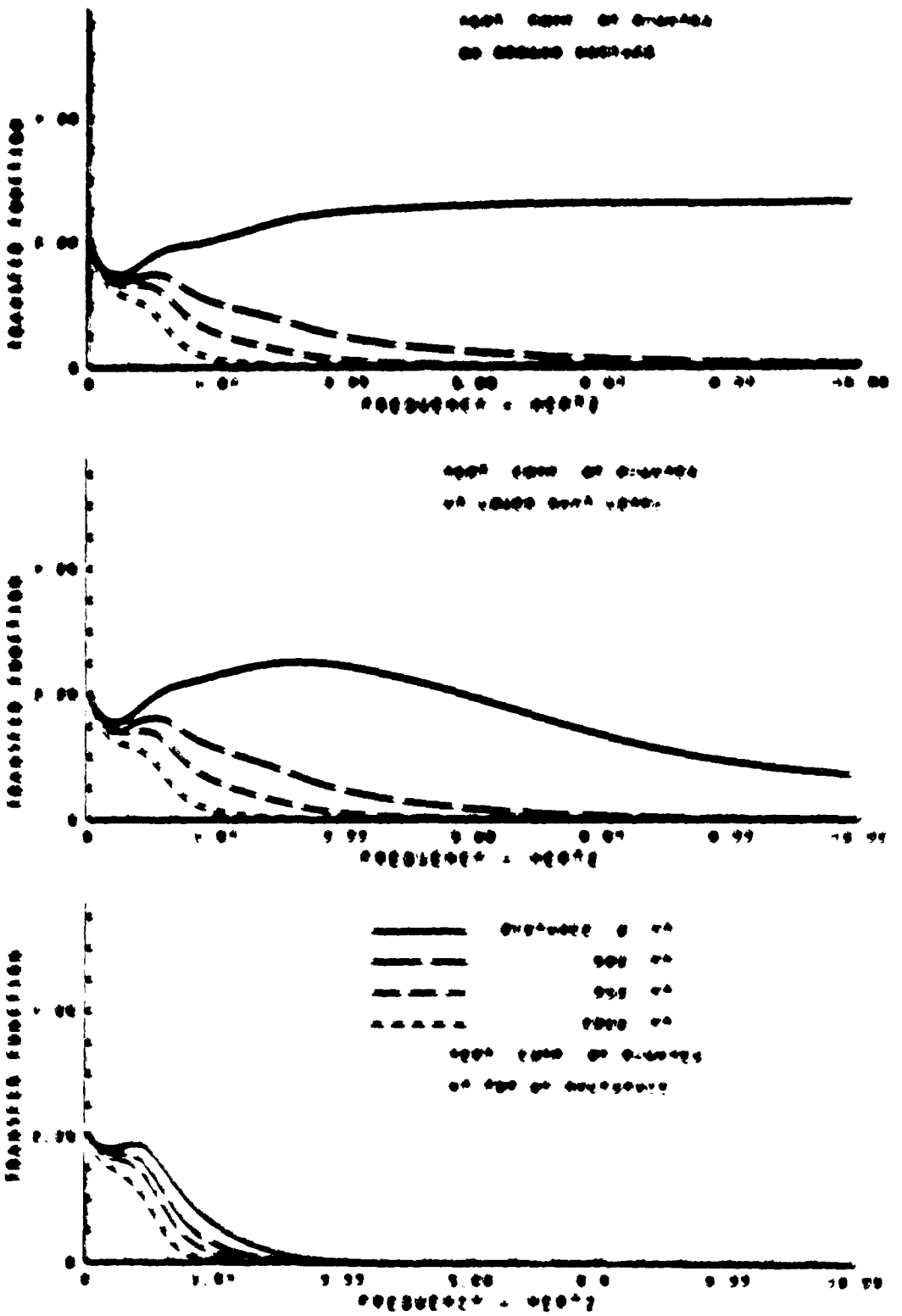

Fig. 5.40 Site Transfer Function on Vertical Component of Ground
- Deep Saturated Site Response to Rayleigh Waves

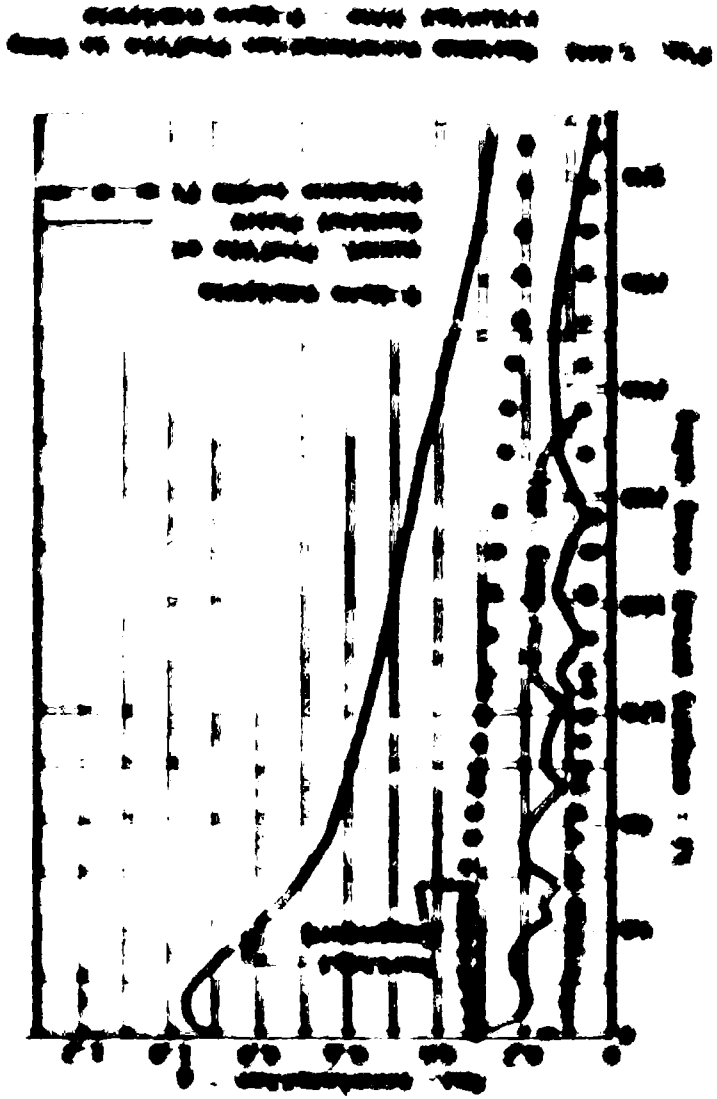

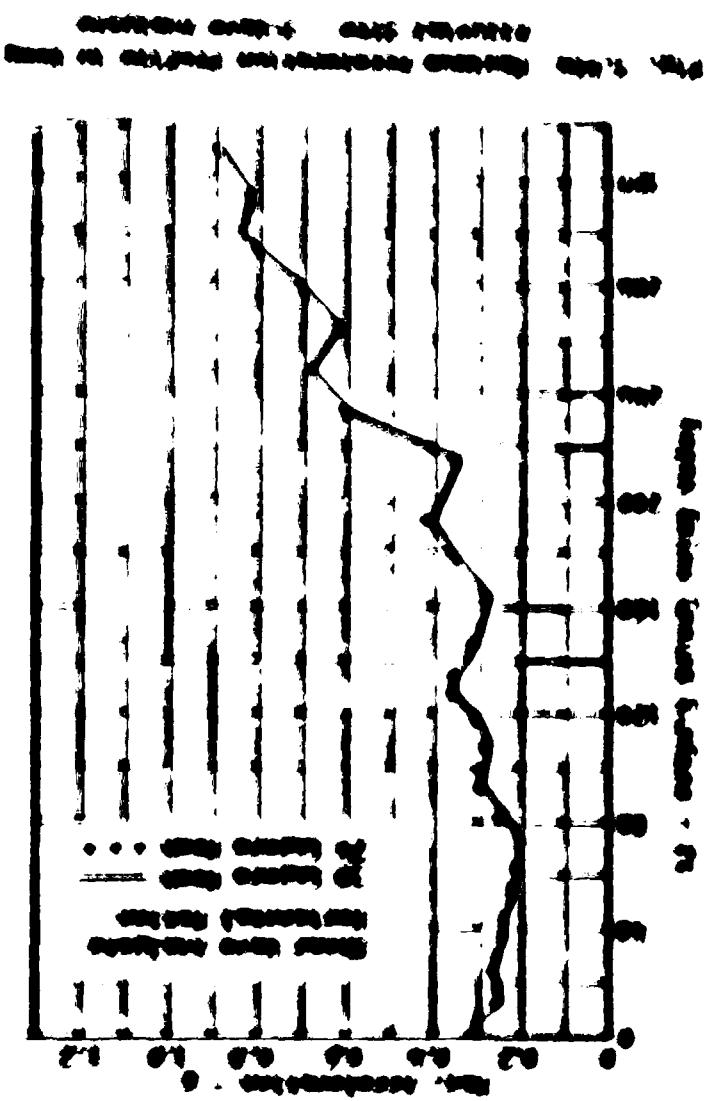

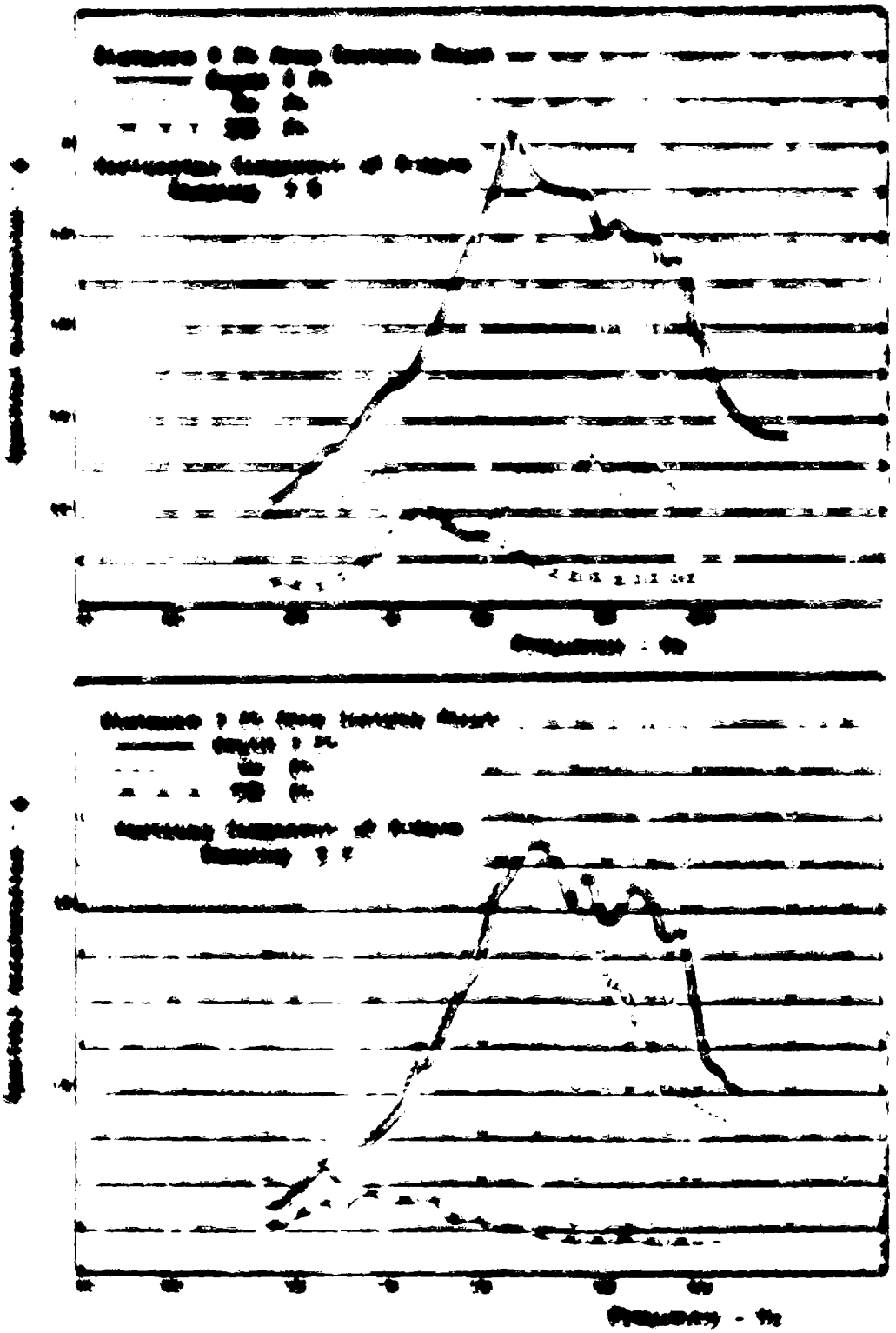

Fig. 5.10 Response [illegible] - Plunger thrusts at different levels in [illegible] ... in ... ft from vertical thrust

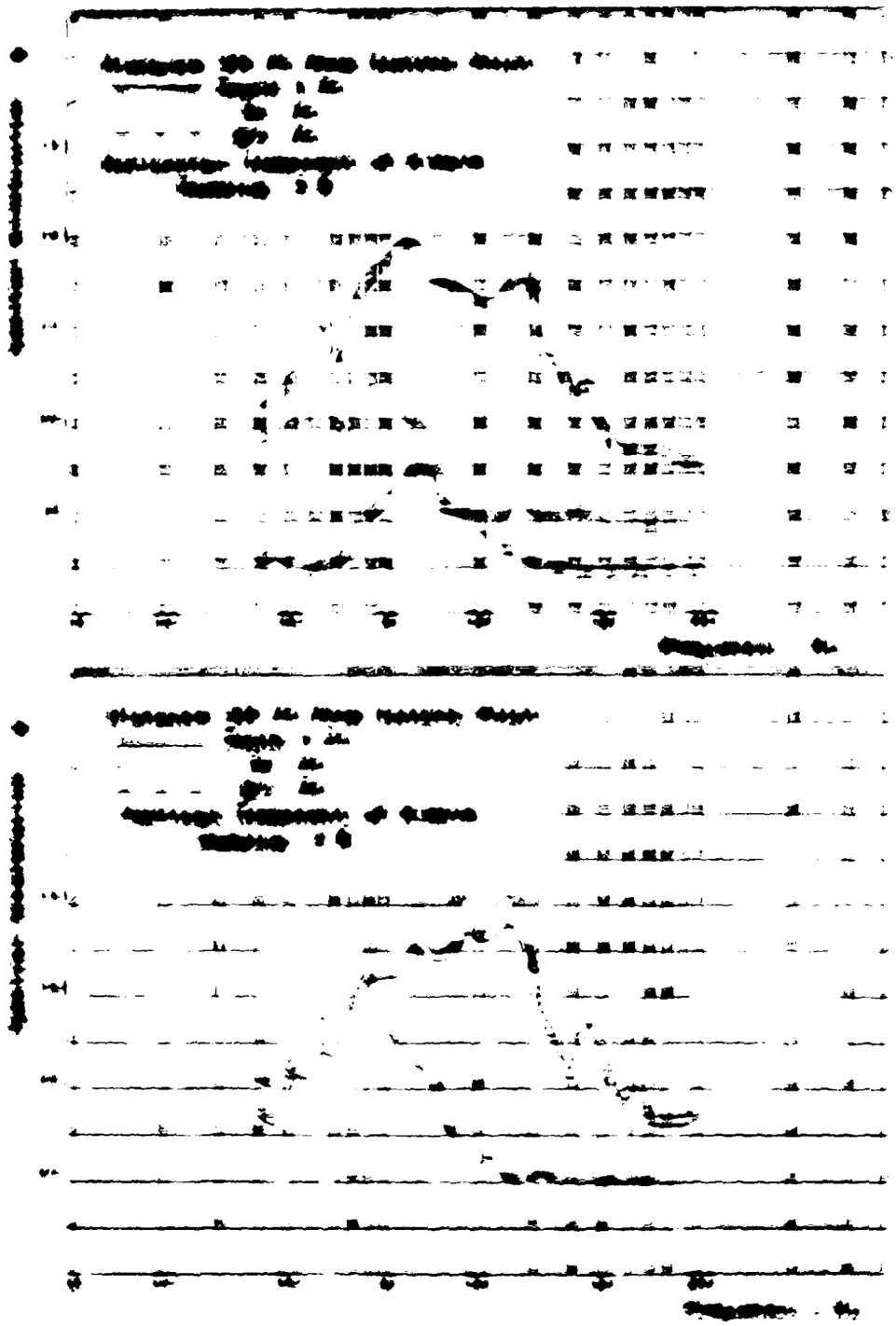

[redacted]

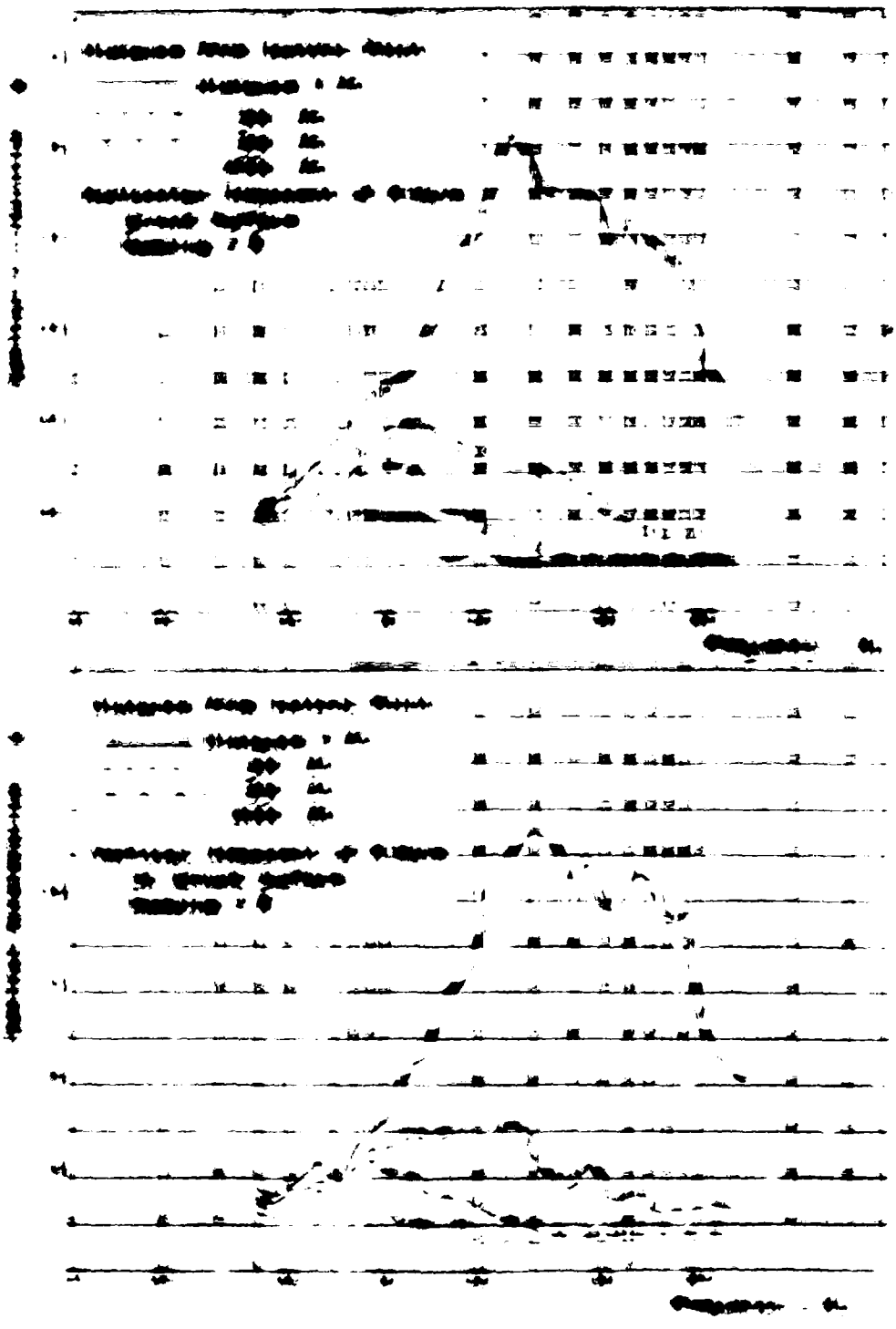

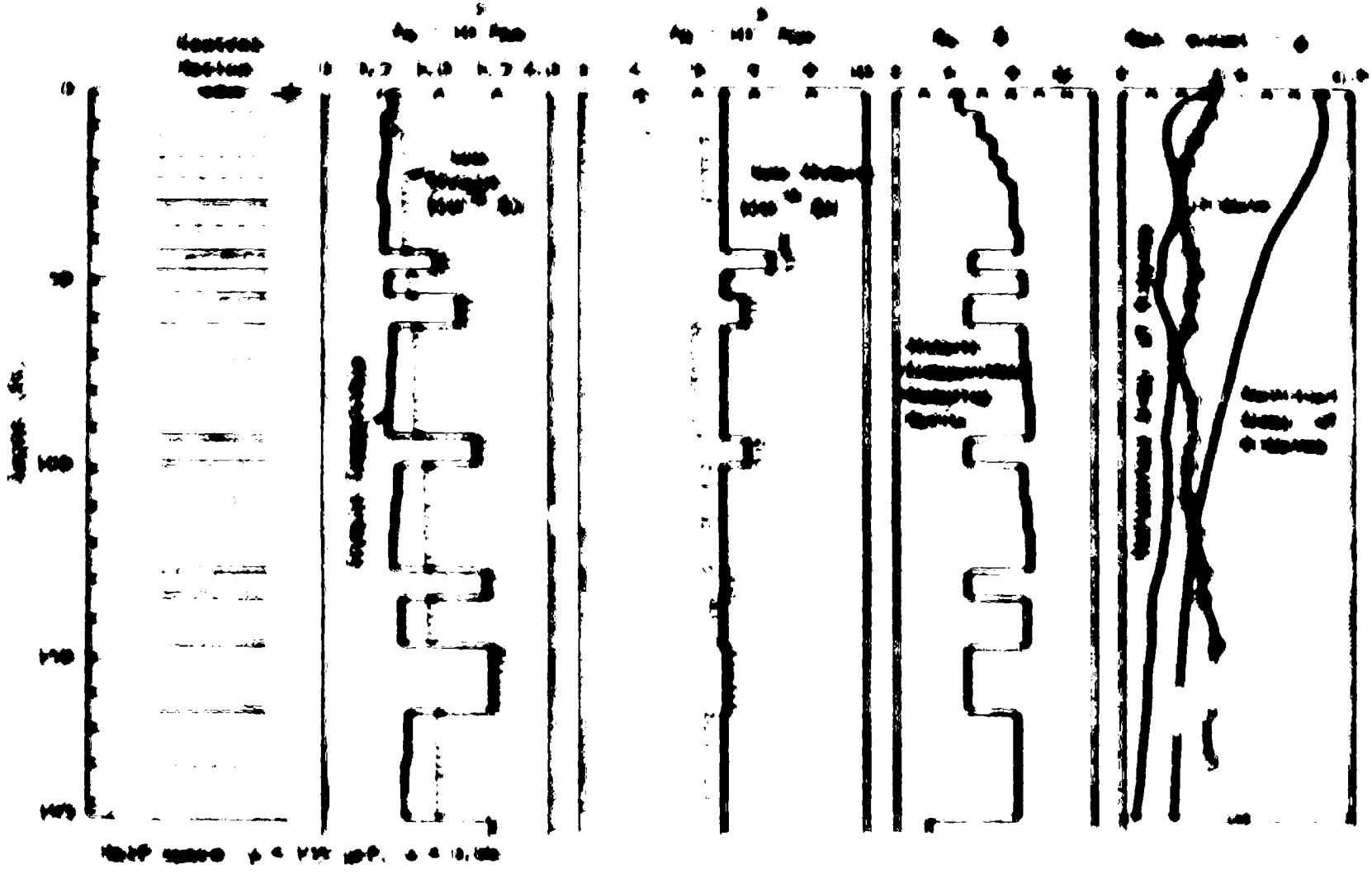

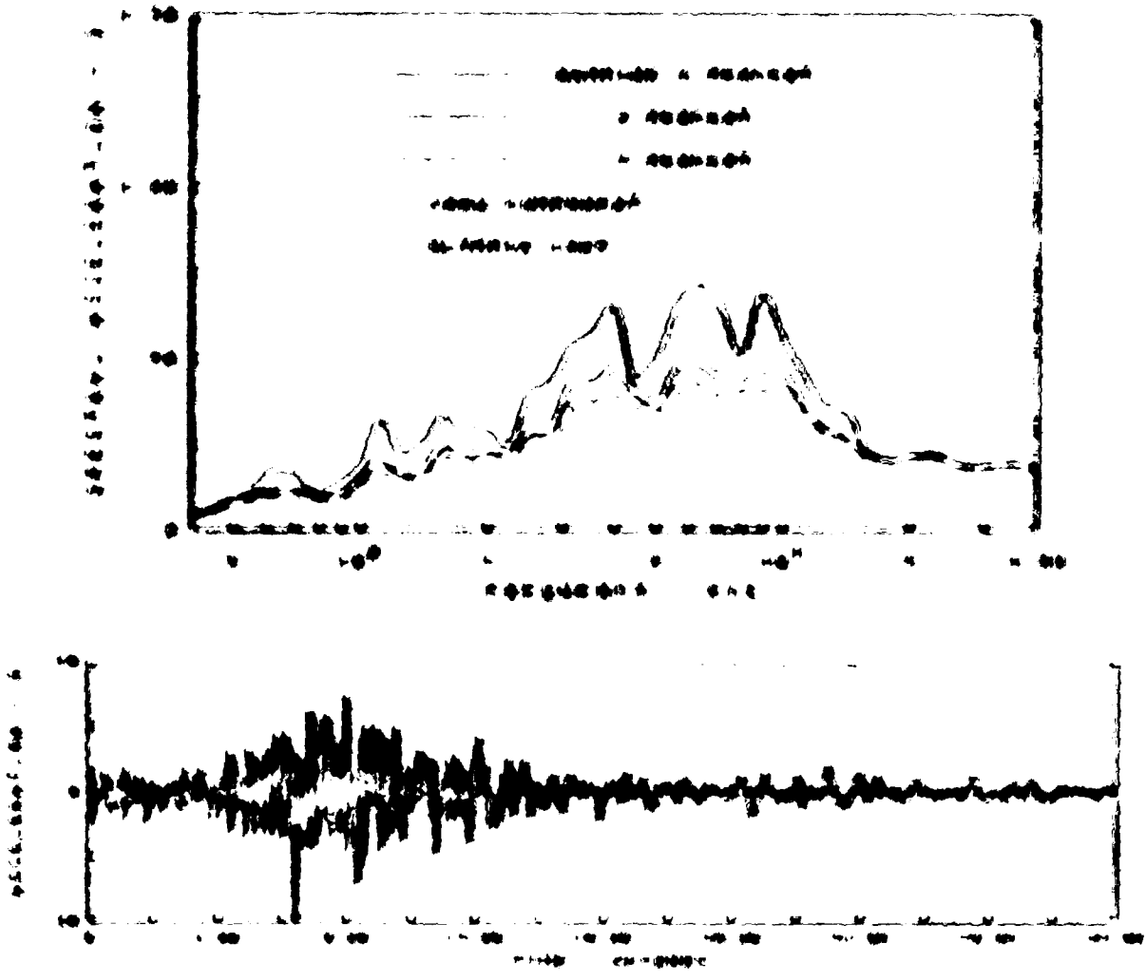

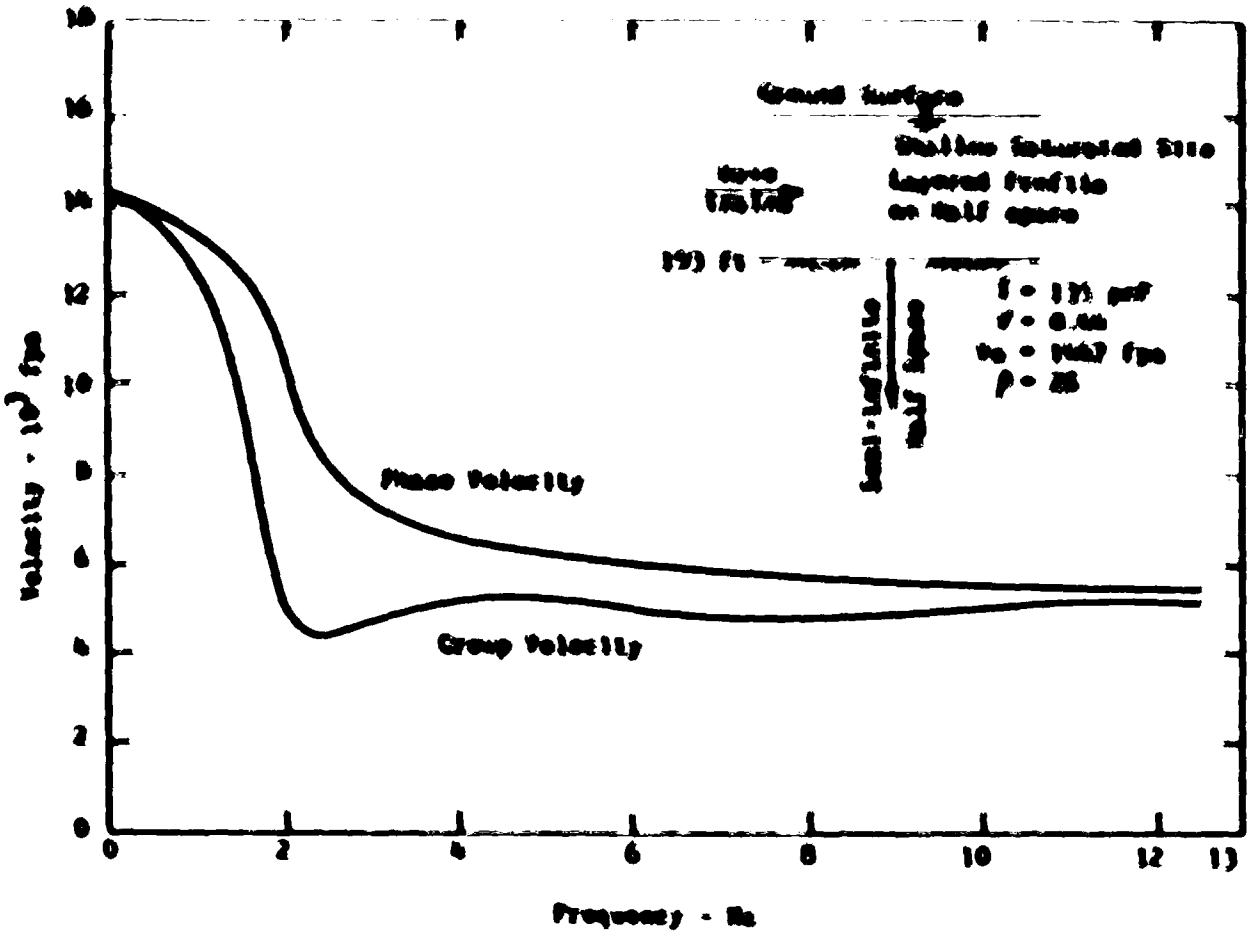

Fig. 5.47 Dispersion Curve for Fundamental Mode of R-Wave in the Shallow Alluvial Site

transfer functions shown in Figs. 5.48 and 5.49. As described before it appears unlikely that surface waves of frequencies higher than 2 Hz can actually exist on the site.

5.7.2 Transient Results

The transient analysis produced the variation with depth of the maximum accelerations and the S-wave compatible strains shown in Fig. 5.45. The results are similar to those found for the deep alluvial site. The response spectra of the horizontal and vertical component of Rayleigh wave motions computed at several different traveling distances are shown in Figs. 5.50 and 5.51. Again, strong decay characteristics of Rayleigh wave propagating in an alluvial site clearly shows that the high frequency Rayleigh wave is not likely to exist in an alluvial site.

5.8 Summary for All Sites

What has been demonstrated in this chapter is that the numerical methods developed in Chapters 3 and 4 can indeed be applied to actual field problems. This demonstration will continue in the next chapter where some of the results obtained will be applied to a number of soil-structure interaction problems.

Perhaps even more important, some of the results obtained in this chapter provide important information on the likelihood of certain types of wave fields actually existing in nature and on the relative importance of horizontal wave propagation to engineering projects. This is most strikingly demonstrated by the computed rapid attenuation of fundamental mode Rayleigh waves in soil sites which seems to preclude the existence of high frequency Rayleigh waves on such sites. This observation does not preclude the possibility that higher-mode

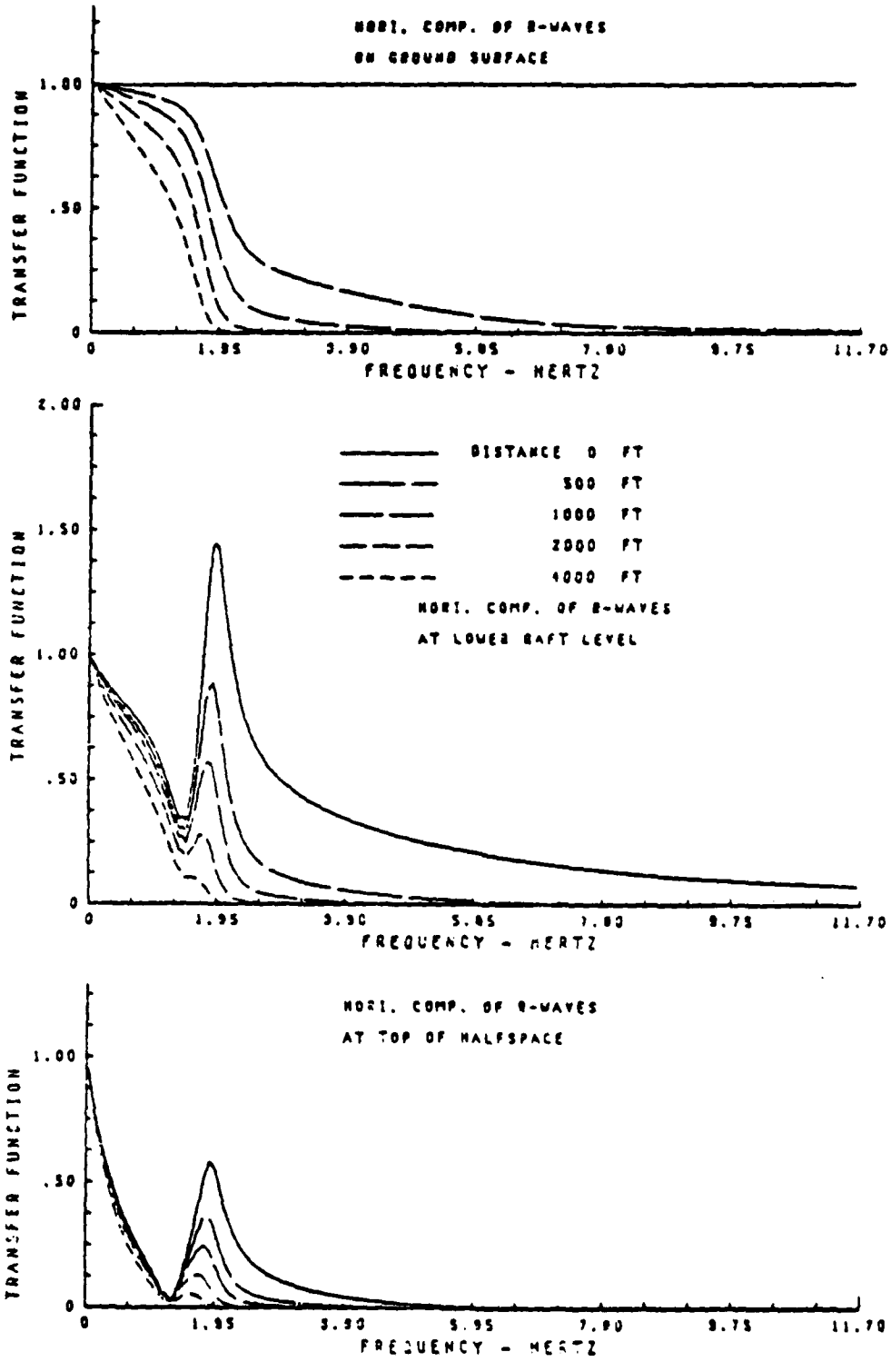

Fig. 5.48 Site Transfer Function on Horizontal Component of R-Wave - Shallow Alluvial Site Response to Rayleigh Waves

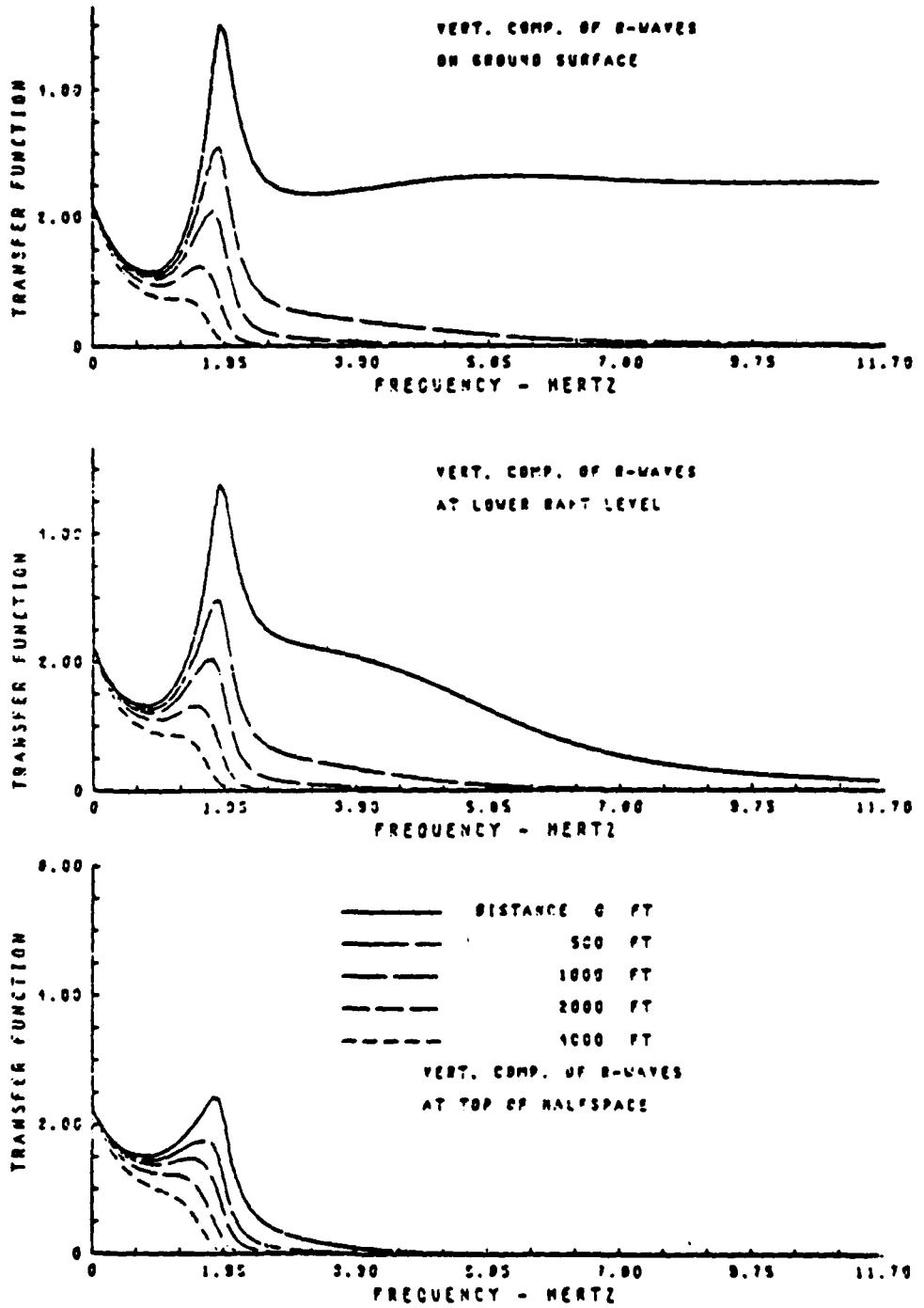

Fig. 5.49 Site Transfer Function on Vertical Component of R-Wave - Shallow Alluvial Site Response to Rayleigh Waves

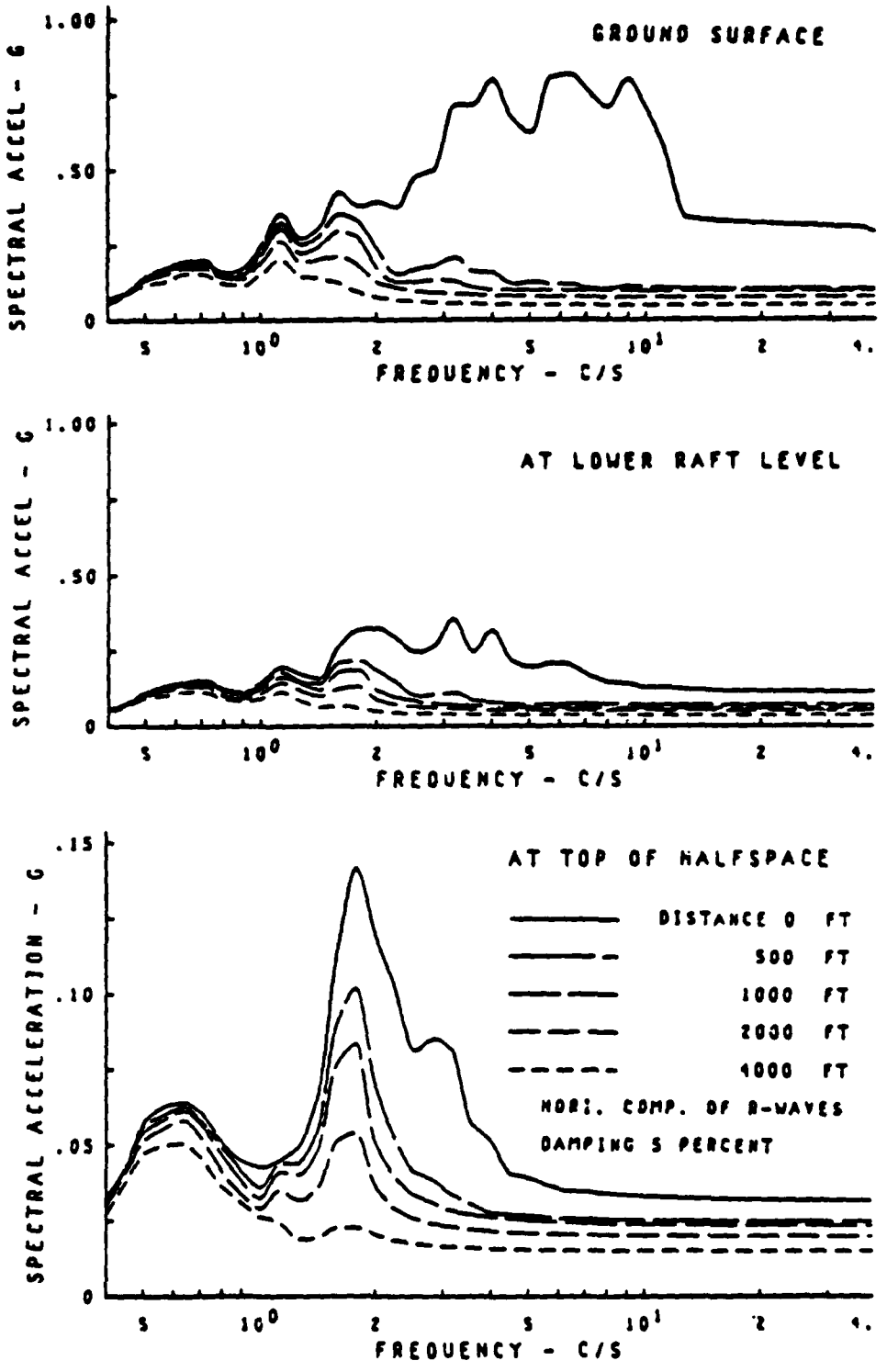

Fig. 5.50 Response Spectra of Horizontal Component of R-Wave Motion Travelling at Different Distance - Shallow Alluvial Site

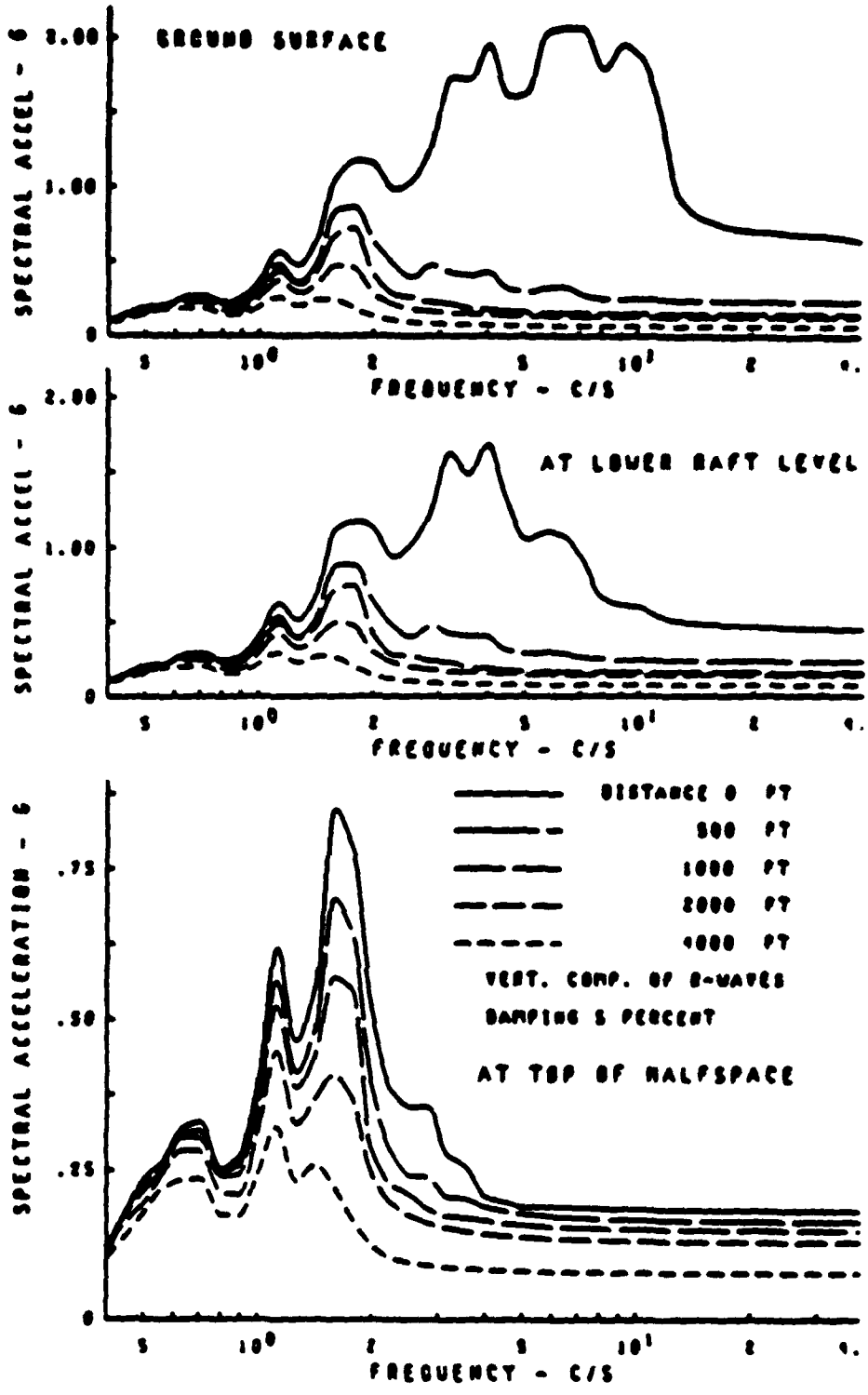

Fig. 5.51 Response Spectra of Vertical Component of R-Wave Motion Travelling at Different Distance - Shallow Alluvial Site

Rayleigh waves could exist. As discussed in Section 6.3.3 it is possible that modes of the lower decay type could exist on such sites and further investigations should be made in this area. It should be observed, however, that such modes will have longer wavelengths than the fundamental modes and they will therefore behave more like vertically propagating waves as far as engineering structures are concerned.

The results also show that there is a great need to establish realistic partitioning functions which describe the relative contribution of wave types to control motions. This relationship should be site and frequency dependent.

[illegible]

[illegible] - [illegible]

6.1 [illegible]

The dynamic response of a structure during earthquakes is dependent on the characteristics of earthquake ground motions, the material properties and geometries of both the structure and the foundation, the local soil conditions as well as the geological environment of the site. The effects of soil-structure interaction must be considered in the analysis of various types of structures. A complete soil-structure interaction analysis consists of two parts: a site response analysis for free field motions and an interaction analysis for structural response. Experience has shown that the free-field ground motion characteristics is one of the most important factors involved in the analysis of soil-structure interaction.

Current methods for the site response analysis part of the problem were discussed in Chapter I and some new methods involving vertical body waves and surface waves were presented in Chapters 3-5. In this chapter it will be demonstrated how these methods can be applied in the solution of some complete soil-structure interaction problems.

6.2 Method of Analysis

An overview of current methods of soil-structure interaction analysis has been presented by Lysmer (1978). Only one method, which clearly shows how the spatial variation of the free-field motions enter into the soil-structure interaction problem, will be discussed herein. The method was first suggested by Clough and Penzien (1975). It was first used by Aydinoglu (1977) on a problem involving a surface

[illegible]

The use of the concept of the superposition theorem is illustrated in Fig. 6.1. The three-bolted column of steel flanges are shown at the bottom of the figure supported by the flexible soil-pile system. Each pile, having one of its three ends in the bolted connection, has the displacement given in Fig. 6.1(b) due to displacement, rotation, and twist. Thus at this end, the structure connects to pile-cap at the ground and the bolted represents the free-field problem. The structural nodes above ground level are assumed to be fixed at first and the displacement only for subsequent convenience to ensure that the displacement vector for the three nodes have the same dimension.

The boundary between the soil mass which is being replaced and that which is being replaced is assumed to be located far away from the structure. Thus the sensitive nature, δ_{ij}, are the same for the complete interaction model, Fig. 6.1(a), and the site response model, Fig. 6.1(b).

Using the formulation of the complex response method, [illegible] the real part, where $[k]$ contains the complex displacement amplitudes at all nodes, the total displacements, $\{u\}$, of the complete model, Fig. 6.1(a), can be written

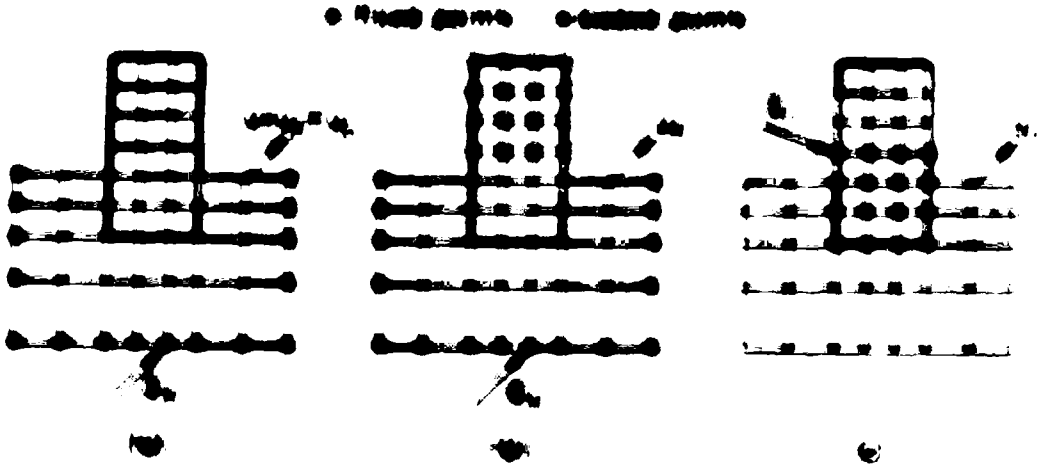

[illegible]

$$|\psi\rangle + |\psi_{sc}\rangle = |\psi_L\rangle \qquad (6.4)$$

where $|\psi_{sc}\rangle$ are the scattered wavefunctions of the outer atom as in Fig. 6.1(b) and $|\psi_L\rangle$ are the exact wavefunctions

The expansions of these two wavefunctions in Fig. 6.1 are

$$\text{wavefunction inside} \quad \sum_{l,m} c_{lm}^{\beta} j_l(kr) Y_{lm}(\theta,\phi) + \psi_{sc} \qquad (6.5)$$

$$\text{wavefunction outside} \quad \sum_{l,m} c_{lm}^{\alpha} h_l^{+}(kr) Y_{lm}(\theta,\phi) + \psi_{sc} \qquad (6.6)$$

where (6.5) and (6.6) describe the same one continuous wavefunction

The wave matching follows as before

Multiply expansion of Eq. (6.5) by Eq. (6.6) and subtract of Eq. (6.6) results in

$$\sum_{l,m} c_{lm}^{\beta} j_l(kr) Y_{lm}(\theta,\phi) = \psi_L \qquad (6.7)$$

where

$$\psi_L + \sum_{l,m} c_{lm}^{\alpha} h_l^{+}(kr) Y_{lm}(\theta,\phi) = \sum_{l,m} c_{lm}^{\beta} j_l(kr) Y_{lm}(\theta,\phi) \qquad (6.8)$$

$$\sum_{l,m} c_{lm}^{\alpha} h_l^{+}(kr) Y_{lm}(\theta,\phi) = \psi_{sc} \qquad (6.9)$$

$$\sum_{l,m} c_{lm}^{\beta} j_l(kr) Y_{lm}(\theta,\phi) = \psi_{sc} \qquad (6.10)$$

Equation (6.8) is the expansion of wavefunction inside the outer atom as in Fig. 6.1(a) and which gives the outer atom as though there are neither

Prior to be matched with expansion (6.5) and (6.6) which represent the wavefunction in each and continuous between the atomic core and the overlapping hard sphere region we set $r=a$ and obtain corresponding to discrete set of values of α on the core edge outside the boundary and because the vector $|\psi_{sc}\rangle$ represents wave waves for any discrete of α values corresponding to the finite radius as Fig. 6.1(b)

For the outer radius the total vector $|\psi_L\rangle$ depends only on the free-field because within the overlapped region there are the core radiation produced has been solved for the outside boundary as the previous diagram the total vector $|\psi_{sc}\rangle$ can be obtained from Eq. (6.9) The interaction displacements $|\psi_L\rangle$ can be found from

[redacted]

[redacted]

[redacted]

[redacted]

[redacted]

- [redacted]
- [redacted]
- [redacted]

[redacted]

[redacted]

[redacted]

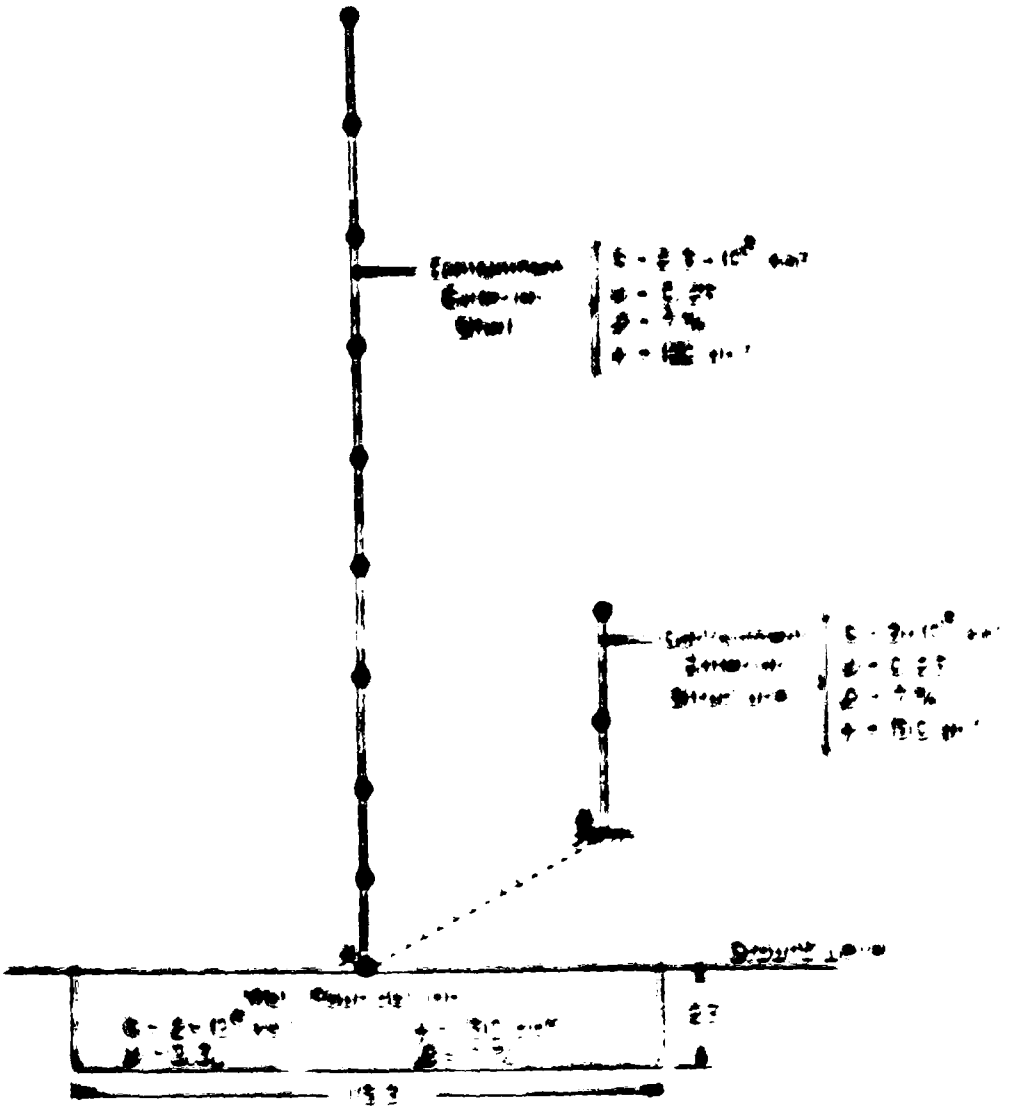

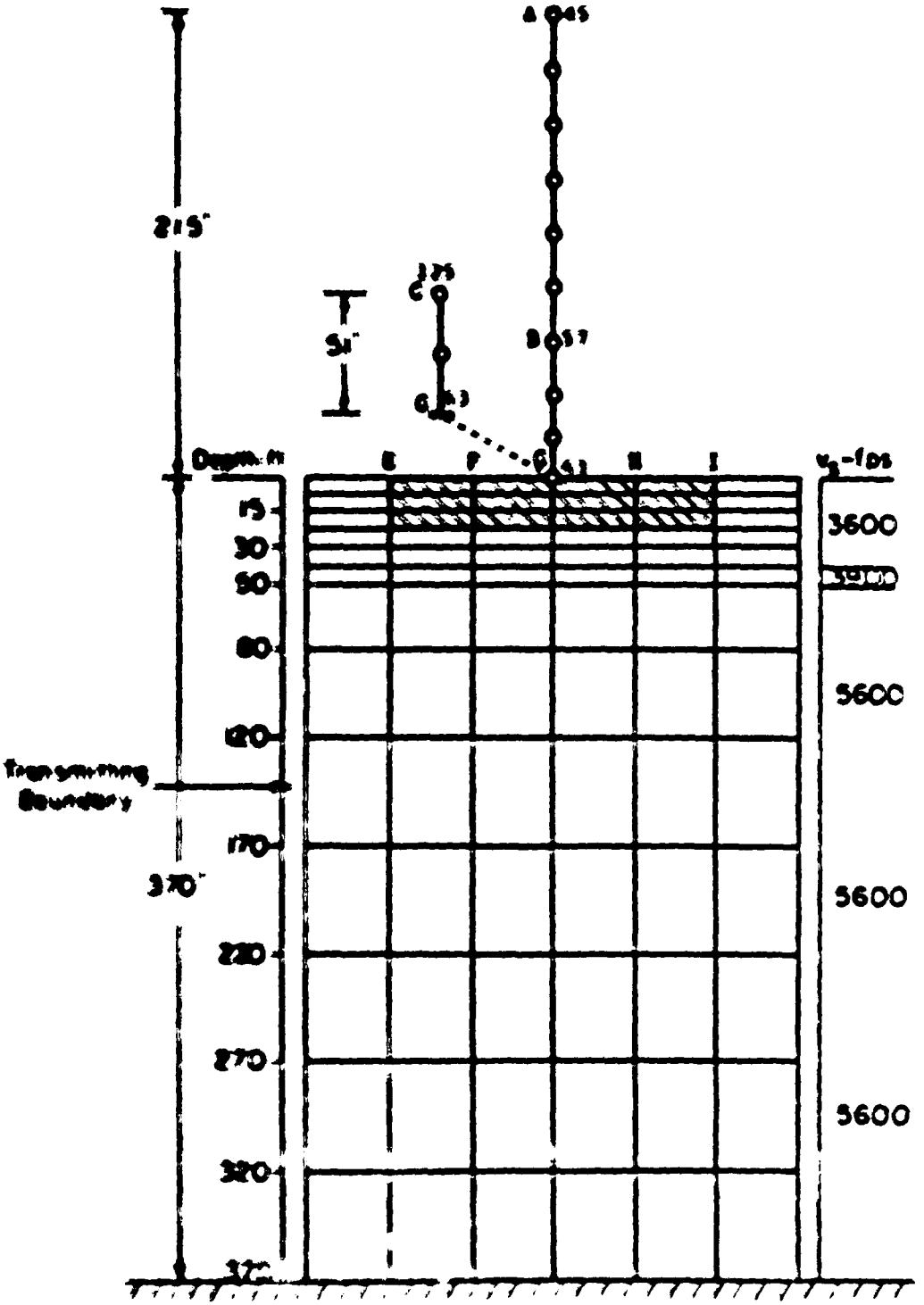

Fig. 6.1 Finite Element Model for Soil Structure Interaction Analysis - Rock Site

3-dimensional radiation damping effect. This technique is identical to that used in the FLUSH program, Lysmer (1975), and will not be discussed futher. The rigid base at a depth of 370 feet has been shown by Gomez-Masso (1978), who cooperated in these calculations, to be sufficiently deep to simulate a half space for this model. It should be mentioned here that the site response analysis associated with this analysis employed the variable depth method for Rayleigh waves. Thus the above rigid base occurs only in the interaction model

6.3.3 The Results

The results of the CREAM analyses are presented in terms of 2% acceleration response spectra for the components of motion at key nodes of the structural model. In each case the results of the Rayleigh wave analysis and the combined body wave analysis are plotted together for easy comparison.

As can be seen from Fig. 6.4 the motions computed for Point G at the middle of the base slab are nearly identical for the two cases which is not surprising since this point is also the control point in the free field. Generally, the S + P-wave analysis is conservative for horizontal motions while the R-wave analysis is conservative for vertical motions.

The horizontal motions along the length of the base slab were all the same as at Point G, which is not surprising since the slab is very rigid. However, rocking induced some variations in the vertical motions as illustrated in Fig. 6.5. As expected, the Rayleigh waves produce slightly more rocking than the body wave excitation. The vertical motion at the left end of the slab (Point E) is larger than at the right end (Point F). This is so because the Rayleigh waves travel from left to right and thus attenuate in that direction.

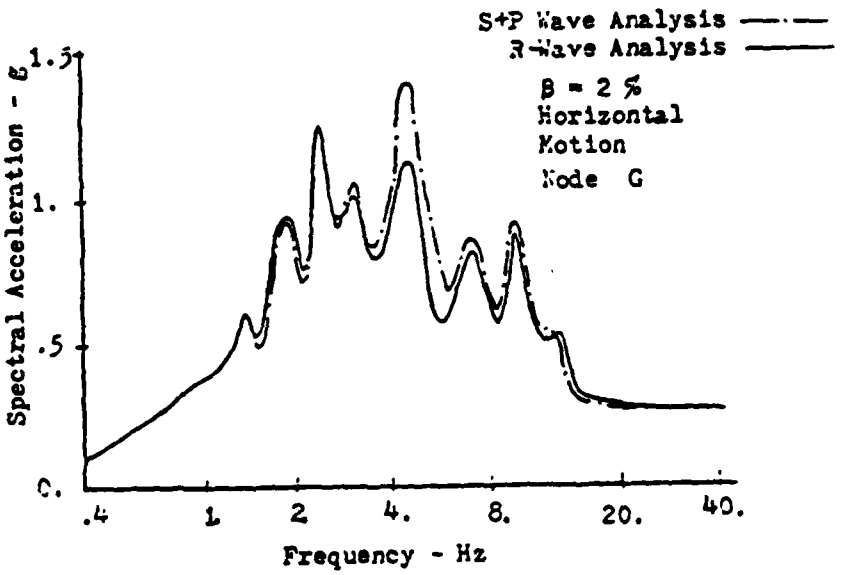

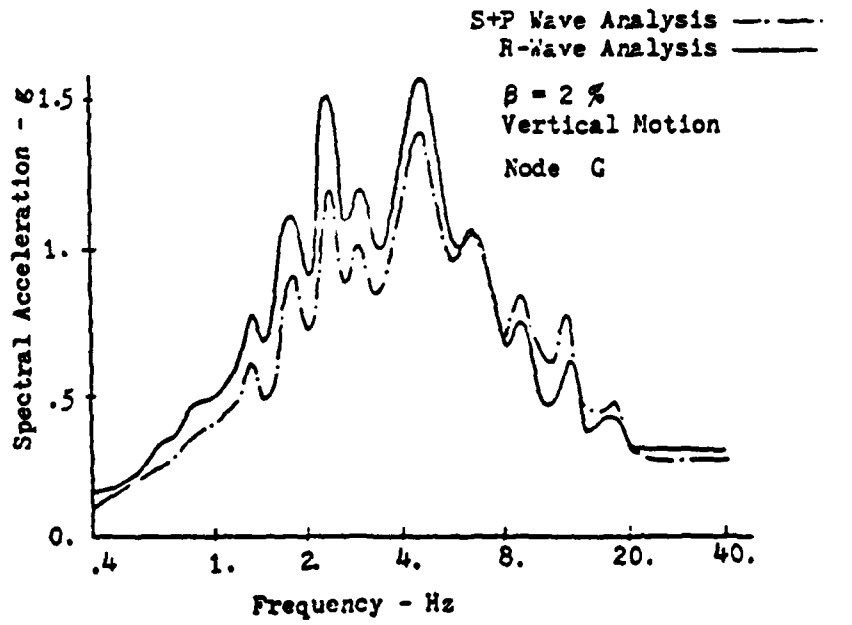

Fig. 6.4 Horizontal and Vertical Response Spectra at Node G (on Top of the Slab) - Rock Site

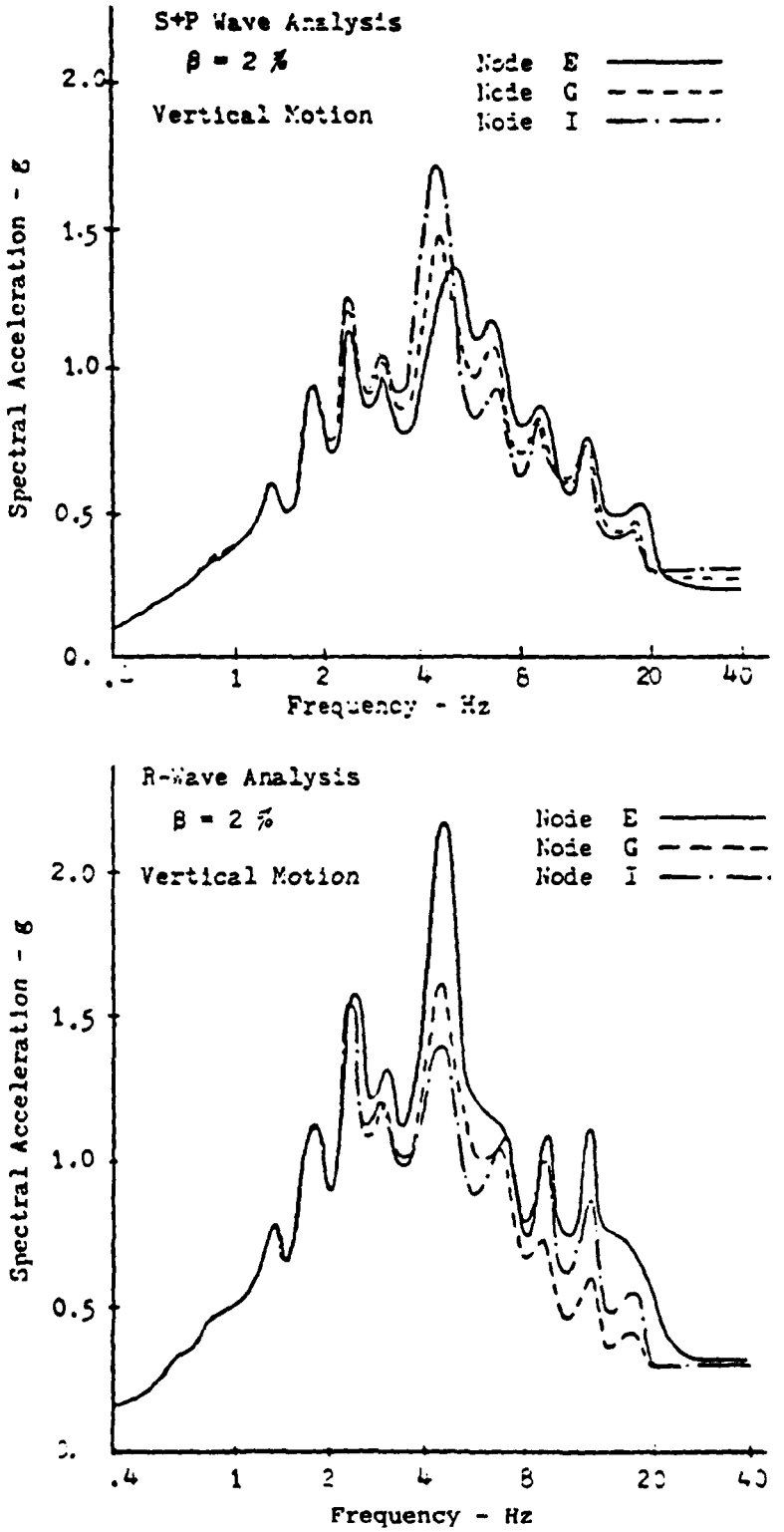

Fig. 6.5 Spectral Acceleration of Vertical Motion along the Top of the Foundation Slab - Rock Site

Due to the rocking of the base slab, the Rayleigh wave excitation produces higher horizontal motions at higher points in the structure. This is illustrated by the response spectra shown in Fig. 6.6. The vertical motions at the same points are shown in Fig. 6.7. These motions appear to follow the same trend as the motion of Point G on the base slab, i.e. the Rayleigh wave field gives higher response in the low frequency range (<5 Hz) and lower response in the high frequency range than the body wave field. However, the differences are not large.

In the entire analysis the largest difference observed between results obtained from the two seismic environments occured at Point C at the top of the internal structure. The response spectra computed for the motions at this point are shown in Fig. 6.8. For this one point it appears that at frequencies higher than 8 Hz the spectrum for the horizontal motion produced by the Rayleigh wave field is nearly double as high as the corresponding spectrum for the body wave field.

In view of the above results it appears that Rayleigh wave motions may be critical for the design of structures on rock. In making this statement, it should, however, be remembered that no seismic environment consists entirely of Rayleigh waves and that such waves may not even exist in the high frequency range (>4 Hz) where the largest differences were observed.

6.4 Structure on Sand Site

The analysis discussed above was repeated using the same structural model but this time embedded into the sand site studied in Section 5.5. The computational model used is shown in Fig. 6.9.

6.4.1 Free-Field Motions

Contrary to the analysis of the rock site previously studied, at this site the location of the control point was found to be of crucial

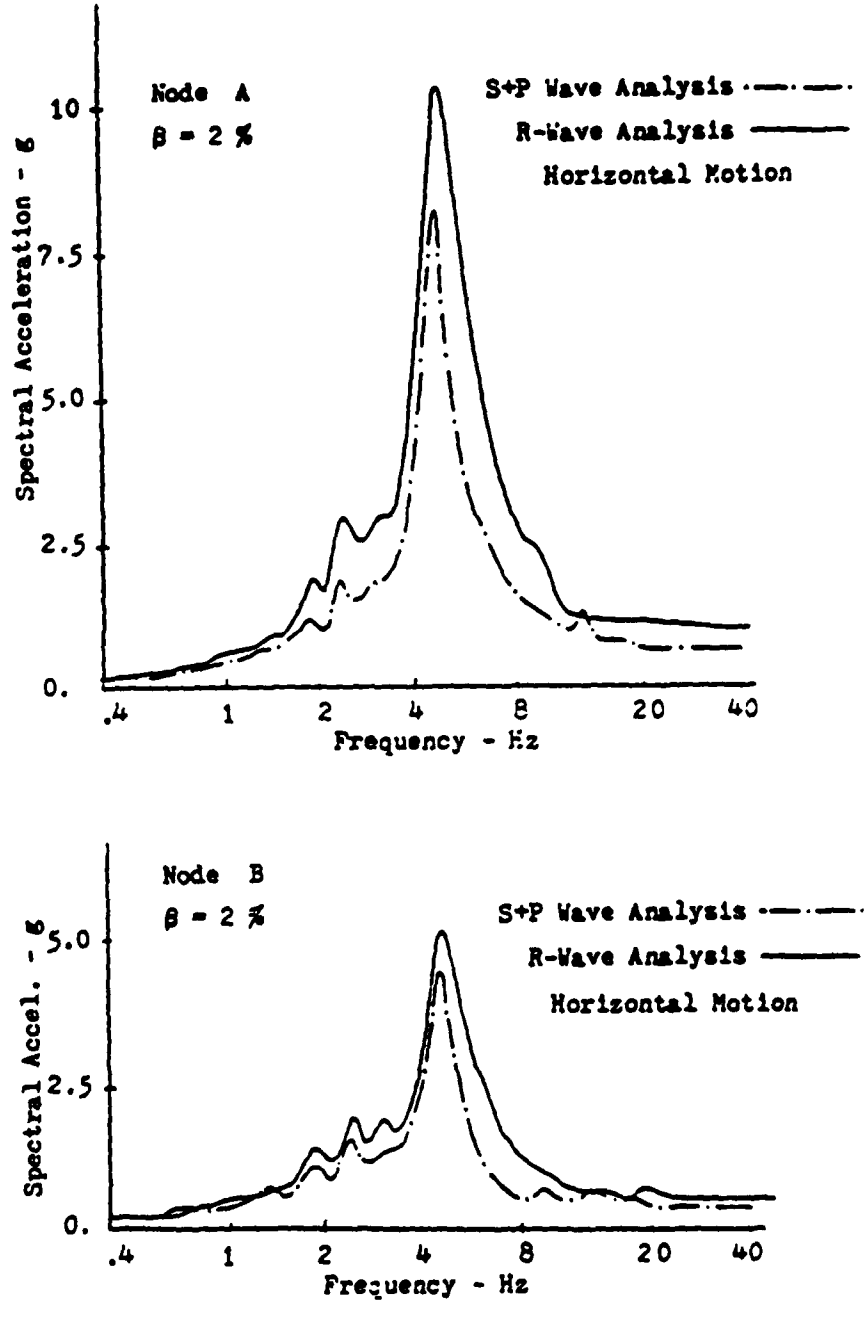

Fig. 6.6 Response Spectra of Horizontal Motions at Node A and B - Rock Site

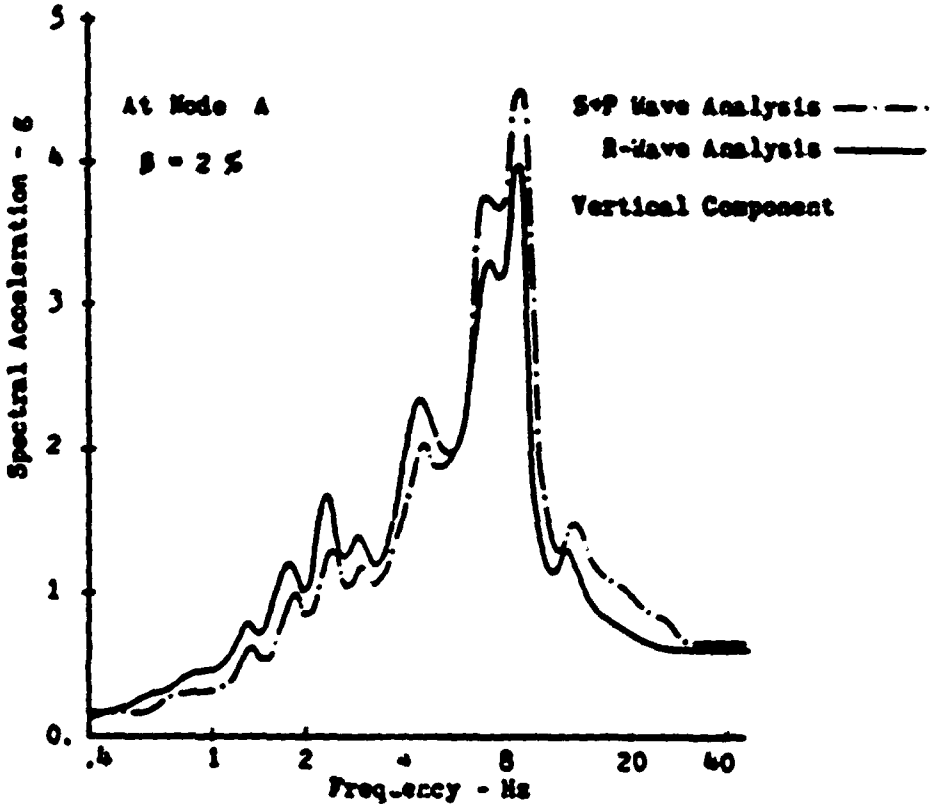

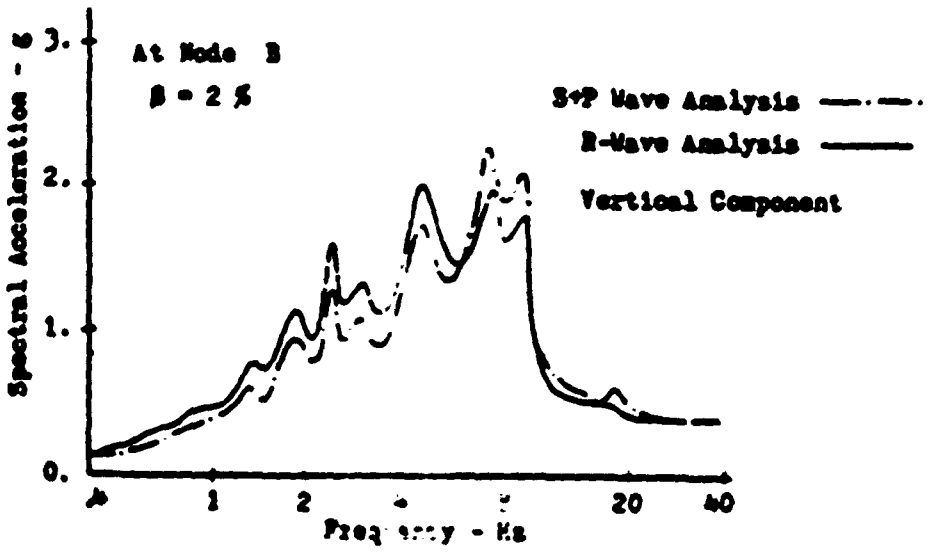

Fig. 6.7 Response Spectra of Vertical Motions at Nodes A and B - Rock Site

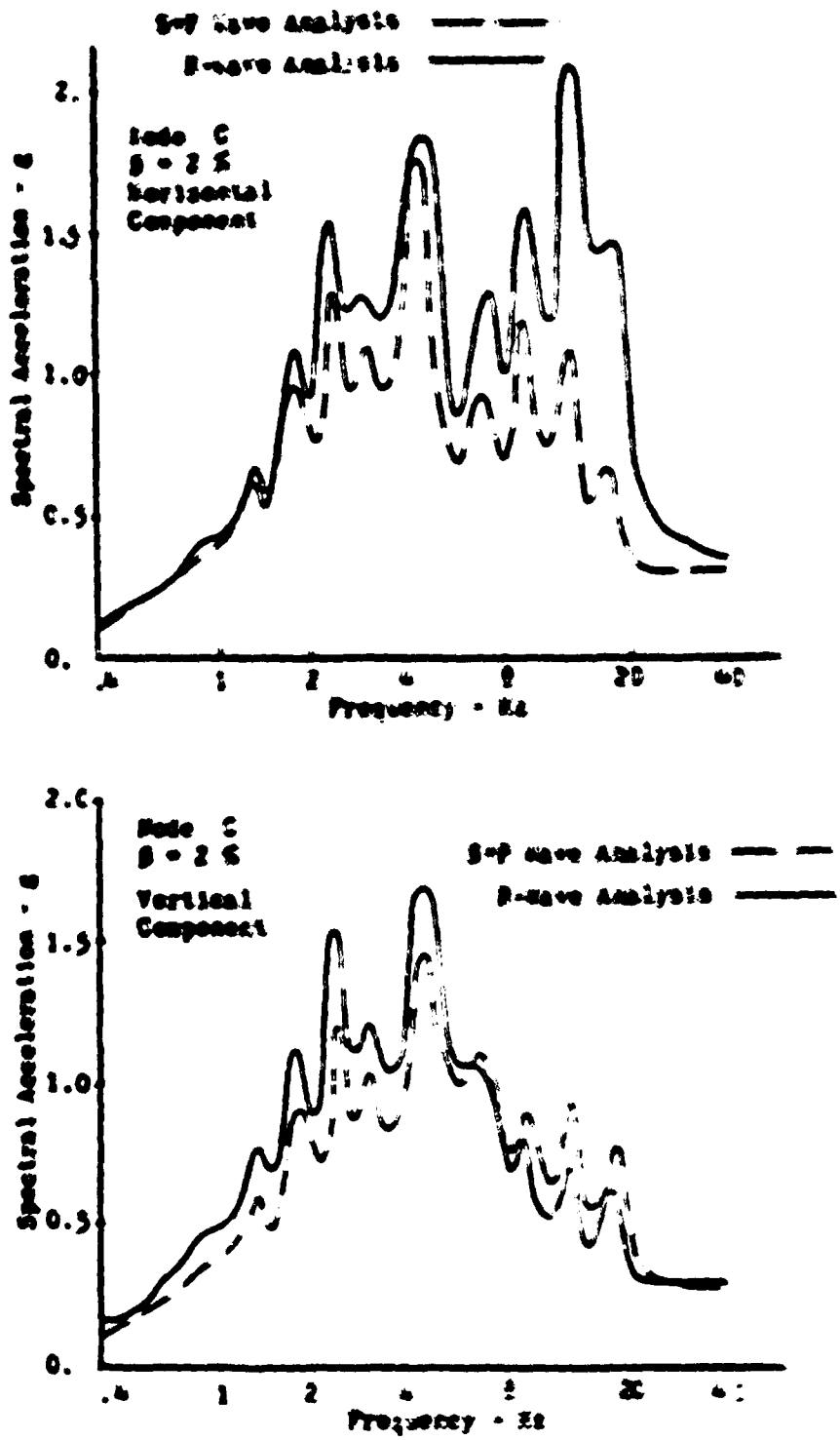

Fig. 6.8 Response Spectra of Horizontal and Vertical Motions at Nodal Point C - Rock Site

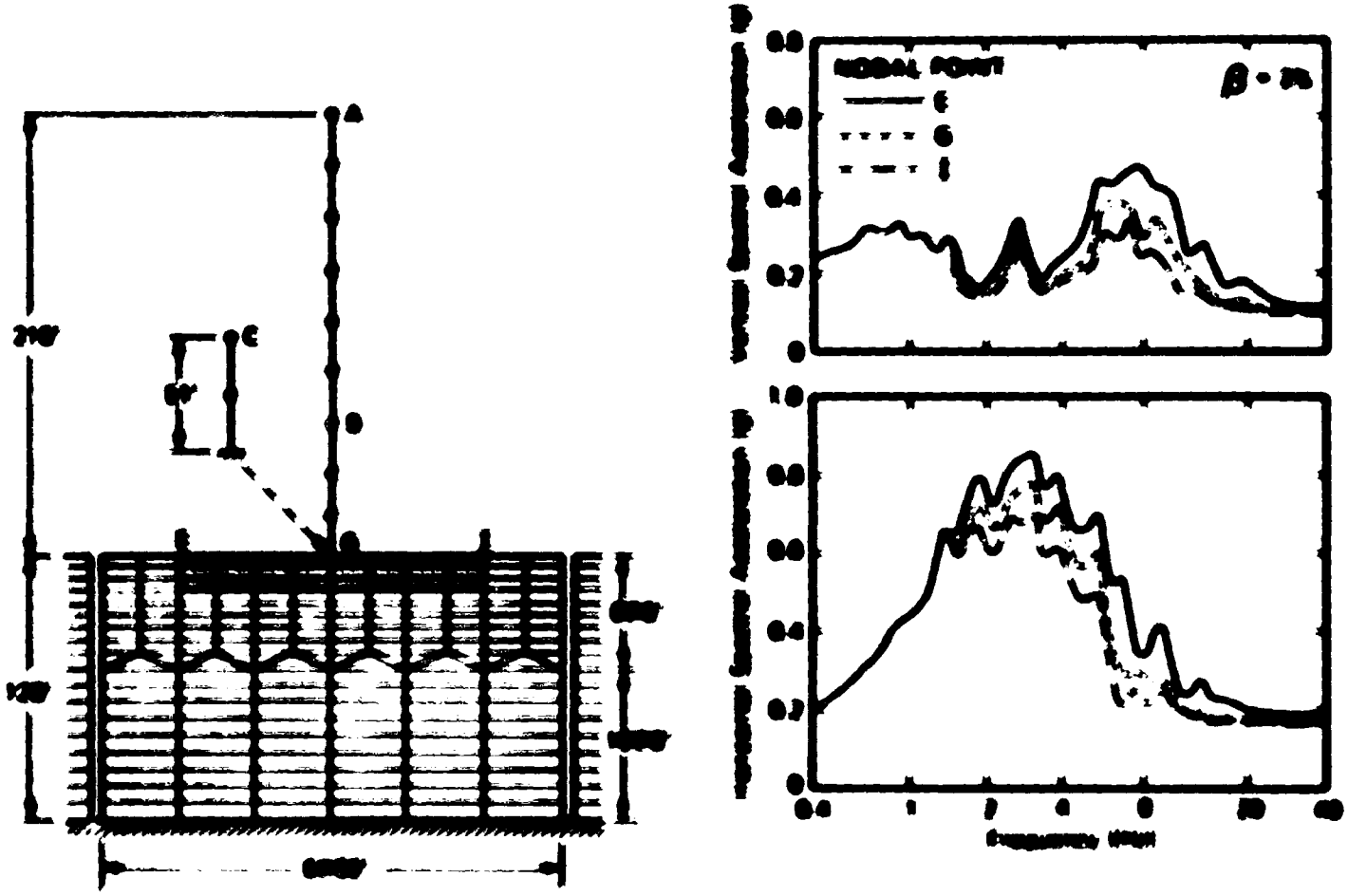

Fig. 6.9 Finite Element Mesh and Response from Field Tests for a Typical Site

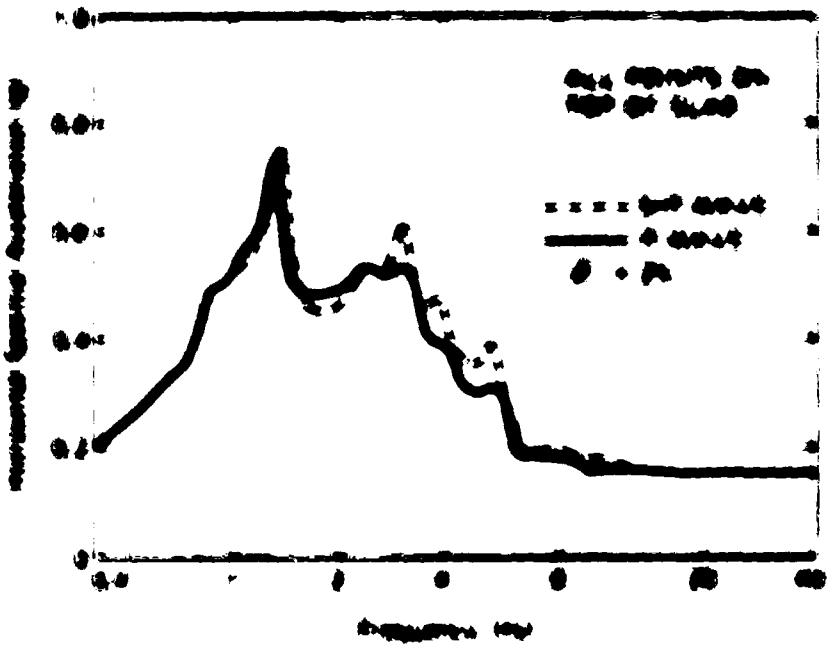

Fig. 6 (a) Electrostatic Temperature Sensors during the Ice on the Mountain-top Site (Base Case)

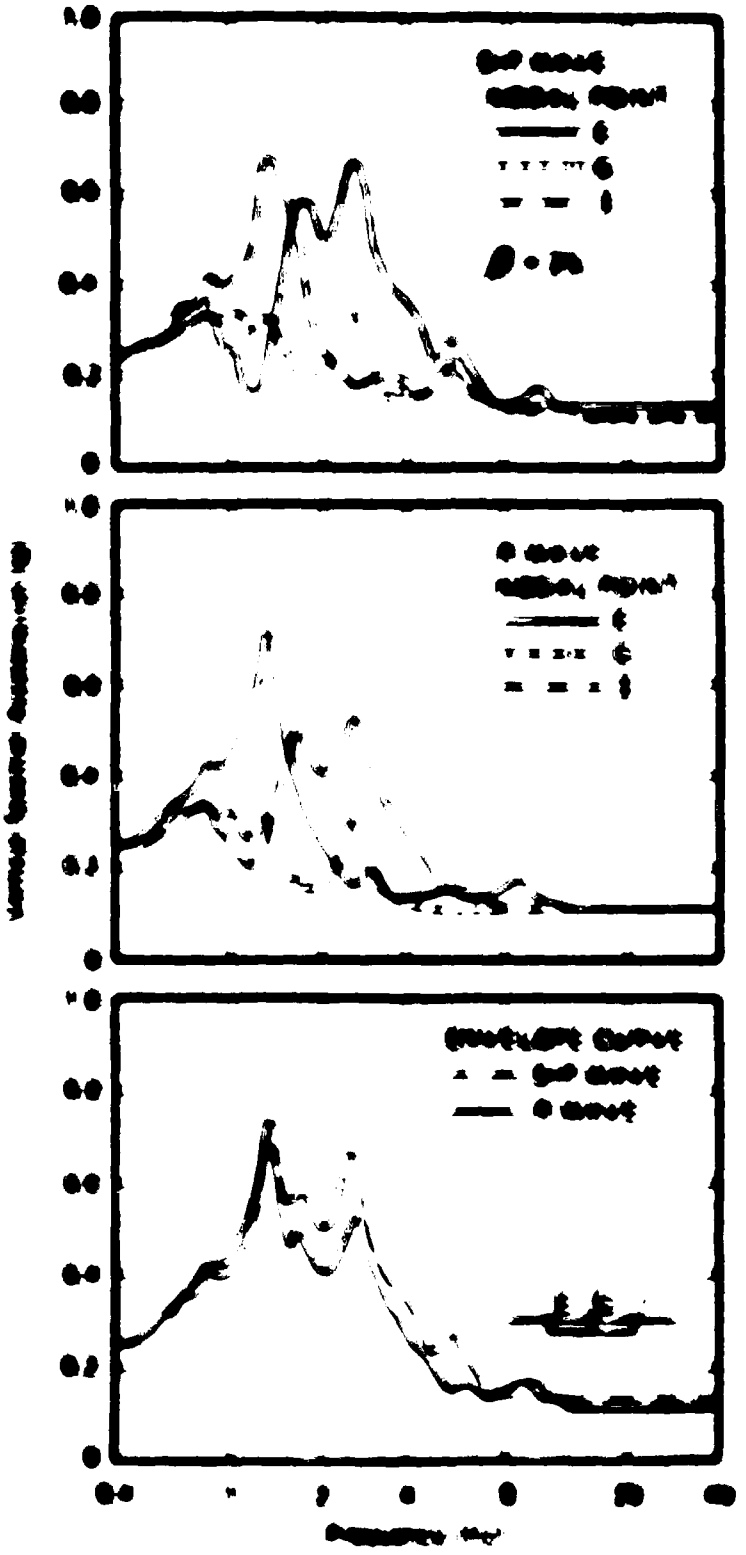

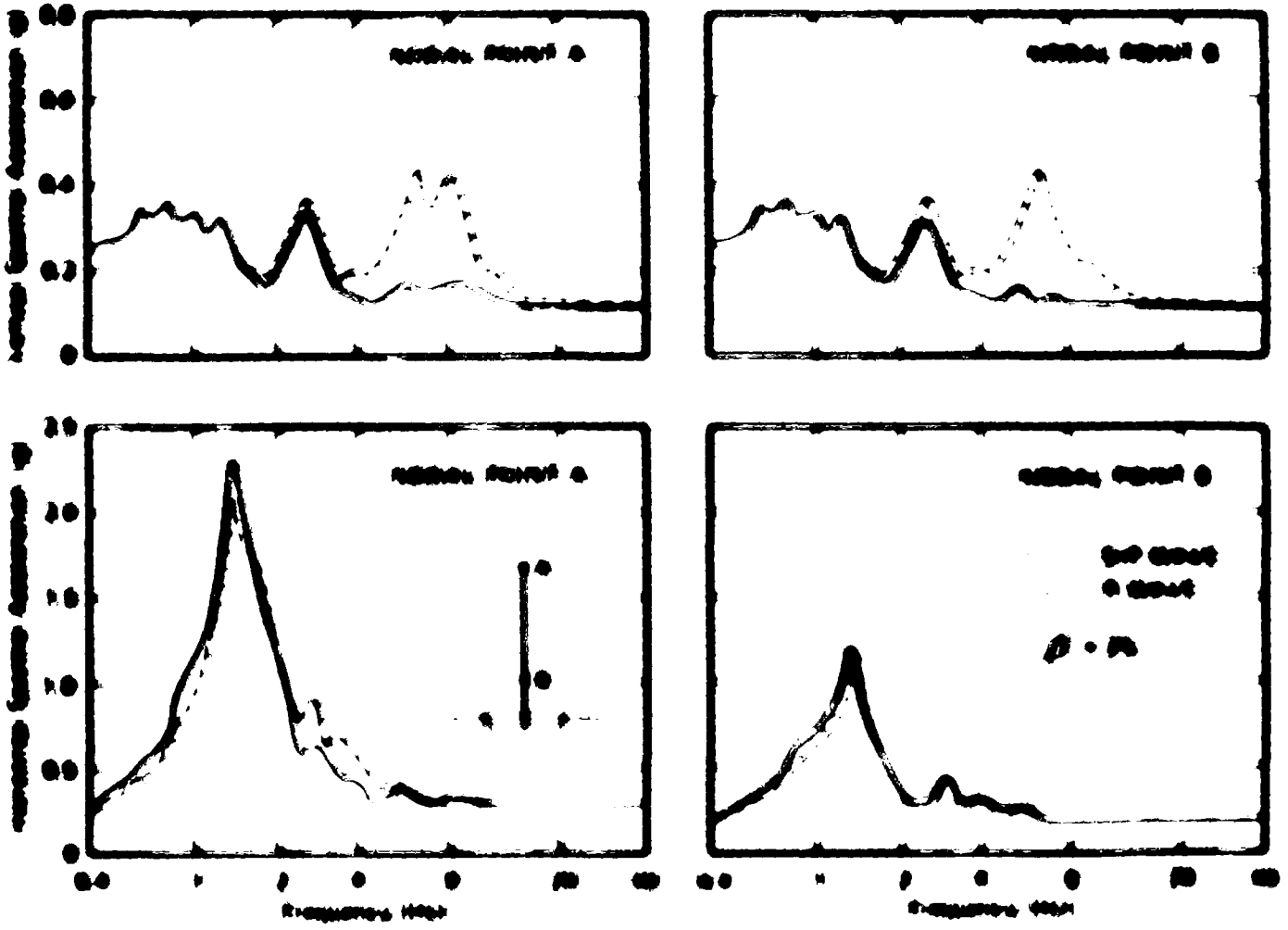

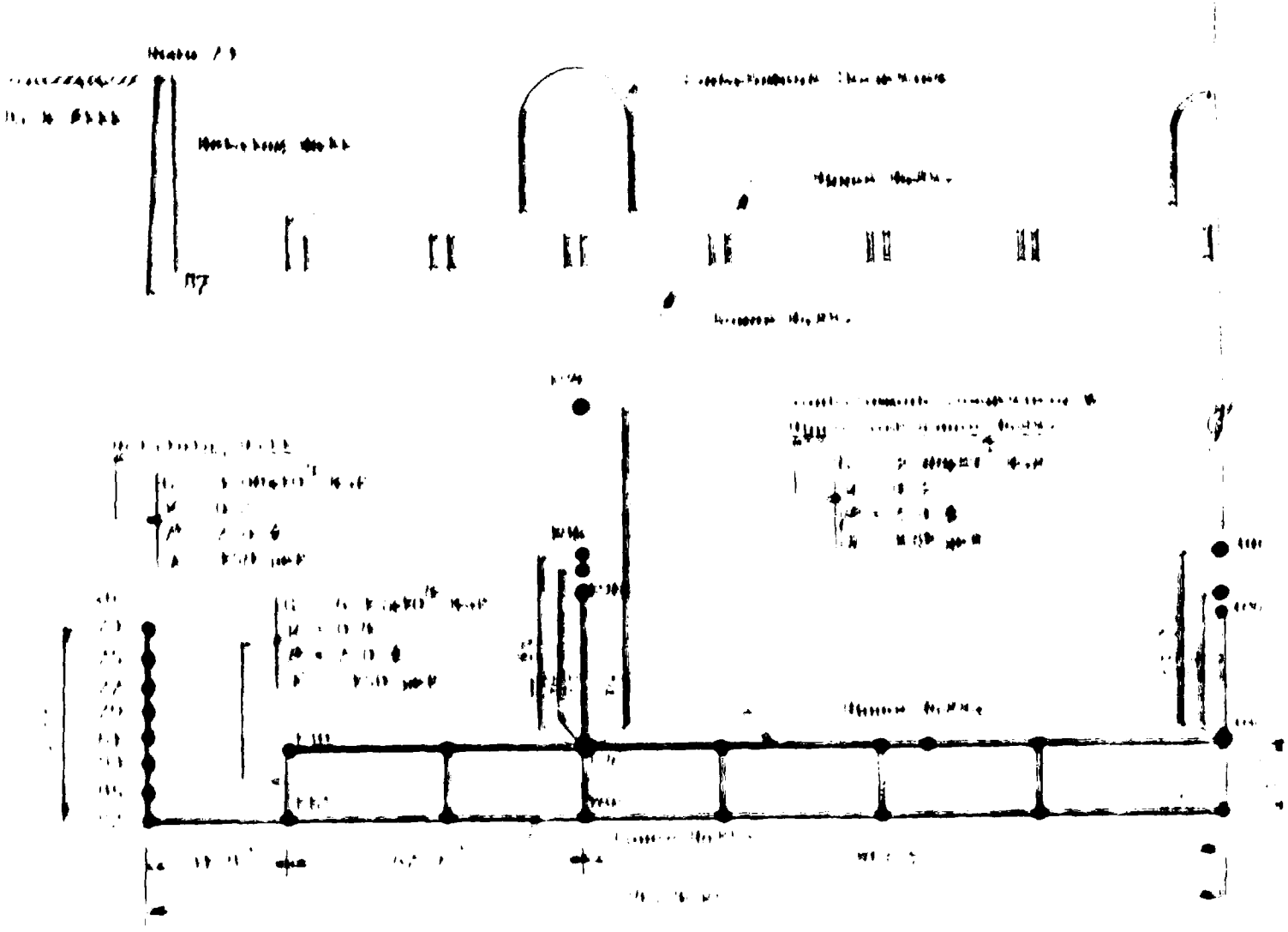

field and the sign of the control motion are not known. Hence, it is necessary to consider both arrival from the left and from the right. This amounts to using the envelopes of the spectra for Points E and I for design. These envelopes are shown in the lower part of Fig. 6.11 and indicate virtually no difference between the design motions obtained from the two analyses. The same is true for points at different elevations in the structure, see Fig. 6.12, except for the high frequency range where body waves appear to give higher vertical motions.

The conclusion from the above results must be that Rayleigh waves are not important for the design of structures on sand sites, in fact, they might not even exist.

6.7 Retaining Wall on Alluvial Site

The last example involves a large retaining wall (height = 44 ft) which is part of a raft system for a nuclear power plant proposed for the alluvial site previously analyzed in Section 5.6. The main dimensions and the structural model for the plant and raft system are shown in Fig. 6.13. The heavy lines in this figure indicate beam elements.

Three seismic environments were considered

- Vertically propagating S-waves
- Rayleigh waves with control point at top of retaining wall
- Rayleigh waves with control point 500 ft from retaining wall

The control motion was in all cases horizontal and identical to that used in Section 5.6, see Fig. 5.36. It had a maximum acceleration of 0.32 g and the cut-off frequency on all analyses was 10.5 Hz.

The computational model for the interaction analysis is shown in Fig. 6.14. As for the previous studies it includes transmitting boundaries and a rigid base.

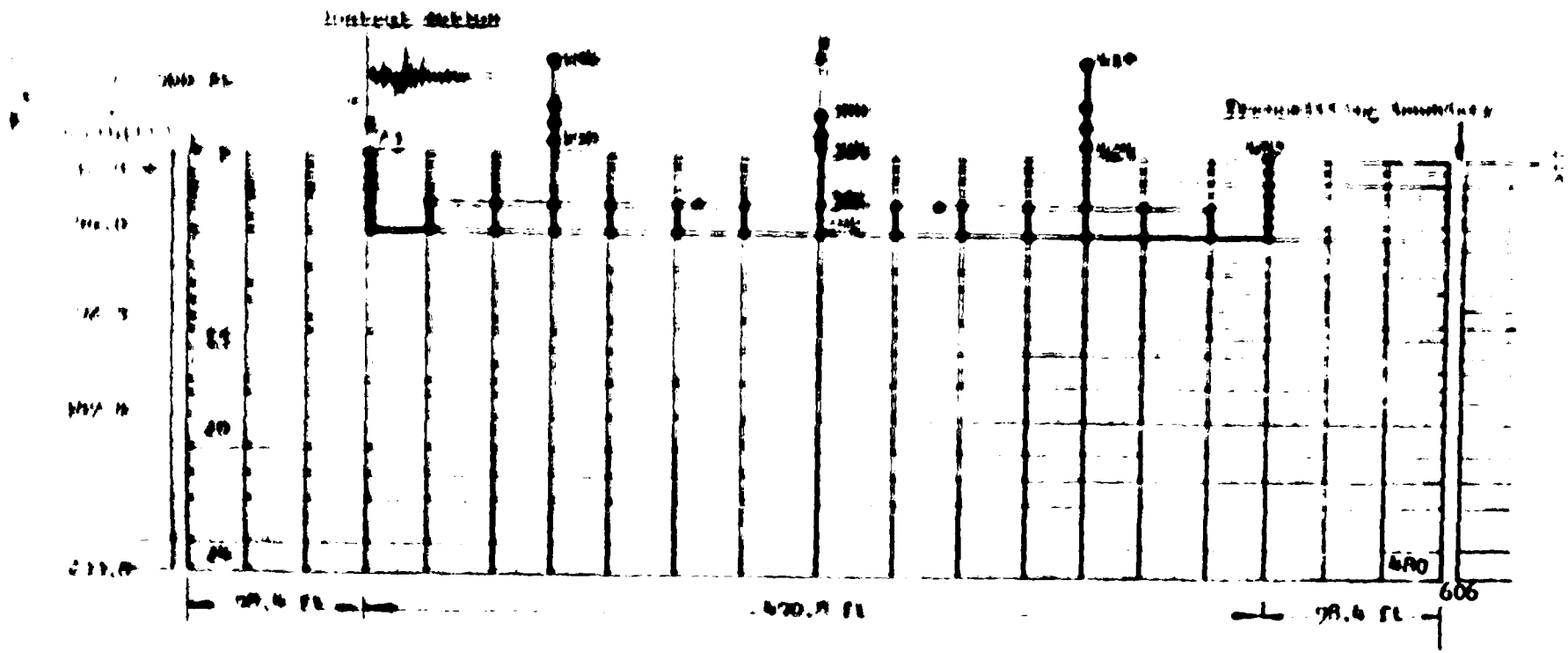

Fig. 6.14 Finite Element Model for Interaction Analysis

Since the purpose of this investigation was to determine the behavior of the retaining wall, only results which relates to this scope will be presented below.

6.5.1 Maximum Accelerations

The maximum accelerations along the retaining wall are shown in Fig. 6.15 for the S-wave case and in Fig. 6.16 and 6.17 for the R-wave cases. In each case the motions are compared with the corresponding free-field motion. Except for the close-in Rayleigh wave case the interaction effects appear to be insignificant (<10%). This was generally true for all points in the structural system. In all cases all points of the wall had essentially the same vertical acceleration which is reasonable for such a stiff structure.

The horizontal accelerations induced by shear waves are generally larger than those induced by Rayleigh waves. This observation does, as will be shown below, not mean that the shear wave field is the critical load case.

6.5.2 Shear Forces and Bending Moments

The computed maximum shear forces in the retaining wall are shown in Figs. 6.18 and 6.19. As expected, the forces for the case of the close-in Rayleigh wave field are somewhat larger than for the case when the control point is located 500 ft from the wall. Much more significant is the observation that the shear forces induced by the Rayleigh wave field are several times larger than those induced by the S-wave fields. This is so because, as discussed in Section 5.5.3, the normal stresses on vertical planes are much higher in Rayleigh wave fields than they are in vertically propagating fields (even vertically propagating P-waves will generate smaller stresses on vertical planes than R-waves within normal depths of embedment).

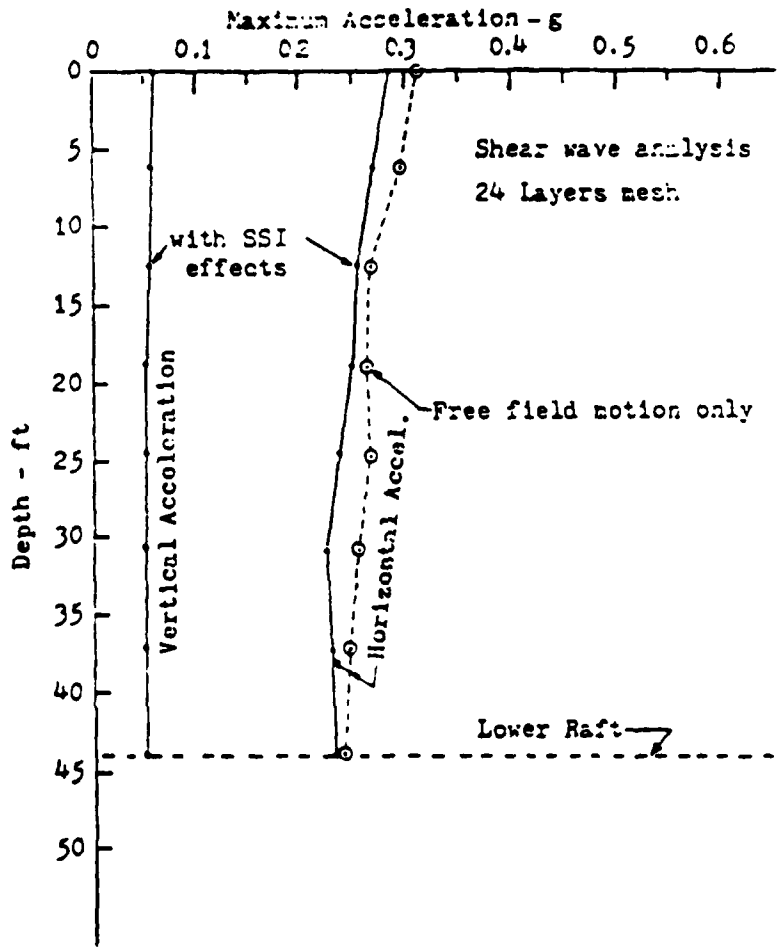

Fig. 6.15 Acceleration Profile along the Retaining Wall in Case of Shear Wave Analysis

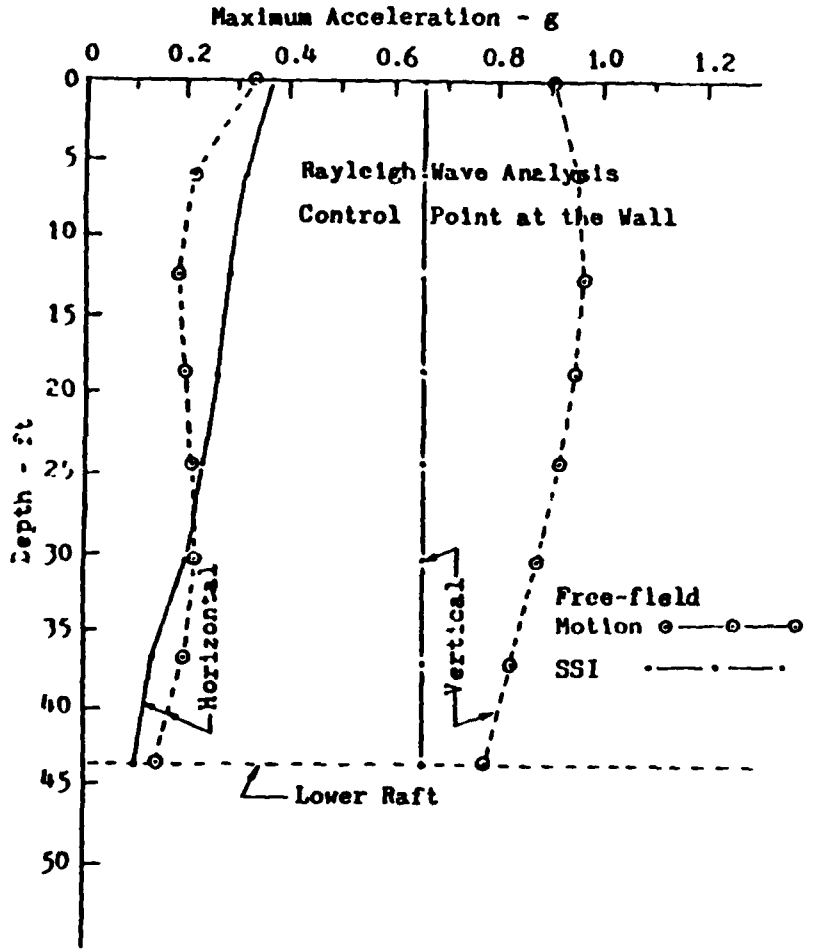

Fig. 6.16 Acccleration Profile along the Retaining Wall, Rayleigh Wave Analysis for the Case Control Point at the Wall

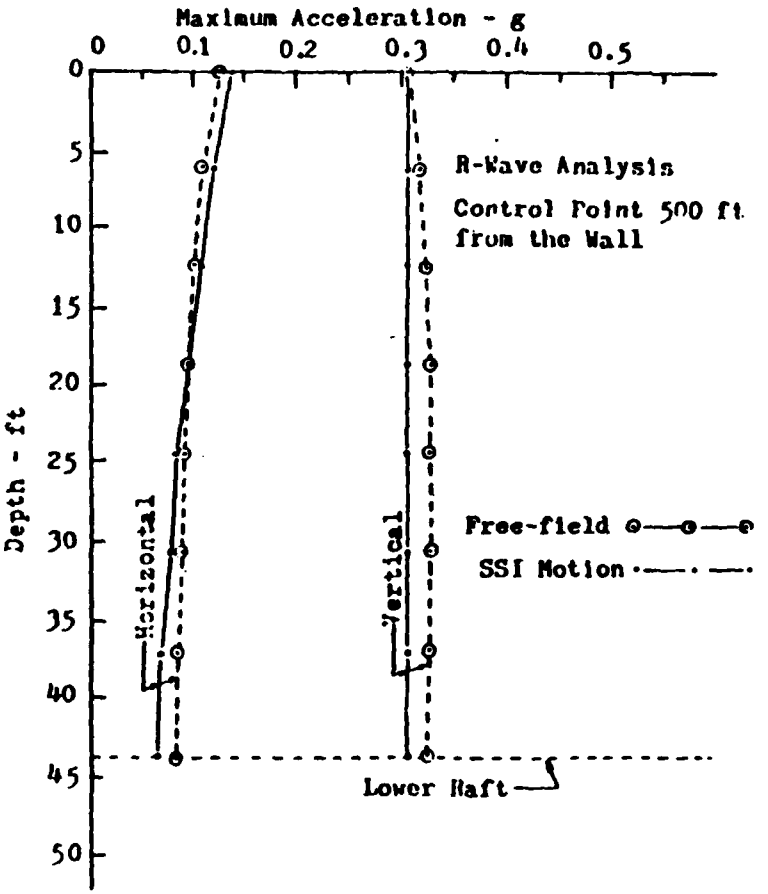

Fig. 6.17 Acceleration Profile along the Wall, Rayleigh Wave Analysis for the Case of Control Point 500 ft from the Wall

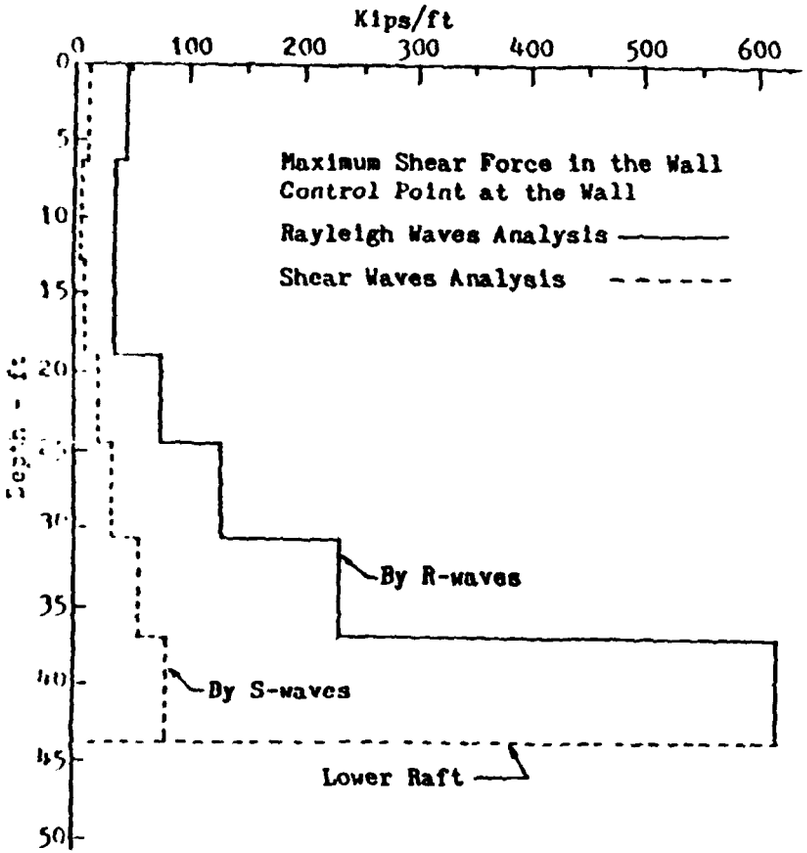

Fig. 6.18 Comparison of Maximum Shear Force in the Wall by R-wave and S-wave Analysis - Control Point at the Wall

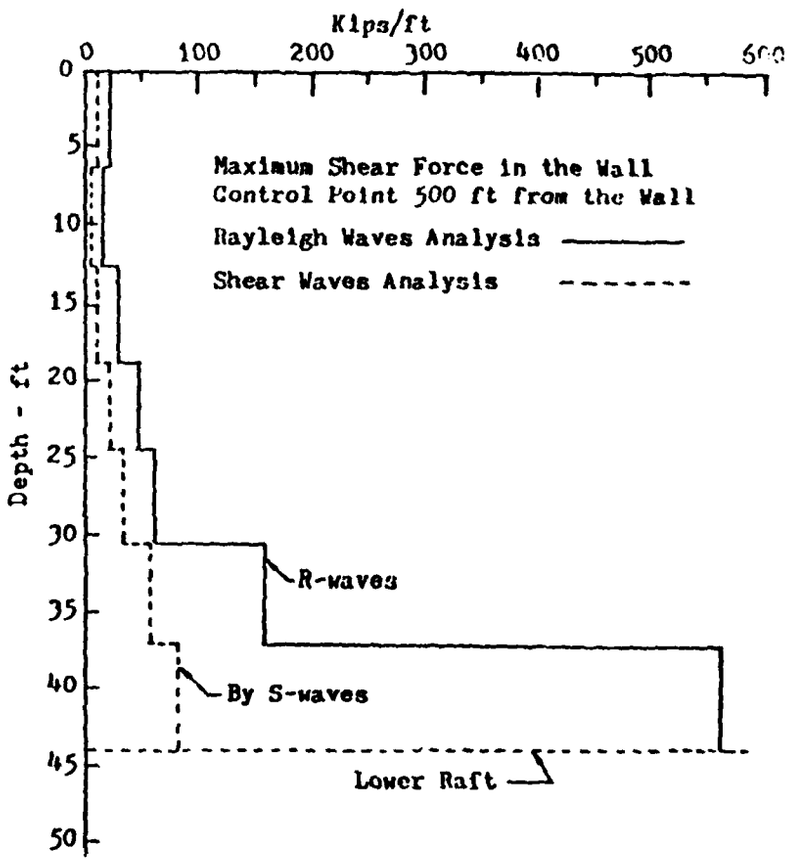

Fig. 6.19 Comparison of Maximum Shear Force in the Wall by R-wave and S-wave Analysis - Control Point 500 ft Away from the Wall

As shown in Figs. 6.20 and 6.21 the situation is similar for bending moments in the wall.

6.5.3 Design Considerations

The high bending moments developed in the retaining wall turned out to be the most critical item in the design of the raft system. The practical solution to the problem was to design the wall for a bending moment which was computed from a field consisting of 1/3 Rayleigh waves and 2/3 vertically propagating shear waves. This decision was based on the arguments presented in Section 5.5.3, according to which it is unlikely that a strong Rayleigh wave field can exist on the site. Even then the design moment turned out to be several times larger than the moment computed by say a FLUSH analysis which assumes vertically propagating waves.

More important than the design decision made, the above analysis illustrates a case for which even a small content of Rayleigh waves in a control motion may be critical, even though such waves create smaller accelerations in the structure than vertically propagating waves.

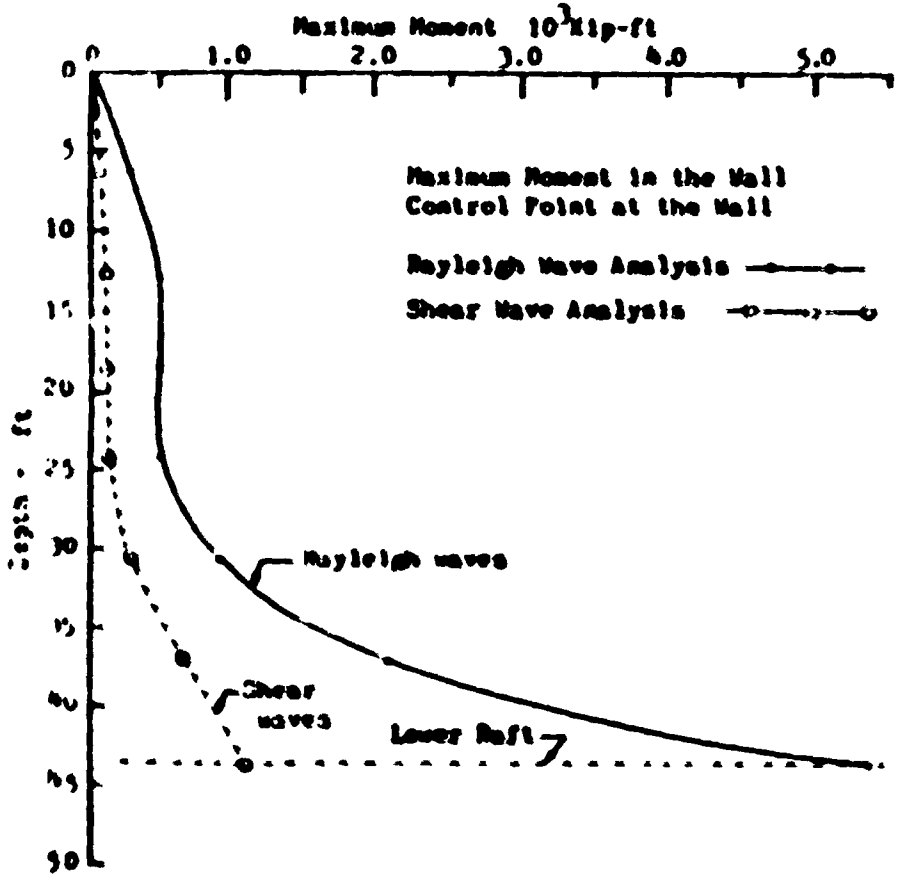

Fig. 6.20 Comparison of Maximum Bending Moment in the Wall Control Point at the Wall

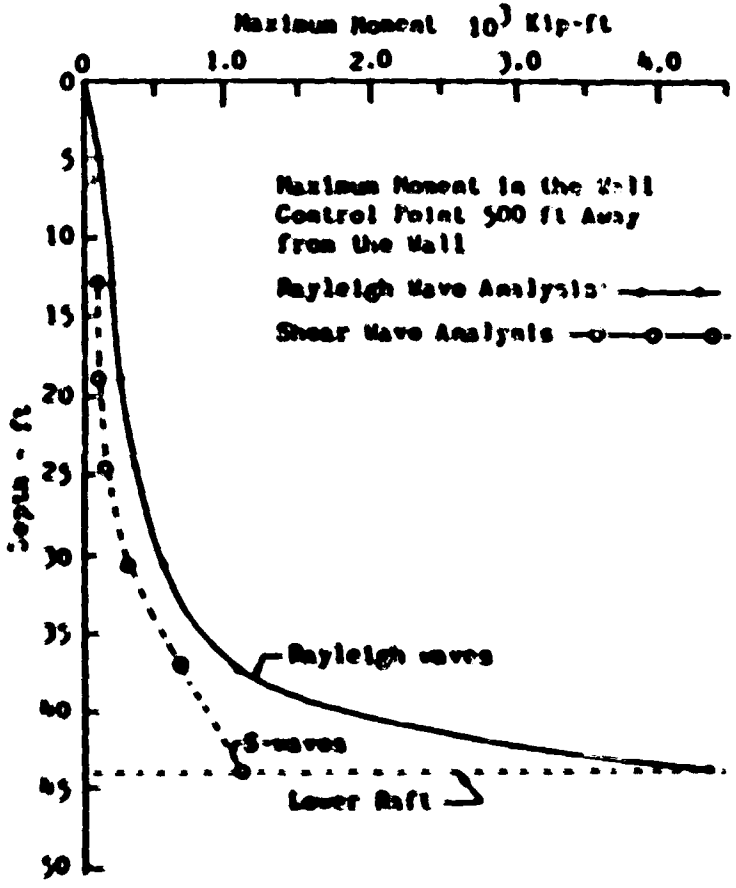

Fig. 6.21 Comparison of Maximum Bending Moment in the Wall, Control Point 500 ft to the left of the Wall

CHAPTER 7

SUMMARY AND CONCLUSIONS

Methods have been developed for harmonic and transient site response analysis of a horizontally layered site. The methods are of the finite element type and are based on the following assumptions:

- The site consists of horizontal soil and rock layers resting on a semi-infinite half space.
- All material properties are linearly viscoelastic. Nonlinearities can be approximated by the equivalent linear method.
- The site is located at some distance from the epicenter.
- A control motion is given at some point in the site: usually at the ground surface.
- The control motion consists of a known proportion of incident body waves and fundamental Rayleigh and Love waves.

The methods work in the frequency domain and have been implemented in two practical computer codes: SITE and LOVE. The codes have been verified by reproduction of exact solutions from literatures.

Examples have been presented of complete analysis of a rock site, a dry cohesionless site and an alluvial site.

The connection has been established between soil-structure interaction analysis which was the main topic of the research and site response analysis and several examples have been presented to show how the site response solutions obtained by program SITE can be applied to soil-structure interaction problems involving surface waves.

The research has advanced the state-of-the-art in the following areas:

- The establishment of a unified finite element approach for [illegible] body waves and surface waves.
- Proper treatment of the underlying mathematics that opens the door for both body waves and surface waves into the finite element method.
- Procedures for extracting the fundamental surface wave modes from among the many modes which can exist in a viscoelastic layered system.
- Documentation procedures for presenting the [illegible] propagation wave fields.
- Practical computer programs for the above procedures.

In addition to the above theoretical developments the results of the case studies presented have provided a deeper insight into the relative importance of [illegible] propagating waves and the practical factors the engineer can expect to control the [illegible] propagation waves in layers.

- The air impact problem is the central factor that is the time history and frequency content. And, most important, also is the relative content of wave types at different frequencies.

The research presented herein provides an answer to the first question. However, as to the second question, the results from the case studies involving Rayleigh waves clearly demonstrate that

- the content of high frequency [illegible] fundamental Rayleigh waves in motions at soil site must be very small.

This is so because such waves will attenuate to insignificant amplitudes within a few hundred feet of their source. This result

[illegible]

[illegible]

- [illegible]

[illegible]

[illegible]

[illegible]

[illegible]

- [illegible]

[illegible]

- [illegible]

---

*[illegible]

[illegible]

- [illegible]

[illegible]

[illegible]

- [illegible]

[illegible]

[illegible]

REFERENCES

Anderson, J. (1976) "A Dislocation Model for the San Fernando Earthquake," Bull. Seism. Soc. Am., Vol. 66, pp. 637-660, 1976.

Aydinoglu, M. N. and Bycroft, G. N. (1978) "Dynamic Interaction between Soil and a Group of Structures," Proc. 6th Conf. Earthq. Engrg., Vol. 6, pp. 139-146, New Delhi, 1978.

Bahuin, M. A. (1976) "Body wave spectra and crustal structure in Southeastern New York and Northern New England," Ph.D. Dissertation, Univ. of Calif., Berkeley, September 1976.

Bell, B. A. (1976) "San Fernando Aftershock Sequence and the Pacoima Dam Strong Motion Record," Bull. Seism. Soc. Am., Vol. 66, pp. 1335-1341, 1976.

Bernhaus, M. (1977) "Soil Amplification Factor of Surface Waves," Proc. 6th World Conf. Earthq. Engrg., Vol. 6, pp. 6-100, New Delhi, 1977.

Bycroft, G. N. (1976) "Interdependent Body and Surface Plane Waves in a Semi-infinite Viscoelastic Half-space," Ph.D. Dissertation, Univ. of Calif., Berkeley, 1976.

Bycroft, G. N. (1978) "Plane and Plane Waves in Linear Viscoelastic Media," J. of Sound. Vib., Vol. 59, No. 10, pp. 2481-2493, May 1978.

Bycroft, G. N. (1978) "Plane Waves in Linear Viscoelastic Media," Geophys. J. Roy. Soc., Vol. 52, pp. 533-542, April 1978.

Bullen, K. E. (1963) "An Introduction to the Theory of Seismology," 3rd edition, Cambridge University Press, 1963.

Carpenter, A. B. (1976) "Elastic Wave Velocities in Soils," Department of Engineering, Univ. of Calif., Los Angeles, Internal Report, December 1976.

Chandra, U. (1979) "Angles of Incidence of S-Waves," Bull. Seism. Soc. Am., Vol. 69, No. 3, pp. 903-913, 1979.

Clough, R. W. and Penzien, J. (1975) "Dynamic of Structures," McGraw Hill, Inc., 1975.

Constantopoulos, I. V. (1973) "Amplification Studies for a Nonlinear Hysteretic Soil Model," MIT Research Report R73-46, Department of Civil Engineering, Massachusetts Institute of Technology, Cambridge, 1973.

Constantopoulos, I. V., et al. (1973) "A Comparison of Linear and Exact Nonlinear Analysis of Soil Amplification," Proc. 5th World Conf. on Earthq. Engrg., Rome, Session 5B, 1973.

Cooley, J. W. and Tukey, J. W. (1965) "An Algorithm for the Machine Calculation of Complex Fourier Series," Mathematics of Computation, Vol. 19, No. 90, pp. 297-301, 1965.

Cooper, H. F., Jr. (1967) "Reflection and Transmission of Oblique Plane Waves at a Plane Interface between Viscoelastic Media," J. Acoust. Soc. Am., Vol. 42, pp. 1064-1069, 1967.

Eastman, J., Ewing, M. and Oliver, J. (1960) "Study of Shear Velocity Distribution by Mantle Rayleigh Waves," Bull. Seis. Soc. Am., Vol. 50, pp. 87-115, 1960.

Drake, L. A. (1972) "Love and Rayleigh Waves in Horizontally Layered Media," Bull. Seis. Soc. Am., Vol. 62, No. 5, pp. 1241-1258, October 1972.

Drake, L. A. (1972) "Rayleigh Waves in an Alluvial Valley," Nature Physical Science, Vol. 240, pp. 113-114, December 1972.

Drake, L. A., and Mal, A. K. (1972) "Love and Rayleigh Waves in the San Fernando Valley," Bull. Seis. Soc. Am., Vol. 62, No. 6, pp. 1673-1690, December 1972.

Drnevich, V. P., Hall, J. R., Jr. and Richart, F. E., Jr. (1966) "Large Amplitude Vibration Effects on the Shear Modulus of Sand," Univ. of Michigan, Report for Corps of Engineers, U. S. Army, WES, Contract DA-22-079-Eng-340, October 1966.

Dunkin, J. (1965) "Computation of Modal Solutions in Layered, Elastic Media at High Frequencies," Bull. Seis. Soc. Am., Vol. 55, pp. 335-358, 1965.

Eisenberg, A. (1972) "Observations of Body Wave Amplitudes and Their Implication Concerning the Structure of the Earth's Mantle," Ph.D. Thesis, Univ. of Calif., Berkeley, 1972.

Ewing, W. M., Jardetzky, W. S., and Press, F. (1957) "Elastic Waves in Layered Media," McGraw-Hill, 1957.

Finn, W. D. L., Lee, K. W., and Martin, G. R. (1977) "An Effective Stress Model for Liquefaction," J. Geot. Engrg. Div., ASCE, Vol. 103, No. GT6, pp. 517-533, June 1977.

Finn, W. D. L., Martin, G. R. and Lee, K. W. (1978) "Comparison of Dynamic Analysis for Saturated Sands," Proc. ASCE Geotech. Engrg. Specialty Conf. on Earthq. Engrg. and Soil Dynamics, ASCE, Vol. 1, pp. 472-491, Pasadena, California, June 1978.

Ghaboussi, J. and Dikmen, S. U. (1978) "Liquefaction Analysis of Horizontally Layered Sands," J. Geot. Engrg. Div., ASCE, Vol. 104, No. GT3, pp. 341-356, March 1978.

Idriss, I. M. and Seed, H. B. (1966) "An Analysis of Ground Motions During the 1957 San Francisco Earthquake," Bull. Seis. Soc. Am., Vol. 56, No. 6, December, 1966.

Idriss, I. M. and Seed, H. B. (1967) "Response of Horizontal Soil Layers during Earthquake," Report of ITTE, University of California, Berkeley, 1967.

Idriss, I. M. and Seed, H. B. (1968) "Seismic Response of Horizontal Soil Layers," Journal of the Soil Mechanics and Foundations Division, ASCE, Vol. 94, No. SM4, July, pp. 1003-1031.

Idriss, I. M. Lysmer, J., Hwang, R., and Seed, H. B. (1973) "QUAD 4- A computer program for Evaluating the Seismic Response of Soil Structure by Variable Damping Finite Element Procedures," Earthquake Engineering Research Center, EERC 73-16, Univ. of Calif., Berkeley, July 1973.

Idriss, I. M., Dobry, R., Doyle, E. H., and Singh, R. D. (1976) "Behavior of Soft Clays Under Earthquake Loading Conditions," Proc. Offshore Technology Conference, Paper No. OTC 2671, Dallas, May 1976.

Kanamori, H. and Anderson, D. L. (1975), "Physical Mechanisms of Large Seismic Wave Attenuation," Rev. of Geophysics and Space Physics, Vol. 13, pp. 1-43, 1975.

Kawamoto, T. (1968), "Damping in Composite Structures," Proc. 2nd World Conf. Earthq. Engrg., Tokyo, 1960.

Kondner, R. L. (1963), "Hyperbolic Response of a General Yielding Structure," J. Engrg. Mech. Div., ASCE, Vol. 89, No. EM2, April 1964.

Newmark, N. M. (1967) "A Method for Calculating Nonlinear Seismic Response of Two Dimensions," Bull. Seis. Soc. Am., Vol. 57, No. 5, pp. 1213-1236, October 1967.

Newmark, N. M. and Chan, S. P. (1979) "A Comparison of Nonlinear Dynamic Response of Earthquakes," Bull. Seis. Soc. Am., Vol. 69, No. 5, pp. 1213-1236, October 1979.

Ozawa, A. (1978) "Shaking Table Tests and Analysis of Soil-Structure Systems," Ph.D. Dissertation, Univ. of Calif., Berkeley, May 1978.

Parmelee, R. (1967) "Relation between the Nature of Surface Layer and the Amplitude of Earthquake Motions," Bull. Tokyo Earthquake Research Institute, 1967.

Parmelee, R. (1967) "Relation between the Nature of Surface Layer and the Amplitude of Earthquake Motions," Bull. Tokyo Earthquake Research Institute, Vol. 45, pp. 1-7, Tokyo, 1967.

Pawsey, S. Whitman, R. V., Dobry, R., and Esteban, P. (1978) "Nonlinear Dynamic and Design," Vol. 48, pp. 377-392, 1978.

Knopoff, L., Frederichs, R., Gangi, A., and Porter, L. (1957) "Surface Amplitudes of Reflected Body Waves," Geophysics Vol. 22, No. 4, pp. 842-847, 1957.

Knopoff, L. (1964) "Q, Review of Geophysics," Vol. 2, 1964, pp. 625-659, 1964.

Kondner, R. L. and Zelask, J. S., (1963) "A Hyperbolic Stress-Strain Formulation for Sands," Proc. 2nd Pan-Am. Conf. on SMFE, Brazil, Vol. 1, 1963.

Levshin, A. L. (1962) "Propagation of Surface Waves in Unconsolidated Formations," Bull. Acad. Sci. USSR, Geop. Ser. 12, pp. 1094-1104, 1962.

Liang, G. C. and Duke, C. M. (1977) "Separation of Body and Surface Waves in Strong Motion Records," Proc. 6th World Conference on Earthquake Engineering, Vol. 2, pp. 215-220, New Delhi, India, January 1977.

Liou, C. P., Streeter, V. L. and Richart, F. E., Jr. (1977) "Numerical Model for Liquefaction," J. Geot. Engrg. Div., ASCE, Vol. 103, No. GT6, pp. 589-606, June 1977.

Lockett, F. J., (1962) "The Reflection and Refraction of Waves at an Interface between Viscoelastic Media," J. Mech. Phys. Solids, 10, pp. 53-64, 1962.

Love, A. E. H., (1927) "A Treatise on the Mathematical Theory of Elasticity," Dover, 1927.

Lysmer, J., (1969a) "Lumped Mass Methods for Rayleigh Waves," Geotechnical Engineering Report, Univ. of Calif., Berkeley, 1969.

Lysmer, J. and Kuhlemeyer, R. L. (1969b) "Finite Dynamic Model for Infinite Media," J. Engrg. Mech. Div., ASCE, Vol. 95, No. EM4, pp. 859-877, August 1969.

Lysmer, J. and Drake, L. A. (1971) "The Propagation of Love Waves across Non-Horizontally Layered Structures," Bulletin of the Seismological Society of America, Vol. 61, No. 5, pp. 1233-1256, 1971.

Lysmer, J., Seed, H. B. and Schnabel, P. B. (1971) "Influence of Base-Rock Characteristics on Ground Response," Bull. Seis. Soc. Am., Vol. 61, No. 5, pp. 1213-1232 October 1971.

Lysmer, J. and Drake, L. A. (1972) "A Finite Element Method for Seismology," Methods in Computational Physics, Vol. 11, Chapter 6, Academic Press, 1972.

Lysmer, J. and Waas, G. (1972) "Shear Waves in Plane Infinite Structures," Jour. Eng. Mech. Div. ASCE Vol. 98 No. EM1, pp. 85-105, February 1972.

Lysmer, J., Udaka, T., Seed, H. B. and Hwang, R. (1974) "LUSH a Computer Program for Complex Response Analysis of Soil-Strucuture Systems," Earthquake Engineering Research Center Report No. EERC 74-4, Univ. of Calif., Berkeley, 1974.

Lysmer, J. et al. (1975a) "FLUSH--A Computer Program for Approximate 3-D Analysis of Soil-Structure Interaction Problems," Report No. EERC 75-30, Univ. of Calif., Berkeley, December 1975.

Lysmer, J. et al., (1975b) "Efficient Finite Element Analysis of Seismic Structure-Soil-Structure Interaction," Report No. EERC 75-34, Univ. of Calif., Berkeley, 1975.

Lysmer, J. (1978) "Analytical Procedures in Soil Dynamics," Earthquake Engineering Research Center, UCB/EERC-78129, Univ. of Calif., Berkeley, December 1978.

Martin, P. P. (1975) "Non-Linear Methods for Dynamic Analysis of Ground Response," Ph.D. Thesis, University of California, Berkeley, June 1975.

Martin, P. P. and Seed, H. B. (1978) "A Simplified Procedure for Effective Stress Analysis of Ground Response," paper submitted to J. Geot. Engrg. Div., ASCE, 1978.

Matumoto, T., (1953) "Transmission and Reflection of Seismic Waves through Multilayered Elastic Medium," Bull. Earthq. Res. Inst., Vol. 31, September 1953.

McDonal, F. J. et al. (1958) "Attenuation of Shear and Compressional Waves in Pierra Shale," Geophysics, Vol. 23, 1958, pp. 421-439, 1958.

Meissner, R. (1965) "P and SV Waves from Up-Hole Shooting," Geophysical Prospecting, The Hague, The Netherlands, Vol. 13, pp. 443-459, 1965.

Mooney, H. M. and Bolt, R. A. (1966) "Dispersive Characteristics of the First Three Rayleigh Modes for a Single Surface Layer," Bull. of Seism. Soc. Am., Vol. 56, No. 1, pp. 43-67, February 1966.

Nair, G. P. (1975) "Response of Soil-Pile Systems to Seismic Waves," Ph.D. Dissertation, McMaster University, January 1975.

Nair, G. P. and Emery, J. J. (1975) "Spatial Variations in Seismic Motions," Second Canadian Conference on Earthquake Engineering, Preprint No. 5, Hamilton, Ontario, June 1975.

Ohsaki, Y. and Iwasaki, R. (1973) "On Dynamic Shear Moduli and Poisson's Ratio of Soil Deposits: Soils and Foundations" Japan, ASCE, Vol. 13, No. 4, pp. 61-73, 1973.

Okamoto, S. (1973) "Introduction to Earthquake Engineering," John Wiley and Sons, Inc., New York, 1973.

Papadakis, C. K. (1973) "Soil Transients by Characteristics Method," Ph.D. Dissertation, The University of Michigan, 1973.

Phinney, R. A. (1964), "Structure of the Earth's Crust from Spectral Behavior of Long-Period Body Waves," J. Geoph. Res. 69, pp. 2997-3018, 1964.

Ramberg, W. and Osgood, W. R. (1943) "Description of Stress-Strain Curves by Three Parameters," Technical Note 902, NACA, July 1943.

Rayleigh, Lord (1885) "On Wave Propagated along the Plane Surface of an Elastic Solid," Proc. Roy. Math. Soc., 17, pp. 4-11, 1885.

Richart, F. E., Jr., Hall, J. R., Jr. and Woods, R. D. (1970) "Vibrations of Soils and Foundations," Prentice-Hall, Inc., 1970.

Roesset, J. M. and Whitman, R. V. (1969) "Theoretical Background for Amplification Studies," Research Report No. R69-15, Soils Publication No. 231, Massachusetts Institute of Technology, Cambridge, 1969.

Scanlan, R. H. (1976) "Seismic Wave Effects on Soil/Structure Interaction," Earthquake Engineering and Structural Dynamics, Vol. 4, pp. 379-388, June 1976.

Schiff, A. and Bogdanoff, J. L. (1967) "Analysis of Current Methods of Interpreting Strong Motion Accelerogram," Bull. Seis. Soc. Am., Vol. 57, pp. 857-874, 1967.

Schnabel, P. B., Lysmer, J. and Seed, H. B. (1972) "SHAKE--A Computer Program for Earthquake Response Analysis of Horizontally Layered Sites," Report No. EERC 72-12, Earthquake Engineering Research Center, Univ. of Calif., Berkeley, December 1972.

Schnabel, P. B. and Seed, H. B. (1972) "Accelerations in Rock for Earthquakes in the Western United States," Report No. EERC 72-2, Univ. of Calif., Berkeley, July 1972.

Schnabel, P. B., Seed, H. B. and Lysmer, J. (1971) "Modification of Seismograph Records for the Effect of Local Soil Conditions," Report No. EERC 71-8, Univ. of Calif., Berkeley, December 1971.

Schnabel P. B. (1973), "Effects of Local Geology and Distance from Source on Earthquake Ground Motions," Ph.D. Dissertation, Univ. of Calif., June 1973.

Seed, H. B. and Idriss, I. M. (1969) "The Influence of Soil Conditions on Ground Motions during Earthquakes," J. Soil Mech. Found. Div., ASCE, Vol. 94, No. SM1, pp. 99-137, January 1969.

Seed, H. B., Idriss, I. M. and Kiefer, F. W. (1969) "Characteristics of Rock Motions during Earthquakes," J. Soil Mech. Found. Div., ASCE, Vol. 95, No. SM5, September 1969.

Seed, H. B. and Idriss I. M. (1970) "Analysis of Ground Motions at Union Bay, Seattle During Earthquake and distant Nuclear Blasts, Bull. Seism. Soc. Am. Vol. 60, pp. 125-136, 1970.

Seed, H. B. and Idriss, I. M. (1970) "Soil Moduli and Damping Factors for Dynamic Response Analysis," Report No. EERC 70-10, Univ. of Calif., Berkeley, December 1970.

Seed, H. B., Ugas, C. and Lysmer, J. (1976a) "Site Dependent Spectra for Earthquake Resistant Design," Bull. Seis. Soc. Am. Vol. 66, No. 1, pp. 221-243, February 1976.

Seed, H. B., Murarka, R., Lysmer, J. and Idriss, I. M. (1976b) "Relationships between Maximum Acceleration, Maximum Velocity, Distance from Source and Local Site Condition for Moderately Strong Earthquakes," Bull. Seis. Soc. Am., Vol. 66, No. 4, pp. 1323-1342, August 1976.

Sezawa, K. and Kanai, K. (1935) "The M2 Seismic Wave," Bull. Earthquake Research Institute, Tokyo, Vol. 13, pp. 471-475, 1935.

Sezawam J. (1927) "Dispersion of Elastic Waves Propagated on the Surface of Stratified Bodies and on Curved Surfaces," Bulletin of the Earthquake Research Institute, Vol. 3, 1927, pp. 1-18, 1927.

Shannon and Wilson Inc. and Agbabian Assoc. (1971) "Soil Behavior Under Earthquake Loading Conditions," Interim Report No. 1 to U.S. AEC, 1971.

Shima, E. (1970) "Seismic Surface Wave Detected by the Strong Acceleration Seismograph," Bull. of Earthquake Research Institute, The Univ. of Tokyo, Japan, Vol. 2., No. 20, 1970.

Silva, W. (1976) "A Variational Formulation for Love Waves in a Layered Anelastic Solid," G. J. R. Astr. Soc. Vol. 45, pp. 445-450, 1976.

Silva, W. (1976) "Body Waves in a Layered Anelastic Solid," Bull. Seis. Soc. Am., Vol. 66, No. 5, pp. 1539-1554, October 1976.

Silva, W. (1978) "Wave Propagation in Anelastic Media with Application to Seismology," PhD Dissertation, Univ. of Calif., Berkeley, 1978.

Silver, M. L. and Seed, H. B. (1969)," The Behavior of Sands under Seismic Loading Conditions," Report No. EERC 69-16, Univ. of Calif., Berkeley, 1969.

Stokoe, K. H. and Lodde, P. F. (1978) "Dynamic Response of San Francisco Bay Mud," ASCE Conf. on Earthq. Engrg. and Soil Dynamics, Pasadena, California, June 1978.

Stoneley R. (1955) "Rayleigh Waves in a Medium with Two Surface Layers," Roy. Astro. Soc., Geoph. Suppl., Vol. 7, No. 2, October 1955.

Stoneley, R. (1957) "The Attenuation of Rayleigh Waves with Depth in a Medium with Two Surface Layers," Roy. Astro. Soc., Geoph. Suppl., Vol. 7, No. 5, April 1957.

Streeter, V. L., Wylie, E. B., and Richart, F. E., Jr. (1974) "Soil Motion Computations by Characteristics Method," J. Geot. Engrg. Div., ASCE, Vol. 100, No. GT3, pp. 1539-1554, October 1974.

Suzuki, T., (1932) "On the Angle of Incidence of the Initial Motion Observed at Hongo and Mitaka," Bulletin of the Earthquake Research Institute, Vol. 10, 1932, pp. 517-535, 1932.

Swanger, W. J. and Boore, D. M. (1978) "Simulation of Strong-Motion Displacements using Surface-Wave Modal Superposition," Bull. Seis. Soc. Am., Vol. 68, No. 4, pp. 247-263, March 1978.

Taylor, P. W. and Larkin, T. J. (1978) "Seismic Site Response of Nonlinear Soil Media," J. Geot. Engrg. Div., ASCE, Vol. 104, No. GT3, pp. 369-383, March 1978.

Teng, T. L. (1967) "Reflection and Transmission from a Plane Layered Core-Mantle Boundary," Bull. Seis. Soc. Am., Vol. 57, No. 3, pp. 477-499, June 1967.

Thomson, W. T. (1950) "Transmission of Elastic Waves Through a Stratified Solid Medium," J. Appl. Physics, Vol. 21, February 1950.

Thrower, E. N. (1965) "The Computation of the Dispersion of Elastic Waves in Layered Media," J. Sound Vib. Vol. 2, pp. 210-225, 1965.

Toki, K. (1977) "Disintegration of Accelerograms into Surface and Body Waves," Proc. 6th World Conference on Earthquake Engineering, Vol. 2, pp. 209-214, New Delhi, India, January 1977.

Trifunac, M. D. (1970) "Low Frequency Digitization Errors and a New Method for Zero Baseline Correction of Strong-Motion Accelerograms," Earthquake Engineering Research Laboratory, EERL 70-67, California Institute of Technology, Pasadena, 1970.

Trifunac, M. D. (1971a) "Response Envelope Spectrum and Interpretation of Strong Earthquake Ground Motion," Bull. Seis. Soc. Am., Vol. 61, pp. 343-356, 1971.

Tsai, N. C. (1969) "Influence of Local Geology on Earthquake Ground Motion," Ph.D. Dissertation, California Institute of Technology, Pasadena, 1969.

Tsai, N. C. and Housner, G. W. (1970) "Calculation of Surface Motions of a Layered Half-Space," Bull. Seism. Soc. Am., Vol. 60, No. 5, pp. 1625-1651, October 1970.

Udaka, T. (1975) "Analysis of Response of Large Embankments to Traveling Base Motions," PhD Dissertation, Univ. of Calif., Berkeley, December 1975.

Valera, J. E., Seed, H. B., Tsai, C. F. and Lysmer, J. (1977) "Soil-Structure Interaction Effects at the Humboldt Power Plant in the Ferndale Earthquake of June 7, 1975." Report No. UCB/EERC 77/03, Univ. of Calif. Berkeley, 1977.

Viktorov, I. A. (1967) "Rayleigh and Lamb Waves." trans. by W. P. Mason, Plenum Press, 1967.

Waas, G. (1972) "Linear Two-Dimensional Analysis of Soil Dynamic Problems in Semi-Infinite Layered Media." Ph.D Dissertation, Univ. of Calif., Berkeley, June 1972; also Tech Report S-71-16, U. S. A. W. E. S., September 1972.

Watson, T. H. (1970) "A Note on Fast Computation of Rayleigh Wave Dispersion in the Multilayered Elastic Half-Space." Bull. Seis. Soc. Am. Vol. 60, No. 1, pp. 161-166, February 1970.

White, R. V. (1970) "Seismic Response of a Very Deep Soil Deposit." Research Report No. 870-38, Massachusetts Institute of Technology, Cambridge, June 1970.

Wong, H. L. (1975) "Dynamic Soil/Structure Interaction." Report No. EERC 75-01, Ph.D. Dissertation, California Institute of Technology, Pasadena, May 1975.

Wong, H. L. and Luco, J. E. (1976) "Dynamic Response of Rigid Foundations of Arbitrary Shape." Earthquake Engineering and Structural Dynamics, Vol. 4, pp. 579-587, 1976.

Woods, R. D. (1978) "Measurement of Dynamic Soil Properties." Proc. of the ASCE Geotech. Eng. Div., Specialty Conf. on Earthquake Engineering and Soil Dynamics, pp. 91-178, June 1978.

Yamahara, H. (1970) "Ground Motions during Earthquakes and the Input Loss of Earthquake Power to an Excitation of Building Soils and Foundations." Soil and Foundations, Japan Soc. Civil Engrg., Vol. 10, No. 2, pp. 165-181, June 1970.

Yashimi, Y. et al. (1977) "Soil Dynamic and its Application to Foundation Engineering." Proc. 9th Int. Conf. Soil Mech. Found. Engrg., Vol. 2, pp. 605-650, 1977.

Zienkiewicz, O. C., Chang, C. T. and Bettess, P. (1978) "Drained Seismic Response and Liquefaction," submitted for publication in the Int. J. Numerical and Analytical Methods in Geomechanics, 1978.

[illegible]

[illegible]

[illegible]

[illegible]

[illegible]

[illegible]

[illegible]

EERC 75-19 "The Inelastic Behavior of Critical Regions of Reinforced Concrete Components as Influenced by Moment, Shear and Axial Force," by G.H. Atalay and J. Penzien - 1975 (PB 258 842)A11

EERC 75-20 "Dynamic Properties of an Eleven Story Masonry Building," by R.M. Stephen, J.P. Hollings, J.G. Bouwkamp and D. Jurukovski - 1975 (PB 246 945)A04

EERC 75-21 "State-of-the-Art in Seismic Strength of Masonry - An Evaluation and Review," by R.L. Mayes and R.W. Clough - 1975 (PB 249 048)A07

EERC 75-22 "Frequency Dependent Stiffness Matrices for Viscoelastic Half-Plane Foundations," by A.K. Chopra, P. Chakrabarti and S. Dasgupta - 1975 (PB 248 121)A07

EERC 75-23 "Hysteretic Behavior of Reinforced Concrete Framed Walls," by T.Y. Wong, V.V. Bertero and E.P. Popov - 1975

EERC 75-24 "Panel Tests for Alternate Configurations of Precast Wall Structural Systems," by V.V. Bertero, E.P. Popov and S. Endo - 1975

EERC 75-25 "Influence of Seismic History on the Liquefaction Characteristics of Sands," by H.B. Seed, K. Mori and C.K. Chan - 1975 (Superseded by EERC 75-28)

EERC 75-26 "The Generation and Dissipation of Pore Water Pressures during Soil Liquefaction," by H.B. Seed, P.P. Martin and J. Lysmer - 1975 (PB 252 648)A03

EERC 75-27 "Identification of Research Needs for Improving Aseismic Design of Building Structures," by V.V. Bertero - 1975 (PB 248 136)A05

EERC 75-28 "Evaluation of Soil Liquefaction Potential during Earthquakes," by H.B. Seed, I. Arango and C.K. Chan - 1975 (NUREG 0026)A13

EERC 75-29 "Representation of Irregular Stress Time Histories by Equivalent Uniform Stress Series in Liquefaction Analyses," by H.B. Seed, I.M. Idriss, F. Makdisi and N. Banerjee - 1975 (PB 252 635)A03

EERC 75-30 "FLUSH - A Computer Program for Approximate 3-D Analysis of Soil-Structure Interaction Problems," by J. Lysmer, P.B. Udaka, C.-F. Tsai and H.B. Seed - 1975 (PB 258 781)A07

EERC 75-31 "ALUSH - A Computer Program for Seismic Response Analysis of Axisymmetric Soil-Structure Systems," by E. Berger, J. Lysmer and H.B. Seed - 1975

EERC 75-32 "SAP IV and SAPIVD - Computer Programs for Soil-Structure Interaction Analysis with Horizontally Travelling Waves," by P. Chan, J. Lysmer and H.B. Seed - 1975

EERC 75-33 "Predicting the Performance of Structures in Regions of High Seismicity," by J. Penzien - 1975 (PB 248 130)A03

EERC 75-34 "Efficient Finite Element Analysis of Seismic Structure - Soil - Direction," by J. Lysmer, H.B. Seed, T. Udaka, R.N. Hwang and C.-F. Tsai - 1975 (PB 253 570)A07

EERC 75-35 "The Nonlinear Behavior of a Fixed Steel Model of a Three-Story Steel Frame Subjected to Earthquake Loading," by R.W. Clough and L.-Y. Lu - 1975 (PB 248 961)A05

EERC 75-36 "Earthquake Simulator Study of a Steel Frame Structure, Volume II - Analytical Results," by D.T. Tang - 1975 (PB 252 926)A10

EERC 75-37 "NONSAP - A General Purpose Computer Program for Analysis of Non-Linear Structural Response," by D.P. Mondkar and G.H. Powell - 1975 (PB 252 926)A10

EERC 75-38 "Nonlinear Response Spectra for Probabilistic Seismic Design and Damage Assessment of Reinforced Concrete Structures," by M. Murakami and J. Penzien - 1975 (PB 259 530)A05

EERC 75-39 "Study of a Method of Feasible Directions for Optimal Elastic Design of Frame Structures Subjected to Earthquake Loading," by S.J. Walker and K.S. Pister - 1975 (PB 257 781)A06

EERC 75-40 "An Alternative Representation of the Elastic-Viscoelastic Analogy," by G. Dasgupta and J.L. Sackman - 1975 (PB 252 170)A03

EERC 75-41 "Effect of Multi-Directional Shaking on Liquefaction of Sands," by H.B. Seed, R. Pyke and G.R. Martin - 1975 (PB 258 781)A03

EERC 76-1 "Strength and Ductility Evaluation of Existing Low-Rise Reinforced Concrete Buildings - Screening Method," by T. Okada and B. Bresler - 1976 (PB 257 906)A11

EERC 76-2 "Experimental and Analytical Studies on the Hysteretic Behavior of Reinforced Concrete Rectangular and T-Beams," by S.-Y.M. Ma, E.P. Popov and V.V. Bertero - 1976 (PB 260 843)A12

EERC 76-3 "Dynamic Behavior of a Multistory Triangular-Shaped Building," by J. Petrovski, R.M. Stephen, E. Gartenbaum and J.G. Bouwkamp - 1976 (PB 273 279)A07

EERC 76-4 "Earthquake Induced Deformations of Earth Dams," by N. Serff, H.B. Seed, F.I. Makdisi & C.-Y. Chang - 1976 (PB 292 065)A08

UCB/EERC-79/01 "Hysteretic Behavior of Lightweight Reinforced Concrete Beam-Column Subassemblages," by B. Forzani, E.P. Popov, and V.V. Bertero - 1979

UCB/EERC-79/02 "The Development of a Mathematical Model to Predict the Flexural Response of Reinforced Concrete Beams to Cyclic Loads, Using System Identification," by J.F. Stanton and H.D. McNiven - 1979

UCB/EERC-79/03 "Linear and Nonlinear Earthquake Response of Simple Torsionally Coupled Systems," by C.L. Kan and A.K. Chopra - 1979

UCB/EERC-79/04 "A Mathematical Model of Masonry for Predicting Its Linear Seismic Response Characteristics," by Y. Mengi and H.D. McNiven - 1979

UCB/EERC-79/05 "Mechanical Behavior of Lightweight Concrete Confined by Different Types of Lateral Reinforcement," by M.A. Manrique, V.V. Bertero and E.P. Popov - 1979

UCB/EERC-79/06 "Static Tilt Tests of a Tall Cylindrical Liquid Storage Tank," by R.W. Clough and A. Niwa - 1979

UCB/EERC-79/07 "The Design of Steel Energy Absorbing Restrainers and Their Incorporation Into Nuclear Power Plants for Enhanced Safety: Volume 1 - Summary Report," by P.N. Spencer, V.F. Zackay, and E.R. Parker - 1979

UCB/EERC-79/08 "The Design of Steel Energy Absorbing Restrainers and Their Incorporation Into Nuclear Power Plants for Enhanced Safety: Volume 2 - The Development of Analyses for Reactor System Piping," "Simple Systems" by M.C. Lee, J. Penzien, A.K. Chopra, and K. Suzuki "Complex Systems" by G.H. Powell, E.L. Wilson, R.W. Clough and D.G. Row - 1979

UCB/EERC-79/09 "The Design of Steel Energy Absorbing Restrainers and Their Incorporation Into Nuclear Power Plants for Enhanced Safety: Volume 3 - Evaluation of Commerical Steels," by W.S. Owen, R.M.N. Pelloux, R.O. Ritchie, M. Faral, T. Ohhashi, J. Toplosky, S.J. Hartman, V.F. Zackay, and E.R. Parker - 1979

UCB/EERC-79/10 "The Design of Steel Energy Absorbing Restrainers and Their Incorporation Into Nuclear Power Plants for Enhanced Safety: Volume 4 - A Review of Energy-Absorbing Devices," by J.M. Kelly and M.S. Skinner - 1979

UCB/EERC-79/11 "Conservatism In Summation Rules for Closely Spaced Modes," by J.M. Kelly and J.L. Sackman - 1979

UCB/EERC-79/12 "Cyclic Loading Tests of Masonry Single Piers Volume 3 - Height to Width Ratio of 0.5," by P.A. Hidalgo, R.L. Mayes, H.D. McNiven and R.W. Clough - 1979

UCB/EERC-79/13 "Cyclic Behavior of Dense Coarse-Grained Materials in Relation to the Seismic Stability of Dams," by N.G. Banerjee, H.B. Seed and C.K. Chan - 1979

UCB/EERC-79/14 "Seismic Behavior of Reinforced Concrete Interior Beam-Column Subassemblages," by S. Viwathanatepa, E.P. Popov and V.V. Bertero - 1979

UCB/EERC-79/15 "Optimal Design of Localized Nonlinear Systems with Dual Performance Criteria Under Earthquake Excitations," by M.A. Bhatti - 1979

UCB/EERC-79/16 "OPTDYN - A General Purpose Optimization Program for Problems with or without Dynamic Constraints," by M.A. Bhatti, E. Polak and K.S. Pister - 1979

UCB/EERC-79/17 "ANSR-II, Analysis of Nonlinear Structural Response, Users Manual," by D.P. Mondkar and G.H. Powell - 1979

UCB/EERC-79/18 "Soil Structure Interaction in Different Seismic Environments," A. Gomez-Masso, J. Lysmer, J.-C. Chen and H.B. Seed - 1979

UCB/EERC-79/19 "ARMA Models for Earthquake Ground Motions," by M.K. Chang, J.W. Kwiatkowski, R.F. Nau, R.M. Oliver and K.S. Pister - 1979

UCB/EERC-79/20 "Hysteretic Behavior of Reinforced Concrete Structural Walls," by J.M. Vallenas, V.V. Bertero and E.P. Popov - 1979

UCB/EERC-79/21 "Studies on High-Frequency Vibrations of Buildings I: The Column Effects," by J. Lubliner - 1979

UCB/EERC-79/22 "Effects of Generalized Loadings on Bond Reinforcing Bars Embedded in Confined Concrete Blocks," by S. Viwathanatepa, E.P. Popov and V.V. Bertero - 1979

UCB/EERC-79/23 "Shaking Table Study of Single-Story Masonry Houses, Volume 1: Test Structures 1 and 2," by P. Gülkan, R.L. Mayes and R.W. Clough - 1979

UCB/EERC-79/24 "Shaking Table Study of Single-Story Masonry Houses, Volume 2: Test Structures 3 and 4," by P. Gülkan, R.L. Mayes and R.W. Clough - 1979

UCB/EERC-79/25 "Shaking Table Study of Single-Story Masonry Houses, Volume 3: Summary, Conclusions and Recommendations," by R.W. Clough, R.L. Mayes and P. Gülkan - 1979

UCB/EERC-79/26 "Recommendations for a U.S.-Japan Cooperative Research Program Utilizing Large-Scale Testing Facilities," by U.S.-Japan Planning Group - 1979

UCB/EERC-79/27 "Earthquake-Induced Liquefaction Near Lake Amatitlan, Guatemala," by H.B. Seed, I. Arango, C.K. Chan, A. Gomez-Masso and R. Grant de Ascoli - 1979

UCB/EERC-79/28 "Infill Panels: Their Influence on Seismic Response of Buildings," by J.W. Axley and V.V. Bertero - 1979

UCB/EERC-79/29 "3D Truss Bar Element (Type 1) for the ANSR-II Program," by D.P. Mondkar and G.H. Powell - 1979

UCB/EERC-79/30 "2D Beam-Column Element (Type 5 - Parallel Element Theory) for the ANSR-II Program," by D.G. Row, G.H. Powell and D.P. Mondkar

UCB/EERC-79/31 "3D Beam-Column Element (Type 2 - Parallel Element Theory) for the ANSR-II Program," by A. Riahi, G.H. Powell and D.P. Mondkar - 1979

UCB/EERC-79/32 "On Response of Structures to Stationary Excitation," by A. Der Kiureghian - 1979

UCB/EERC-79/33 "Undisturbed Sampling and Cyclic Load Testing of Sands," by S. Singh, H.B. Seed and C.K. Chan - 1979

UCB/EERC-79/34 "Interaction Effects of Simultaneous Torsional and Compressional Cyclic Loading of Sand," by P.M. Griffin and W.N. Houston - 1979

UCB/EERC-80/01 "Earthquake Response of Concrete Gravity Dams Including Hydrodynamic and Foundation Interaction Effects," by A.K. Chopra, P. Chakrabarti and S. Gupta - 1980

UCB/EERC-80/02 "Rocking Response of Rigid Blocks to Earthquakes," by C.S. Yim, A.K. Chopra and J. Penzien - 1980

UCB/EERC-80/03 "Optimum Inelastic Design of Seismic-Resistant Reinforced Concrete Frame Structures," by S.W. Zagajeski and V.V. Bertero - 1980

UCB/EERC-80/04 "Effects of Amount and Arrangement of Wall-Panel Reinforcement on Hysteretic Behavior of Reinforced Concrete Walls," by R. Iliya and V.V. Bertero - 1980

UCB/EERC-80/05 "Shaking Table Research on Concrete Dam Models," by A. Niwa and R.W. Clough - 1980

UCB/EERC-80/06 "Piping With Energy Absorbing Restrainers: Parameter Study on Small Systems," by G.H. Powell, C. Oughourlian and J. Simons - 1980

UCB/EERC-80/07 "Inelastic Torsional Response of Structures Subjected to Earthquake Ground Motions," by Y. Yamazaki - 1980

UCB/EERC-80/08 "Study of X-Braced Steel Frame Structures Under Earthquake Simulation," by Y. Ghanaat - 1980

UCB/EERC-80/09 "Hybrid Modelling of Soil-Structure Interaction," by S. Gupta, T.W. Lin, J. Penzien and C.S. Yeh - 1980

UCB/EERC-80/10 "General Applicability of a Nonlinear Model of a One Story Steel Frame," by B.I. Sveinsson and H. McNiven - 1980

UCB/EERC-80/11 "A Green-Function Method for Wave Interaction with a Submerged Body," by W. Kioka - 1980

UCB/EERC-80/12 "Hydrodynamic Pressure and Added Mass for Axisymmetric Bodies," by F. Nilrat - 1980

UCB/EERC-80/13 "Treatment of Non-Linear Drag Forces Acting on Offshore Platforms," by B.V. Dao and J. Penzien - 1980

UCB/EERC-80/14 "2D Plane/Axisymmetric Solid Element (Type 3 - Elastic or Elastic-Perfectly Plastic) for the ANSR-II Program," by D.P. Mondkar and G.H. Powell - 1980

UCB/EERC-80/15 "A Response Spectrum Method for Random Vibrations," by A. Der Kiureghian - 1980

UCB/EERC-80/16 "Cyclic Inelastic Buckling of Tubular Steel Braces," by V.A. Zayas, E.P. Popov and S.A. Mahin - June 1980

UCB/EERC-80/17 "Dynamic Response of Simple Arch Dams Including Hydrodynamic Interaction," by C.S. Porter and A.K. Chopra - July 1980

UCB/EERC-80/18 "Experimental Testing of a Friction Damped Aseismic Base Isolation System with Fail-Safe Characteristics," by J.M. Kelly, K.E. Beucke and M.S. Skinner - July 1980

UCB/EERC-80/19 "The Design of Steel Energy-Absorbing Restrainers and their Incorporation into Nuclear Power Plants for Enhanced Safety (Vol 1B): Stochastic Seismic Analyses of Nuclear Power Plant Structures and Piping Systems Subjected to Multiple Support Excitations," by M.C. Lee and J. Penzien - 1980

UCB/EERC-80/20 "The Design of Steel Energy-Absorbing Restrainers and their Incorporation into Nuclear Power Plants for Enhanced Safety (Vol 1C): Numerical Method for Dynamic Substructure Analysis," by J.M. Dickens and E.L. Wilson - 1980

UCB/EERC-80/21 "The Design of Steel Energy-Absorbing Restrainers and their Incorporation into Nuclear Power Plants for Enhanced Safety (Vol 2): Development and Testing of Restraints for Nuclear Piping Systems," by J.M. Kelly and M.S. Skinner - 1980

UCB/EERC-80/22 "3D Solid Element (Type 4-Elastic or Elastic-Perfectly-Plastic) for the ANSR-II Program," by D.P. Mondkar and G.H. Powell - 1980

UCB/EERC-80/23 "Gap Friction Element (Type 5) for the ANSR-II Program," by D.P. Mondkar and G.H. Powell - 1980

UCB/EERC-80/24 "U-Bar Restraint Element (Type 11) for the ANSR-II Program," C. Oughourlian and G.H. Powell - 1980

UCB/EERC-80/25 "Testing of a Natural Rubber Base Isolation System by an Explosively Simulated Earthquake," by J.M. Kelly 1980

UCB/EERC-80/26 "Input Identification from Structural Vibrational Response," by Y. Hu - 1980

UCB/EERC-80/27 "Cyclic Inelastic Behavior of Steel Offshore Structures," by V.A. Zayas, S.A. Mahin and E.P. Popov - 1980

UCB/EERC-80/28 "Shaking Table Testing of a Reinforced Concrete Frame with Biaxial Response," M.G. Oliva and R.W. Clough 1980

UCB/EERC-80/29 "Dynamic Properties of a Twelve-Story Prefabricated Panel Building," by J.G. Bouwkamp, J.P. Kollegger and R.M. Stephen - 1980

UCB/EERC-80/30 "Dynamic Properties of a Eight-Story Prefabricated Panel Building," by J.G. Bouwkamp, J.P. Kollegger and R.M. Stephen - 1980

UCB/EERC-80/31 "Predictive Dynamic Response of Panel Type Structures Under Earthquakes," by J.P. Kollegger and J.G. Bouwkamp 1980

UCB/EERC-80/32 "The Design of Steel Energy-Absorbing Restrainers and their Incorporation into Nuclear Power Plants for Enhanced Safety: Vol 3, Testing of Commercial Steels in Low-Cycle Torsional Fatigue," by P. Spencer, E.R. Parker, E. Jongewaard and M. Drory - 1980

UCB/EERC-80/33 "The Design of Steel Energy-Absorbing Restrainers and their Incorporation into Nuclear Power Plants for Enhanced Safety: Vol 4, Shaking Table Tests of Piping Systems with Energy-Absorbing Restrainers," by S.F. Stiemer and W.G. Godden - 1980

UCB/EERC-80/34 "The Design of Steel Energy-Absorbing Restrainers and their Incorporation into Nuclear Power Plants for Enhanced Safety: Vol 5, Summary Report," by P. Spencer 1980

UCB/EERC-80/35 "Experimental Testing of an Energy Absorbing Base Isolation System," by J. Kelly, M.S. Skinner and K.E. Beucke - 1980

UCB/EERC-80/36 "Simulating and Analyzing Artificial Non-Stationary Earthquake Ground Motions," by R.F. Hao, R.M. Oliver and K.S. Pister - 1980

UCB/EERC-80/37 "Earthquake Engineering at Berkeley," - 1980

UCB/EERC-80/38 "Inelastic Seismic Analysis of Large Panel Buildings," by V. Schricker and G.H. Powell - 1980

UCB/EERC-80/39 "Dynamic Response of Embankment, Concrete-Gravity and Arch Dams Including Hydrodynamic Interaction," by J.F. Hall and A.K. Chopra - 1980

UCB/EERC-80/40 "Inelastic Buckling of Steel Strut Under Cyclic Load Reversal," by R.G. Black, W.A. Wenger and E.P. Popov - 1980

UCB/EERC-80/41 "Influence of Site Characteristics on Building Damage During the October 3, 1974 Lima Earthquake," by P. Repetto, I. Arango and H.B. Seed - 1980

UCB/EERC-80/42 Evaluation of a Shaking Table Test Program on Response Behavior of a Two Story Reinforced Concrete Frame," by J.M. Blondet, R.W. Clough and S.A. Mahin - 1980

UCB/EERC-80/43 "Modelling of Soil-Structure Interaction by Finite and Infinite Element," by F. Medina - 1980

UCB/EERC-81/01 "Control Cyclic Response of Piping Systems and other Structures by Base Isolation," edited by J.M. Kelly - 1981

UCB/EERC-81/02 "OPTNSR - An Interactive Software System by Optimal Design of Statically and Dynamically Loaded Structures with Nonlinear Response," by M.A. Bhatti, V. Ciampi and K.S. Pister - 1981

UCB/EERC-81/03 "Analysis of Local Variations in Free Field Seismic Ground Motion," by J.-C. Chen, J. Lysmer and H.B. Seed - 1981